An Investigation Into Novel Red Emitting Phosphors and Their Applications

A thesis submitted for the degree of Doctor of Philosophy

by
Roni Stone

Wolfson Centre for Materials Processing
Brunel University
September 2011

To my parents. . .

Abstract

An Investigation Into Novel Red Emitting Phosphors and Their Applications

New red emitting phosphors, based on the double tungstate/molybdates, were discovered. Some were able to retain their luminous efficacy after substituting Y^{3+} for Eu^{3+}, reducing the cost of the phosphor. This substitution was attempted for existing commercial red emitting phosphors and proved unsuccessful.

Another set of phosphors based on these lattices were discovered and the emitted luminous efficacy was 140% greater than other reported Eu^{3+} phosphors. The best of these was $Na_2WO_4MoO_4Eu_{0.44}Al_{1.34}Sm_{0.011}$.

The integration of phosphors to the lighting application was also studied, including improvements in light extraction for existing phosphors. ACEL panels are currently applied to many applications and were briefly examined. The more recent OLED technology was investigated and comparisons can be drawn with the ACEL panels. LEDs were also a focus of the work with a new method developed for remote application of phosphors to LEDs, based on a dome shaped encapsulant, and this was adopted commercially by a high brightness LED manufacturer.

The studies on the phosphors reported herein were aimed at integrating these into commercial applications. Although this was not achieved as brightness and particles size were problematic, if it is demonstrated that further development of the synthetic methods produce phosphors with suitable attributes, this may lead to the integration in applications.

Table of Contents

i

List of Figures

List of Tables

List of Abbreviations

CIE   -   Commission internationale de l'éclairage

CCT   -   Colour Correlated Temperature (K)

CRI   -   Colour Rendering Index

FESEM   -   Field Emission Scanning Electron Microscope

SEM   -   Scanning Electron Microscope

XRD   -   X-Ray Diffraction

ACEL   -   Alternating Current Electroluminescence

LED   -   Light Emitting Diode

OLED   -   Organic Light Emitting Diode

PLED   -   Polymer Light Emitting Diode

lm   -   Lumens

lm/W   -   Lumens per Watt

LE   -   Luminous Efficacy (lm/W)

QE   -   Quantum Efficiency (%)

cd   -   Candela

cd/m^{-2} -   Candela's per square metre

Acknowledgements

Chapter 1

Introduction

A modern world of wasteful consumption requires a greater degree of efficiency in usage habits and technical advancements. Energy consumption such as electricity is high on the agenda, as though an individual's usage may be low, the total sum of all runs into a vast amount. A solution here, like most developments in our world, will be based on scientific improvements researched and implemented by universities and companies around the world. The Wolfson Centre at Brunel University is one such research institute. My small contribution begins here.

1.1 Thesis Introduction

Lighting is a large part of the modern world. Improvements in efficiency in this area will lead to energy savings. The areas investigated were done so in an attempt to improve the properties of the phosphors and to increase photon extraction from LED devices.

Lighting, both general lighting (e.g. white light emitters) and display lighting, is often based on high brightness blue LEDs. Green and red LEDs are not yet of the same luminous efficacy and so phosphors are used to convert light to other wavelengths. However, red phosphors have problems with their performance including a low luminous efficacy, poor temperature dependence and poor stability such as susceptibility to degradation when coming into contact with water [1] [2]. Improvements in this area can be achieved by either synthesising novel phosphors, or making changes to existing phosphors to improve their properties in the relevant areas without loss in their existing traits.

The properties required of phosphors for general and display lighting can be summarised in understanding that for general lighting, a CRI of above 85 is crucial and this usually requires a broad band emitting phosphor. In display lighting, a wide colour gamut is key to allow for the greatest number of colours to be displayed. A narrow band emitter is not a hindrance here; the CIE coordinates of the emitter (defined in section 1.2.3) are the key measure for display lighting.

In both cases a high luminous efficacy is necessary. This depends heavily on the wavelength of the emission; for comparison commercial phosphors were measured at

the outset of the work. Excited at 465nm, $SrS:Eu^{2+}$ was measured at $119\,lm/W$ with peak emission at 615nm and $SrS:Eu^{2+}$ at $43\,lm/W$, with a peak emission at 655nm. The aim is to match or exceed a luminous efficacy at similar emission wavelengths with additional properties of a reduction in degradation or improvement in performance at temperatures of above $150\,^{\circ}C$.

Another method in increasing the efficiency of light emitting devices is from improvements in photon extraction from the package. This includes how and where the phosphor is applied in relation to the LED chips. Scattering and reflection of the phosphor and the other elements of the package, including the encapsulant, were the areas under consideration. Attributes of the phosphor such as temperature dependence will invariably depend upon the packaging. The closer that the phosphor lies to the LED chip, the higher the temperature the phosphor will experience.

Phosphors have been in use for some time and have found many uses within lighting. The existing technology of ACEL panels (chapter 6) and the newer technology of OLEDs (chapter 8) were both investigated for their suitability to the application of phosphors.

1.2 Lighting Introduction

The most logical place to commence a work on lighting is the visible light we see around us. However, this is just a small part of the electromagnetic spectrum (figure 1.1), and those areas just outside the visible region, specifically the ultra violet region, can also play an important role.
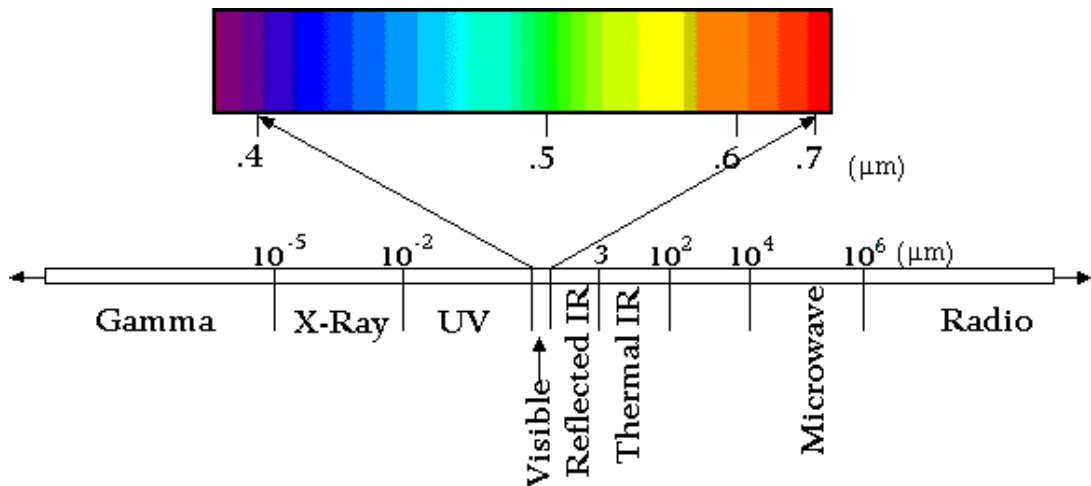
Figure 1.1: The electromagnetic spectrum with the visible region expanded with an inset [3]

1.2.1 Electromagnetic Spectrum

The electromagnetic spectrum comprises waves that have an electric and magnetic component, as described by Maxwell in the mid 19th century. These are perpendicular to each other as the wave propagates through space and a more detailed treatise can

be found in many general physics books [4]. All parts of the spectrum are governed by the same laws, although it will be the 200nm to 800nm region that is the main interest in this work.

1.2.2   Photopic Eye Response

How the human eye responds to the electromagnetic spectrum is of importance. Effective in the wavelength range from 390nm to 750nm the eye is sensitive to both colour and luminosity. There are three types of cells in the eye sensitive to light; rods, cones and retinal ganglion cells. There are approximately 4.6 millions cones, and 92 millions rods in the eye which are used to detect light, colour and movement [5]. The retinal ganglion cells are most sensitive to blue light but are only used in the control of the circadian clock [6].

The eye responds differently in light conditions and dark conditions using cones, rods or the combination of the two. In high intensity conditions ($>1\,\mathrm{cdm^{-2}}$) rods and cones are used while under low intensity ($<0.01\,\mathrm{cdm^{-2}}$) only the rods are active. This is referred to as photopic and scotopic conditions, respectively. The response to photons by the eye is not uniform at all wavelengths, and the photopic and scotopic responses also differ from each other. For lighting levels in between these conditions a mixture of the rods and cones are used; this is known as the mesopic response. An accurate description of how these curves graduate from one to the other is not fully understood, although an attempt to define it has been discussed [7].

Ogden Rood helped develop an accurate method for measuring the photopic eye response, known as 'Flicker' photometry [8] meant to measure the behaviour of the response curves. It was not until 1923, that Gibson and Tyndall conducted a more thorough study, the results of which led to an internationally accepted photopic response curve, which peaks at 555nm at a value of 683 lm/W.

This was revised in 1978 to make an adjustment in the sensitivity function below 450nm which was underestimated up to this point [9]. This revised function is shown in figure 1.2. A comparison of the photopic and scotopic response curves is shown in figure 1.3 [10].

Photometric definitions are based on an integration of the energy of the radiation at different wavelengths over the standard photopic response curve. To define the efficacy of light consisting of more than one wavelength, the area under its emission curve is integrated with each wavelength multiplied by the photopic response curve function.

1.2.3   Measuring Visible Light

CIE coordinates

From the onset of the 20th century, as well as advances in understanding the eye response to light stimulation, the standard for light measurements were being advanced. It was known that mixing the three primary colours in suitable ratios could produce
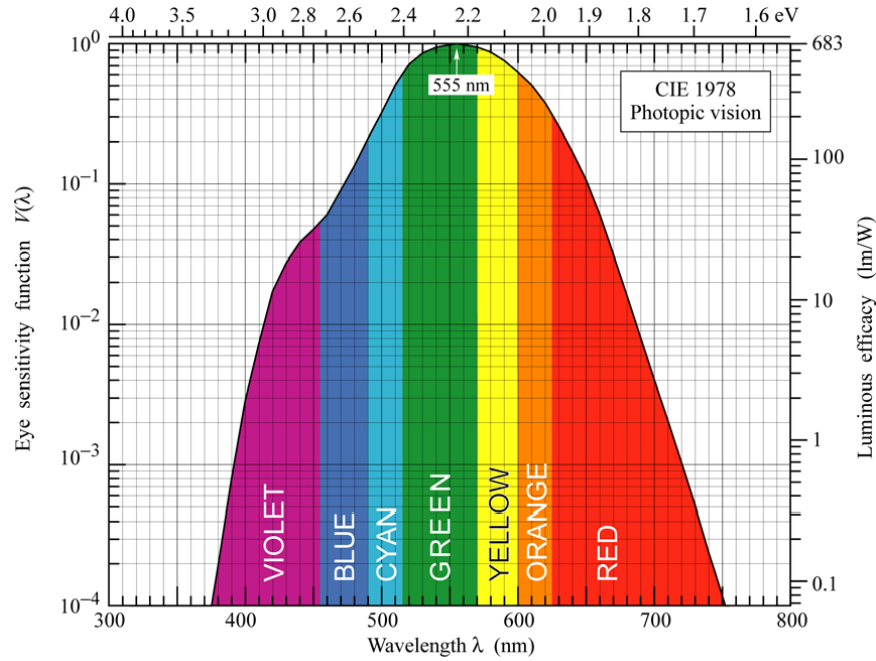
Figure 1.2: Eye sensitivity function, $V(\lambda)$ and luminous efficacy measured in lumens per watt of optical power [9]

any of the set of possible colours. Based on this principle, the CIE (International Commission on Illumination) colour space for chromaticity was created. Initially this was measured experimentally to create an RGB colour space based on the receptors in the human eye. However, their coefficients, which can be seen in figure 1.4, included some negative values, which led to the creation of an XYZ colour space where all colours are created by mixing without subtraction. These spectral functions are shown in figure 1.5.

From the tristimulus XYZ values, the chromaticity values are calculated. $x = \frac{X}{(X+Y+Z)}$ and $y = \frac{Y}{(X+Y+Z)}$. Since by definition $x + y + z = 1$, z is unnecessary to show as it can be derived from x and y.

In 1931 the CIE proceedings agreed on the XYZ colour space which is to this day the widely used measurement. This colour space in (x,y) is shown in figure 1.6.

From any two points in this colour space, all points between them can be formed by mixing these two colours. From any three points (which will form a triangle) all points within their triangle can be formed by mixing the colours in appropriate combination.

However, mixing equal amounts of colours will not result in the emission at the midpoint of the colours mixed. A correction for this was attempted in 1960 by introducing CIELUV colour space which involved a transform from the (x, y) coordinates to (u, v) colour space. This was updated again in 1976 by a simple factor to where $u' = u$ and $v' = 1.5v$.

The problem that this colour space introduced was that when mixing colour points their resultant will not be situated on a line between the initial points, unless they are constant in lightness.
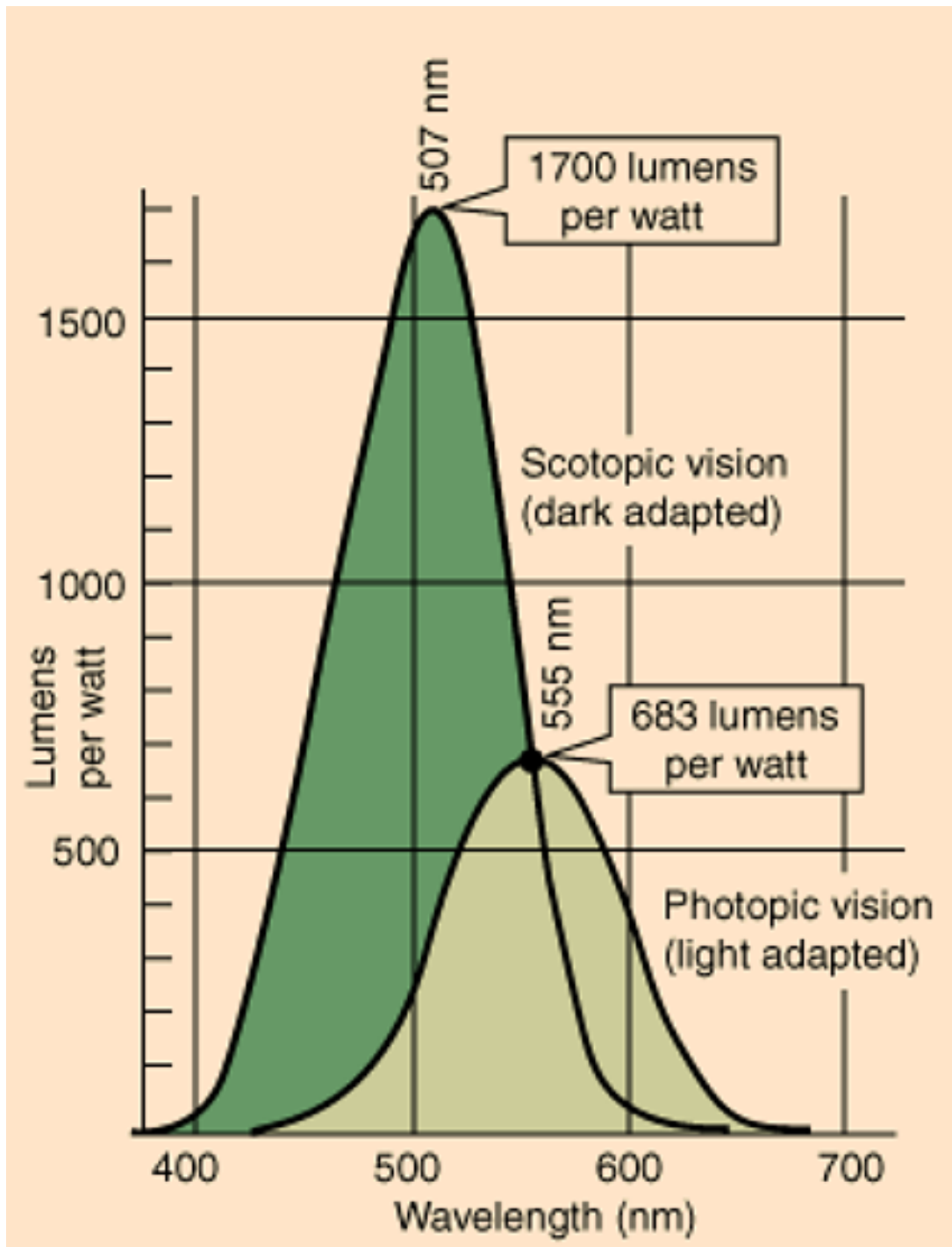
Figure 1.3: Eye sensitivity function for photopic (555nm peak) and scotopic (507nm peak) response functions [10]

Colour Temperature

The line that runs through the 1931 CIE diagram (figure 1.7) is the Planckian locus (or blackbody locus) which shows the locus of colour that an incandescent black body emitter would take in this colour space. Low temperature blackbody emitters are located in the red region of the spectrum and the shift to high temperatures corresponds to a shift in emission colour to blue. It should be noted that when referring
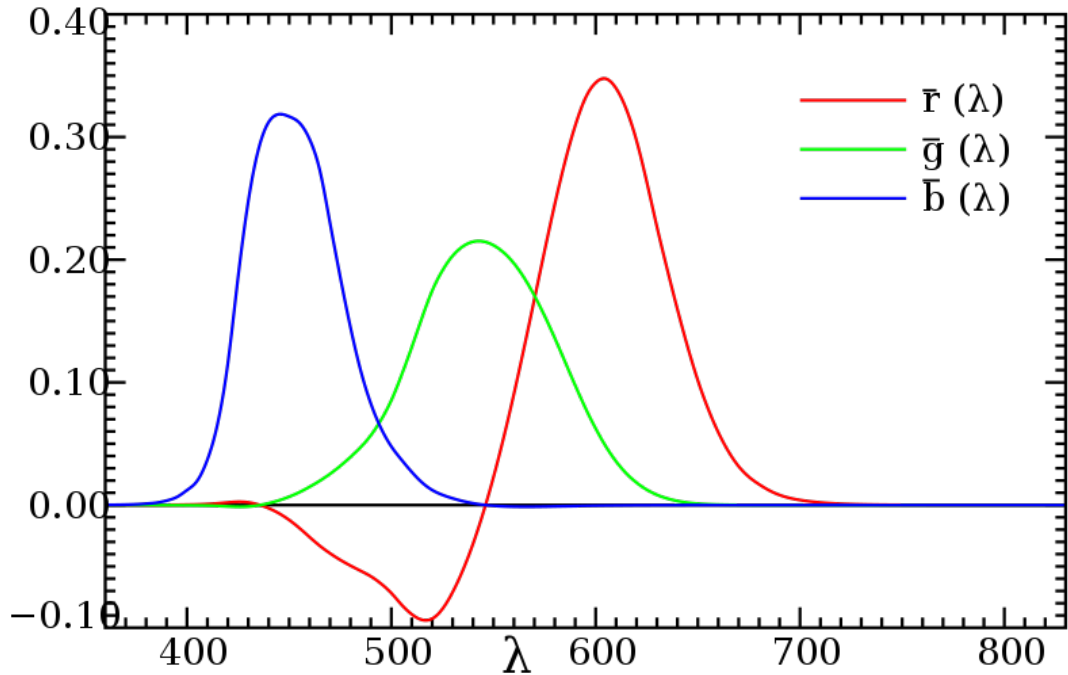
Figure 1.4: Colour matching function on the y-axis versus wavelength in nm on the x-axis

colloquially to the temperature of lighting, warm is often used for red lighting and cool for blue; the opposite to blackbody designation.

As there are a variety of light combinations that will appear white, the difference between them is often denoted by the colour temperature. This temperature is derived from the blackbody temperature. However, much white light emission will not be directly situated on the Planckian locus and they are designated by their colour correlated temperature (CCT). This is the nearest point to the Planckian based on the colour points of the emission. This is of course only relevant if the emission is close enough to a white emission. The CIE recommends that "The concept of correlated color temperature should not be used if the chromaticity of the test source differs more than $[\Delta_{uv} = 5 \times 10^{-2}]$ from the Planckian radiator" [11].

In (u, v) and (u', v') colour space, normals to the Planckian give lines of colour correlated temperature, equal to the point of intersection with the Planckian locus.

Colour Rendering Index

There is a further measure of the quality of white light, and this is the colour rendering index. Using daylight as the reference for a perfect white light emitter, this measures the quality of the white light in comparison. This comparison is made by measuring the distance between eight chromaticity points (R1 to R8) on the reference light source and test source. Each can be measured between 0 and 100, where 100 was defined as having no difference. The average of all of these gives the overall colour rendering, R_a, or CRI. Further individual reference points have been described by the CIE from R9 to R15 and these represent either a specified saturated colour, or a skin tone.

As each colour temperature will have a unique spectrum, comparing CRI is most
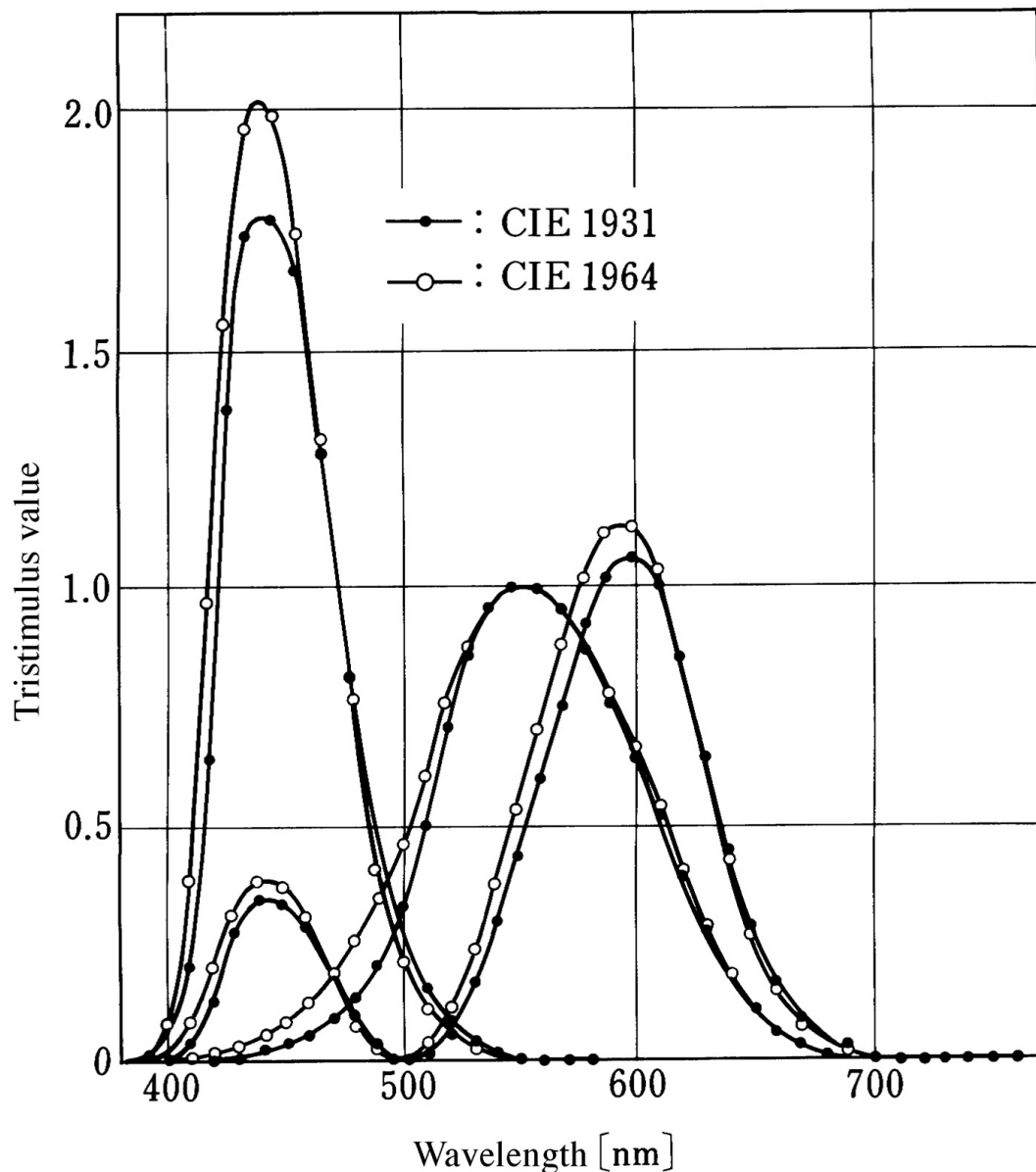
Figure 1.5: Curves of spectral tristimulus values. CIE 1964 supplementary standard colorimetric observer and CIE 1931 standard colorimetric observer. (From CIE, Testing of Supplementary Systems of Photometry, TC1-21, in preparation.)

appropriate at similar colour temperatures.

This is an imperfect measurement as it compares only averages over eight chosen chromaticity points and not the entire spectrum. In some applications, more weight needs to be considered to certain aspects of the spectrum, e.g. in medical applications a high level red (R8) and deep red (R9) light is required to see colour accurately within the human body.

Furthermore, a high CRI is not necessarily the result of a complete emission within the visible spectrum, and for these reasons alternative methods have been proposed to compare the entire spectrum of as reference source to a test source. The National Institute of Standards and Technology (NIST) have proposed a 'Colour Quality Scale' (CQS) to replace the CRI. In this scheme, fifteen evenly spaced measurements on
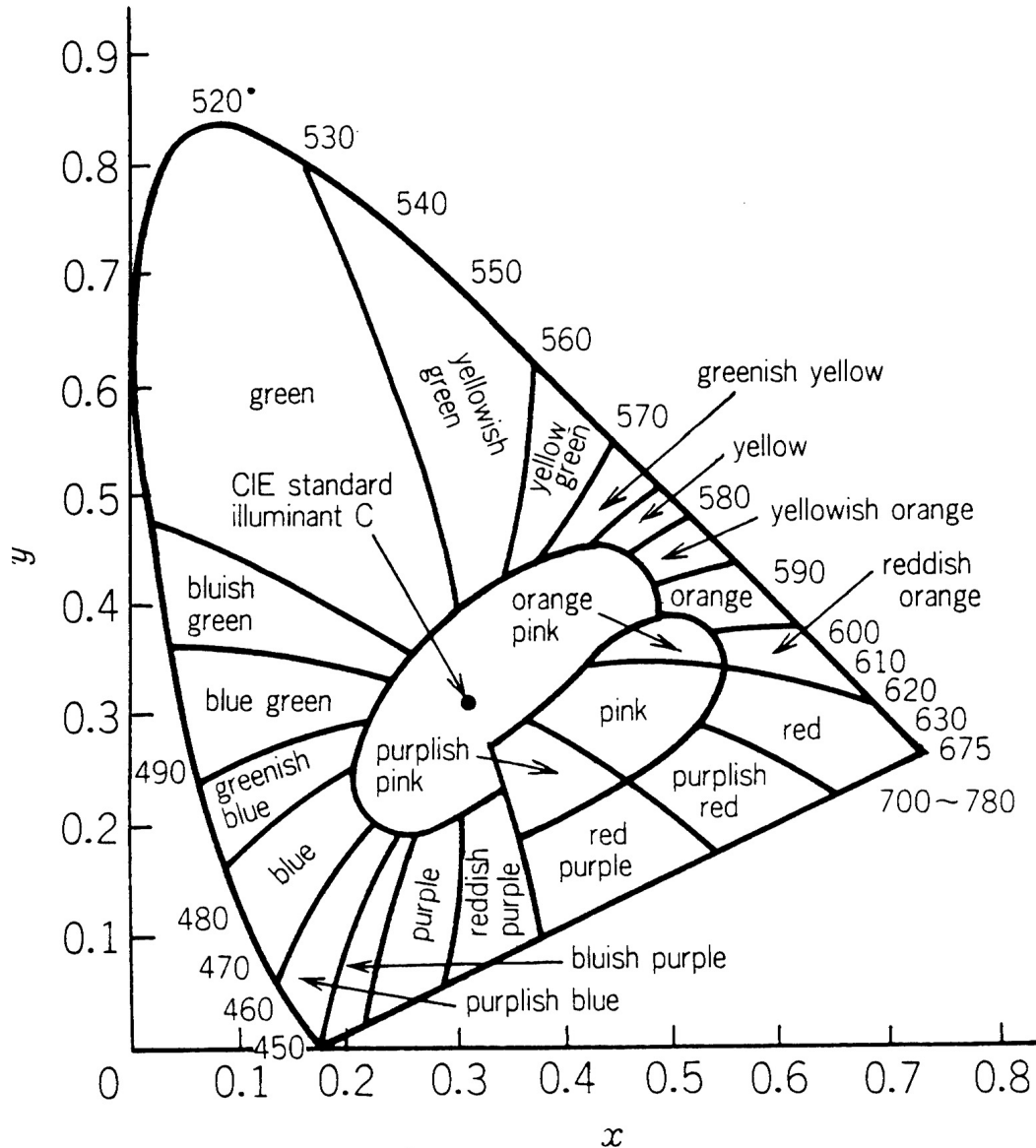
Figure 1.6: CIE Chromaticity diagram. (From Kelly, K.L., J. Opt. Soc. Am., 33, 627, 1943.)

the 1976 CIE (L*a*b) colour space would be defined against which measurements would be made. Currently CRI measurements are made against 8 points in the 1960 CIE(W*U*V). A detailed investigation at the benefits and application has been published [12].

1.3 Luminescence

Luminescence is the emission of electromagnetic radiation by a process other than thermal radiation. There are many different types of luminescence that can occur, defined by the manner in which the material is excited. Among others, these include:

- Photoluminescence - when the excitation occurs by photons. There are two types which are distinguished by the lifetime.

- – fluorescence - short lifetime, these are allowed transitions and usually will be measured to emit in ~0.1 μs or less.

- – phosphorescence - long lifetime, these emit via forbidden transitions and have longer lifetimes, from 0.1 μs or longer [13].

- electroluminescence - when the excitation is caused by an electric field.

- cathodoluminescence - when the excitation is caused by an energetic electrons.

Phosphorescence is a phenomenon not to be confused with afterglow, where afterglow is the emission from a trapped electron or hole [14]. The terminology of organic phosphors is also different, where phosphorescence refers to emission from a triplet state, and fluorescence from a singlet state.

In this work the focus will be on photoluminescence, although consideration of electroluminescence in certain cases will be required.
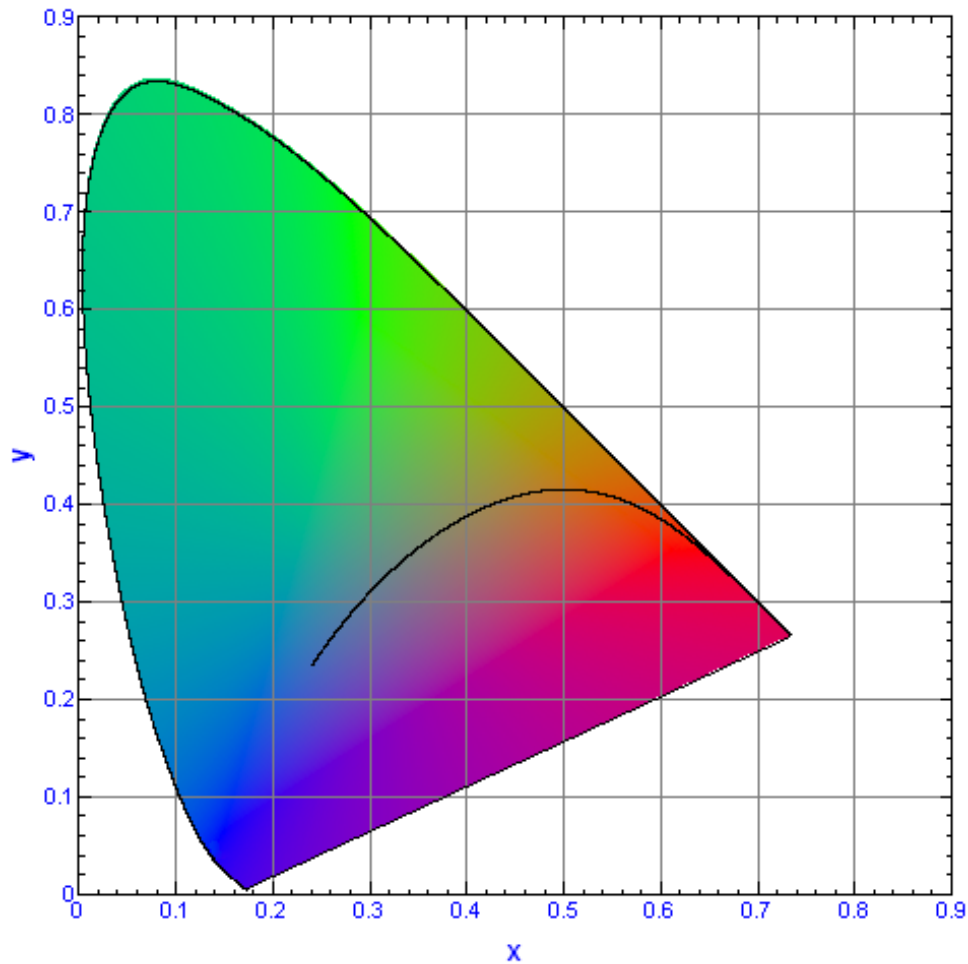
Figure 1.7: CIE Chromaticity diagram, including Planckian Locus

1.4 Phosphors

The beginnings of modern day phosphor research began after an accidental discovery in 1866 by the French chemist, Théodore Sidot [15]. Studying crystal growth in ZnS crystals, copper impurities led to phosphorescence, which became the starting point for research into phosphorescent materials.

Phosphors have since become widespread in their use, which has included radiation detectors [16] [17], televisions, flat panel displays, general, display and high brightness lighting. LED lighting has seen an increase in market share in recent years, following greater awareness of energy efficiency and is predicted to rise rapidly in the coming years [18].

The emission in luminescence of inorganic materials is through one of two processes, either an activator (localised luminescent centre) or semiconductor luminescence and these are shown schematically in figure 1.8 [13].
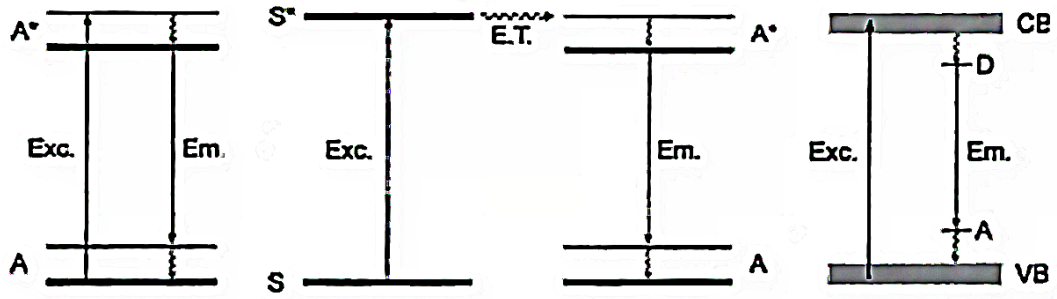
Figure 1.8: Schematic illustrations of luminescent processes on isolated centres (left, centre) and semiconductors (right) [13]

In the former case, the exciting energy, from any of the methods listed earlier, can be absorbed directly by the activator, or absorbed by a sensitiser (or coactivator) and transferred to the activator. Energy can also be absorbed by the host lattice and transferred to the activator.

This energy transfer leads to an electron within the activator being promoted to a higher excited state, before this energy is lost. The return to a lower energy state is mediated via two competing methods, light emission and phonon emission. Light emission is the return to a lower state with the emission of a photon. Phonon emission is the loss of energy without emission of a photon, usually through vibrational emission which will produce heat.

Stokes' law states that the emission will be at a lower energy than the excitation energy. There are materials which can emit photons at higher energy, and these are referred to as anti-stokes converters. The anti-stokes processes can make use of two (or more) lower energy photons to emit a higher energy photon, or the incoming photon can combine with thermal energy to emit at a higher energy [19].

The excited states are defined quantum mechanically and are at discrete intervals; the emission energy, and therefore frequency, for each material will be at fixed values which can be derived (see the following section (1.4.1) for more detail on this in the

case of the rare earth elements). Whilst normally in the visible region, the emission can be in the ultra violet or the infra red, depending on the composition of the material.

Usually, the emission will be due to the presence of an activator, although there are some host lattices which do not include any such 'impurities'. This occurs in ZnS, tungstates and molybdates where the emission can originate from the ions in the lattice such as Zn^{2+} [20] or W^{6+} [21]. In the case of the latter, the energy transfer is from the oxygen in $(WO_4)^{2-}$ to the d-level of the tungsten ion. The lack of dopant necessary to generate visible emission leads to a label for this type of emitter as 'self-activated'.

The decay time of the phosphors is a measure of the length time taken for the brightness of the phosphor to decrease to $1/e$ after the excitation source is removed. The reasons for the differences are discussed more specifically for the rare earth elements below and will be seen to be important for considering the application of the phosphor.

1.4.1 Rare Earth Element Phosphors

Rare earth ions are the preferred activators for light emitting phosphors. Those in the periodic table from cerium to ytterbium, when in the 2+ or 3+ (and sometimes 4+) oxidation states, can have energy levels which lead to luminescence in the visible region. When in their excited state, they can relax via light emission or phonon emission. These processes compete against each other and the greater the light emission, the higher the quantum efficiency of the phosphor. External factors such as temperature can affect this ratio where increasing temperature will increase non radiative losses. This is described in more detail in section 1.4.2.

The nature of the host lattice and activator(s) determine the excitation and emission spectra of these elements. These are dependent on the type of transition that occurs; for charge transfer (C-T) and allowed transitions (i.e. d-f) the bands are broad, but in the case of the trivalent rare earth elements the f-f transition is not allowed and leads to line emission. In the latter case there are no large vibrations in the optical centre which is well shielded by the 5s and 5p shells (there is no large difference in chemical bonding between the ground and excited states) and so the emission is a narrow band [22]. Eu^{3+} is an example of this and the emission spectrum is shown in figure 1.9.

The effect of host lattice on the activator must be considered in other cases. In both charge transfer transitions and allowed transitions (such as d-f) the host lattice can affect the bonding which leads to a broad band emission. In contrast to its 3+ oxidation state, Eu^{2+} shows this broad band behaviour and its emission spectrum, in a strontium sulphide lattice, is shown in figure 1.10.

The decay of the excited state has a lifetime, which is also based upon the transition. Allowed transitions have a higher probability of occurrence and will have a shorter lifetime. Forbidden transitions have longer lifetimes for the opposite reason.

It should be noted that transitions which are referred to as forbidden are able to occur when their selection rules are 'relaxed'. This is based on the sites at which the
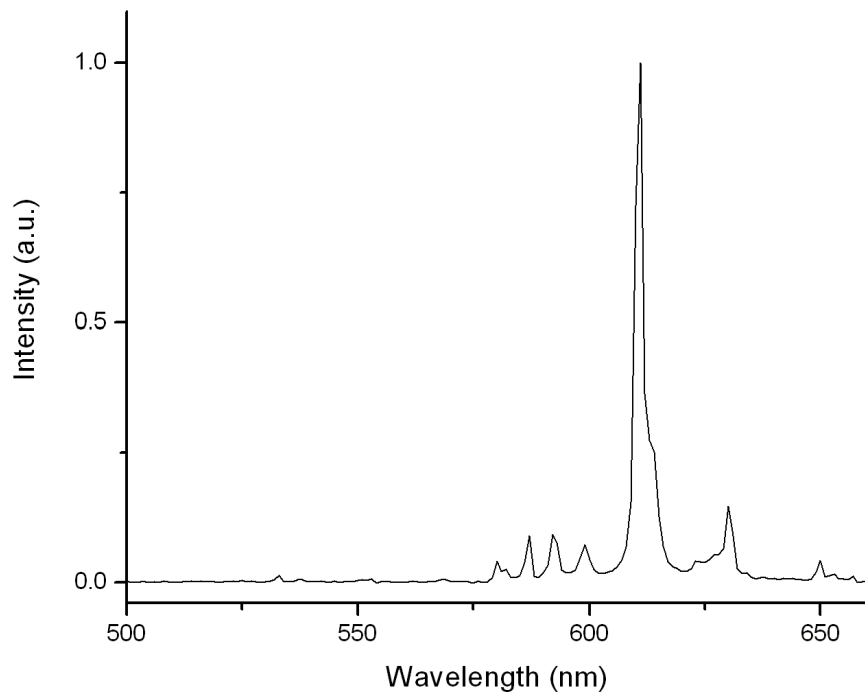
Figure 1.9: Emission spectrum of Y_2O_3:Eu^{3+}
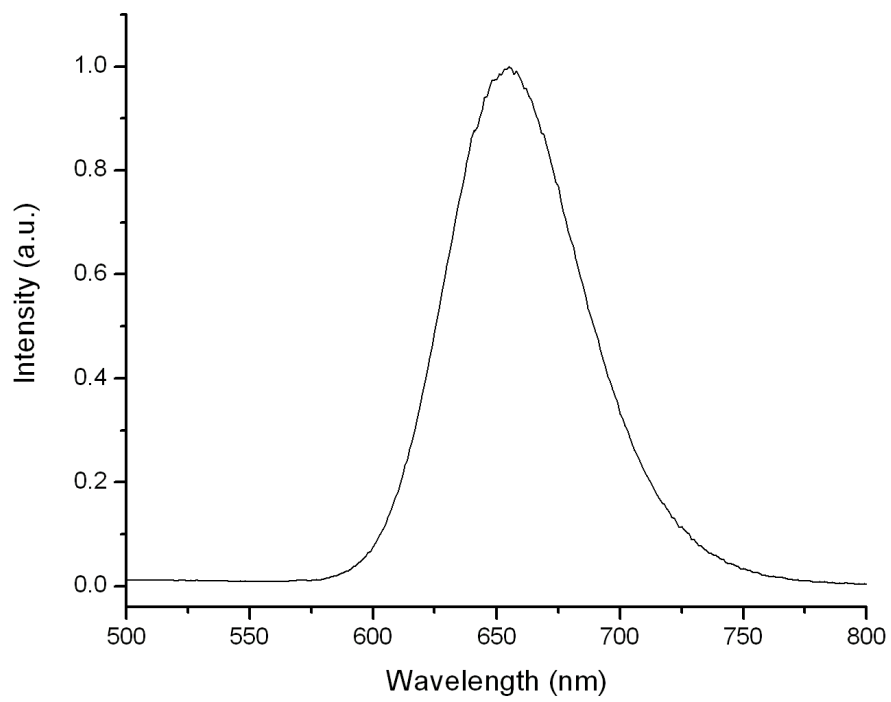
Figure 1.10: Emission spectrum of SrS:Eu^{2+}

activators are found, which do not have inversion symmetry. These are said to 'steal' some of the intensity from an allowed transition, such as the 5d-4f [22]. Relaxation can occur through vibrations [23] as well as through sites occupied by the rare earth ion which lack symmetry [24] [25].

The Dieke diagram, figure 1.11 [26], gives the configurations of the rare earth levels. Altering the stoichiometry of such materials can lead to changes in the energy of the emission [27]. Ce^{3+} ions find it energetically favourable to promote one electron to the 5d shell in an excited state and as such will behave similarly to the divalent materials. Such behaviour includes a broad band emission spectrum which is sensitive to changes in the host lattice. $(Y,Gd)AG:Ce^{3+}$ is an example of this where altering the gadolinium to yttrium ratio will shift the emission bands.

For narrow emitters, whilst the peak locations do not change, the relative heights may change based on the host lattice, due to the sites where the rare earth is located. As an example, under vacuum UV radiation $Y_2O_3:Eu^{3+}$ has its maximum peak emission at 611nm, $(Y, Gd)BO_3:Eu^{3+}$ has its maximum peak emission at 595nm. The former exhibits this emission from an electric dipole transition $(^5D_0 \rightarrow {}^7F_2)$ while the latter is due to a magnetic dipole transition $(^5D_0 \rightarrow {}^7F_1)$ as the Eu^{3+} ions are at a site which forbids the electric dipole transition [28].

The spectrum of Eu^{3+}, in $Y_2O_3:Eu^{3+}$ is shown in figure 1.9 and compared with that of $SrS:Eu^{2+}$ shown in figure 1.10, shows the difference between the divalent and trivalent ions. Furthermore, the emission of the divalent europium activated phosphors can be located across the whole visible spectrum, depending on the host lattice, examples of which are shown in table 1.1 [29].

Table 1.1: Peak emission wavelength of Eu^{2+} in variety of host lattices [29]

Phosphor	Peak emission wavelength (nm)
$SrB_4O_7:Eu^{2+}$	368
$Sr_2P_2O_7:Eu^{2+}$	420
$BaMgAl_{10}O_{17}:Eu^{2+}$	453
$Sr_4Al_{14}O_{25}:Eu^{2+}$	490
$Ba_2SiO_4:Eu^{2+}$	505
$SrGa_2S_4:Eu^{2+}$	535
$Sr_2SiO_4:Eu^{2+}$	575
$SrS:Eu^{2+}$	615

1.4.2 Quenching

Quenching is the reduction in radiative emission in the phosphor and can be caused by external factors such as an increase in temperature, or stoichiometric factors such as an increased amount of activator or sensitiser in the lattice (i.e. concentration quenching).

The amount of activator present has a saturation limit, usually in the region of 1-5% for rare earth phosphors. Further addition of the rare earth does not usually lead to an increase in emission but rather an increase in the non radiative losses, which

Figure 1.11: Energy levels for f shell transitions of trivalent lanthanides [26]

leads to 'concentration quenching'. This non-radiative decay is a result of one of many possible factors, the most common of which include lattice defects, which act as sites where the energy is lost non-radiatively and cross relaxation between the activators and impurities. Cross relaxation occurs when part of the energy of the excited state is transferred to a nearby similar ion.

In phosphors that contain a sensitiser and an activator, the sensitiser can undergo radiative or non radiative decay by itself, or by energy transfer to the activator. If there is spectral overlap, the sensitiser's radiative decay can be absorbed by the activator. This will depend on the transfer rate to the activator, the decay rate of the sensitiser, and the distance between the two ions. To prevent a separate emission from any coactivator introduced as a sensitiser, its concentration must be kept low to ensure it will be in close proximity to the preferred activator.

The distance between the ions is important even in cases where only one activator is present. Energy transfer between similar ions is possible and will quench the emission. Again, the distance between the ions is important and in this case the higher energy states of the excited ions can transfer part of their energy to excite a ground state ion. This results in the loss of emission at higher energies, and can occur for concentrations as low as 1%, in the case of Eu^{3+}, where blue emission is not seen above these concentrations [29]. Further detailed analysis can be found in many books [29] [30].

Temperature Effects

The temperature can affect the emission of phosphors and of interest here are the effects of high temperatures, of the order that will occur in lighting applications. The operating temperatures of LEDs can reach $200\,°C$ [31] and the effects that this had on the emission of the phosphors were studied in this work.

The quenching temperature is derived from the quantum efficiency and can be explained by a few factors; the following can be reduced to decrease the effect of thermal quenching [32]:

1. Increasing the bond strength. (As the bonds get weaker, the ground and excited state have a larger displacement. A larger displacement increases the probability of the excited state to decay directly to the ^7F state which is a non radiative transition [33]).

2. Lowering the vibrational frequency, which reduces the probability of tunnelling from the excited state to the ground state.

3. For a broad band emission, the shorter the distance between maximum wavelengths of emission and excitation, the more efficient the radiative process.

Another model which describes the temperature quenching effect is based on the possibility of thermal excitation of electrons to the conduction band, which will then undergo non radiative emission [33] [34].

1.5 Europium $3+$

This work focuses on the preparation and application of novel phosphors. At the outset of the work, the intention was to focus on red phosphors as these have the

greatest scope for improvement, as discussed in section 1.1. Europium is a key rare earth for this part of the spectrum due to the emission band of the 3+ oxidation state at 615nm with a relatively high photopic response (44% of the maximum, higher than 465nm blue emission, and of course higher than longer wavelength red emitters). As discussed in section 1.4.1, the peak positions of this emission will not shift based on the host lattice, but the relative strengths of the transitions will shift based on site symmetry.

A commercial Eu^{3+} phosphor was measured in order to be used as a comparison with any phosphors synthesised at a later date. In the host lattice Y_2O_3 the peak wavelength was 611nm, and its colour points were measured as (0.64, 0.35). The colour points are of interest for display lighting as discussed in section 1.1.

1.6 Synthesis

In the synthesis of phosphors, whether by solid state method, precipitation or otherwise, there will need to be a step where the activator is diffused into the host lattice, and this is done by firing, usually at temperatures greater than $600\,°C$. This may be for a period as short as 30 minutes, although can be for 24 hours or longer. For ions which favour a lower oxidation state, a reducing atmosphere may be required (e.g. in the formation of Eu^{2+}). This is achieved using a tube furnace and a H_2/N_2 mixture to control the gas surrounding the firing.

Effects of the firing need to be taken into account, notably agglomeration of particles, especially in the case where particle size needs to be controlled for any application. Grinding following the firing can have adverse effects on the luminous output as it will introduce defects into the particles. The use of novel synthetic methods to create uniform small particles has been investigated for some time [35] [36].

In the preparation of phosphors, a flux may be included solely in order to improve the properties of the particle size in its growth period. There are many materials which can fulfil this role, including halides such as LiCl [37].

1.7 Applications

Many factors need to be considered when assessing the suitability of a phosphor in commercial applications. These include efficacy, emission (colour and spectrum), excitation wavelengths, decay time, quenching effects, stability, particle morphology, availability (current and projected) of materials and cost [13] [38].

Being able to create homogeneous phosphor particles of controlled thickness has been a field of research for some time [39] and its importance is well known. This is advantageous in both the application of phosphors (e.g. for reduced scattering effects) as well as in the manufacturing process, where small particles are necessary for high quality screen printing.

1.7.1 Degradation

Degradation of phosphor performance has been linked to atmospheric moisture and is especially important in the case of electroluminescent devices [40] and mentioned specifically for these devices in section 6.2. This degradation affects sulphide phosphors in particular and many coatings have been investigated to minimise it. Coatings to prevent degradation include SiO_2, Al_2O_3, TiO_2, silicon resin and many other materials [41] [42] [43]. For most applications, coatings are necessary else the lifetime of the device will be prohibitively short.

1.7.2 Existing Technologies

Phosphors are already prevalent in a myriad of existing technologies from early scintillation devices to lighting, such as ACEL panels and fluorescent tubes, as well as the most modern lighting such as LEDs. Many of the later applications attempted to use the existing phosphors, although of course as the excitation and emission requirements changed, so did the phosphors that were used. The most common phosphors are listed in table 1.2 [13], with LED phosphors of note specified in the next section.

Table 1.2: Table of common phosphors [13]

Emission colour	Cathode Ray Tube	Plasma Panel Display	Fluorescent Lamp	X-ray-Intensifying / Scintillation
blue	$ZnS:Ag^+,Cl^-$	$BaMgAl_{10}O_{17}:Eu^{2+}$	$BaMgAl_{10}O_{17}:Eu^{2+}$ $Sr_4Al_{14}O_{25}:Eu^{2+}$ $Sr_3(PO_4)_5Cl:Eu^{2+}$	$NaI:Ti^+$ $Ba(F,Br):Eu^{2+}$ $LaBr_3:Ce^{3+}$ $Bi_4Ge_3O_{12}$ $Gd_2SiO_5:Ce^{3+}$ / $Lu_2SiO_5:Ce^{3+}$ $LuAlO_3:Ce^{3+}$ $YTaO_4:Nb^{5+}$
green	$ZnS:Cu^+,Au^+,Al^{3+}$ $ZnS:Cu^+,Al^{3+}$	$BaAl_{12}O_{19}:Mn^{2+}$ $Zn_2SiO_4:Mn^{2+}$ $BaMgAl_{10}O_{17}:Eu^{2+},Mn^{2+}$	$GdMgB_5O_{10}:Ce^{3+},Tb^{3+}$ $LaPO_4:Ce^{3+},Tb^{3+}$ $CeMgAl_{11}O_{19}:Tb^{3+}$	$CsI:Ti^+$ $Gd_2O_2S:Tb^{3+}$
yellow			$Y_3Al_5O_{12}:Ce^{3+}$	
red	$Y_2O_2S:Eu^{3+}$	$Y_2O_3:Eu^{3+}$	$Y_2O_3:Eu^{3+}$ $(Y,Gd)(P,V)O_4:Eu^{3+}$	
white			$Ca_5(PO_4)_3(F,Cl):Sb^{3+},Mn^{2+}$	

1.8 LEDs

Following the rise in use of LEDs since the mid 1990s, and now included for a wide variety of products and applications, phosphors are required which can be excited by UV and blue wavelength light. While some existing phosphors are suitable for this application, novel phosphors may be required in these products to improve their efficiency in a manner described in section 1.1. The most common of the phosphors used are $Y_3Al_5O_{12}:Ce^{3+}$ (yellow), $CaS:Eu^{2+}$ (red) and $SrS:Eu^{2+}$ (orange). LEDs are now commonly used in applications such as general lighting, display lighting and high end lighting, as well as televisions, all of which have their own priorities in the phosphors' performance. Some require a wide colour gamut, others require a high CRI and some need a reasonable combination of both. Lifetime of the phosphors must also

be considered in applications such as television where phosphorescence can reduce the sharpness of the image. This is noticeable when the picture is fast moving (the colours need to move rapidly across the screen) and a long lifetime phosphor is employed, a 'trail' of this phosphor is seen across the screen.

LEDs are semiconductor materials which, when excited by electric fields, emit light. The first patent on these were for infra-red emitting devices by Baird and Pittman and Texas Instruments in 1961 [44]. One year later Holonyak at General Electric built a red emitting LED. Craford, a student of Holonyak built the first yellow emitting device in 1972. No high brightness blue materials were discovered until 1994, created by Nakamura et al working at Nichia [45]. His double heterostructure device is shown in figure 1.12.
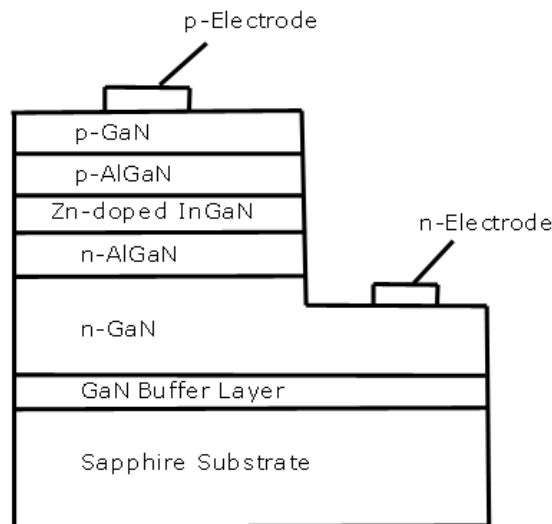
Figure 1.12: The structure of the InGaN/AlGaN double-heterostructure blue LED [45]

The n-type material is labelled such when it provides electrons. The p-type material is one that accepts electrons. When these are used together a p-n junction is formed.

In this blue emitting diode, an electric field is applied to overcome the energy gap between the materials; an electron is promoted creating an electron hole pair. When these recombine a photon is emitted. This occurs at energies based on the band gap energy of the material and this energy defines the frequency of the emission. The emission spectra of LED materials is a narrow emission band.

Using this knowledge, a material of known band gap energy can be selected which will emit at a desired wavelength. It is further possible to alter the band gap with the introduction of elements into the material structure, e.g. indium into gallium

nitride increases the wavelength of the emitted photons. This comes at the expense of efficiency due to more defects present in the structure of the material. These are caused by the size difference between the atoms [46]. This leads to little emission once into the green wavelength region of the spectrum, the consequences of which are discussed in section 3.1. Also discussed in more details is the possibility of white light generation with the option to use down conversion phosphors.

Using LEDs in lighting applications has many advantages, primarily the low power consumption. These devices are set to enter the market with performance recently reported at over 92 lm/W [47]. Prototypes have been developed to deliver over 150 lm/W [48] which will provide huge savings in the running costs of these devices. However, the overall cost of the product is larger due to the cost of manufacturing the device and materials used, even when factoring in the vast increase in lifetime of the LEDs. Their small size and durability is also a useful advantage over other light fittings.

LEDs do have other disadvantages including their high running temperature at high currents. Even though the input energy is converted directly to light emission, losses associated with this are in the form of thermal energy and heat sinks are required for high brightness LEDs. Furthermore high temperatures can reduce performance of phosphors used as colour converters with the device which are sensitive to thermal quenching.

1.9 OLEDs

As the name suggests, organic light emitting diodes are light emitting device based on organic substances. These have a similar structure to semiconductor LED devices, and a typical OLED structure is shown in figure 1.13 [49].
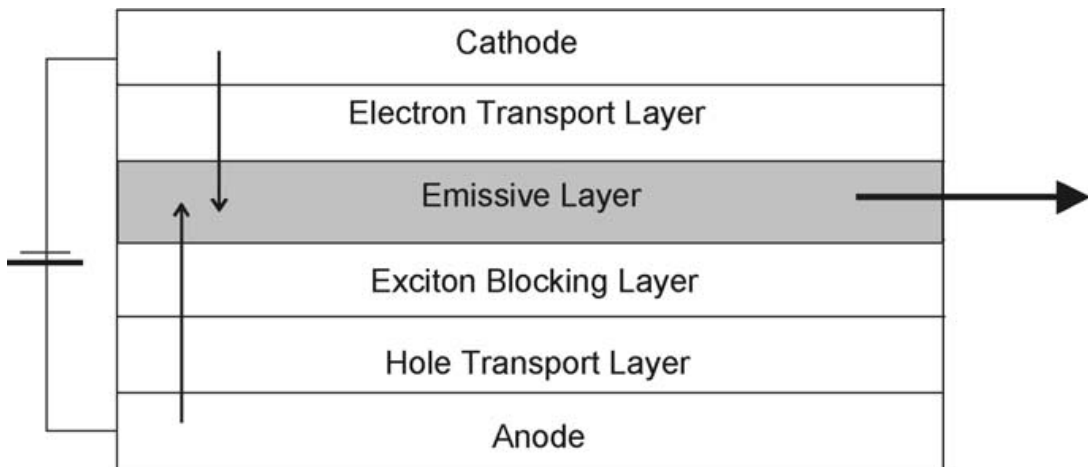
Figure 1.13: A typical OLED structure [49]

Whilst this work is not intended to give a full account of OLED technology, there are detailed summaries available in the literature [50], its increased use in display and lighting and the similarities shared with LEDs in the use of colour converting

phosphors for generation of light make it worthwhile investigating. OLED lighting is forecast to increase hugely over the next 5-10 years in both usage and revenue, from to over $1 billion dollars in 2015 [51].

There are two main processes to manufacture OLEDs; the first is to use small molecule materials, and the second is to minimize the number of layers and use one material for all the functions [52]. This second method typically utilises polymers and are often referred to as PLEDs and review articles are available which discuss them in detail [53].

References

[1] Dirk Poelman and Philippe Smet. Europium-doped phosphors for lighting : the past, the present and the future. In *International workshop on advanced nanovision science, Abstracts*, pages 18–21. Ghent University, Department of Solid state sciences, 2011.

[2] R. Withnall, J. Silver, G. Fern, T. Ireland, A. Lipman, and B. Patel. Experimental and theoretical luminous efficacies of phosphors used in combination with blue-emitting LEDs for lighting and backlighting. *Journal of the SID*, 16(2):359 – 366, 2008.

[3] NASA. Electromagnetic spectrum http://ls7pm3.gsfc.nasa.gov/images/rmpics/emspec.gif.

[4] David Halliday Robert Resnick and Kenneth S. Krane. *Physics*, volume 2, pages 600 – 800. Wiley, 2001.

[5] Christine A. Curcio, Kenneth R. Sloan, Robert E. Kalina, and Anita E. Hendrickson. Human photoreceptor topography. *The Journal of Comparative Neurology*, 292(4):497–523, 1990.

[6] David M. Berson, Felice A. Dunn, and Motoharu Takao. Phototransduction by retinal ganglion cells that set the circadian clock. *Science*, 295:1070 – 1073, 2002.

[7] J. A. S. Kinney, M. Ikeda, D. Palmer, K. Sagamwa, and P. Trezona. *Mesopic Photometry: History, Special Problems and Practical Solutions*. CIE Publication no. 81, 1989. Commission Internationale de l' Eclairage, Vienna, Austria.

[8] Frank P. Whitman. On the photometry of differently colored lights and the "flicker" photometer. *Phys. Rev. (Series I)*, 3(4):241–249, Jan 1896.

[9] J. J. Vos. Colorimetric and photometric properties of a 2-deg fundamental observer. *Color Research and Application*, 3:125 – 128, 1978.

[10] S. J. Williamson and H. Z. Cummins. *Light and Color in Nature and Art*, page 173. Wiley, 1983.

[11] János Schanda. *CIE Colorimetry*, pages 25–78. John Wiley & Sons, Inc., 2007.

[12] Wendy Davis and Yoshi Ohno. Color quality scale. *Optical Engineering*, 49(3):033602, 2010.

[13] Claus Feldmann, Thomas Jüstel, Cees R. Ronda, and Peter J. Schmidt. Inorganic luminescent materials: 100 years of research and application. *Advanced Functional Materials*, 13(7):511 – 516, 2003.

[14] GFJ Garlick. *Handbook der Physik*, chapter 26, page 1. Springer, 1958.

[15] Shinkichi Tanimizu. *Phosphor Handbook*, pages 247 – 248. Taylor & Francis Group, LLC, 2007.

[16] Amar Sinha, B.D. Bhawe, C.G. Panchal, A. Shyam, M. Srinivasan, and V.M. Joshi. High sensitivity neutron imaging system for neutron radiography with a small neutron source. *Nuclear Instruments and Methods in Physics Research B*, 108:408 – 412, 1996.

[17] Mitsuru Ishii and Masaaki Kobayashi. Single crystals for radiation detectors. *Progress in Crystal Growth and Characterization of Materials*, 23:245 – 311, 1992.

[18] ElectroniCast. http://www.ledsmagazine.com/products/32128, Jan 2011.

[19] François Auzel. Upconversion and anti-stokes processes with f and d ions in solids. *Chemical Reviews*, 104(1):139–174, 2004.

[20] Takao Koda and Shigeo Shionoya. Nature of the self-activated blue luminescence center in cubic ZnS:Cl single crystals. *Phys. Rev.*, 136(2A):A541–A555, Oct 1964.

[21] S Rothschild. Some unusual phosphors. *British Journal of Applied Physics*, 6(S4):S32, 1955.

[22] G Blasse and B.C. Grabmaier. *Luminescent Materials*, pages 11 – 32. Springer-Verlag, 1994.

[23] K. K. Pukhov, T. T. Basiev, F. Auzel, F. Pelle, and J. Heber. Multiphonon sideband intensities in rare earth ions in crystal. *Laser Physics*, 11(7):844–852, 2001.

[24] S.H. Shin, J.H. Kang, D.Y. Jeon, and D. Sik Zang. Enhancement of cathodoluminescence intensities of Y_2O_3:Eu and Gd_2O_3:Eu phosphors by incorporation of Li ions. *Journal of Luminescence*, 114(3-4):275–280, 2005.

[25] M. Yangand Y. Sui, S. Wang, X. Wang, Y. Sheng, Z. Zhang, T. Lü, and W. Liu. Enhancement of upconversion emission in $Y_3Al_5O_{12}$:Er^{3+} induced by Li^+ doping at interstitial sites. *Chemical Physics Letters*, 492(1-3):40–43, 2010.

[26] G. H. Dieke. *Spectra and Energy Levels of Rare Earth Ions in Crystals*, page 84. Interscience, 1968.

[27] Y. C. You, J. S. Choi, Y. R. Do, T. W. Kim, and H. L. Park. Tunable color emission in a $Ba_{1-x}Sr_xY_2S_4$:Eu^{2+} phosphor. *Solid State Communications*, 99(12):961 – 963, 1996.

[28] C. R. Ronda, T. Jüstel, and H. Nikol. Rare earth phosphors: fundamentals and applications. *Journal of Alloys and Compounds*, 275-277:669 – 676, 1998.

[29] Cees R. Ronda. *Emission and excitation mechanisms of phosphors*, pages 1 – 20. Weinheim: Wiley-VCH, 2008.

[30] G Blasse and B.C. Grabmaier. *Luminescent Materials*, pages 91 – 107. Springer-Verlag, 1994.

[31] Enfis. *E-mail to R Stone*, July 2008.

[32] G Blasse and B.C. Grabmaier. *Luminescent Materials*, pages 80–84. Springer-Verlag, 1994.

[33] P Dorenbos. Thermal quenching of Eu^{2+} 5d-4f luminescence in inorganic compounds. *Journal of Physics: Condensed Matter*, 17(50):8103, 2005.

[34] U. Happek, S. A. Basun, J. Choi, J. K. Krebs, and M. Raukas. Electron transfer processes in rare earth doped insulators. *Journal of Alloys and Compounds*, 303-304:198 – 206, 2000.

[35] J. Silver, M. I. Martinez-Rubio, T. G. Ireland, G. R. Fern, and R. Withnall. The effect of particle morphology and crystallite size on the upconversion luminescence properties of erbium and ytterbium co-doped yttrium oxide phosphors. *The Journal of Physical Chemistry B*, 105(5):948–953, 2001.

[36] M. I. Martinez-Rubio, T. G. Ireland, G. R. Fern, J. Silver, and M. J. Snowden. A new application for microgels? Novel method for the synthesis of spherical particles of the Y_2O_3:Eu phosphor using a copolymer microgel of NIPAM and acrylic acid. *Langmuir*, 17(22):7145–7149, 2001.

[37] Yun Chan Kang, Hyun Sook Roh, Seung Bin Park, and Hee Dong Park. Use of LiCl flux in the preparation of Y_2O_3:Eu phosphor particles by spray pyrolysis. *Journal of the European Ceramic Society*, 22(9-10):1661 – 1665, 2002.

[38] Shinkichi Tanimizu. *Phosphor Handbook*, page 370. Taylor & Francis Group, LLC, 2007.

[39] A. Vecht, C. Gibbons, D. Davies, X.P. Jing, P. Marsh, T. Ireland, J. Silver, A. Newport, and D. Barber. Engineering phosphors for field emission displays. *Journal of Vaccum Science and Technology B*, 17:750–757, 1999.

[40] Kenton D Budd. *Encapsulated electroluminescent phosphor and method for making same*. United States Patent 5593782, January 1997.

[41] Thomas Juestel, Cornelis Reinder Ronda, Walter Mayr, Peter Schmidt, and Volker Ulrich Weiler. *Light-emitting device with coated phosphor*. US patent 7202598, April 2007.

[42] Chongfeng Guo, Benli Chu, and Qiang Su. Improving the stability of alkaline earth sulfide-based phosphors. *Applied Surface Science*, 225(1-4):198 – 203, 2004.

[43] Xiong Zhaoxian, Chen Yayong, Chen Zhihui, and Song Chunxiao. Modification of luminescent properties of red sulphide phosphors for white LED lighting. *Journal of Rare Earths*, 24(1, Supplement 1):133 – 136, 2006.

[44] Cees R. Ronda. *Emission and excitation mechanisms of phosphors*, pages 179 – 190. Weinheim: Wiley-VCH, 2008.

[45] S. Nakamura, T. Mukai, and M. Senoh. Candela-class high-brightness InGaN/AlGaN double-heterostructure blue-light-emitting diodes. *Appl. Phys. Lett.*, 64:1687 – 1689, 1994.

[46] Z. L. Li, P. T. Lai, and H. W. Choi. Failure analysis of InGaN/GaN LEDs with emission wavelength between 440 nm and 550 nm. *Phys. Status Solidi C*, 7(7 - 8):2202 – 2204, 2010.

[47] U.S Department of Energy. L prize competition winner, http://www.lightingprize.org/overview_60watttest.stm, August 2011.

[48] Cree. Cree prototype lamp of more than 1300 Lumens at 152 Lumens per Watt, http://www.cree.com/press/press_detail.asp?i=1312203835951, August 2011.

[49] Rachel C. Evans, Peter Douglas, and Christopher J. Winscom. Coordination complexes exhibiting room-temperature phosphorescence: Evaluation of their suitability as triplet emitters in organic light emitting diodes. *Coordination Chemistry Reviews*, 250:2093 – 2126, 2006.

[50] P. Coppo. *SPR Photochemistry*, volume 37, pages 393 – 406. A. Albini ed., 2009.

[51] Jennifer Colegrove. Oled lighting in 2009 and beyond: The future. Technical report, DisplaySearch, 2009.

[52] Cees R. Ronda. *Emission and excitation mechanisms of phosphors*, pages 191 – 217. Weinheim: Wiley-VCH, 2008.

[53] R. H. Friend, R. W. Gymer, A. B. Holmes, J. H. Burroughes, R. N. Marks, C. Taliani, D. D. C. Bradley, D. A. Dos Santos, J. L. Brédas, M. Lögdlund, and W. R. Salaneck. Electroluminescence in conjugated polymers. *Nature*, 397:121 – 128, 1999.

Chapter 2

Characterisation of Phosphors

To investigate the phosphors, measurements are carried out to characterise them over a wide range of properties. The most important of these include the luminous efficacy, the excitation and emission spectra of the phosphors and the performance at high temperature (i.e. thermal quenching.) There are further properties that are of importance which were examined and these include the particle size and structure.

The methods used to characterise phosphor samples included integrating spheres, a scanning electron microscope (SEM) and an X-Ray diffractometer. Further equipment used in the preparation of application of phosphors such as screen printing, are described here.

Additionally, phosphor powders were on occasion illuminated under a UV lamp of 254nm or 366nm and viewed/compared by eye.

2.1   Integrating Sphere

Integrating spheres are hollow spheres coated internally with a highly reflective coating to diffuse the light evenly within the sphere. Integrating spheres were used to measure the light emission properties of the phosphor. These are the excitation and emission spectra, luminous efficacy and quantum efficiency values, CIE (x, y) coordinates, CRI, CCT(K) and thermal quenching. Those that were used in this work included a Bentham Integrating Sphere and a Pro-Lite Integrating Sphere.

Integrating spheres work by using their coating and spherical shape to allow a uniform scattering to create an even distribution of the power from the light source inside the sphere. A small hole in the sphere is used to allow measurement of the emission.

The Bentham spheres measured the light emission from the phosphor powder using an external light source to provide the excitation wavelength. This provided qualitative or quantitative measurements of excitation and emission spectra as well as luminous efficacy results. Temperature measurements from room temperature to 225 °C were possible with this equipment.

The measurement of light emitting applications, such as LEDs, rather than those that use excitation from an external source, utilised the Pro-Lite integrating sphere.

2.1.1 Bentham Integrating Sphere

A xenon lamp source was used to provide a range of wavelengths to excite the phosphor. To measure the powders a Bentham spectrometer was used which consists of an M300 programmable grating monochromater photometer system, with computer controlled wavelength scanning and intensity data collection using in the visible region an 1800 lines/mm grating. A built-in stepping motor and sine drive allowed the wavelength scanning to be completely controlled from a remote stepping drive unit (SMD3B), which itself was controlled by a computer via a BUS interface. This qualitatively measured the emission and excitation spectra directly from the powder. Comparisons between phosphors is only possible when normalised and quantitative results are not attainable.

A second Bentham sphere, seen in figure 2.1 was utilised and also consisted of a xenon lamp source along with a similar monochromater photometer system and wavelength scanning system. The difference in this was that it was possible to ascertain quantitative results. This also contained a heater unit, fan and an infra red sensor to measure the temperature of the phosphor. This was employed for measuring phosphor performance at high temperatures and was used to reach temperatures of up to 225 °C.

To take the measurements, after the monochromater calibration, the power of the lamp is measured. Following this, a reflective powder, Ba_2SO_4, was used to measure the output at the desired excitation wavelength, which was then followed by measurement of the phosphor powder at the same excitation wavelength. The surface area and height of these powders must remain consistent for all measurements in order that they may be accurately compared. From the data provided in these results, the luminous efficacy and quantum efficacy can be extracted and calculated. The excitation and emission spectra are measured directly by the emission monochromater.

Both integrating spheres were capable of measuring the CIE (x,y) coordinates of the phosphor powder.

2.1.2 Pro Lite Integrating Sphere

The Pro-Lite Integrating Sphere used was the Labsphere LMS-200, a 50cm diameter bench top integrating sphere. These are designed for the measurement of the total flux of lamps by comparing with a standard lamp of known output.

This was connected to an external power supply unit (PSU) to provide the power to the lamps fitted in the sphere. Calibrated using the auxiliary lamp within the sphere for each light fitting that was used, the software provided runs the measurement on the light emission within the sphere.

This measured the total emission from light sources, primarily LEDs and organic LEDs (OLEDs) with or without a phosphor applied to the package. The measurements obtained from this sphere include the resulting emission spectrum and lumen output of the system. Luminous efficacy measurements require knowledge of the input power provided by an external PSU to calculate. Further measurement taken include CRI

Figure 2.1: Bentham Integrating Sphere

Figure 2.2: Pro-Lite Integrating Sphere

(including a break down of individual R numbers from R1-R14), colour correlated temperature (CCT) and CIE (x,y) coordinates.

If the direct emission from a source is more useful than the total light output, as may be the case for characteristics for display lighting, alternative equipment, such as a spectroradiometer, can provide additional insight.

2.2 JETI

The JETI is a spectroradiometer that takes direct measurements of luminescence from diffuse light sources such as screens, room illuminance and lamps. It measures radiance, irradiance, dominant wavelength, CCT(K), CRI and CIE (x,y) coordinates. This measures the emission over a fixed area and is useful for calculating $\mathrm{cd\,m^{-2}}$ (luminance). The spectral range is from 380nm to 780nm and the luminance range from $0.1\,\mathrm{cd\,m^{-2}}$ to $70{,}000\,\mathrm{cd\,m^{-2}}$.

2.3 X-Ray Diffraction

X-ray diffraction (XRD) is used to investigate the crystal structure of materials using the pioneering work in X-Rays of Röntgen, von Laue, Moseley, Bragg and many others. X-rays were discovered by Röntgen in 1895 but it was not until 1912 that von Laue pioneered the use of X-rays to determine the structure of matter based on the patterns measured on a detection film of a crystal in the path of X-rays. This method used here to investigate the phosphors involved Bragg diffraction to analyse their structure. Constructive interference from the planes of the crystal are only present for certain angles. Based on the diffraction pattern the lattice spacing can be determined [1] [2].

The parameters that are obtained and used in this work are the lattice constants, namely size of the lengths of unit cell (a, b and c) in angstrom and angles (alpha beta and gamma) between them. From these parameters, the lattice is determined. The diffraction pattern can also be used to compare and contrast phosphor powders [1]. An example of a unit cell with the parameters labelled is shown in figure 2.3. Depending on these parameters, the unit cell will be one of the 14 Bravais lattices, from triclinc, the least symmetric, to cubic, the most.
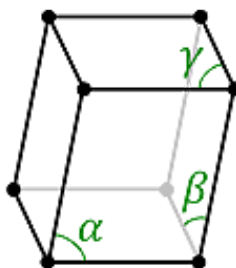
Figure 2.3: Unit cell, showing angles α, β and γ

X-ray diffraction data for this work was collected using a Bruker powder diffractometer (Advance D8) with copper tube and LynxEye detector. The LynxEye detector is a position sensitive, silicon based, semiconductor detector. Powder samples are loaded into plastic holders which were rotated during the measurements which last up to 7 hours. The rotation reduces any preferential orientation that would exist in the powder sample. The greater length of time reduces the background noise, especially prevalent in lower angle detection. This XRD equipment is equipped with an automatic sample changer and accommodates up to 8 holders.
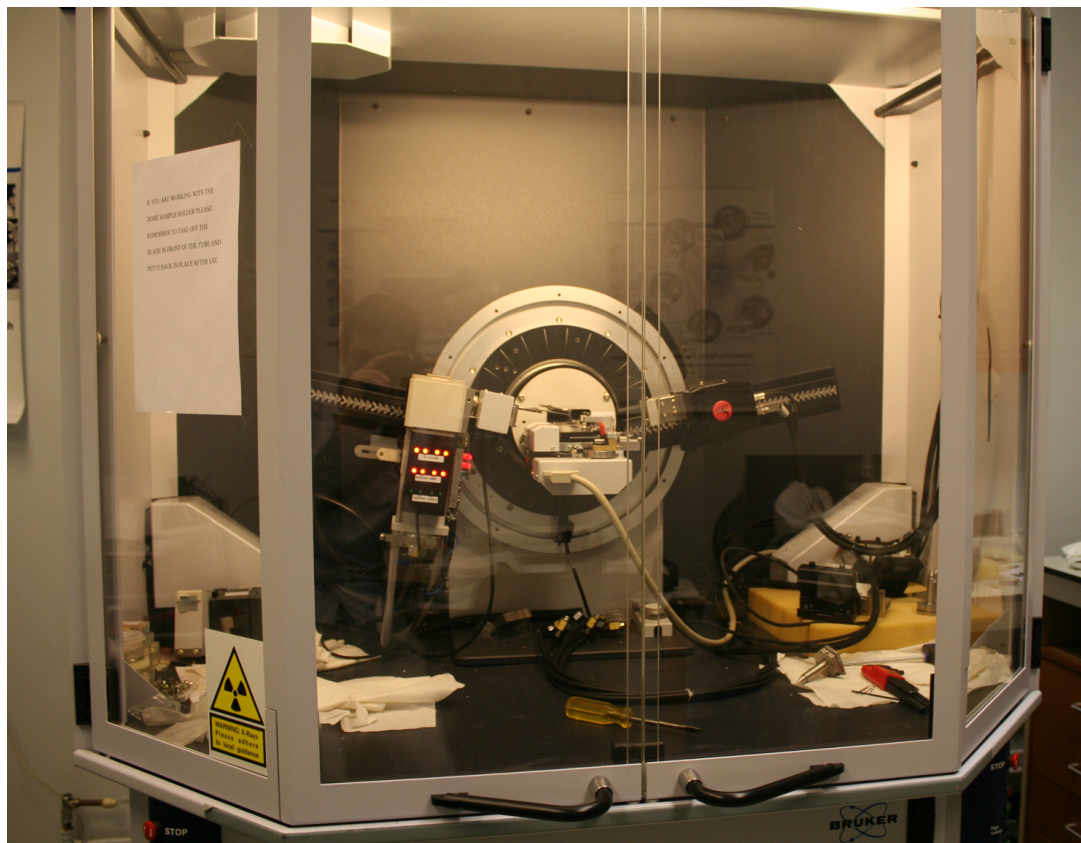
Figure 2.4: Bruker X-Ray diffractometer

2.4 Field Emission Scanning Electron Microscope

In a field emission gun scanning electron microscope (FESEM or SEM) a high energy beam of electrons is fired at a sample where it will interact with atoms on the surface. Carbon conducting tape was fixed atop an aluminium stub, which was then coated with the sample material. The excess of this was removed using pressurised air. This was then coated in a thin layer of gold, a procedure especially important for materials that were poorly conductive, deposited by low vacuum sputter coater. This prevents the samples from charging under the electron beam which would lead to their appearance as bright diffuse objects detracting from a clear image. Fine particles also benefit from a coating to reduce the effects of beam penetration [3].

The SEM was used to view particle size and morphology with various points, including over varied magnification, taken to ensure uniformity and consistency. These images were exported directly and are those shown in this work.

The SEM was a Zeiss Supra 35VP field emission scanning electron microscope, with a high-vacuum and variable operating pressure capabilities.

2.5 Speedmixer

The speedmixer was a DAC 150 FVZ-K which is a small mixer that can be used to grind or mix materials in solid state as well as liquid. Running from 500-3500rpm and
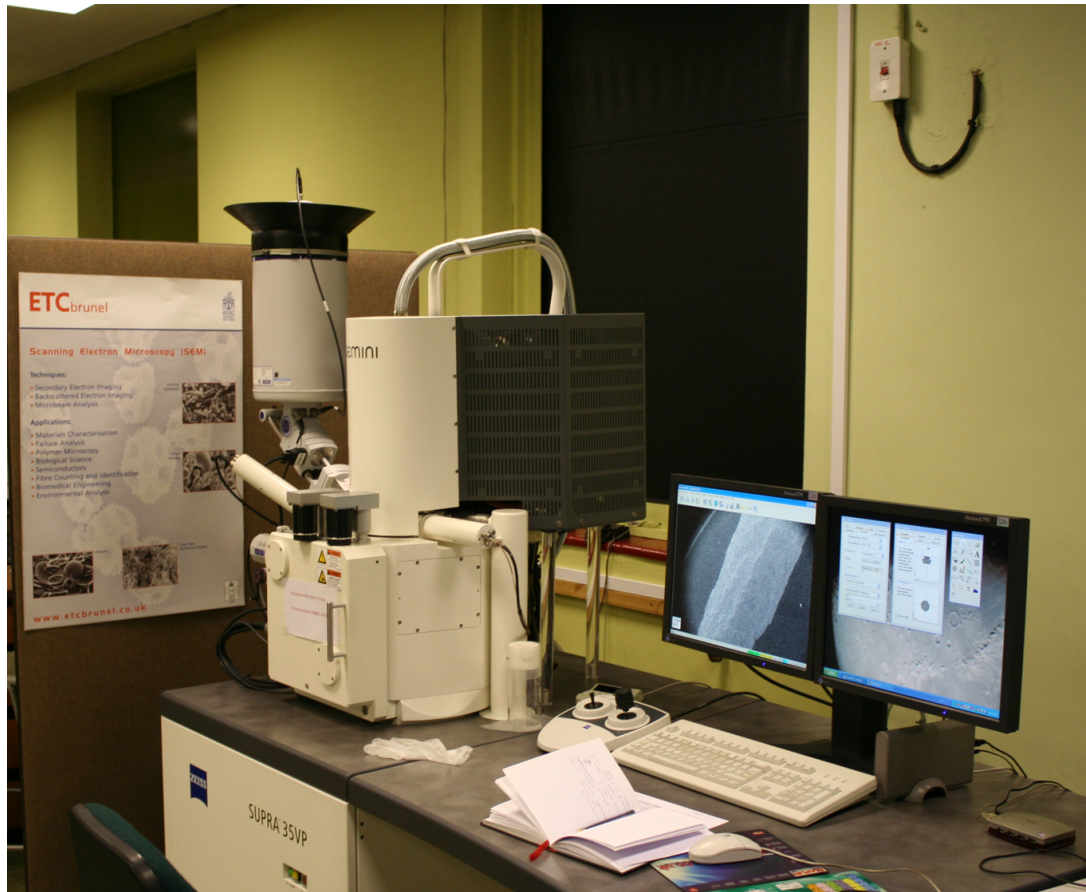
Figure 2.5: Scanning Electron Microscope

for materials up to 100g, it also has attachments where a material can be extracted directly into a syringe. Materials were mixed in this using a plastic container and only to a speed where they would not rise to reach the lid of the said container. As there is a discontinuity in the container at this point, the material may separate from the main body where losses could be incurred in the mixture which would lead to a final composition different to that from the intended stoichiometry.

For solid state mixing, this was run at speeds of up to 2300rpm for 90s. The time and speed depended on the mass of mixture, with a greater mass requiring a lower mixing speed for a greater length of time. In the case of mixing binder with phosphor for screen printing this was run at up to 2500rpm for 90s with similar considerations for weight and length of run.

When mixing two part silicones using this speedmixer, any air in the silicones is removed and this removes any degassing step that would otherwise be required prior to curing. The viscosity of the solution was also taken into account where lower viscosity materials can be run at high speeds.

2.6 Screen Printing

The screen printer used was a DEK 247, an automatic screen printer with a maximum print area of 305 x 305mm, shown in figure 2.6. This is used to deposit phosphors onto screens which were then applied to light sources. This can then allow the overall package of a light source and phosphor to be measured in an integrating sphere. The key benefit of this equipment is that the automated print cycle allowed consistency in the weight of ink deposited onto the substrate and allows a repeatable process to be taken.

The printer is designed to take frame mounted removable screens, shown in figure 2.7, which allow control over the weight of material printed with each pass of the printer. All the screens used were of a nylon mesh and a metal frame. The variables between each screen were thread diameter and number of threads per inch. Those used here had 48 threads per cm and a thread diameter of 80μm.

Figure 2.6: DEK 247 screen printer

Careful control over the ratio between binder and phosphor applied allowed more precision in the weight of the phosphor deposited. This ratio was suggested by the binder manufacturer, there is some leeway to allow an increase or decrease in the amount of phosphor mixed and therefore printed. While the weight of material may remain constant, when more phosphor is applied a thicker coat is achieved. While this can be calculated based on the operating variables [4], experimentally measured values are more accurate.

For successful printing of the phosphors, the particle size must not be so large that there is difficulty in printing between the threads. Once particle size exceeds the order of 100μm a new screen would be required with fewer threads per centimetre or smaller

Figure 2.7: Typical screen used with screen printer. Printable area in centre (yellow) is of size 65mm x 48mm

thread size. In any event, particle size of this order or less is necessary to achieve an even coating in the quality of printing which will in turn lead to an even distribution of light output.

Following printing onto the substrate, which was either glass or acetate, the mixture of binder and phosphor was dried in an oven at $80\,^{\circ}\mathrm{C}$ for approximately ten minutes until dry. Multiple layers can be printed which will increase the thickness of the layer and in some cases improve the uniformity of the deposit. Allowing each layer to dry before printing successive layers is referred to as 'dry' printing whereas printing in succession before any drying occurs was referred to as 'wet' printing.

References

[1] B. D. Cullity. *Elements of X-Ray Diffraction.* Addison-Wesley, 1978.

[2] A. Guinier. *X-ray diffraction in crystals, imperfect crystals, and amorphous bodies.* Dover Books on Physics, 1994.

[3] Brunel University ETC. Printed guide, Introduction to SEM, Feb 2008.

[4] The Gwent Group. Data for nylon mesh, http://www.gwent.org/gem_table1.html, Jan 2011.

Chapter 3

White Light Emission

Attempts to create a perfect white light will often constitute the search for individual colours which can later be combined as the designer sees fit. This is the logical progression that research has taken, and with the invention of colour television, the three primary colours were successfully generated with the inclusion of phosphors. Phosphor technology has continued to spread into a great many applications. As with all commercial applications, greater efficiency and cheaper costs are pursued, and one goal is an improvement in phosphors in these areas. In these respects, the red emitting phosphors are of a lower standard than their green and blue counterparts as discussed in section 1.1. This has therefore been a focus of study. Furthermore, new and changing technology can create the need for phosphors with altered properties, such as the location of the excitation bands. Therefore, this work begins with a chapter on analysis of existing phosphors and their properties, and whether they can be adjusted to satisfy the needs of newer applications and their potential in the near future.

3.1   White Light from LEDs

The discovery of high power blue LEDs in 1994 by Nakamura [1] established the use of LEDs to power lighting systems that cover the entire colour spectrum. This high brightness blue emitter was based on indium gallium nitride (InGaN) chips using an organo-metallic vapor phase epitaxy growth technique [2]. Prior to this, white light emission from an LED source was not considered suitable for commercial applications as the luminous flux was not high enough to compete with existing technologies, such as ACEL panels and fluorescent tubes. It was not until 2003 that commercial white LEDs achieved $74 \, \mathrm{lmW^{-1}}$ [3], equal to the generally reported $74 \, \mathrm{lmW^{-1}}$ efficiency of fluorescent tubes. Improvements in LEDs based on InGaN and AlInGaN for the orange/red part of the spectrum [4] combined with high brightness blue and green LEDs allowed one to create any combination within their colour gamut, including a mix that produced a white light emission.

White light can be generated in many different ways from LEDs [5]. Multicolour LED systems with a red, green and blue component can be used, or alternatively, they can be based upon a single colour LED system using either blue LEDs or ultra violet

LEDs (UVLEDs) as the source of photons. These single colour systems use one or more phosphors to provide a combination of wavelengths of light that gives an output which appears white. By varying this combination, the emission can be tailored to appear at a desired colour temperature.

One more method utilises organic dyes in conjunction with light emitting devices. These have advantages and are used with other technologies such as OLEDs and ACEL panels, but they are not currently suited to LEDs. A critical drawback when using dyes is their degradation which is pronounced when used in conjunction with high brightness sources, as in the case of LEDs, where the energy of the blue and UV photons can break the bonds in the dyes.

3.1.1 RGB Chip Method

This method of white light generation combines blue, green and red LEDs. When mixed they can provide the range of colours that lie within their colour gamut. This method requires the use of a blue wavelength equal to or lower than 470nm and a red emitter of at least 610nm to reach the full range of colour temperatures on the Planckian locus (figure 3.1). One of the greatest advantages of this system lies in that there is no quantum deficit when the energy is converted into photons and this leads to a high efficiency, restricted solely by the LED chips and their packaging [6].

However, there are problems associated with using a three chip system. Difficulties arise in attaining a high CRI due to narrow emission bands, although tuning of the emission is possible [5] to give an optimised, if somewhat artificially high, CRI. This is high as the LED emission peaks will match the CRI measured peaks, although gaps in the spectrum outside of these points are not filled. Another issue is that similar colour chips can have a relatively wide range of efficacies when new. This is further complicated as wavelength and luminous flux can change with temperature during usage as well as over the lifetime of operation [7]. This is very different to the stable emission incandescent and fluorescent lighting provides. Controlling these factors for a combination of LEDs over the course of their lifetime is a necessary requirement for general illumination and is possible [8]; however, this is costly due to the necessary electric circuitry.

Furthermore, the lifetime of the three colour LEDs may differ causing large colour shifts in the device over time.

There is also a lack of high efficiency green LEDs [9] as shown in figure 3.2 and those that are currently used degrade faster than at other wavelengths [10]. This is due to an increase in defects produced during the synthesis process as the emission wavelength shifts towards the green from the blue or red. Altogether these problems suggest this method currently appears to be an unsuccessful avenue to pursue for lighting solutions. However, research continues in this area, with Osram and SORAA announcing in late 2010 a 2% efficiency in their green laser semiconductor with a target of 10% [11].
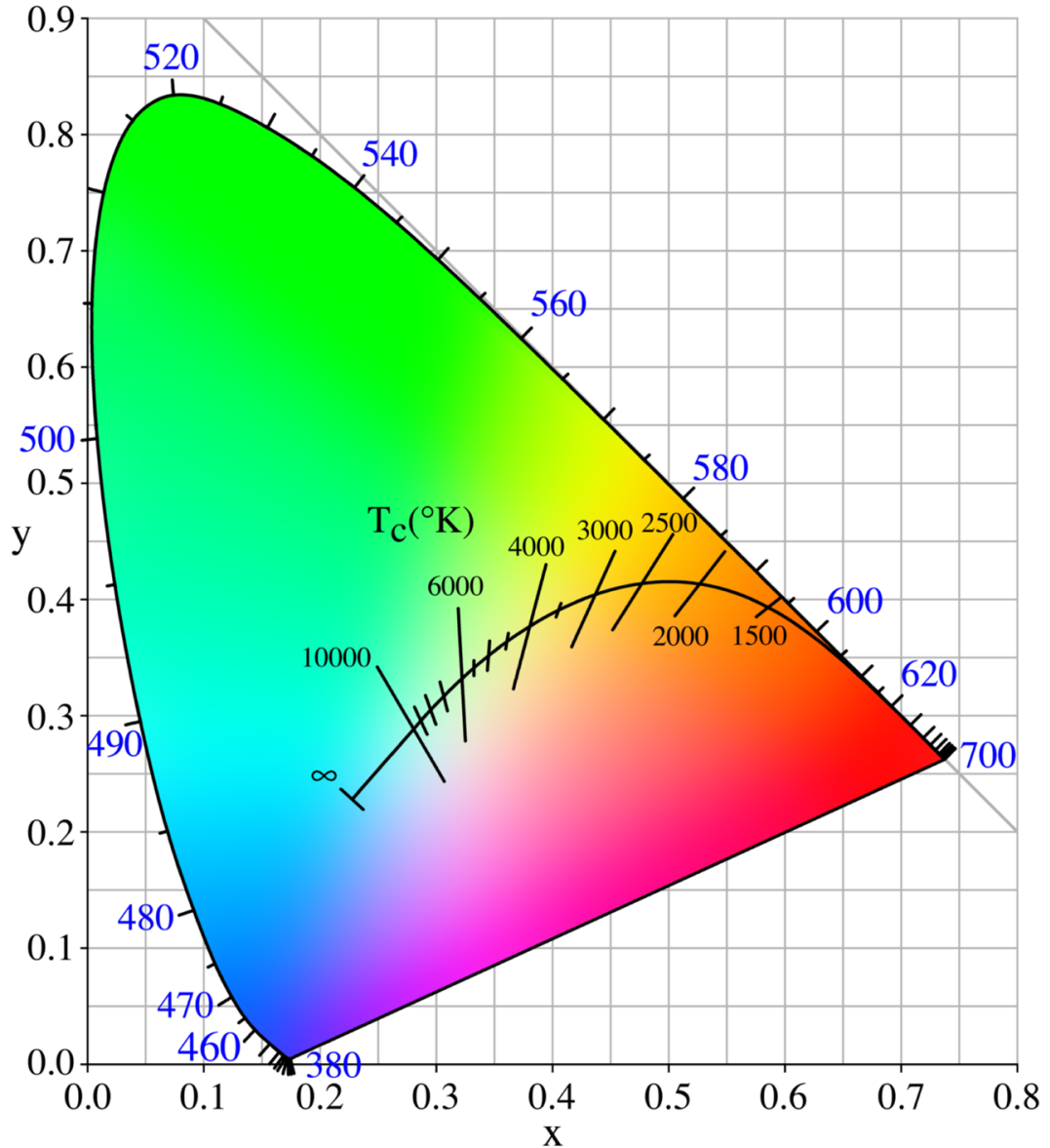
Figure 3.1: 1931 CIE chromaticity diagram with Planckian

3.1.2 Phosphor Method

Other methods are available which give a more efficient, cheaper system and they are the focus of the work here. The multi chip method is used only in specific applications, such as the backlight for flatscreen televisions [12], as the significant problems associated with it are difficult to overcome cheaply, even with recent advances. Coupled with a higher efficiency of blue and UV LEDs over red and especially green counterparts, white light generation often focuses on these LEDs used in conjunction with phosphors. Blue LEDs will have a smaller Stokes shift in the down conversion of photons from the pump source. They also have the benefit that their emission is in the blue region of the spectrum which leads to a high efficiency in this region.

Using blue emitting devices it is common to pursue one of two avenues for white lighting, depending on the properties required from the white emission. These are to
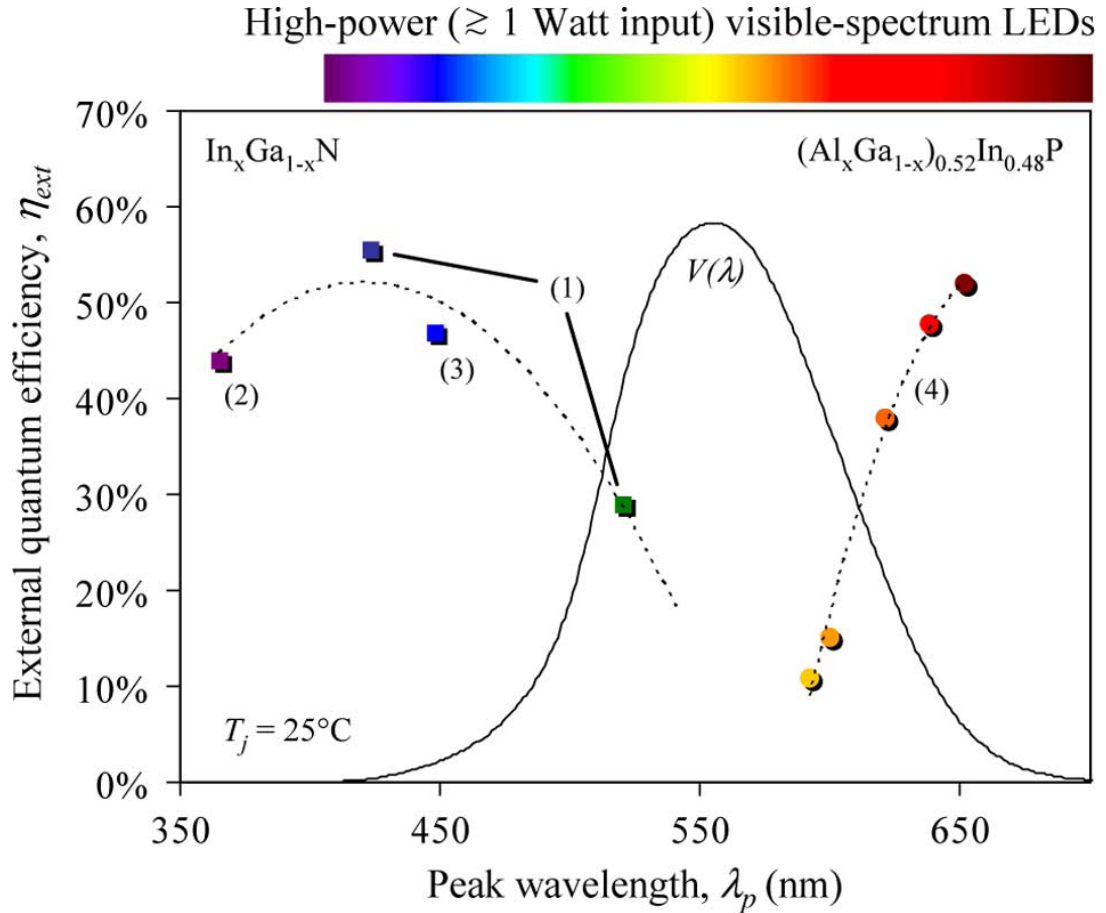
Figure 3.2: External quantum efficiencies for high-power visible-spectrum LEDs (T = 25 C), all from [9]: (1) InGaN TFFC LEDs, 350 mA; (2) InGaN VTF LED, 1000 mA; (3) InGaN CC LEDs employing patterned substrates; and (4) Production performance, AlGaInP TIP LEDs, Philips Lumileds Lighting Co., 350 mA. V (λ) is the luminous eye response curve from CIE. Dashed lines are guides to the eye. © 2007 IEEE

use either one yellow/green phosphor such as cerium doped yttrium aluminum garnet (YAG:Ce^{3+}) or a two phosphor combination using a yellow/green and a red phosphor, such as europium doped strontium thiogallate ($SrGa_2S_4$:Eu^{2+}) with europium doped calcium sulphide (CaS:Eu^{3+}) [13].

Using phosphors with blue or UV LEDs as the source also has its disadvantages. There is a reduction in efficiency of the overall package when including a colour conversion step, due to this process introducing non-radiative losses such as energy dissipating through lattice vibrations. This is an additional loss to the Stokes' shift, which is unavoidable when using a down conversion phosphor. The efficiency of the phosphor itself may have scope for improvement. Another obstacle is the 'halo effect' which is caused from the difference in light outputs when using a directional LED and a phosphor which emits over a 2π solid angle. This is observed when viewing the emission from the side of the device [14]. However, this effect can be corrected by moulding a lens containing the phosphor and results a more uniform emission, based on viewing angle [15].

UV emitting chips with a combination of up to three phosphors to produce the

white light [16] have additional problems which includes the possibility of degradation to the packaging from the UV emission [17].

3.2 Yttrium Aluminium Garnet

Colour conversion phosphors have been around well before their application in LED chip packages. The scope of their usage covered oscilloscopes, CRT televisions, electroluminescent and fluorescent tube lighting, however, it was found that many of the phosphors for those devices were not suited to blue and UV LED excitation primarily because their excitation bands did not lie in the regions where the LEDs emitted. For this reason, the red emitting phosphor that was used for cathode ray tube televisions YVO:Eu^{3+} [18] was not suitable for use with blue LEDs. However, cerium doped yttrium aluminium garnet ($Y_3Al_5O_{12}$:Ce^{3+}, or YAG:Ce^{3+}) was found to be well suited to this application [19] [20].

YAG:Ce^{3+} can be used as the sole phosphor in conjunction with blue LEDs to generate a white light emission. The CRI measured in this arrangement is ~80. For comparison, those of fluorescent tubes range from as low as 50 to greater than 90; the lowest acceptable values for CRI in general lighting begin at around 70, although would need to be greater than 85 to be good. A combination of YAG:Ce^{3+} and a blue LED will not generate a higher value of CRI as the combined emission spectrum lacks a component in the red. Figure 3.3 shows the combined emission of a blue LED, of peak wavelength 465nm, with a commercially available YAG:Ce^{3+} phosphor. This was measured to compare to the existing standard for white light based upon the mix of blue and yellow which appears white. This showed CIE (x,y) coordinates of (0.29, 0.31), a CCT of 8000K and a CRI of 80.

The properties of YAG:Ce^{3+} fulfil many of the requirements for colour conversion from LEDs. It has a broad band excitation in both the UV and blue region from 420nm-500nm as seen in figure 3.4 which will absorb part of the emission from most blue LEDs. (The step structure seen on the main emission band is an artefact from the monochromater used to take the measurement and not a feature of the phosphor). It also has a broad band emission spectra peaking at 555nm (figure 3.5), which covers the yellow, green and the short wavelength edge of the red part of the spectrum.

Furthermore the luminous efficacy is high, as is the quantum efficiency as measured on the Bentham Integrating Sphere and shown in table 3.1. Importantly, YAG:Eu^{3+} is not highly susceptible to temperature quenching as seen in graph 3.6, where at 160 °C its efficacy remains at 80% of its room temperature value.

Table 3.1: Efficacy values of commercial YAG:Ce^{3+} phosphor powder

Efficacy measurement	Value
Luminous Efficacy	321
Max. Theoretical Luminous Efficacy	381
Quantum Efficiency	78
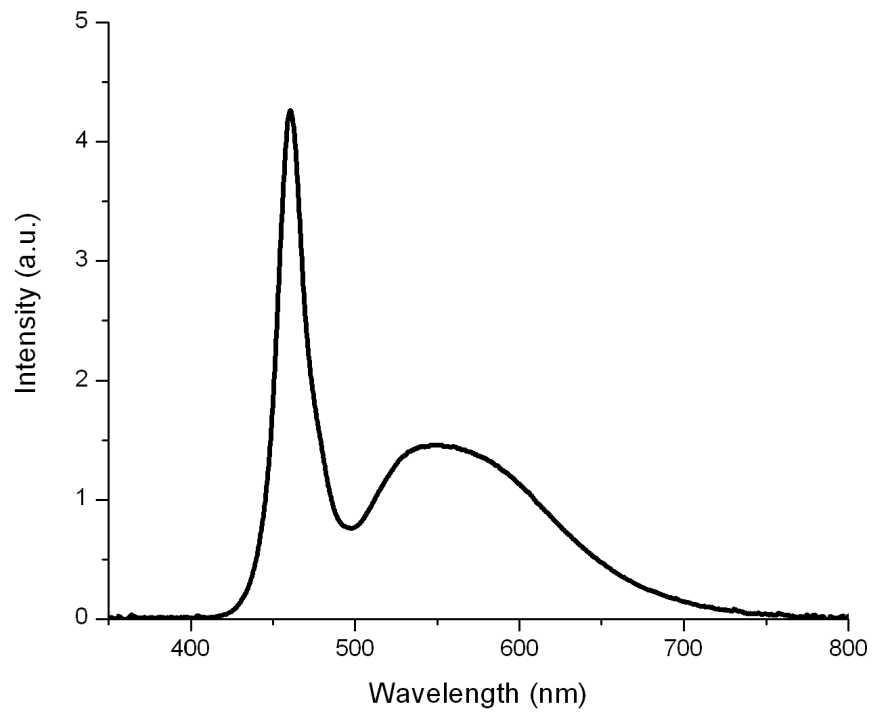
Figure 3.3: Emission spectrum of blue LED at 465nm with YAG:Eu^{3+} phosphor
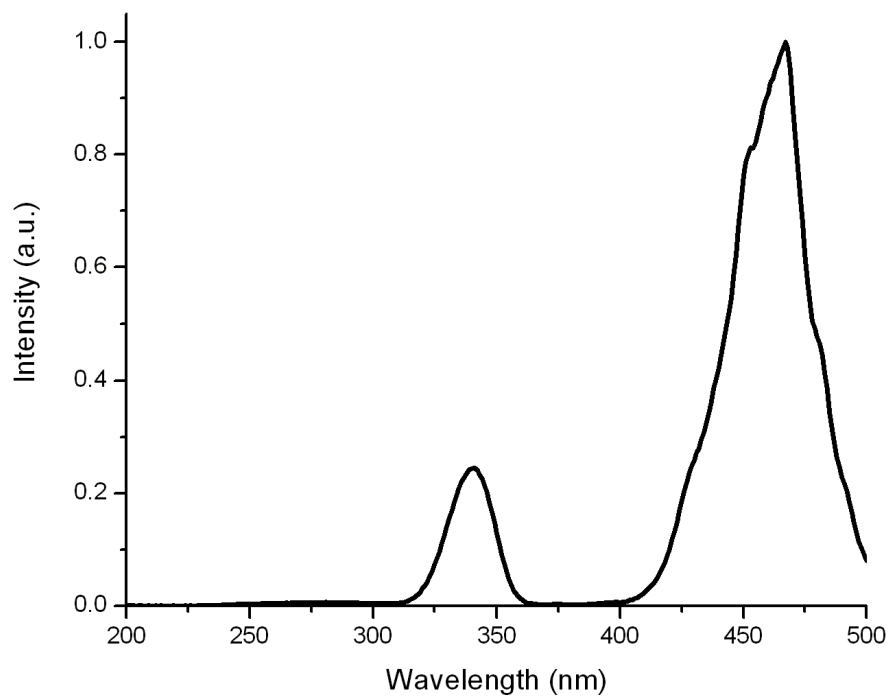
Figure 3.4: YAG:Ce^{3+} excitation spectrum monitored for 555nm wavelength emission
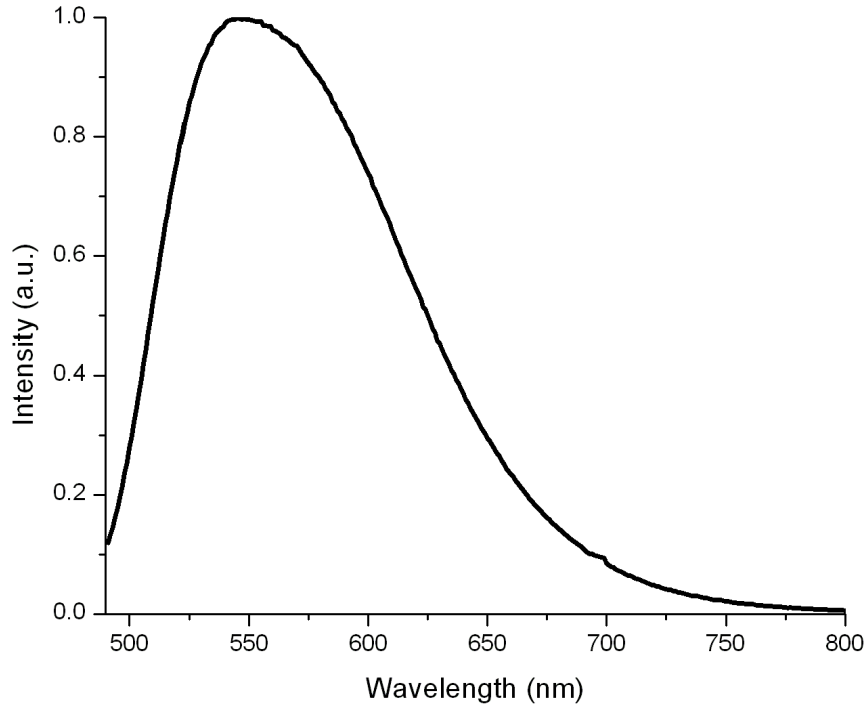
Figure 3.5: YAG:Ce^{3+} emission spectrum, excited at 465nm wavelength light

3.2.1 Optimisation of YAG:Eu^{3+} phosphors

Other factors may affect the luminous efficacies, emission and excitation bands. These include altering the structure of the host lattice or synthesizing uniform particles thus avoiding any grinding after firing the phosphor, an act which may decrease efficacy through introduction of surface defects [21]. Firing time and temperature can also affect the properties of the phosphor. All these factors will reed to be considered in the synthesis of these, and other, phosphors.

3.2.2 Drawbacks of the Single Phosphor Approach

This method for producing white light does have the serious drawback of not being able to achieve a CRI higher than about 80, as mentioned in section 3.1. This is due to a lack of red light in the spectrum of this combination of LED and phosphor as can be seen in graph 3.3. It is possible to shift the emission spectrum of YAG:Eu^{3+} to try to compensate. This is a well known effect which can be achieved by replacing some of the aluminium in the lattice with gadolinium. This shifts the peak of spectrum to longer wavelength, although this comes at the cost of luminous efficacy of the phosphor [5]. These effects can be seen by comparison of the emission spectra of these two phosphors, pumped by a blue emitting LED. These spectra are shown in figure 3.7, where the peak emission wavelength has lengthened from 555nm to 570nm. In this case 20% of the yttrium was replaced by gadolinium. This substitution reduced
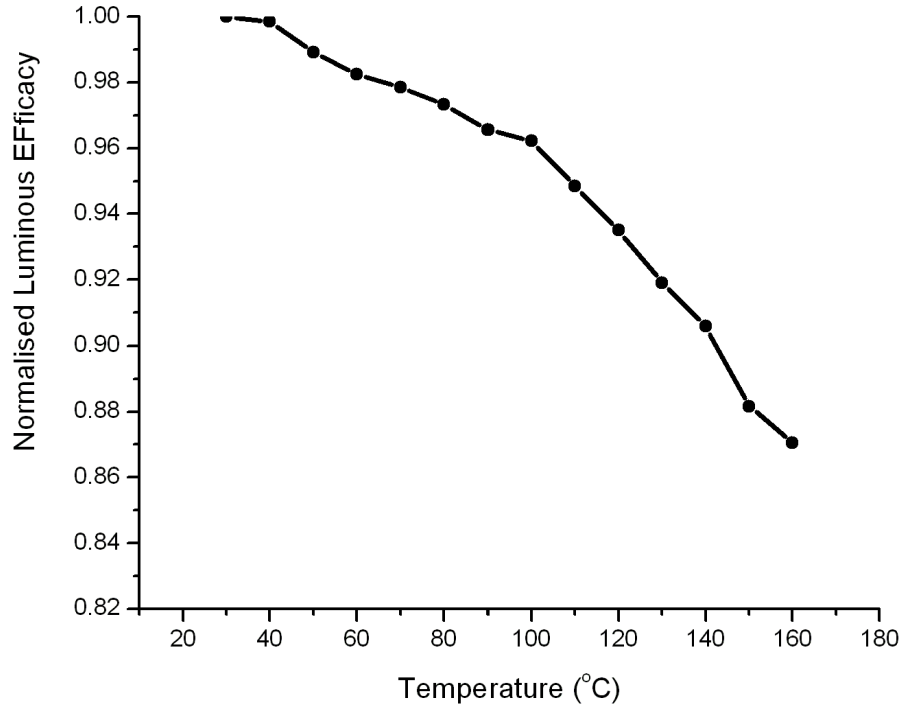
Figure 3.6: YAG:Eu^{3+} temperature dependence, monitored at 535nm emission as the temperature was increased

the efficacy, while the CRI increased from 70 to 80.

Based on this drawback of the single phosphor approach, much work has gone into synthesis of blue wavelength excited phosphors which will emit in the red region of the spectrum.

3.3   Y$_2$O$_3$:Eu^{3+}

Europium has been used in yttrium oxide based lattices, including yttrium oxysulphide, as a red emitting phosphor for many years and in many applications since replacing YVO$_4$:Eu^{3+} [22]. In fact, Y$_2$O$_3$:Eu^{3+} is used as a red emitting phosphor for lighting in fluorescent tubes and it is this compound that we first began the work on preparing red phosphors.

3.3.1   Experimental Method

These phosphors were made using a solution synthesis method. Precursor solutions of Eu(NO$_3$)$_3$ and Y(NO$_3$)$_3$ were prepared using the oxides Eu$_2$O$_3$ and Y$_2$O$_3$ at 99.99% purity as starting materials. The oxides were added to H$_2$O and concentrated nitric acid, heated and stirred until fully dissolved. These solutions were mixed together in measured amounts to produce the desired stoichiometric compound.
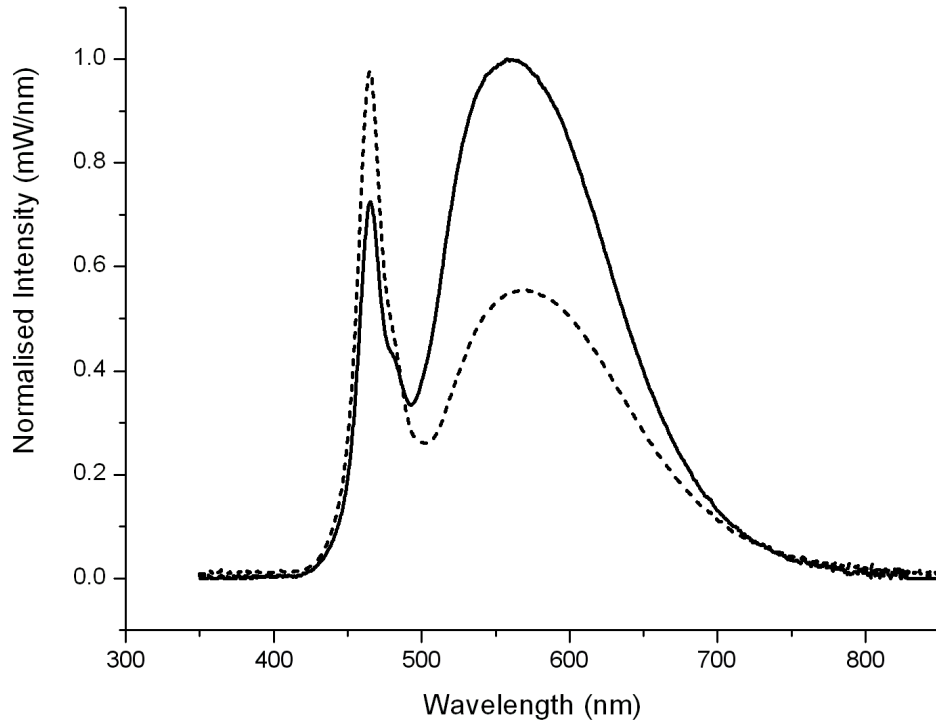
Figure 3.7: YAG:Ce^{3+} (solid line) and (Y,Gd)AG:Ce^{3+} (dashed line) emission spectrum comparison, excited by a blue LED with a 465nm emission peak

$$xY_2O_3 + (1-x)Eu_2O_3 \rightarrow Y_{2x}Eu_{1-2x}O_3, \tag{3.1}$$

This solution was heated to 85 °C and then excess urea added to precipitate the metals as hydroxycarbonates. If necessary, the pH was adjusted to ~8 through addition of nitric acid. This was then filtered and dried in an oven at 110 °C. The resulting powder was fired in a furnace for 17-18 hours at a temperature of 980 °C, in an alumina crucible.

3.3.2 Y$_2$O$_3$:Eu^{3+}

Y$_2$O$_3$:Eu^{3+} is a well established red phosphor and new synthesis methods have been investigated to improve its performance, including production of nanoparticles [23]. This phosphor contains a high europium content, which is the most expensive component of the phosphor. Those made here used much less europium, the highest europium content was that in Y$_{1.84}$Eu$_{0.16}$O$_3$. The emission and excitation spectra of this phosphor is presented in figures 3.8 and 3.9

These phosphors were tested in an integrating sphere at excitation wavelengths of 390nm and 470nm and with the aforementioned phosphor of highest europium content performing best, it was not a high efficacy red emitter, with no calculable emission. A coactivator was then included to investigate if this led to an increase in the efficacy.
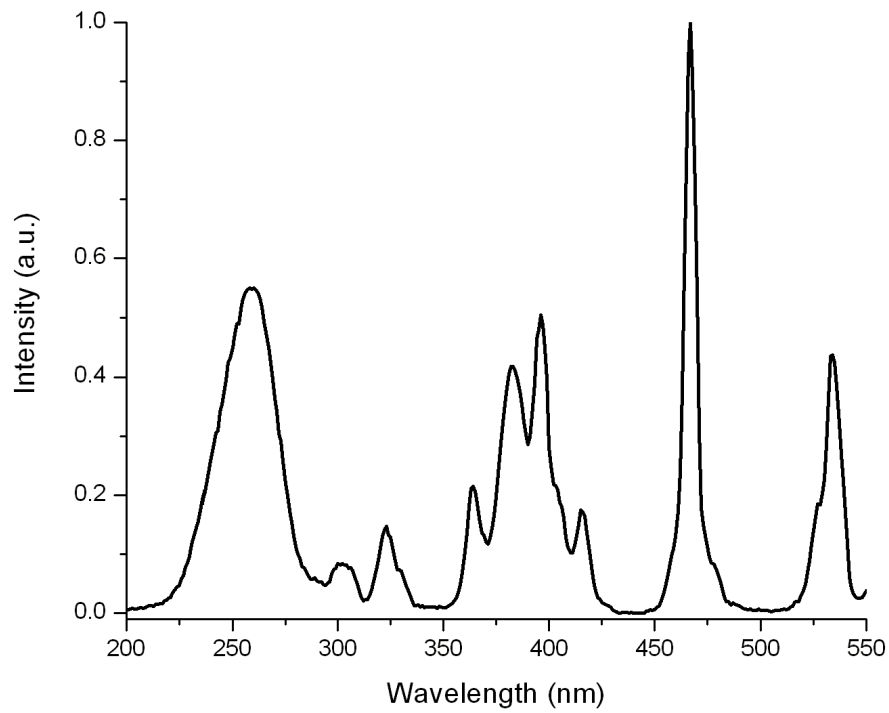
Figure 3.8: Excitation spectrum of Y_2O_3:Eu^{3+} monitored at 611nm
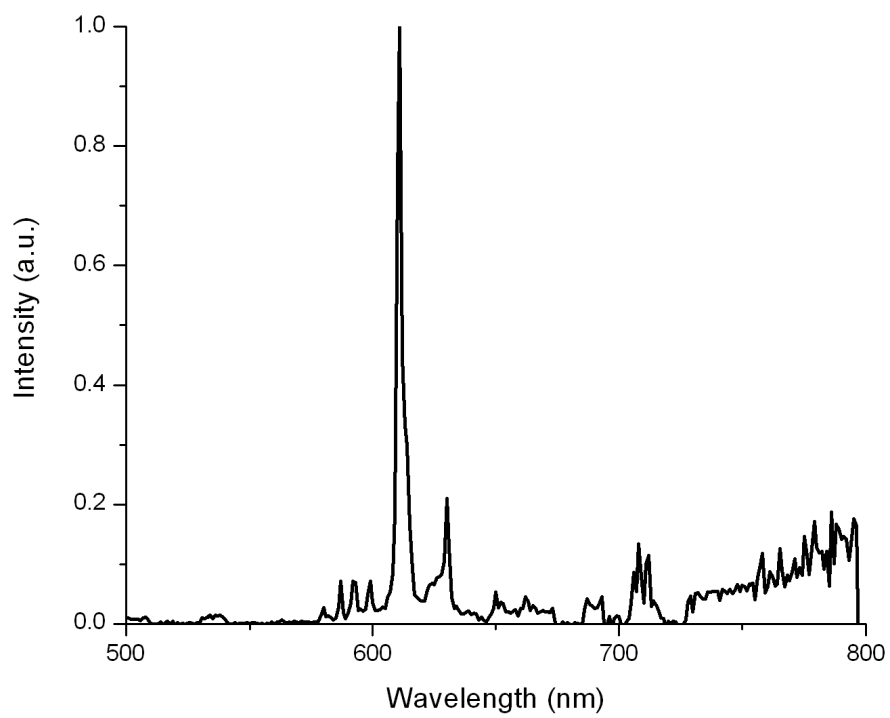
Figure 3.9: Emission spectrum of Y_2O_3:Eu^{3+} excited at 366nm

3.3.3 Bismuth coactivator

Bismuth has been employed as a coactivator in YVO_4 phosphors [24] and was used here to investigate whether there would be a positive effect on the efficacy of this phosphor.

Experimental Method

The synthesis of the phosphors that contain bismuth was similar to the procedure for the Y_2O_3:Eu^{3+} phosphors described in section 3.3.1 above. The only difference is the incorporation to solution of the desired amount of precursor solution $Bi(NO_3)_3$, which was likewise prepared from the oxide Bi_2O_3 at 99.99% purity.

3.3.4 Bismuth Results

The europium content ranged from 5-10% (within the yttrium sites) with the bismuth content between 12-100% relative to europium. Whilst these do show some red luminescence under UV illumination they are of very low efficacies (less than $12 \, \mathrm{lm/W}$) and will not be viable phosphors for use in any current lighting applications. Adding bismuth to the phosphors in all ratios used decreased the emission from the equivalent phosphor with no coactivator. The excitation and emission spectra for the bismuth coactivated phosphors can be seen in figures 3.10 and 3.11 respectively, and whilst the emission does not vary the excitation spectrum is very different.
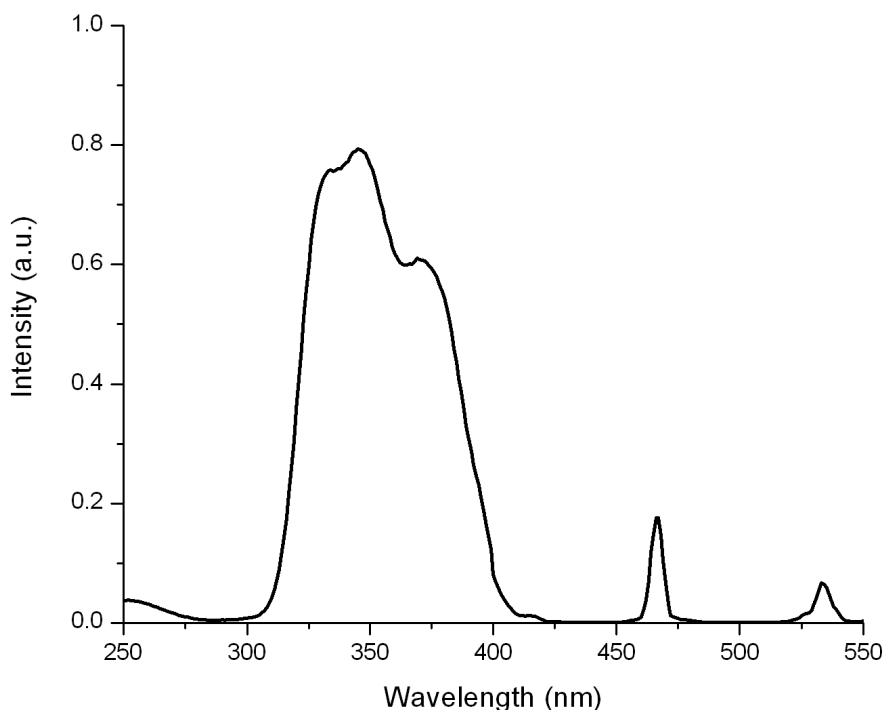
Figure 3.10: Excitation spectrum of Y_2O_3:Eu^{3+},Bi^{3+} monitored at 611nm
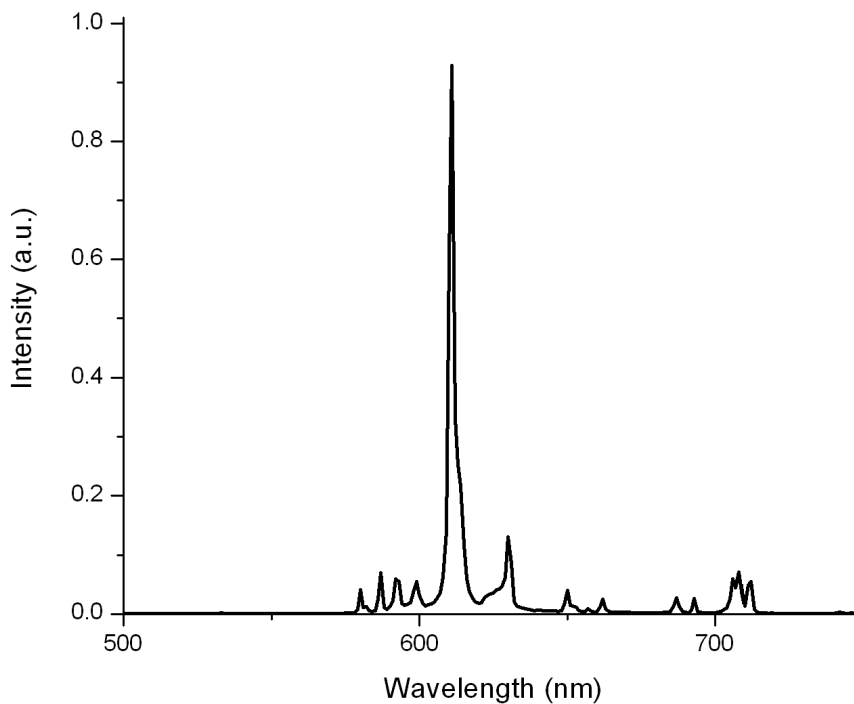
Figure 3.11: Emission spectrum of Y_2O_3:Eu^{3+}, Bi^{3+} excited at 366nm

3.4   Conclusion

Cheaper phosphors by a reduction in the europium content does not appear possible even when using a coactivator in an attempt to increase the efficiency. Reducing the europium content to reduce the cost is not an effective trade off as the luminous efficacy is reduced below useful levels in applications. Coactivators can change the excitation bands especially those at the higher wavelengths (i.e. those above the CT band), as seen from the inclusion of Bismuth in section 3.3.4. This would be useful for phosphors in UV excited applications. However, a change in approach from modification of the existing phosphors is required, as these attempts have not led to a suitable high efficacy phosphor. This begins with a look at alternative host lattices which respond to excitation at different wavelengths of energy.

References

[1] S. Nakamura, T. Mukai, and M. Senoh. Candela-class high-brightness In-GaN/AlGaN double-heterostructure blue-light-emitting diodes. *Appl. Phys. Lett.*, 64:1687 − 1689, 1994.

[2] D.A. Steigerwald, J.C. Bhat, D. Collins, R.M. Fletcher, M.O. Holcomb, M.J. Ludowise, P.S. Martin, and S.L. Rudaz. Illumination with solid state lighting technology. *IEEE Journal of Selected Topics in Quantum Electronics*, 8(2):310 − 320, 2002.

[3] T. Fujii, Y. Gao, R. Sharma, E. L. Hu, S. P. DenBaars, and S. Nakamuraa. Increase in the extraction efficiency of GaN-based light-emitting diodes via surface roughening. *Applied Physics Letters*, 84(6):855 − 857, 2004.

[4] Motokazu Yamada Takashi Mukai and Shuji Nakamura. Characteristics of InGaN-Based UV/blue/green/amber/red light-emitting diodes. *Japanese Journal of Applied Physics*, 38:3976 − 3981, 1999.

[5] R. Withnall, J. Silver, G. Fern, T. Ireland, A. Lipman, and B. Patel. Experimental and theoretical luminous efficacies of phosphors used in combination with blue-emitting LEDs for lighting and backlighting. *Journal of the SID*, 16(2):359 − 366, 2008.

[6] Michael S. Shur and Arturas Zukauskas. Solid-state lighting: Toward superior illumination. *Proceedings of the IEEE*, 93(10):1691 − 1703, 2005.

[7] Arpad Bergh, George Craford, Anil Duggal, and Roland Haitz. The promise and challenge of solid-state lighting. *Physics Today*, 54:42 − 47, 2001.

[8] Subramanian Muthu, Frank J. P. Schuurmans, and Michael. D. Pashley. Red, green, and blue LEDs for white light illumination. *IEEE journal on selected topics in quantum electronics*, 8(2):333 − 338, 2002.

[9] Michael R. Krames, Oleg B. Shchekin, Regina Mueller-Mach, Gerd O. Mueller, Ling Zhou, Gerard Harbers, and M. George Craford. Status and future of high-power light-emitting diodes for solid-state lighting. *Journal of Display Technology*, 3(2):160 − 175, 2007.

[10] Z. L. Li, P. T. Lai, and H. W. Choi. Failure analysis of InGaN/GaN LEDs with emission wavelength between 440 nm and 550 nm. *Phys. Status Solidi C*, 7(7 - 8):2202 – 2204, 2010.

[11] New Scientist. First green semiconductor laser plugs spectrum gap, November 2010.

[12] Robert S. West, Simon Kuppens, Charles Schrama, Yourii Martynov, Nicola Pfeffer, and Huub Konijn. *Multi-colored LED array with improved brightness profile and color uniformity.* US patent number 7,320,531 B2, January 2008.

[13] Hao Wu, Xinmin Zhang, Chongfeng Guo, Jian Xu, Mingmei Wu, and Qiang Su. Three-band white light from InGaN-based blue LED chip precoated with green/red phosphors. *IEEE photonics technology letters*, 17(6):1160 – 1162, 06 2005.

[14] F.K. Yam and Z. Hassan. Innovative advances in LED technology. *Microelectronics Journal*, 36(2):129 – 137, 2005.

[15] Gerd Mueller, Regina Mueller-Mach, Grigoriy Basin, Robert Scott West, Paul S. Martin, Tze-Sen Lim, and Stefan Eberle. *LED with phosphor tile and overmolded phosphor in lens.* International patent number WO/2008/104936, September 2008.

[16] J. K. Sheu, S. J. Chang, C. H. Kuo, Y. K. Su, L. W. Wu, Y. C. Lin, W. C. Lai, J. M. Tsai, G. C. Chi, and R. K. Wu. White-light emission from near UV InGaN-GaN LED chip precoated with blue/green/red phosphors. *IEEE Photonics Technology Letters*, 15(1):18 – 20, 2003.

[17] M. Yamada, Y. Narukawa, H. Tamaki, Y. Murazaki, and T. Mukai. A methodological study of the best solution for generating white light using nitride-based light-emitting diodes. *IEICE Trans. electron*, E88-C:1860 – 1871, 2005.

[18] Albert K. Levine and Frank C. Palilla. A new, highly efficient red-emitting cathodoluminescent phosphor (YVO_4:Eu) for color television. *Applied Physics Letters*, 5(6):118 – 120, 1964.

[19] Shinkichi Tanimizu. *Phosphor Handbook*, page 113. Taylor & Francis Group, LLC, 2007.

[20] Yoshinori Shimizu, Kensho Sakano, Yasunobu Noguchi, and Toshio Moriguchi. *Light emitting device having a nitride compound semiconductor and a phosphor containing a garnet fluorescent material.* US patent number 5,998,925, December 1999.

[21] Gareth Wakefield, Edward Holland, Peter J. Dobson, and John L. Hutchison. Luminescence properties of nanocrystalline Y_2O_3:Eu. *Advanced Materials*, 13(20):1557 – 1560, 2001.

[22] S.J. Dhoble, I.M. Nagpure, J.G. Mahakhode, S.V. Godbole, M.K. Bhide, and S.V. Moharil. Photoluminescence and XEL in Y_2O_3:Eu^{3+} phosphor. *Nuclear Instruments and Methods in Physics Research Section B: Beam Interactions with Materials and Atoms*, 266(15):3437 – 3442, 2008.

[23] Zuoling Fu, Shihong Zhou, Tianqi Pan, and Siyuan Zhang. Preparation and luminescent properties of cubic Eu^{3+}:Y_2O_3 nanocrystals and comparison to bulk Eu^{3+}:Y_2O_3. *Journal of Luminescence*, 124:213 – 216, 2007.

[24] W.J. Park, M.K.Jung, S.J. Im, and D.H. Yoon. Photoluminescence characteristics of energy transfer between Bi^{3+} and Eu^{3+} in $LnVO_4$: Eu, Bi (Ln = Y, La, Gd). *Colloids and Surfaces A: Physiochem. Eng. Aspects*, 313-314:373 – 377, 2007.

Chapter 4

Phosphors with Tungsten Oxide Host Lattices

A search for alternate host lattices begins with materials that have shown some promise in photoluminescence. One such material that has been used in the past for a variety of luminescent applications is tungsten oxide. The approach here will focus on the possibility of creating a high efficacy red emitting phosphor, with absorption in the blue region.

4.1 Tungsten oxide

Tungsten oxides crystals have been of scientific interest for many years including use as host materials for solid state lasers. The properties of the laser will depend on the structure of the lattice and the activator ion that is used, amongst other factors. Whilst most research concentrated on Nd:YAG and Nd:YVO$_4$ lasers, a new host material, Nd:NaY(WO$_4$)$_2$, was reported in 1997 [1].

Further research has shown the alkaline metal tungstates/molybdates, doped with rare earth ions, are suitable as host materials for laser light emission [2], although for lasers, the tungstate crystals have a greater potential than the molybdates with more doped tungsten oxide lattices known to undergo stimulated emission [3]. Molybdenum is mentioned as it has some similarities to tungsten and is a topic of further study in this chapter and the next. Prior to this work in their laser capabilities, calcium tungsten oxide lattices were known to phosphoresce and were used in applications, including scintillation counters [4].

Tungsten oxide combined with hydrogen has long been known to appear in a variety of body colours depending on hydrogen content; with a general formula H$_x$WO$_3$, collectively these are known as the tungsten bronzes [5]. Along with hydrogen, alkaline metals and earth alkaline metals can be intercalated in non stoichiometric coefficients [6]. Changes to the amount of hydrogen or metal can have an effect on the crystal structure as well as the electrical and optical properties [7]. Of all their properties and uses, the phosphorescence is the focus of this chapter.

4.1.1 Calcium Tungstate

Self-activated phosphors (those that do not include activators as a part of their structure, as described in section 1.4), have been in use for practical applications for some time as converters of light from the UV to blue wavelength. An example of this, and one of the earliest known phosphorescent materials, is calcium tungstate ($CaWO_4$). This can be excited by X-ray radiation and has been used for these properties for over 80 years [8]. Further research which has included doping with activators, has expanded their uses to include laser host materials, scintillators and phosphors including X-ray excitation [9] [10] [11] [12].

The structure of $CaWO_4$ is tetragonal (scheelite) with WO_4^{2-} ions in sites of S_4 symmetry loosely bound to Ca^{2+} cations [13]. There have been studies noting the effects of adding activators to this compound, including how the emission will be altered [14] and changes to its structure. Europium – which is of great interest to this work – and terbium, have been researched extensively as activators in this material, including a theoretical approach to their emission properties [15] (see also section 1.4.1).

The interest in the tungstates extended to include the addition of metal ions to improve their luminescence. Lanthanium and gadolinium were reported as materials that increased the luminous efficacies [14], as did the inclusion of the alkaline metals lithium, sodium and potassium [16]. More recently, other alterations to the structure have included the substitution of part or all of the tungsten with molybdenum [17] and this is investigated later in this chapter and the next (sections 4.4 and 5.6.1 respectively).

4.2 Experimental Method

The phosphors discussed in this chapter were synthesised via the solid state method. The raw materials were sourced at 99.9% purity and ground together in either a mortar and pestle, or mixed using the speedmixer (see section 2.5). These were Li_2CO_3, Eu_2O_3, WO_3 and MoO_3. An investigation was undertaken to compare the results obtained by using two methods. Identical phosphors were made using one of the two pathways and then analysed under SEM and in the Bentham Integrating Sphere. The integrating sphere was used to measure both the excitation and emission spectra and the luminous efficacy. These measurements were similar within the margin of error and the speedmixer was used hereafter for mixing the starting materials before firing.

The mixed powders were fired in alumina crucibles at temperatures of 750 °C to 800 °C, for three hours (see table 4.1). After cooling, some phosphors required soaking in water in order to remove them from the crucible. These were then filtered and dried before being ground in a pestle and mortar. Those not soaked were ground only if necessary. The drawback of using this method to create the phosphor is that the mechanical processing of the fired material induces surface damage, such as defects, which was seen to reduce the luminescence.
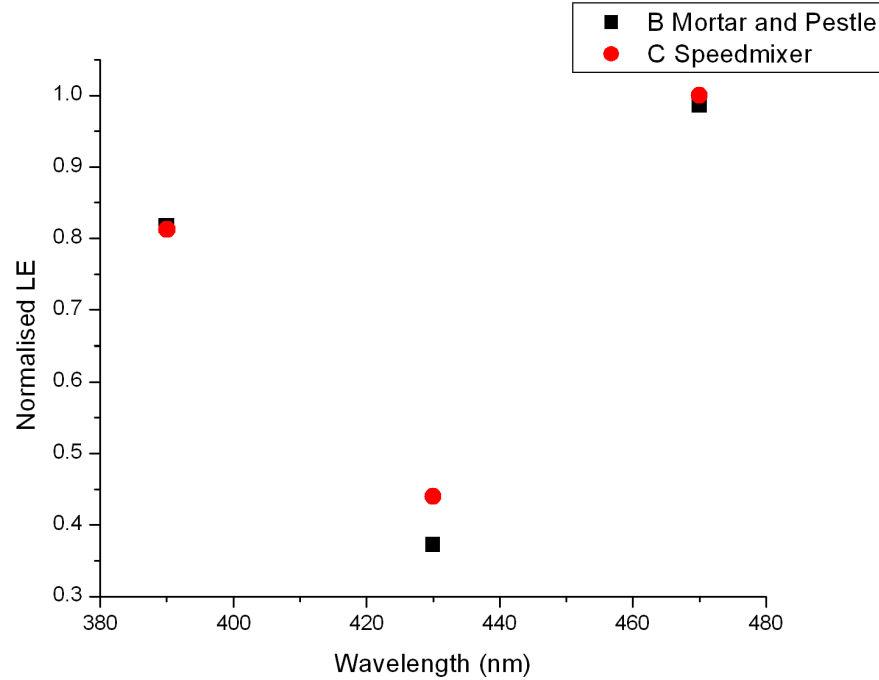
Figure 4.1: Comparison of efficacy results at three separate wavelengths when using either a speedmixer, or grinding raw materials with a mortar and pestle

4.3   Europium Doping of Phosphor Lattices

The structures listed earlier in this chapter (section 4.1.1) phosphoresce and these were doped with activators to alter the emission. Europium, in its 3+ oxidation state, was used as the activator to induce a red emitting phosphor. The addition of Eu^{3+} led to excitation bands above 400nm which are due to the transitions within the $4f^6$ configuration of this europium ion.

The emission relates to the $^5D_0 \longrightarrow {}^7F_2$ electronic transition of the excited europium ion and was expected to lead to a red emission of around 615nm as the emission from this oxidation state is largely unaffected by its surroundings.

$Ca_xEu_{1-x}WO_3$ with x at both 0.8 and 0 were prepared and investigated. The luminous efficacy value extracted from the emission data when excited in the near UV or the blue region, excitation wavelengths of 365nm and 465nm respectively, was below 10 lm/W. However, this compound had appealing properties in its emission and excitation spectra such as the peak excitation wavelengths at just below 400nm and at 465nm (figure 4.2) along with its deep red emission (figure 4.3).

Whilst the luminous efficacy results were poor, this did not immediately discourage further investigation as previous papers have reported bright emission from these structures [18] [19]. Attempts to improve the emission began by looking at alterations to the lattice structure above, commencing with substituting some molybdenum for tungsten in the lattice.
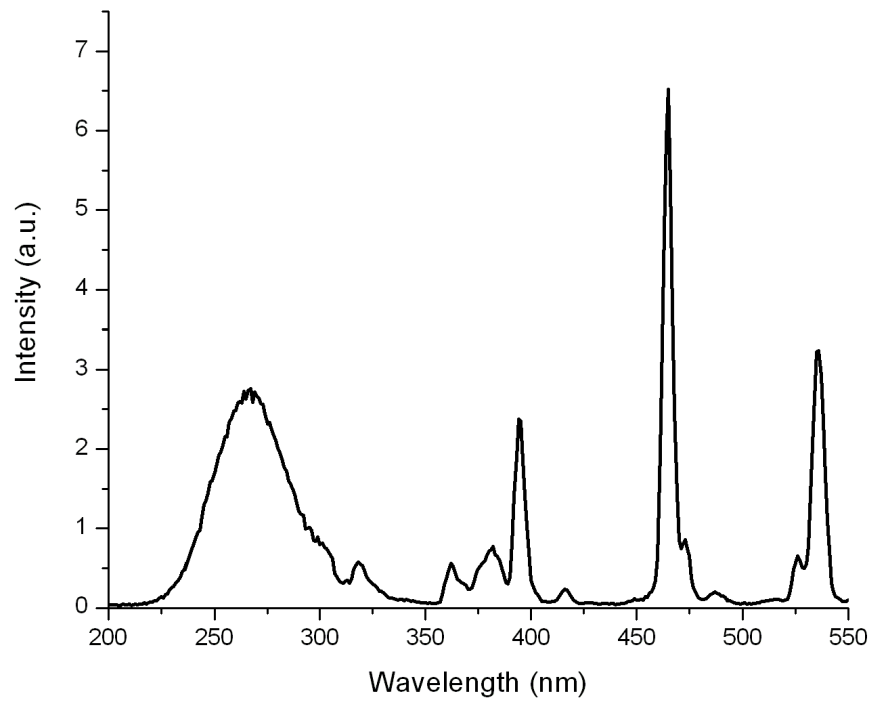
Figure 4.2: Excitation Spectrum of CaWO$_4$:Eu monitored at 615nm
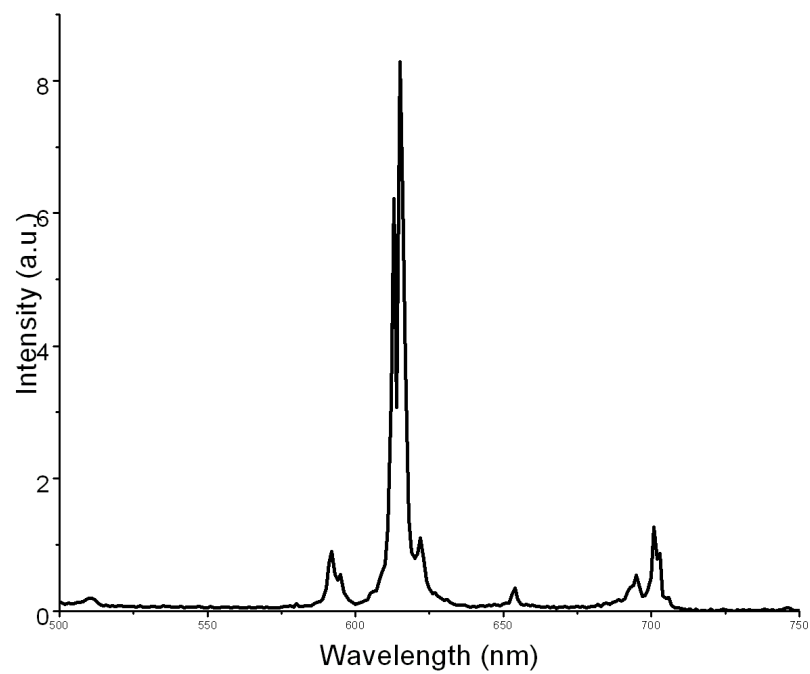
Figure 4.3: Emission Spectrum of CaWO$_4$:Eu excited at 465nm

4.4   Molybdenum Oxide

Molybdenum can be used to partially or fully replace tungsten in the lattice [18]. This affects the lattice structure only slightly as their ionic radii in the 6+ excitation state are similar at 0.59Å and 0.60Å for molybdenum and tungsten respectively.

$Ca_xEu_{1-x}(WO_4)_{0.5}(MoO_4)_{0.5}$ with x at both 0.25 and 0.2 were prepared to compare the excitation spectra, emission spectra and the luminous efficacy. As expected, the positions of the features of the excitation and emission bands remained similar (see figure 4.4) with two noticeable differences in the excitation spectra. The first is seen in the highest energy peak, the charge-transfer band, which is much larger when molybdenum was substituted for tungsten, and the second is seen as a difference in the relative intensities of the peaks. Importantly, the luminous efficacies remained low; at the excitation wavelength peak of 465nm an emission of less than 15 lm/W was recorded on the integrating sphere. There were still more alterations to be made to this lattice in an attempt to improve the luminous efficacy.
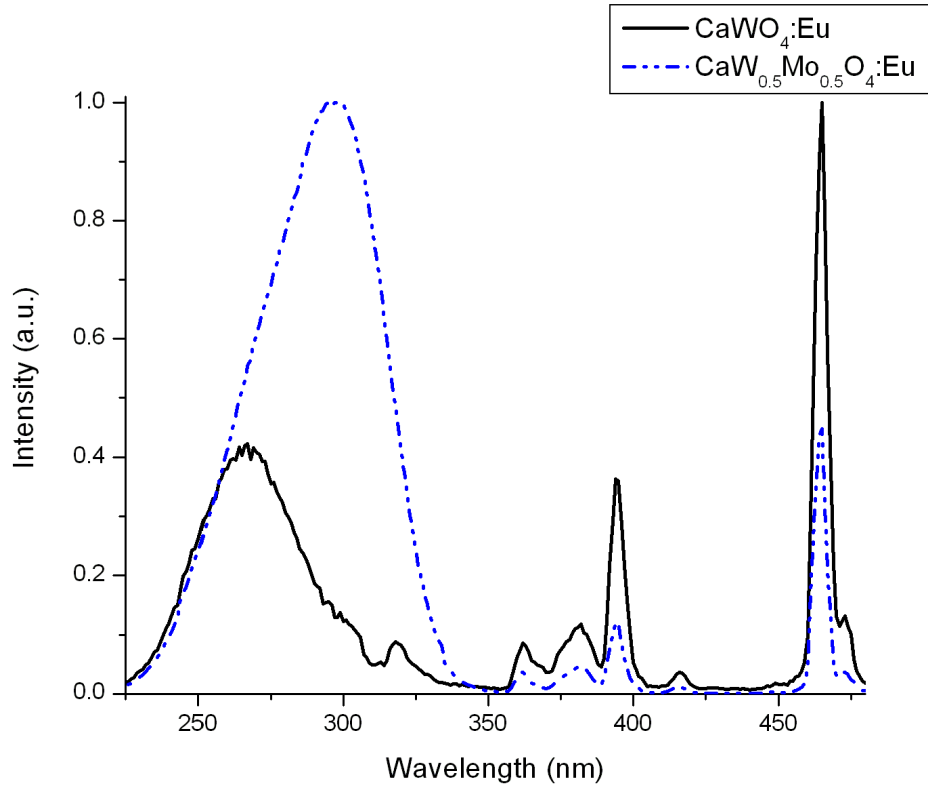
Figure 4.4: Emission Spectra of $CaWO_4$:Eu and $CaW_{0.5}Mo_{0.5}O_4$:Eu
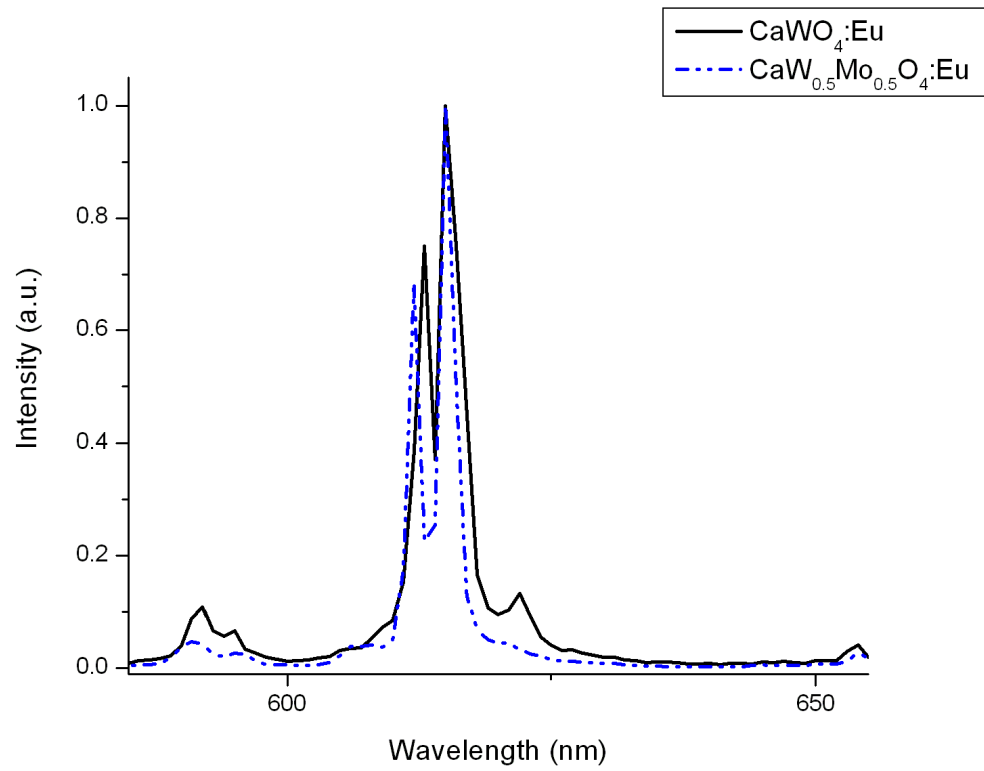
Figure 4.5: Excitation Spectra of $CaWO_4$:Eu and $CaW_{0.5}Mo_{0.5}O_4$:Eu

4.5 Novel Phosphors Developed in this Work

It is only more recently that these europium doped structures have been investigated for their use in solid state lighting [17]. Whilst there has been research into these structures in recent years there is further room for improvement in terms of efficacies and quantum efficiencies for these phosphors. It should be noted that they have many useful properties for commercial applications, such as the narrow band emission at 615nm and good performance at high temperature, which suggests this as an area for further study; as mentioned these are well–suited for use with lighting applications, and in particular, LEDs.

As reported (in section 4.1.1), tungsten and molybdenum based structures can be adapted by varying/controlling their compositions so that they manifest a range of properties. This includes the ratio of tungsten to molybdenum as well as the other elements in the structure. This can involve the inclusion of one of the alkaline metals [20].

4.5.1 Alkaline Metals

Using the double tungstates/molybdates as a starting point, their properties were analysed in detail using the equipment described in chapter 2.

Beginning with phosphors of the form

$$\text{AEu(WO}_4)_{2-x}(\text{MoO}_4)_x, \text{ where A} = \text{(Li, K, Na)}$$
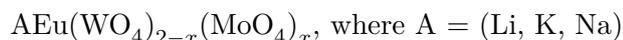
variations in the europium content as well as the structural possibilities above were investigated.

In the formula above, as A was varied the properties of the phosphors, with particular attention paid to the luminous efficacy were measured. x remained constant and equal to one, A had a molar content of 1.6 and the europium molar content was 0.4. Table 4.1 shows these phosphors and their efficacies including the temperatures at which they were fired. These were excited at a wavelength of 470nm.

Table 4.1: Efficacy values of alkaline metals with tungstates/molybdates

Phosphor Composition	Firing		LE (lm W)
	Temperature (°C)	Time	
$\text{Li}_{1.6}\text{Eu}_{0.4}(\text{WO}_4)(\text{MO}_4)$	750	3hrs	287
$\text{Na}_{1.6}\text{Eu}_{0.4}(\text{WO}_4)(\text{MO}_4)$	800	3hrs	0
$\text{K}_{1.6}\text{Eu}_{0.4}(\text{WO}_4)(\text{MO}_4)$	750	3hrs	85

Whilst all were weak, the addition of lithium led to the greatest increase in luminous efficacy of those phosphors.

All the phosphors were required to be soaked in water after firing before being dried and ground briefly with a pestle and mortar to give the final phosphor material. Firing temperature and time for these was similar to that of tungsten and molybdenum oxide lattice phosphors reported in the literature which was between 1-6 hours and

600-900 °C [2] [17] [21]. Grinding the phosphors after firing and prior to testing was important, as for many applications a homogeneous state of smaller particles of the order of 10µm or less is required, for example in the printing process. In this regard, the lithium phosphors were the hardest of those that were made, with potassium phosphors, by comparison being much softer. The uniformity in luminosity over the entire fired sample was also superior for the potassium phosphor over the lithium equivalent; with sodium, the phosphors' properties lay between the two extremes.

4.6   Improving the Efficacy of the new phosphors

The phosphors of the form $A_{1.6}Eu_{0.4}(WO_4)(MoO_4)$ where A = (Li, K, Na), do not provide a great enough emission to be useful in any applications and in order to improve the efficacies many other variations on this formula were tested. Target luminous efficacy values were for greater than 100 lm/W for the phosphor powders (see section 1.1 for comparisons to commercial phosphors). These attempts were either based on previous existing phosphors with an alternative element introduced as part of the lattice. However, not all attempts were simply to alter the structure. Other activators and coactivators were also investigated. While much detail was not focused on them in this thesis, these unsuccessful attempts warrant mention if solely to make others aware of their unsuitability. These are listed in table 4.2

Table 4.2: Novel phosphor formula attempted

Metal Composition in Unsuccessful Phosphors
$LiW_{0.5}Si_{0.22}Eu_{0.22}$
$LiW_{0.5}V_{0.5}Eu_{0.22}$
$LiW_{0.5}Mo_{0.5}Eu_{0.17}Ce_{0.06}$
$LiW_{0.5}Mo_{0.5}Eu_{0.17}Bi_{0.06}$
$LiW_{0.5}Mo_{0.5}Eu_{0.17}Cr_{0.06}$
$LiW_{0.5}Mo_{0.5}Eu_{0.21}Cr_{0.01}$

Cerium, bismuth and chromium were all investigated as coactivators. Amounts varied from 5% to 30% of the europium content, though in no case was there an increase in emission. For the higher concentrations of coactivators, in all cases the luminescene decreased strongly. This would be expected at higher concentrations due to quenching (see section 1.4.2). Literature values for the coactivator relative concentration vary from 5% to 100% [22] [23].

Attempts in changing the structure to improve the luminous efficacy include the replacement of molybdenum with vanadium or silicon. Two of the formulas attempted were $LiEu_{0.22}W_{0.78}Si_{0.22}$ and $LiEu_{0.22}W_{0.5}V_{0.5}$. However, neither of these showed any promise in an increase in luminescence. Under 254nm, 366nm and 465nm excitation no luminescence was visible, with a minor amount captured using an integrating sphere. Measured with the Bentham Spectrometer, over the range of wavelengths from 200nm to 500nm, the excitation spectra showed little difference to the above elements. One example of this is depicted in figure 4.6.
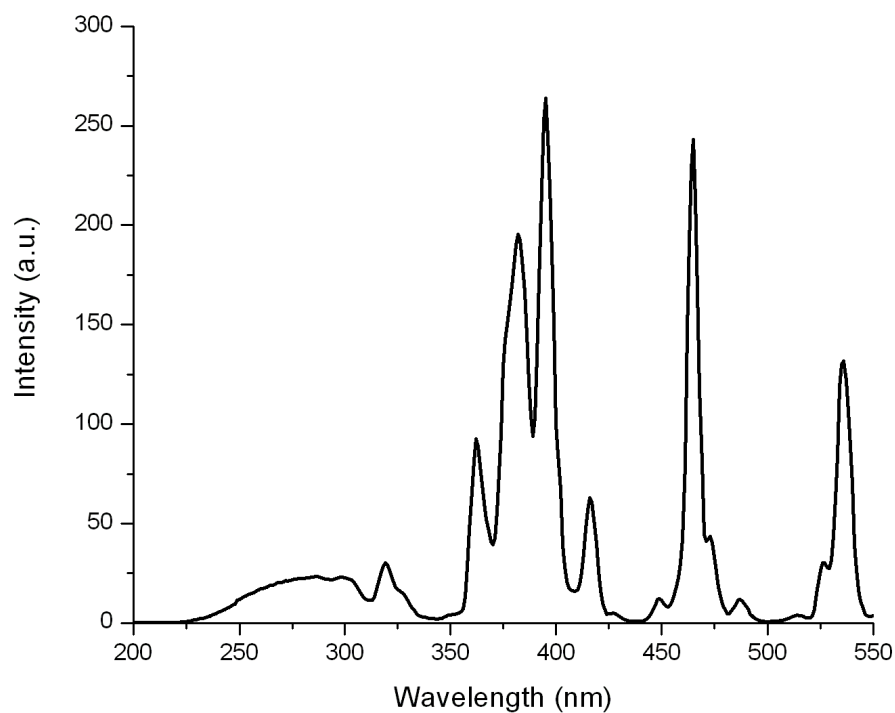
Figure 4.6: Excitation spectrum for $LiEu_{0.22}W_{0.78}Si_{0.22}$ monitored at 615nm

4.7 Conclusion

Many novel phosphors were created and presented in this chapter, either in respect of the host lattice or reduced europium content, although none of them were able to emit at a high efficacy. As with other Eu^{3+} tungstates and molybdates they have useful properties, notably the excitation bands in the right region for blue excitation. Whilst none of these will be suitable for commercial use or deemed worthy of continued investigation due to the low luminous efficacy, there was one compound which when added showed a large increase to the lumen output and that was aluminium oxide. Its incorporation and the effects thereof are discussed at length in the following chapter.

References

[1] Kun Fu, Zheng-Ping Wang, Zhen-Xiang Cheng, Jun-Hai Liu, Ren-Bo Song, Huan-Chu Chen, and Zong-Shu Shao. Effect of Nd^{3+} concentration on the laser performance of a new laser crystal: $Nd:NaY(WO_4)_2$. *Optics & Laser Technology*, 33:593 − 595, 2001.

[2] Taehyung Kim and Shinhoo Kang. Potential red phosphor for UV - white LED device. *Journal of Luminescence*, 122-123(2):964 − 966, 2007.

[3] A. Kaminskii et al. Properties of n^{3+}-doped and undoped tetragonal $PbWO_4$, $NaY(WO_4)_2$, $CaWO_4$, and undoped monoclinic $ZnWO_4$ and $CdWO_4$ as laser-active and stimulated raman scattering-active crystals. *Applied Optics*, 38(21):4533 − 4547, 1999.

[4] V. B. Mikhailik, I. K. Bailiff, H. Kraus, P. A. Rodnyi, and J. Ninkovic. Two-photon excitation and luminescence of a $CaWO_4$ scintillator. *Radiation Measurements*, 38(4-6):585 − 588, 2004. Proceedings of the 5th European Conference on Luminescent Detectors and Transformers of Ionizing Radiation (LUMDETR 2003).

[5] G. Urretavizcaya, F. Tonus, E. Gaudin, J.-L. Bobet, and F.J. Castro. Formation of tetragonal hydrogen tungsten bronze by reactive mechanical alloying. *Journal of Solid State Chemistry*, 180(10):2785 − 2789, 2007.

[6] Facundo J. Castro, Florent Tonus, Jean-Louis Bobet, and Guillermina Urretavizcaya. Synthesis of hydrogen tungsten bronzes H_xWO_3 by reactive mechanical milling of hexagonal WO_3. *Journal of Alloys and Compounds*, 495(2):537 − 540, 2010. 15th International Symposium on Metastable, Amorphous and Nanostructured Materials.

[7] Anders Hjelm and Claes G. Granqvist. Electronic structure and optical properties of WO_3, $LiWO_3$, $NaWO_3$ and HWO_3. *Journal of Luminescence*, 54(4):2436 − 2445, 1996.

[8] M.V. Nazarova, D.Y. Jeona, J.H. Kanga, E.J. Popovicib, L.E. Muresanb, M.V. Zamoryanskayac, and B.S. Tsukerblatd. Luminescence properties of europium-terbium double activated calcium tungstate phosphor. *Solid State Communications*, 131:307 − 311, 2004.

[9] L. F. Johnson, G. D. Boyd, K. Nassau, and R. R. Soden. Continuous operation of a solid-state optical maser. *Phys. Rev.*, 126(4):1406 – 1409, 05 1962.

[10] L.F. Johnson. Optical maser characteristics of rare-earth ions in crystals. *J. Appl Phy*, 34:897 – 912, 1963.

[11] Jeong Ho Ryu, Sin Young Bang, Jong-Won Yoon, Chang Sung Lim, and Kwang Bo Shim. Pulsed laser induced synthesis of scheelite-type colloidal nanoparticles in liquid and the size distribution by nanoparticle tracking analysis. *Applied Surface Science*, 253(20):8408 – 8414, 2007.

[12] R. Grasser and A. Scharmann. Luminescent sites in $CaWO_4$ and $CaWO_4$:Pb crystals. *Journal of Luminescence*, 12-13:473 – 478, 1976.

[13] Michael J. Treadaway and Richard C. Powell. Luminescence of calcium tungstate crystals. *The Journal of Chemical Physics*, 61(10):4003 – 4011, 1974.

[14] Cláudia A. Kodaira, Hermi F. Brito, and Maria Cláudia F. C. Felinto. Luminescence investigation of Eu^{3+} ion in the $RE_2(WO_4)_3$ matrix (RE = La and Gd) produced using the Pechini method. *Journal of Solid State Chemistry*, 171(1-2):401 – 407, 2003. Proceedings from the 23rd Rare Earth Research Conference UC Davis Campus, July 13-16, 2002.

[15] M.V. Nazarov, B.S. Tsukerblat, E.-J. Popovici, and D.Y. Jeon. Optical lines in europium-terbium double activated calcium tungstate phosphor. *Physics Letters A*, 330(3-4):291 – 298, 2004.

[16] Shikao Shi, Jing Gao, and Ji Zhou. Effects of charge compensation on the luminescence behavior of Eu^{3+} activated $CaWO_4$ phosphor. *Optical Materials*, 30:1616 – 1620, 2008.

[17] Chuang-Hung Chiua, Ming-Fang Wang, Chi-Shen Leeb, and Teng-Ming Chen. Structural, spectroscopic and photoluminescence studies of $LiEu(WO_4)_{2-x}(MoO_4)_x$ as a near-UV convertible phosphor. *Journal of Solid State Chemistry*, 180:619 – 627, 2007.

[18] Fang Lei and Bing Yan. Hydrothermal synthesis and luminescence of $CaMO_4$:RE^{3+} (M=W, Mo; RE=Eu, Tb) submicro-phosphors. *Journal of Solid State Chemistry*, 181(4):855 – 862, 2008.

[19] Chaunxiang Qin, Yanlin Huang, Guoqiang Chen, Liang Shi, Xuebin Qiao, Jiuhui Gan, and Hyo Jin Seo. Luminescence properties of a red phosphor europium tungsten oxide Eu_2WO_6. *Materials Letters*, 63:1162 – 1164, 2009.

[20] Kyu-Seog Hwang, Young-Sun Jeon, Seung Hwangbo, and Jin-Tae Kim. Red-emitting $LiEuW_2O_8$ phosphor for white emitting diodes prepared by sol-gel process. *Optica Applicata*, 39(2):375 – 382, 2009.

[21] Kyu-Seog Hwang, Seung Hwangbo, and Jin-Tae Kim. Sol-gel synthesis of red-emitting LiEuW$_2$O$_8$ powder as near-ultraviolet convertible phosphor. *Ceramics International*, 35:2517 – 2519, 2009.

[22] S Neeraj, N Kijima, and A.K Cheetham. Novel red phosphors for solid state lighting; the system Bi$_x$Ln$_{1-x}$VO$_4$; Eu^{3+}/Sm^{3+} (Ln=Y, Gd). *Solid State Communications*, 131(1):65 – 69, 2004.

[23] W.J. Park, M.K. Jung, and D.H. Yoon. Influence of Eu^{3+}, Bi^{3+} co-doping content on photoluminescence of YVO$_4$ red phosphors induced by ultraviolet excitation. *Sensors and Actuators B*, 126:324 – 327, 2004.

Chapter 5

Novel Efficient Phosphors

Serendipity often plays a role in new discoveries, from the glue of post–it notes, to the discovery of penicillin. Although it would be satisfying to proclaim the following novel phosphors were discovered through foresight and ingenuity, in this case, there was a moment of fortune where materials fired at too high a temperature has led to the possibilities of a novel phosphor.

The investigation into new phosphors led to two discoveries of phosphor with host lattices of the form $A_x Eu_y (WO_4)(MoO_4)$. One involved the substitution of yttrium for europium $(A_x Eu_y Y_{1-y}(WO_4)(MoO_4))$ without a loss in efficacy. The second was a novel phosphor which included aluminium and whose properties showed great promise for luminescent applications.

5.1   Alumina

The phosphor $LiEu_{0.22}(WO_4)_{0.5}(MoO_4)_{0.5}$ was synthesised by the solid state method as described in section 4.2. This was fired in an alumina crucible over a range of temperatures, the highest of which was $1400°C$, for 3 hours. They were placed in the furnace at $200°C$ and the temperature was increased at a rate of $19°C$ per minute until the desired firing temperature was reached. This temperature was held for 1–3 hours after which the phosphors were cooled to room temperature at ~$10°C$ per minute. The interesting phosphor, prepared at $1400°C$, was removed from the furnace to find that the majority of this phosphor had either vaporised or infused into the crucible.

Under 366nm UV illumination, the crucible emitted a red light, measured in the Bentham spectrometer with a peak wavelength of 615nm. This indicated an emission due to the europium in its 3+ oxidation state was now present in the crucible and behaved as an activator. To investigate whether this affected just the surface of the crucible, it was cut into two pieces and again illuminated with UV emission, as seen in figure 5.1.

Two conclusions can be drawn from this image; firstly the emission was present throughout the cross section of the crucible and not just the surface, and secondly, this emission was not present in the lower half of the crucible. This second finding was also important as it elucidates the source of the emission. One of the components

Figure 5.1: Image taken showing the cross section of the crucible under 366nm UV radiation where europium has infused into its structure

of the crucible materials is Cr^{3+} which could have been causing this effect. However, from this image it was clear that the lower region of the crucible, which was not in contact with the phosphor powder, did not illuminate at all. This indicated that the phosphor was the cause of this emission and that the structure of the crucible played some part as a host lattice, or affected the host lattice, with an increased luminous flux relative to the phosphor $Eu_{0.22}Li(WO_4)_{0.5}(MoO_4)_{0.5}$. The remaining phosphor powder that was present in the crucible did not appear as bright as the crucible to the naked eye under 366nm illumination. This powder was then tested to measure its luminous efficacy at 615nm emission and found to be $20.6\,lm/W$ at a 365nm excitation wavelength and $120.9\,lm/W$ at 465nm excitation.

$LiEu(WO_4)(MoO_4)$ was synthesised by the same solid state method to compare to this phosphor. XRD data for $LiEu_{0.22}(WO_4)_{0.5}(MoO_4)_{0.5}$ showed all the peaks of that of a known phosphor $LiEu(WO_4)(MoO_4)$ [1] with some additional peaks and is shown in figure 5.2.

This suggested that the former compound has a formulation of the type $(Li_xEu_y)(MoO_4)(WO_4)$ with an excess of some materials or another phase formed. Lattice parameters remained almost identical and are shown in 5.1, confirming this as the same material, albeit with less europium present. $LiEu_{0.22}(WO_4)_{0.5}(MoO_4)_{0.5}$ underwent EDX analysis and showed a 1:1 tungsten to molybdenum ratio, as expected based upon the starting materials. This evidence suggests that the new compound is nonstoichiometric.
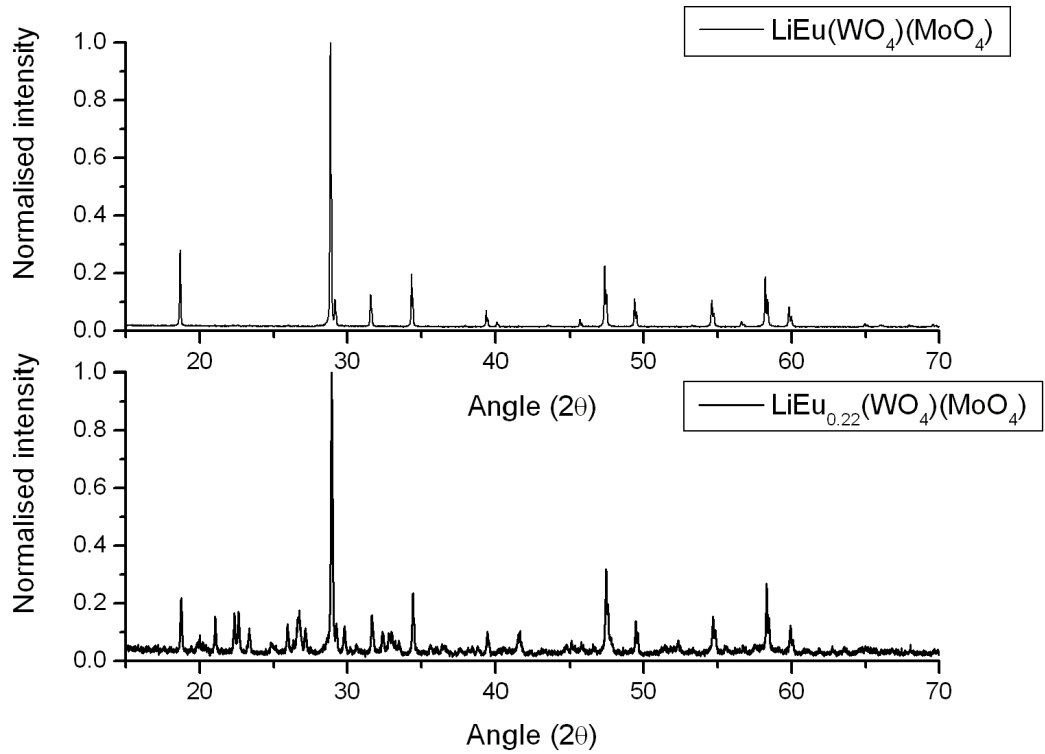
Figure 5.2: XRD overlay showing similarity in phosphors $\text{LiEu}(\text{WO}_4)_{0.5}(\text{MoO}_4)_{0.5}$ and $\text{LiEu}_{0.22}(\text{WO}_4)_{0.5}(\text{MoO}_4)_{0.5}$

Table 5.1: Comparison of lattice parameters with less europium present

	$\text{LiEu}_{0.22}(\text{WO}_4)_{0.5}(\text{MoO}_4)_{0.5}$	$\text{LiEu}(\text{WO}_4)_{0.5}(\text{MoO}_4)_{0.5}$
a (Å)	10.424	10.425
b (Å)	5.214	5.209
c (Å)	6.754	6.745
alpha (°)	112.73	112.73
beta (°)	112.74	112.67
gamma (°)	90.05	90.03

5.2 Aluminium Oxide as Part of the Lattice

The crucible is primarily composed of α-aluminium oxide and so this compound was incorporated into the phosphor starting materials in an attempt to increase the luminous efficacy. These were formed by the solid state method, as described in section 4.2 with the addition of alpha Al_2O_3. The addition of α-aluminium oxide produced phosphors with the general formula:

$$\text{AEu}_{0.22}\text{Al}(\text{WO}_4)_{0.5}(\text{MoO}_4)_{0.5} \text{ where A} = (\text{Li, K, Na}), \tag{5.1}$$

These phosphors were measured for their 615nm emission over two of their peak wavelengths with excitation at 390nm and 470nm. The lithium variant had the greatest measured efficacy as seen in table 5.2.

Table 5.2: Luminous efficacy values of phosphors, measured at 615nm emission

Phosphor formula	470nm excitation efficacy value	390nm excitation efficacy value
Li Eu$_{0.22}$Al(WO$_4$)$_{0.5}$(MoO$_4$)$_{0.5}$	145.4	359.5
NaEu$_{0.22}$Al(WO$_4$)$_{0.5}$(MoO$_4$)$_{0.5}$	68.5	79.4
K Eu$_{0.22}$Al(WO$_4$)$_{0.5}$(MoO$_4$)$_{0.5}$	42.7	47.5

The excitation and emission spectra of these phosphors were quite similar to each other as would be expected and are seen in figures 5.3 and 5.4. The excitation spectra (figure 5.3) showed they all have peaks in the same locations, with the relative heights of each peak differing as the alkali metal is changed. The trend was to higher peaks for lower atomic numbers. Generally, lithium had a higher peak and potassium showed lower peaks. The exception was for the sodium phosphor which showed a slightly higher excitation peak at 473nm and 535nm wavelengths, but fit the trend for all other excitation peaks. The emission spectra (figure 5.4) for lithium and sodium were very similar with the main emission peak split into a double peak at 612nm and 615nm; the 615nm peak was of greater luminous efficacy. However, the potassium phosphor had just one peak emission located at 613nm.

This difference in emission between the spectra at the peak wavelength is associated with the structure of the lattice and crystal field perturbations to which the Eu^{3+} ion will be subjected. While the positions of the peak will not change, the relative strength of the peaks can be affected [2]. This would indicate that the size of the potassium ion has caused an increase in bond length which has affected the structure and is seen in the lattice.

The 615nm and 700nm peaks were the strongest and it was possible to ascribe these to the electric dipole transition of ^{5}D$_0$ –> ^{7}F$_{2,4}$ which were the dominant transitions. This is due to the Eu^{3+} ions sitting in noncentrosymmetric lattice sites. The magnetic dipole transitions of ^{5}D$_0$ –> ^{7}F$_{1,3}$ were weaker, present at around 595nm and 700nm. The ^{5}D$_1$ –> ^{7}F$_j$ transitions, located between 520–570nm. These transitions are well known and described in the literature [1].

XRD analysis showed that only the lithium material contained the same structure as the earlier material, LiEu$_{0.22}$(WO$_4$)$_{0.5}$(MoO$_4$)$_{0.5}$. Lattice parameters were calculated and compared for this phase and showed similarities as seen in table 5.3. The changes in parameters indicate that the size of the lattice decreased. This would suggest that the smaller aluminium ion had replaced some of the europium ions in the lattice. The analysis for LiEu$_{0.22}$Al(WO$_4$)$_{0.5}$(MoO$_4$)$_{0.5}$ also showed a large excess of Al$_2$O$_3$ in the spectrum, analysed in section 5.3.2.

All the phosphors made based on equation 5.1 had poor uniformity with some of the powder emitting low levels of light due to an excess of aluminium. The alkali cation lithium, showed the highest brightness and so the aluminium content of LiEu$_{0.22}$Al$_x$(WO$_4$)$_{0.5}$(MoO$_4$)$_{0.5}$ was selected for further investigation. The aluminium content, x, was adjusted in an attempt to increase the efficacy and improve the uni-
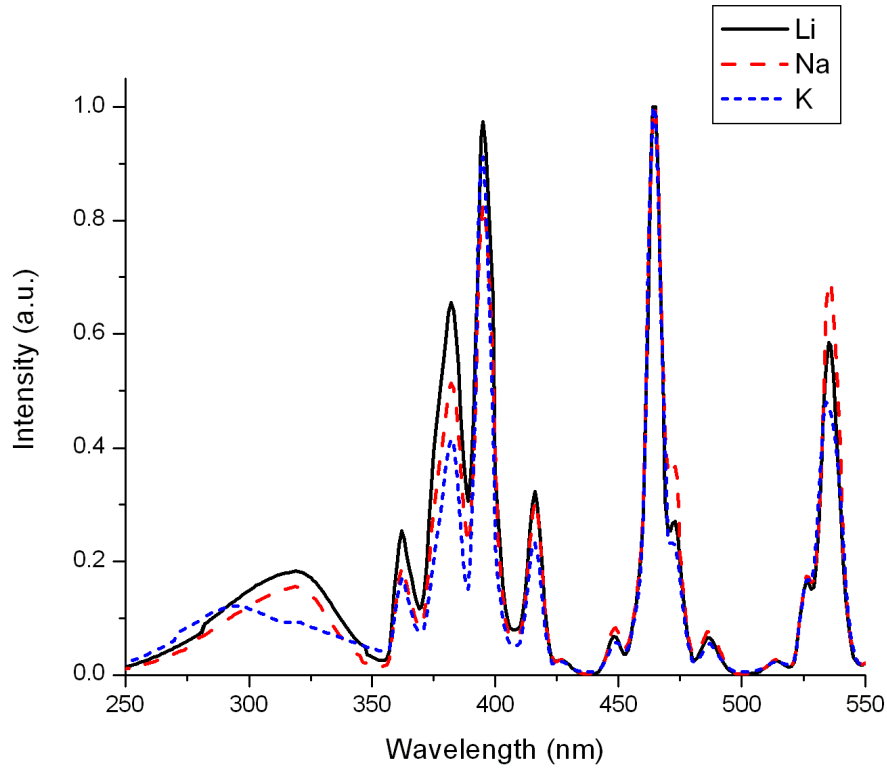
Figure 5.3: Excitation spectra overlay of alakli metal aluminium phosphors, measured at 615nm

Table 5.3: Comparison of lattice parameters with and without aluminium

	$LiEu_{0.22}(WO_4)_{0.5}(MoO_4)_{0.5}$	$LiEu_{0.22}Al(WO_4)_{0.5}(MoO_4)_{0.5}$
a (Å)	10.424	10.420
b (Å)	5.214	5.211
c (Å)	6.754	6.746
alpha (°)	112.73	112.73
beta (°)	112.74	112.66
gamma (°)	90.05	89.93

formity of the emission. The efficacy measurements are seen in figure 5.5. These results show that decreasing the aluminium content decreases slightly the emission at higher excitation wavelengths. However, to ensure that the phosphor powder emits at uniform luminosity, the aluminium content was reduced to below the peak measured efficacy. Without a uniform luminosity the phosphor will not be suitable to any applications and as such the removal of an excess of aluminium (or aluminium oxide) was a key constraint in the synthesis of the phosphor.
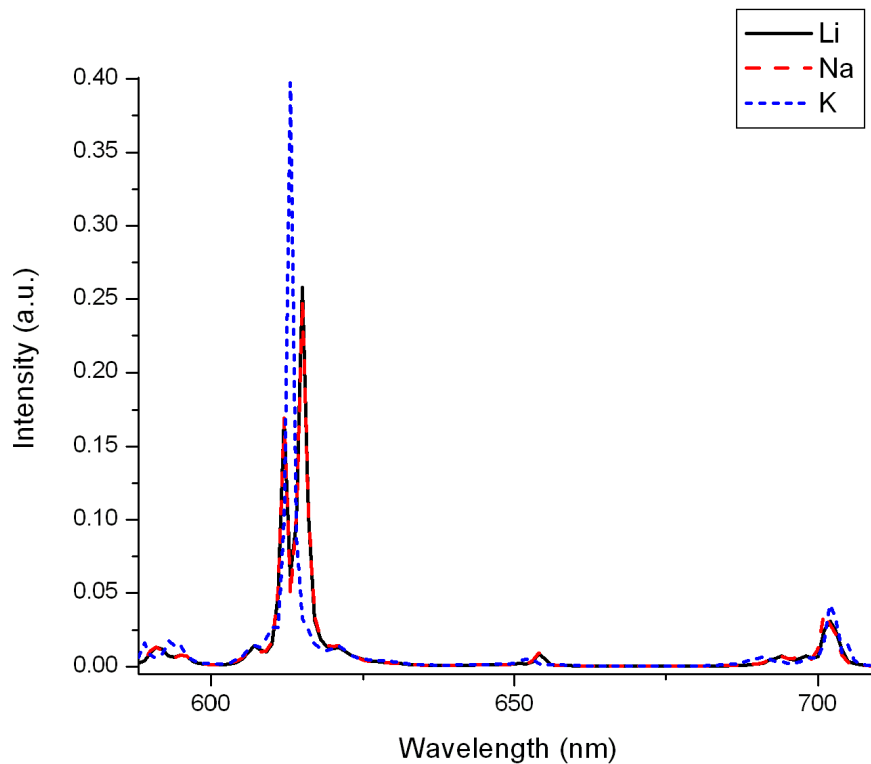
Figure 5.4: Emission spectra overlay of alkali metal aluminium phosphors, measured at 615nm
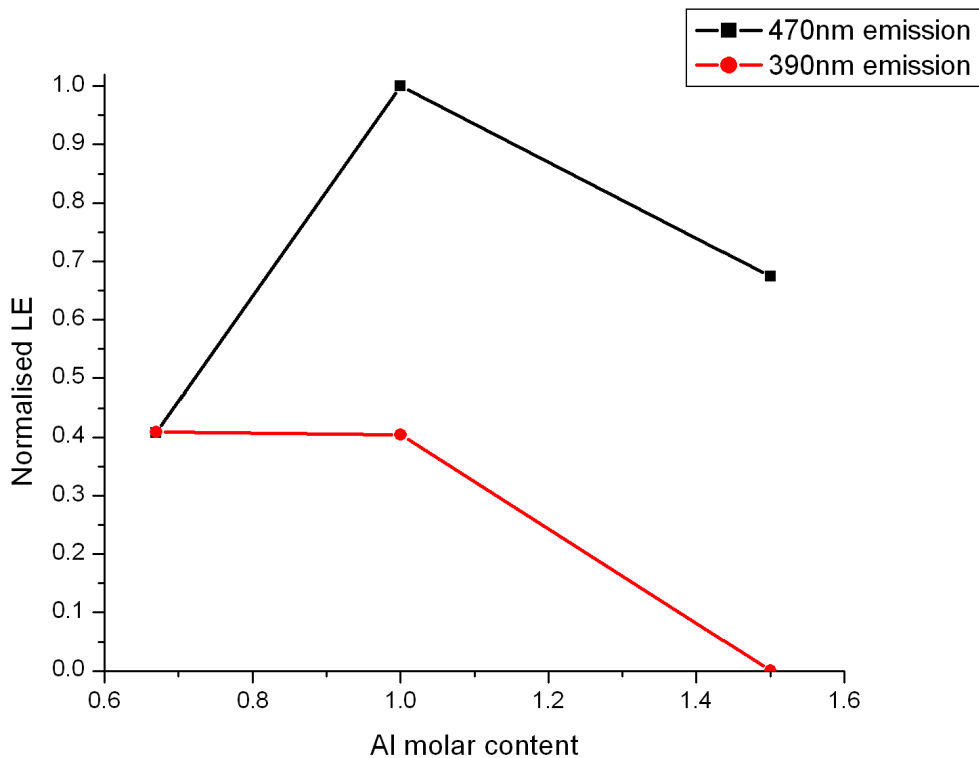
Figure 5.5: Luminous efficacy of $LiEu_{0.22}Al_x(WO_4)_{0.5}(MoO_4)_{0.5}$ as a function of aluminium content, x

5.3 Further Analysis of Phosphors

The starting materials, which form the structure of the phosphors described in the preceding sections of this chapter, were analysed and are presented below. Specifically, these are tungsten oxide, molybdenum oxide and aluminium oxide.

5.3.1 SEM of Starting Materials

All the starting materials are shown at both high and low magnification to see particle size and shape. As described in section 2.4 a large number of images were taken and a the selection shown here are typical images for each compound. They were viewed such that a comparison between the phosphor particles could be described at a later stage and any excess may be more easily identified. Tungsten oxide is shown at low magnification in figure 5.6 and high magnification in figure 5.7. The particles were seen to coalesce to form larger structures. The molybdenum oxide was more disordered with a wide range of particle sizes, seen in both the low and high magnification images of figures 5.8 and 5.9. The aluminium oxide used consisted of very small and very uniform particles, seen in figures 5.10 and 5.11.
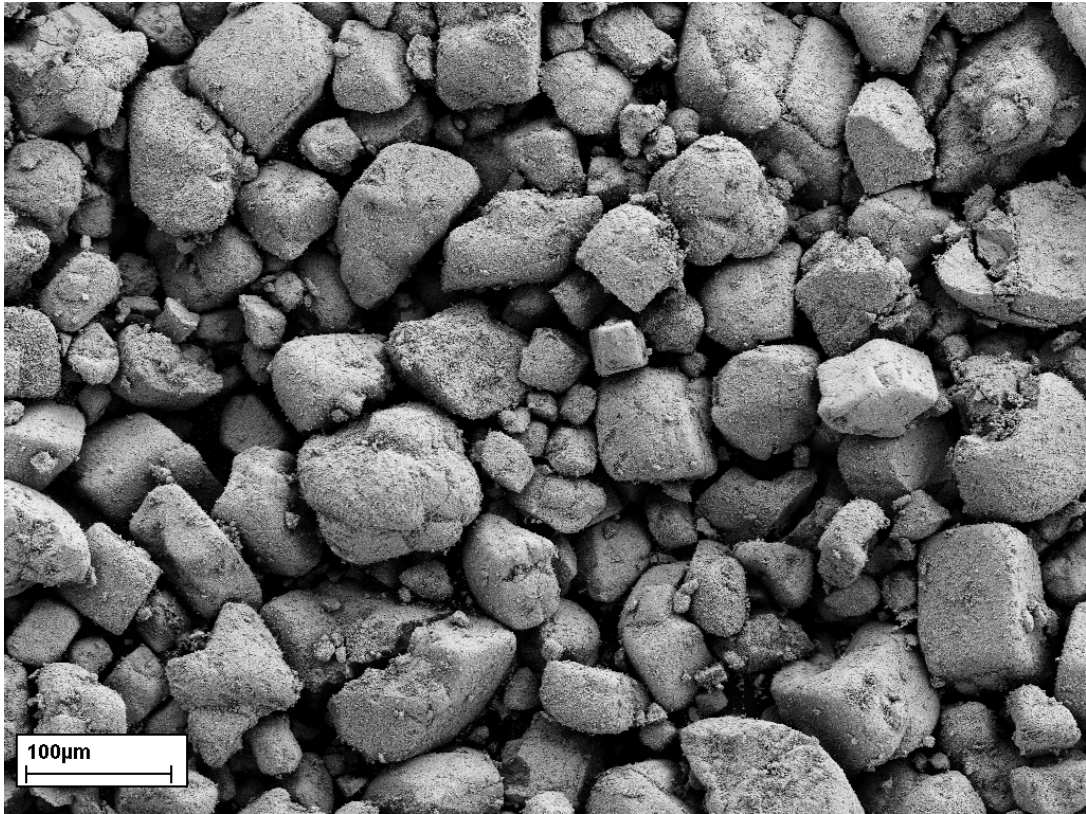
Figure 5.6: Low magnification SEM image of tungsten oxide
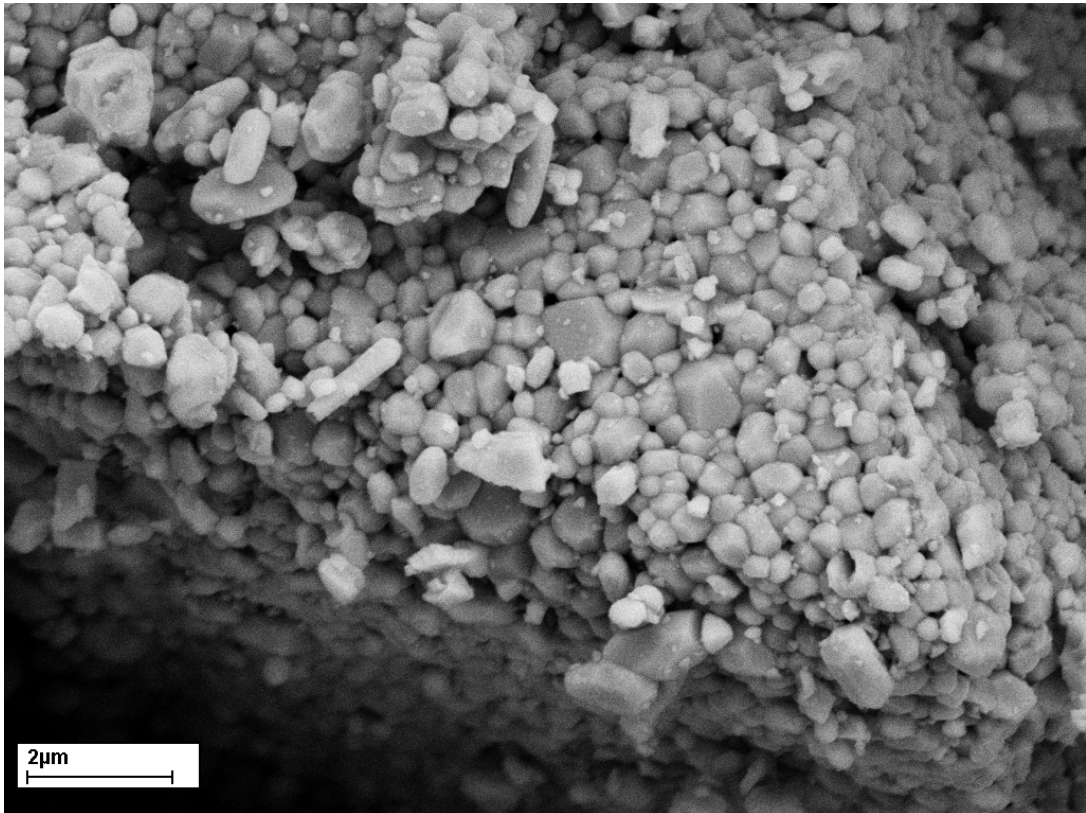
Figure 5.7: High magnification SEM image of tungsten oxide
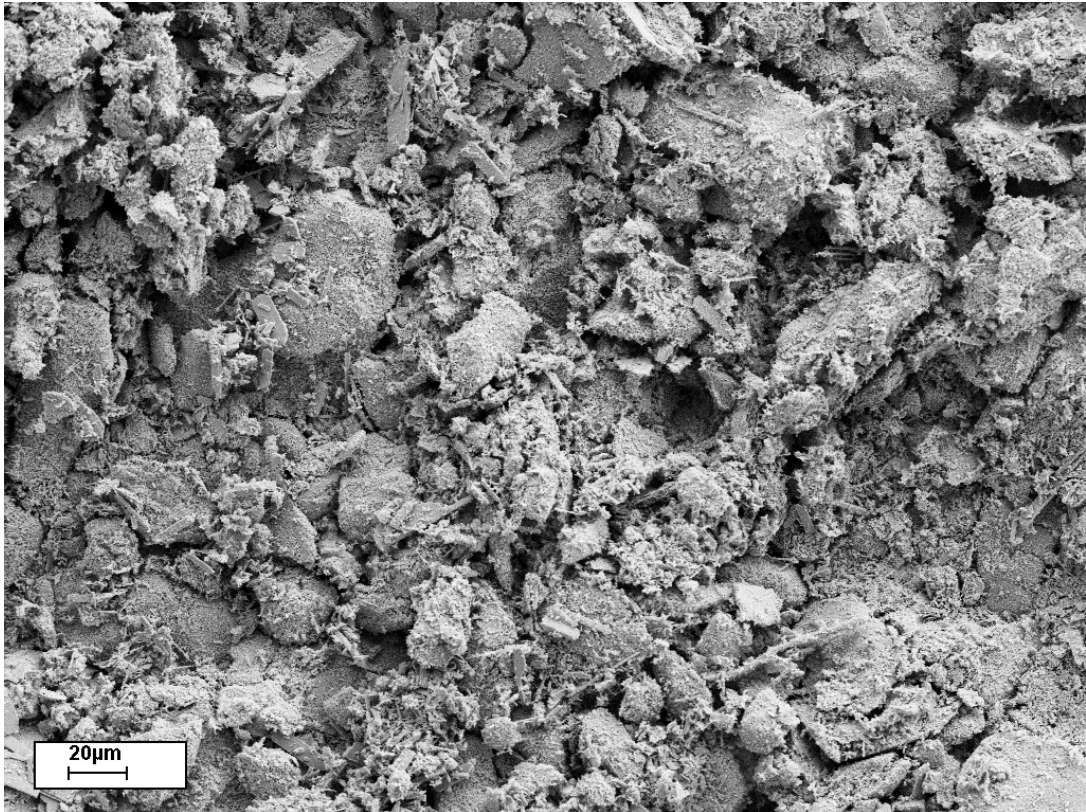
Figure 5.8: Low magnification SEM image of molybdenum oxide
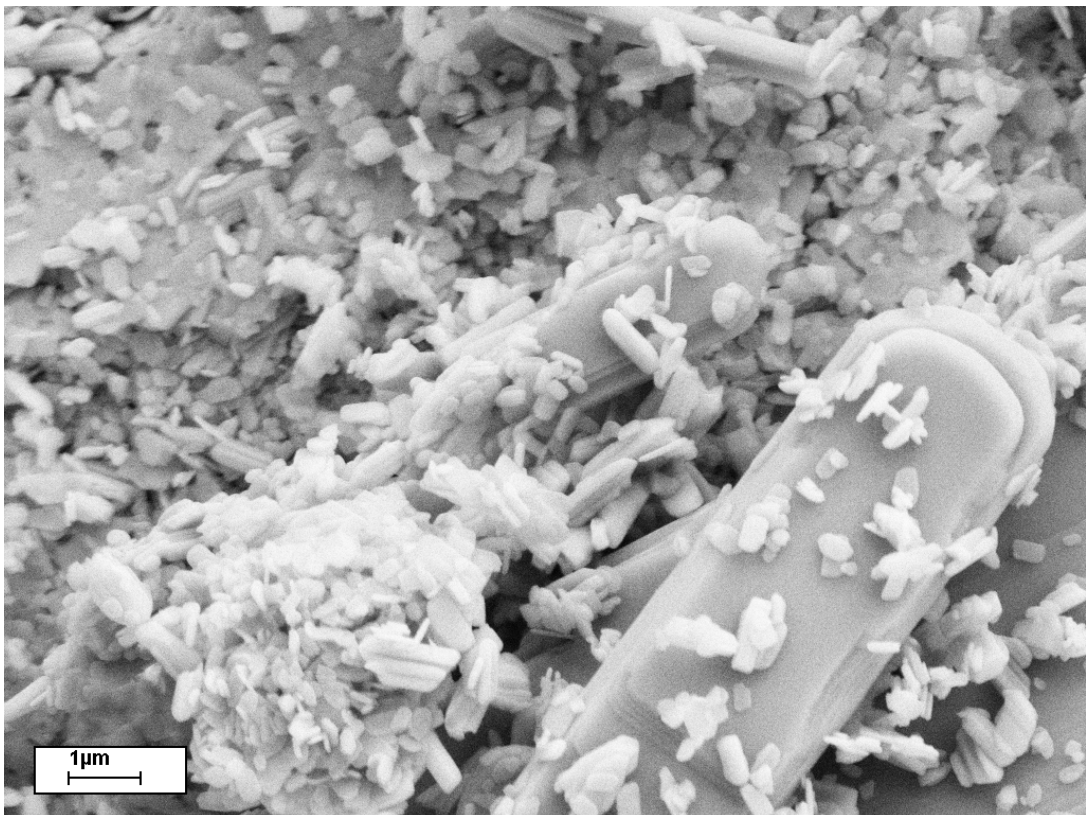
Figure 5.9: High magnification SEM image of molybdenum oxide
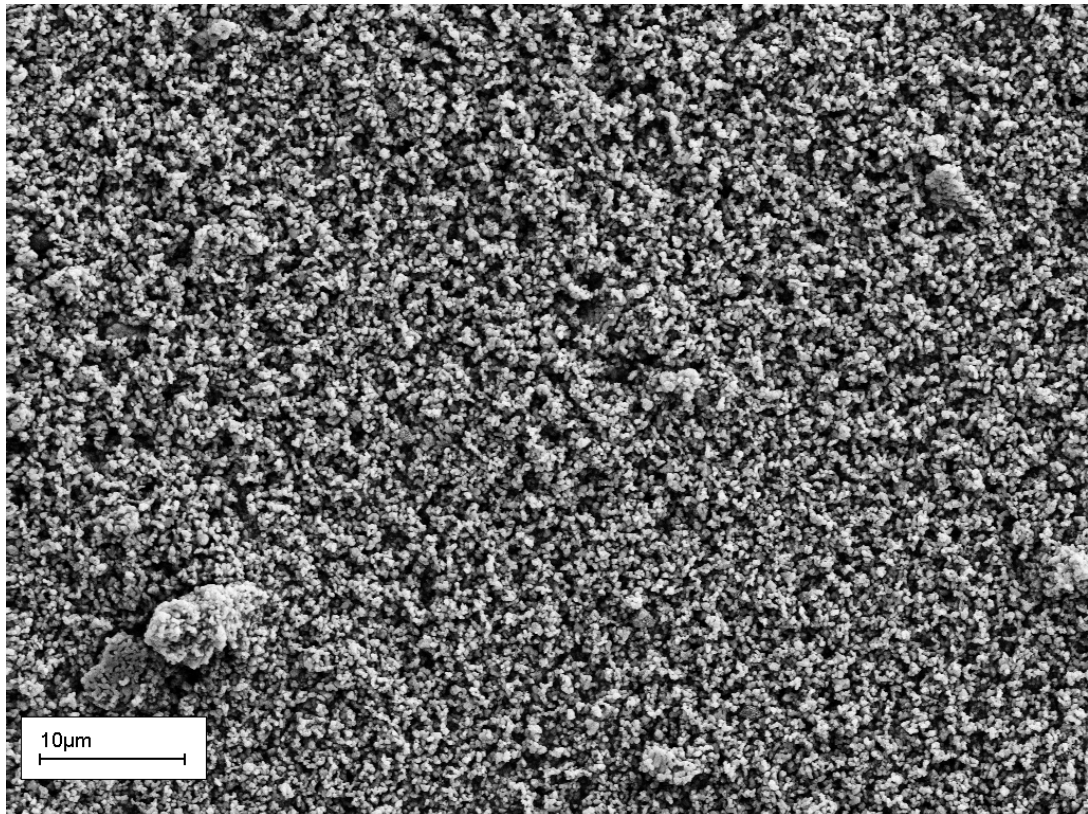
Figure 5.10: Low magnification SEM image of aluminium oxide
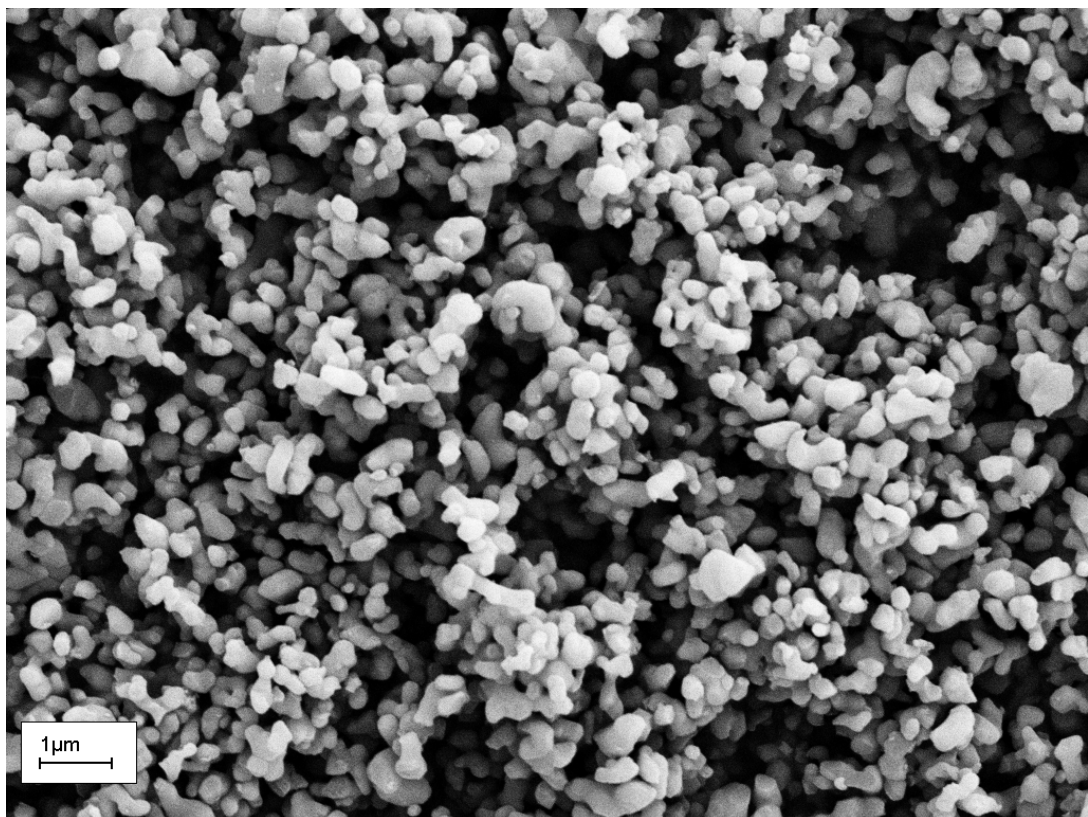
Figure 5.11: High magnification SEM image of aluminium oxide

5.3.2   SEM and XRD Analysis of Phosphors

The SEM images for the phosphors $LiEu_{0.22}Al_{1.5}(WO_4)_{0.5}(MoO_4)_{0.5}$ and $LiEu_{0.22}Al(WO_4)_{0.5}(MoO_4)_{0.5}$ are presented in figures 5.14 and 5.15 respectively, where the shape of the particles was seen to be markedly different. The only difference between these phosphors was the greater aluminium content in the starting materials of the former. This difference is attributed to the aluminium oxide in the starting materials which appeared to cause a difference to the crystal structure. However, as the luminous efficacy is the key property and took priority, as discussed in section 5.2, the lower aluminium content phosphors were those of most interest in this work.

They were compared with the starting materials to see if there was an excess of any of the starting materials. They showed an abundance of the particles of similar size and shape to the smaller particles in tungsten oxide without forming the larger structures seen in figure 5.7. It was difficult to infer from these much about the structural effect due to the greater aluminium content. XRD analysis was used to analyse the structures and is shown in figure 5.12. The top line shows the measured spectrum (blue) and calculated spectrum (red) with the difference between the two spectra illustrated on the line below in grey. In this case, an excess of aluminium oxide was identified from the data, along with the phosphor. There were however further peaks, which were not yet identified. They did not fit for any of the other starting materials, or combinations thereof and are currently unknown.
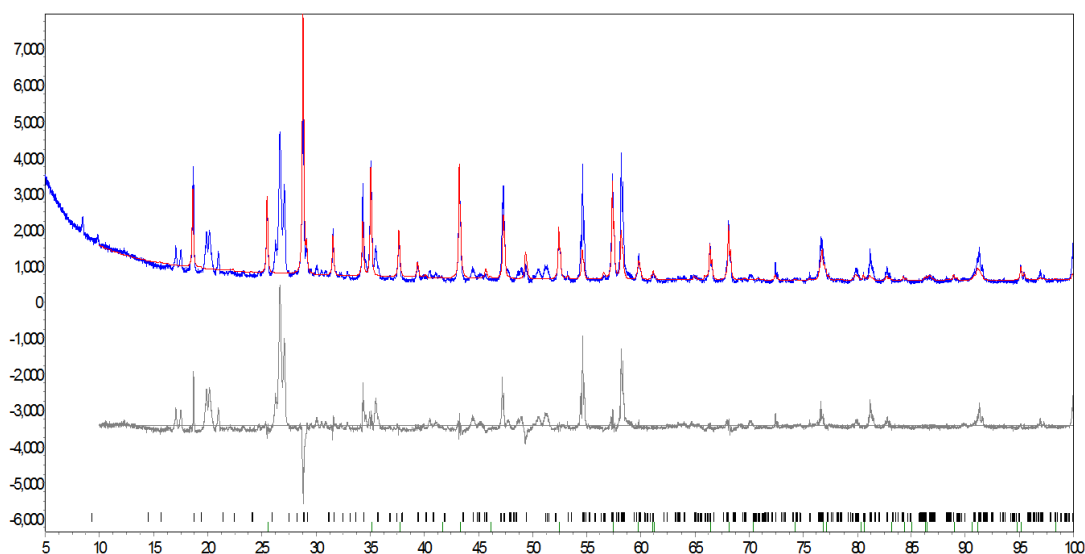
Figure 5.12: Partial fit for analysis of $LiEu_{0.22}Al(WO_4)_{0.5}(MoO_4)_{0.5}$

SEM images for these phosphors were compared and are presented in images 5.13, 5.14 and 5.15 which show no aluminium, 1 mole aluminium and 1.5 moles aluminium, respectively. The particles in the first showed some consistencies in particle size and shape with that in figure 5.14 and marked differences with that in figure 5.15.

Based on these SEM images along with efficacy measurements, the aluminium

content was decreased and gave a phosphor with the formula:

$$\text{Li}(\text{WO}_4)_{0.5}(\text{MoO}_4)_{0.5}\text{Eu}_{0.22}\text{Al}_{0.67}, \tag{5.2}$$
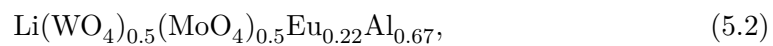
This led to a uniformly emitting higher luminous efficacy phosphor with a measured emission of $145\,\text{lm/W}$ at both 390nm and 470nm excitation. XRD analysis showed only a small excess of aluminium oxide.
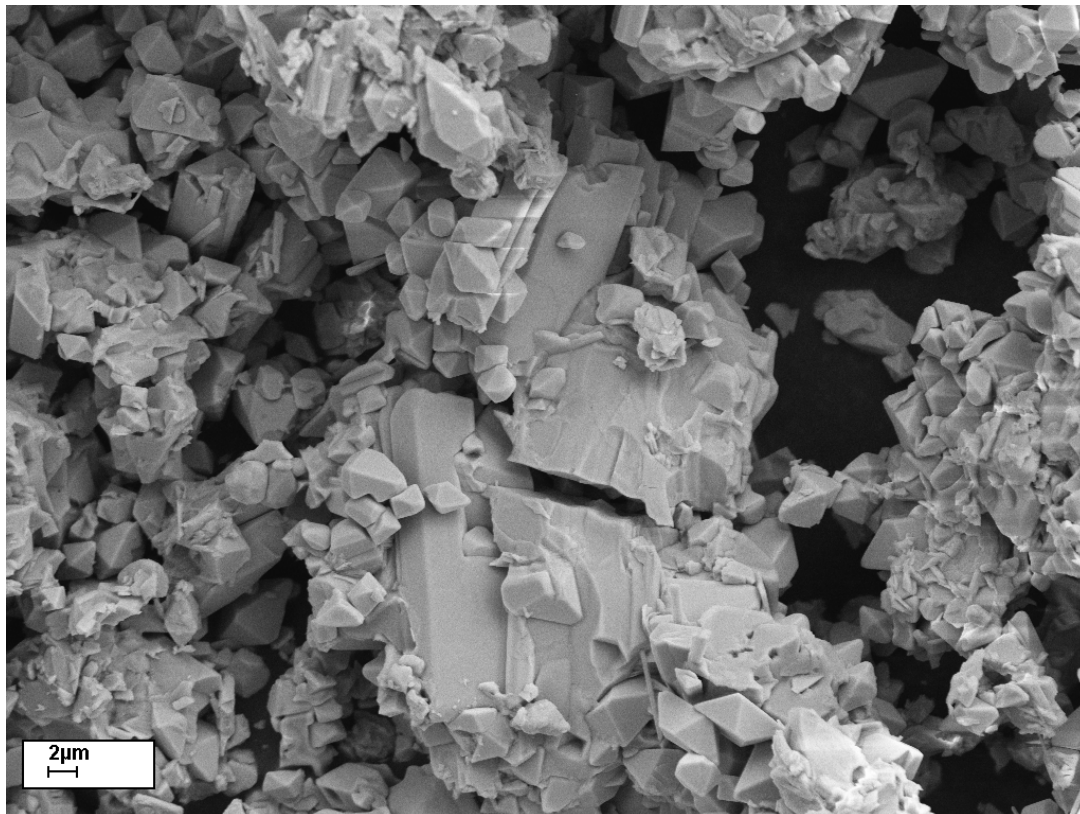
Figure 5.13: SEM image of $\text{LiEu}_{0.22}(\text{WO}_4)_{0.5}(\text{MoO}_4)_{0.5}$
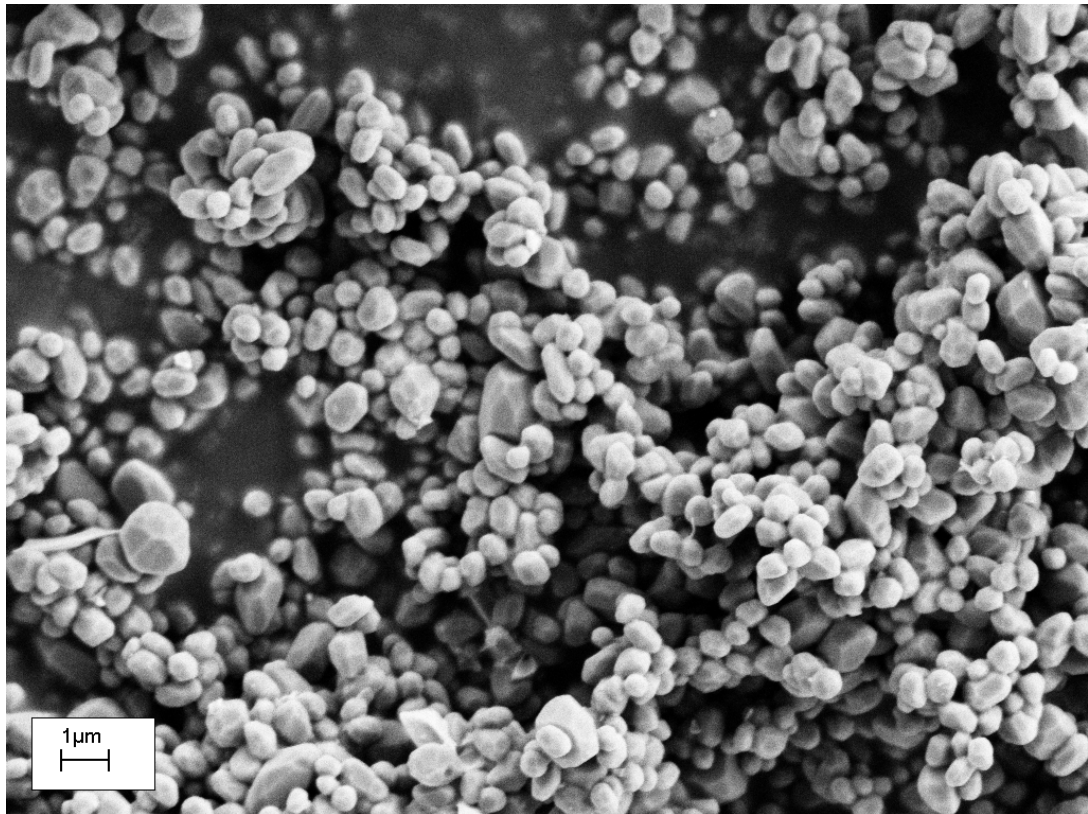
Figure 5.14: SEM image of $LiEu_{0.22}Al(WO_4)_{0.5}(MoO_4)_{0.5}$
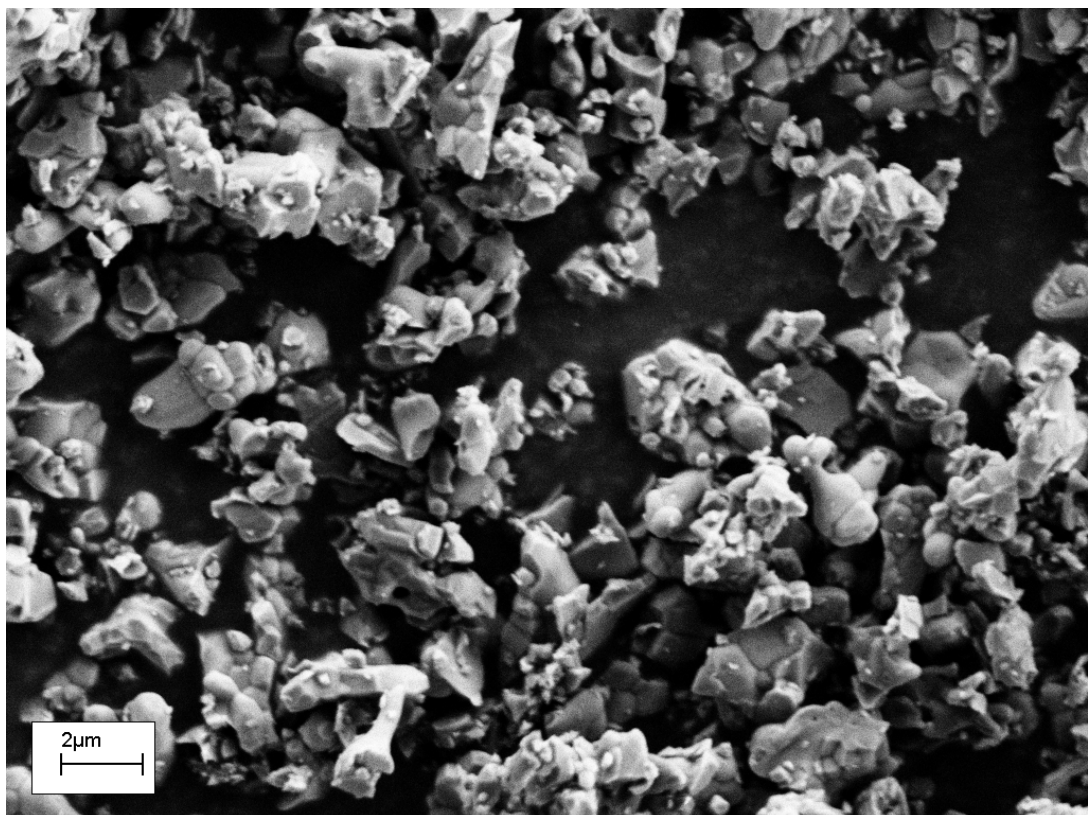
Figure 5.15: SEM image of $LiEu_{0.22}Al_{1.5}(WO_4)_{0.5}(MoO_4)_{0.5}$

5.4 Gadolinium

Gadolinium was substituted in place of aluminium to investigate the effect that this had on the properties of the phosphor. This was made by the solid state method described in section 4.2, with the addition of Gd_2O_3 as a starting material, creating the phosphor $Li(WO_4)_{0.5}(MoO_4)_{0.5}Gd_{0.67}Eu_{0.22}$. This was compared to the phosphor in equation 5.2 which contains aluminium in place of gadolinium, and is otherwise identical. These were compared in the Bentham Integrating Sphere over their measured excitation spectrum, emission spectrum and the luminous efficacies over a range of wavelengths. The efficacies can be seen in table 5.4.

Table 5.4: Comparison of phosphor efficacy utilising either aluminium or gadolinium, measured at 615nm

Composition	LE at excitation wavelength (lm/W)			
	470nm	465nm	395nm	365nm
Aluminium	44.44	127.57	116.18	17.81
Gadolinium	54.96	127.99	108.73	14.88
Relative efficacy	1.24	1.00	0.94	0.84
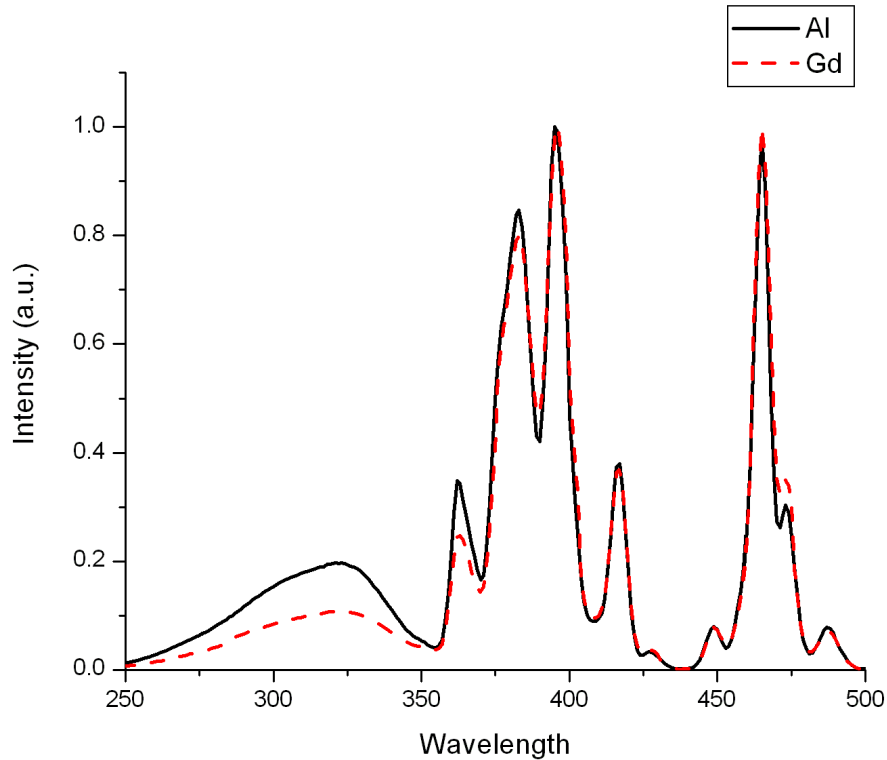
Figure 5.16: Aluminium and gadolinium excitation spectra comparison, measured at 615nm emission

The luminous efficacies were similar with the aluminium reading measured slightly higher at most wavelengths. The excitation spectrum for the aluminium and gadolin-

ium compositions were almost identical and they are seen in figure 5.16. The notable differences were a higher intensity C-T band for aluminium, and a higher peak in the gadolinium spectrum for the shoulder to the 465nm excitation and the peak at 473nm. This second difference could explain the higher measured emission at 470nm for gadolinium, whilst the lower results over all other wavelengths indicates the aluminium phosphor is a more efficient phosphor.

Recently, another phosphor research group has looked at the effects of the addition of gadolinium and aluminium in red emitting phosphor systems. Theirs comprises phosphors of the type $(Y,M)NbO_{4:}Eu^{3+}$ with (M: Gd, Al) [3]. They report that the crystal field distortions around the Eu^{3+} ions through the introduction of one of these elements led to a greater occupancy of asymmetry sites for Eu^{3+} ions and an associated increase in emission.

5.5 Samarium Oxide

Samarium oxide is a known coactivator of europium excited phosphors [4] [5], and has been used in red emitting phosphors based on tungsten structures [6]. Incorporating samarium in small quantities as a coactivator had the effect of increasing the emission from europium and this appears to be due to broadening in the excitation bands. Samarium was added to give the phosphor $Li(WO_4)_{0.5}(MoO_4)_{0.5}Al_{0.67}Eu_{0.22}Sm_{0.01}$, and the excitation spectra of these phosphors, with and without samarium, were compared and are shown in 5.17.

In order to correctly ascertain the line emissions and know whether the coactivator is making a direct contribution to the emission, samarium and europium were looked at when used separately as well as when combined. This has previously been done for other tungsten based phosphors, where the excitation and emission were measured, showing that samarium alone makes little contribution [7]. The effect samarium had when added was primarily in energy transfer to the europium ion from where the photons were emitted.

5.6 Optimisations

The stoichiometry of the phosphors was altered in attempts to improve the properties of the phosphors in accordance with the aims set out at the onset of this work (section 1.1). This includes an increase the efficacy of this phosphor, synthesis of a uniform particle size and to decrease its hardness. Further, the conditions in the production of the phosphor were varied to optimise these same properties. While the requirements of the properties will likely vary depending on their application, a higher efficacy and quantum efficiency will always be desirable. The initial optimisation conditions began with looking at the lattice structure, specifically, the tungsten to molybdenum ratio.
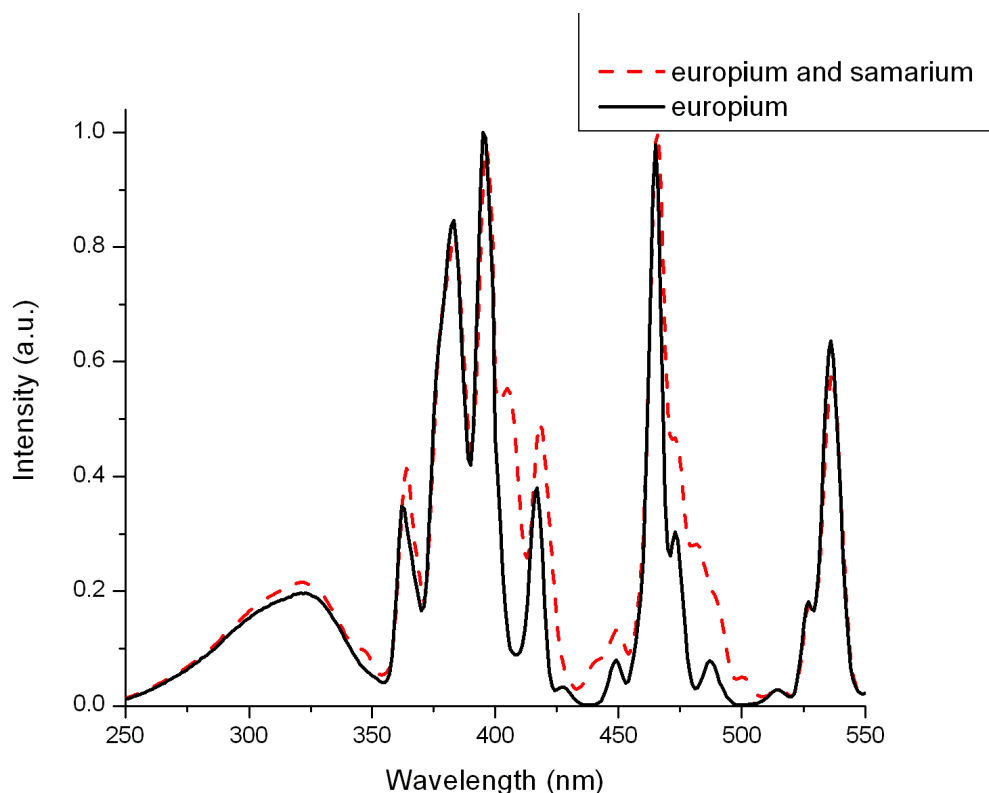
Figure 5.17: Line broadening in the excitation spectrum when samarium is added as a coactivator

5.6.1 Tungsten Molybdenum ratio

For phosphors which have a structure based on double tungstates, molybdenum is a possible replacement for all or part of the tungsten as mentioned in section 4.4. For the most promising of the phosphors listed above, $LiEu_{0.22}(WO_4)_{1-x}(MO_4)_x$, x was varied from 0 to 2 in 0.2 steps. The graph in figure 5.18 shows the luminous efficacy values of the phosphors measured in an integrating sphere, excited at 470nm, 465nm and 390nm wavelengths. When measured at their peak excitation wavelength, these phosphors had a peak luminous efficacy of 120 lm/W.

The high content tungsten phosphors were measured to have a greater luminous efficacy, through the inclusion of some molybdenum, this lead to a higher performance when excited 470nm. As this was the key excitation wavelength, some molybdenum was included in the phosphors created.

5.6.2 Tungstic acid

Particle size plays an important role in both luminous flux and applicability of the phosphors. The ideal is to create a uniform sub-micron phosphor without any reduction in the luminous efficacy, as it will be suited to most applications. To try to improve the consistency and reduce the hardness of the final phosphor tungstic acid was substituted in place of tungsten oxide as a starting material. To test this ef-
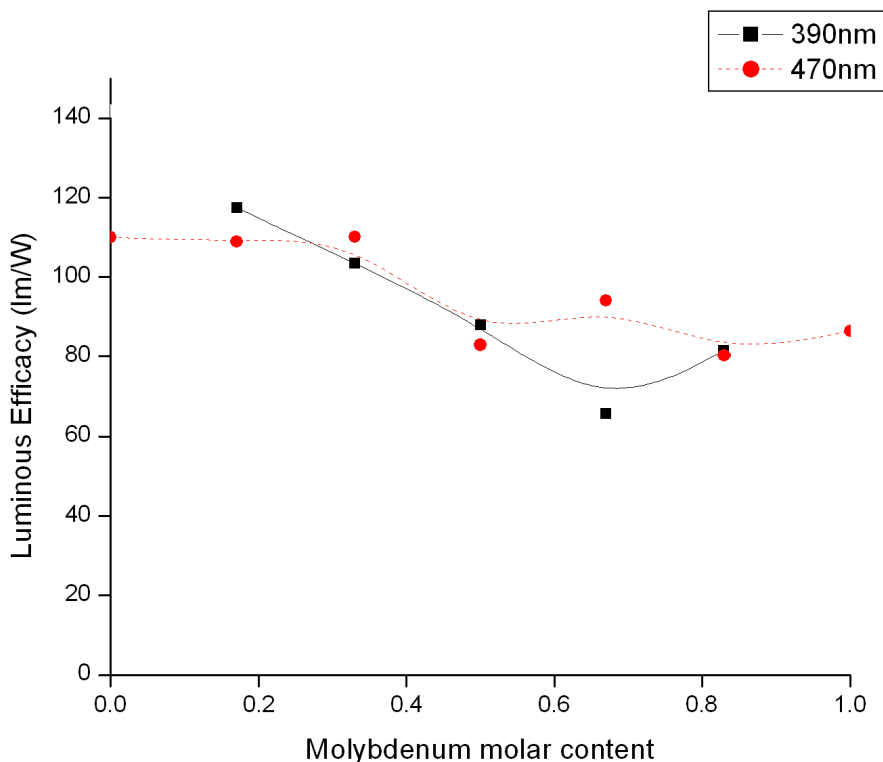
Figure 5.18: Efficacy values over varying molybdenum-tungsten content

fect, some of the phosphors described earlier were repeated and used as a comparison. These results are presented below in table 5.5.

Table 5.5: Luminous efficacy measurements comparing tungsten oxide and tungstic acid as starting materials

Phosphor	Material	Efficacy
$LiEu_{0.22}W_{0.33}M_{0.67}Al_{0.67}Sm_{0.01}$	Tungsten Oxide	63.1
	Tungstic Acid	39.5
$LiEu_{0.22}W_{0.33}M_{0.67}Al_{0.67}Sm_{0.01}$	Tungsten Oxide	69.9
	Tungstic Acid	58.5

These showed that using tungstic acid reduced the efficacy of the phosphors. The physical properties of these phosphors only showed a minor effect following this alteration in the starting materials. Using tungstic acid did not remove the need for grinding following the firing of these phosphors and SEM images of these phosphors can be seen in figures 5.19 and 5.20 below. These showed little difference between the size of the particles in these images, even when viewed at high resolution. Nevertheless, the measured reduction in luminous efficacy is key and thus the tungstic acid was not used further.
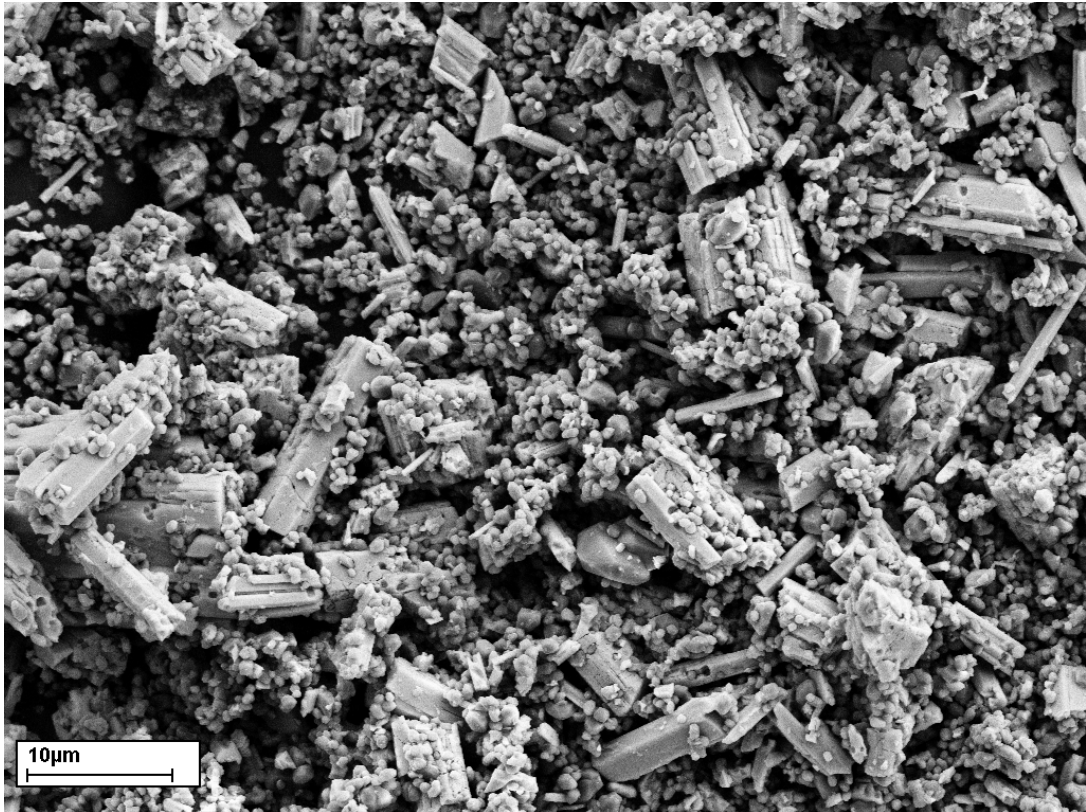
Figure 5.19: SEM image of $LiEu_{0.22}(WO_4)_{0.33}(MoO_4)_{0.67}Al_{0.67}Sm_{0.01}$ using Tungstic Acid
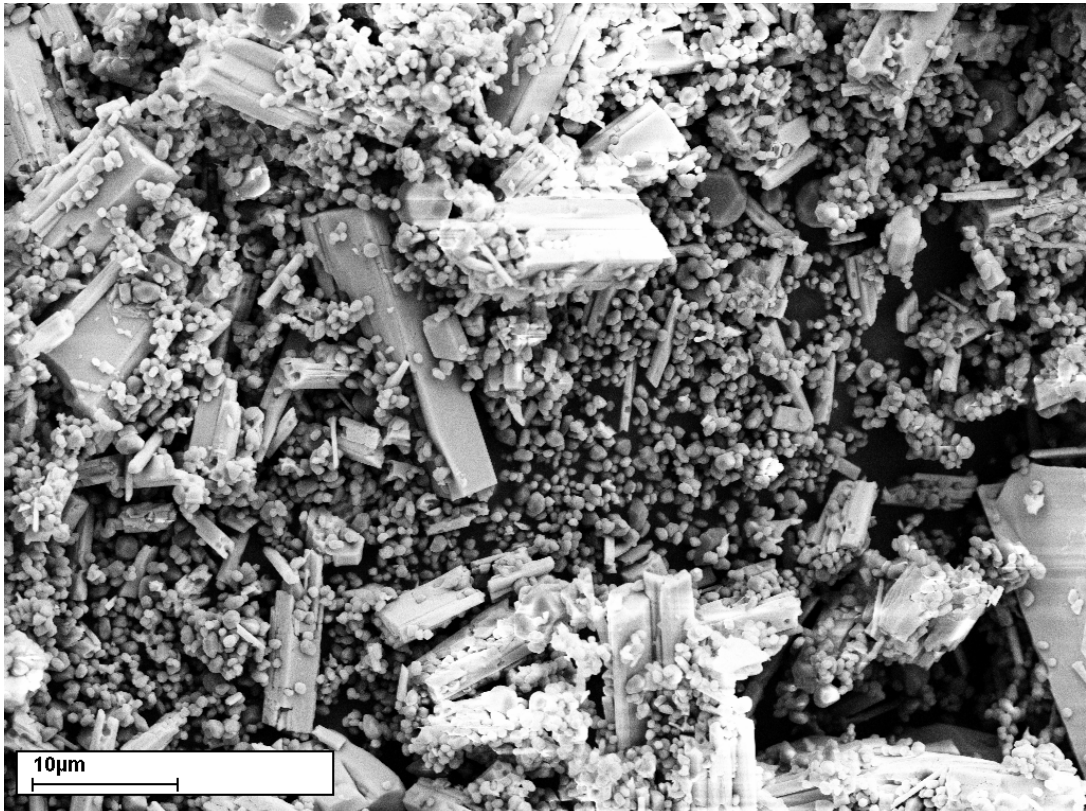
Figure 5.20: SEM image of $LiEu_{0.22}(WO_4)_{0.33}(MoO_4)_{0.67}Al_{0.67}Sm_{0.01}$ using Tungstic Oxide
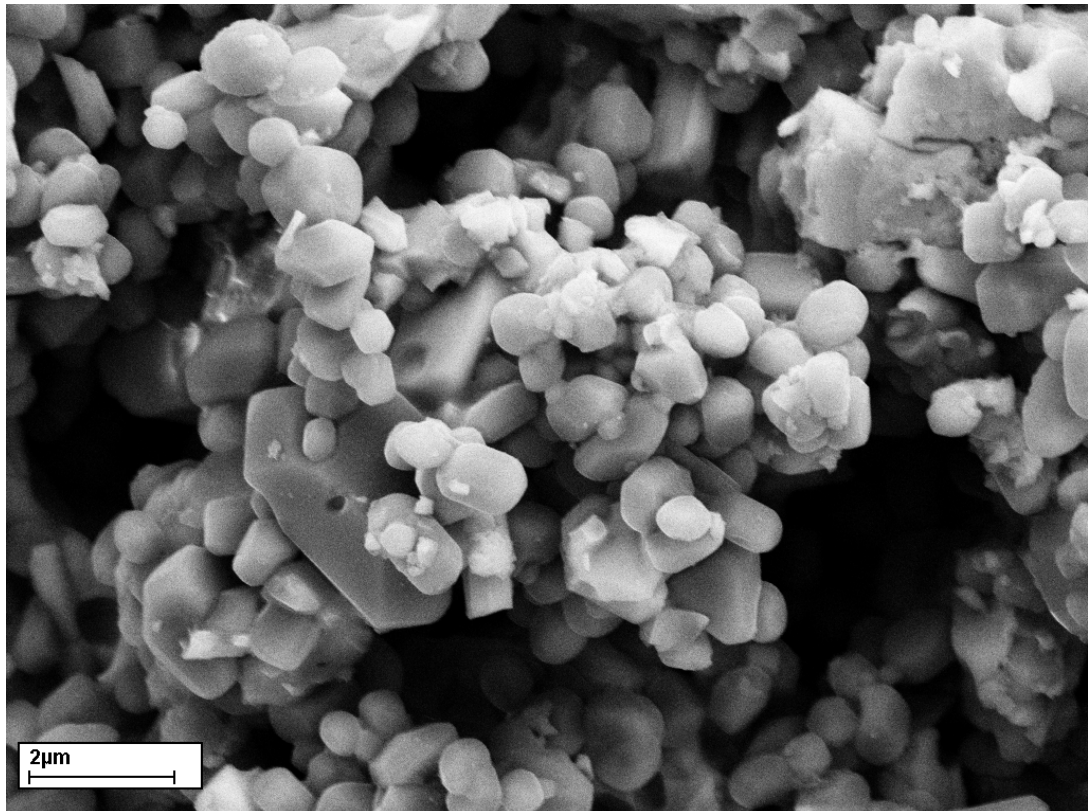
Figure 5.21: SEM image of phosphor with tungstic acid as the starting material
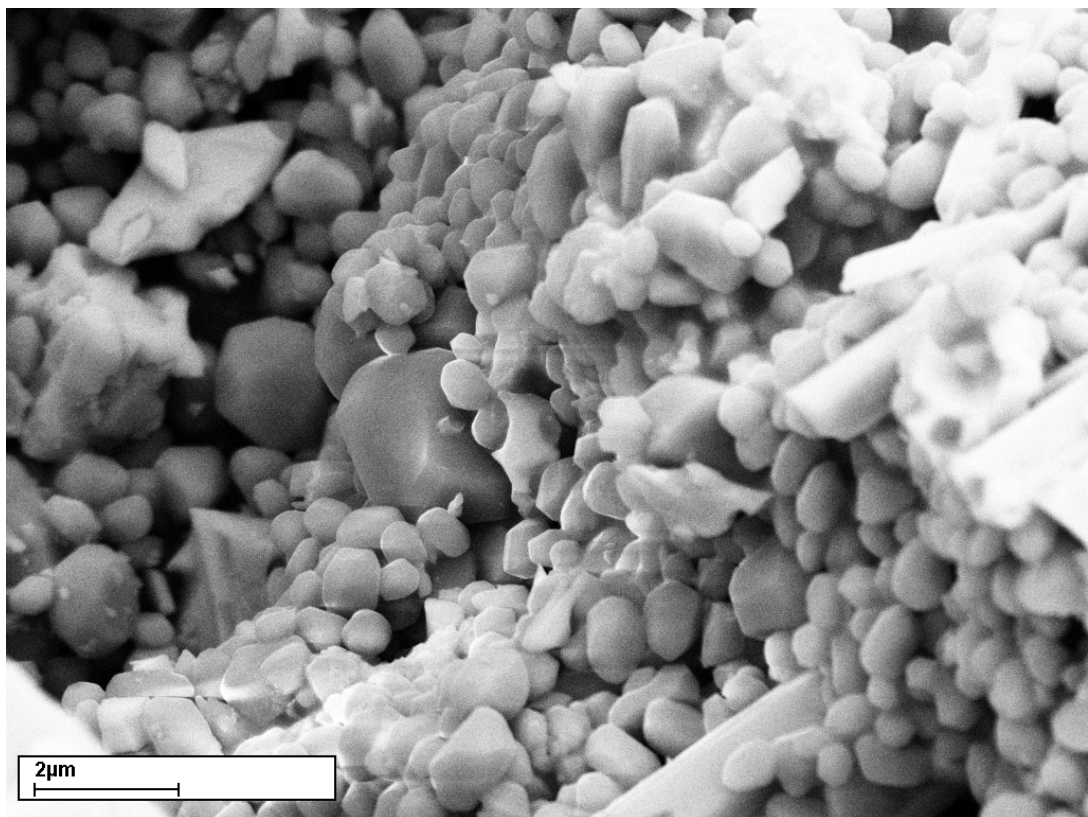
Figure 5.22: SEM image of phosphor with tungsten oxide as the starting material

5.6.3 Europium Content

Europium content has, understandably, a significant contribution to the luminous efficacy and quantum efficiency of these phosphors. Initially, an increase in the europium concentration led to an increase in the lumen output. As with all phosphors, there was a peak activator concentration after which quenching reduced the efficacies. The efficacy were measured for the phosphor $LiEu_xAl_{0.67}(WO_4)_{0.5}(MoO_4)_{0.5}Sm_{0.005}$ as the europium content increased from 0.1 to 0.4. The results can be seen in figure 5.23. This showed a molar concentration at 0.2 was optimal for this lattice.
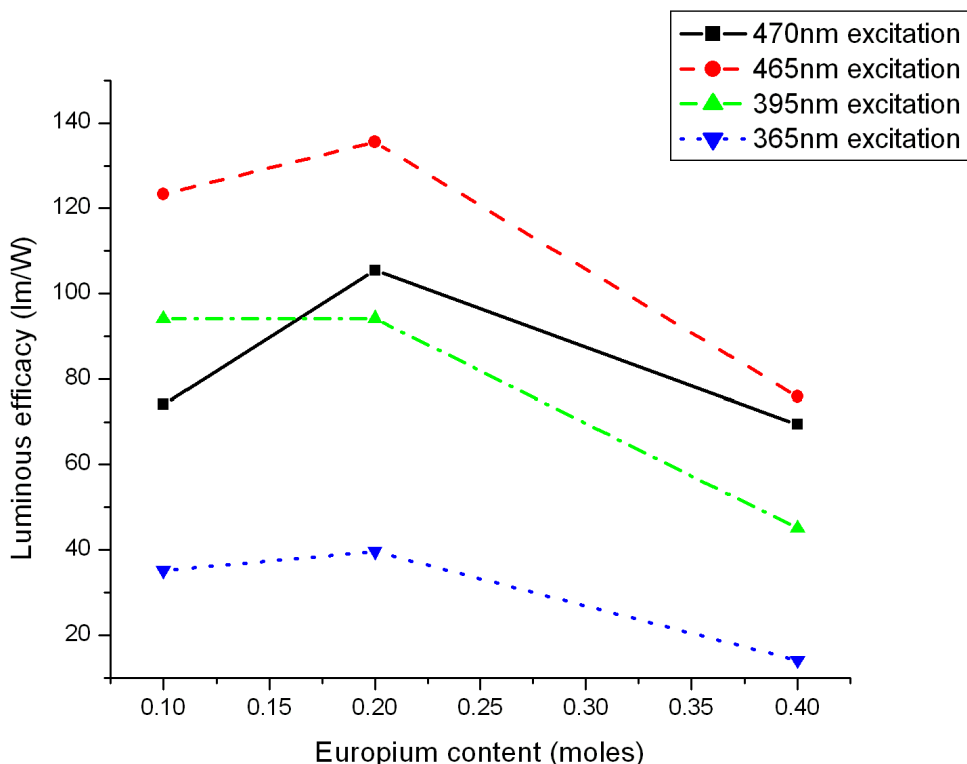
Figure 5.23: Efficacy measurements of $LiEu_xAl_{0.67}(WO_4)_{0.5}(MoO_4)_{0.5}Sm_{0.005}$ as europium concentration varied, excitation shown at four wavelengths

The effect of the coactivator was also investigated for the phosphor $LiEu_{0.2}Al_{0.67}(WO_4)_{0.5}(MoO_4)_{0.5}Sm_x$. Whilst this is at a small concentration relative to the europium, its effects can sometimes be great (as discussed in section 1.4.2). Figure 5.24 shows the measured luminous efficacy output as the samarium content was varied between 0.0025 and 0.015.

This appeared to have a similar effect to the lumen output as did the europium content, although the scale at which this occurred was much smaller, as expected for a coactivator.

Whilst not a key consideration during this part of the research, when commercialising products the cost of manufacture is important and with europium as one of the more expensive components of the phosphor, a reduced content potentially sacrificing some lumen output is a consideration.
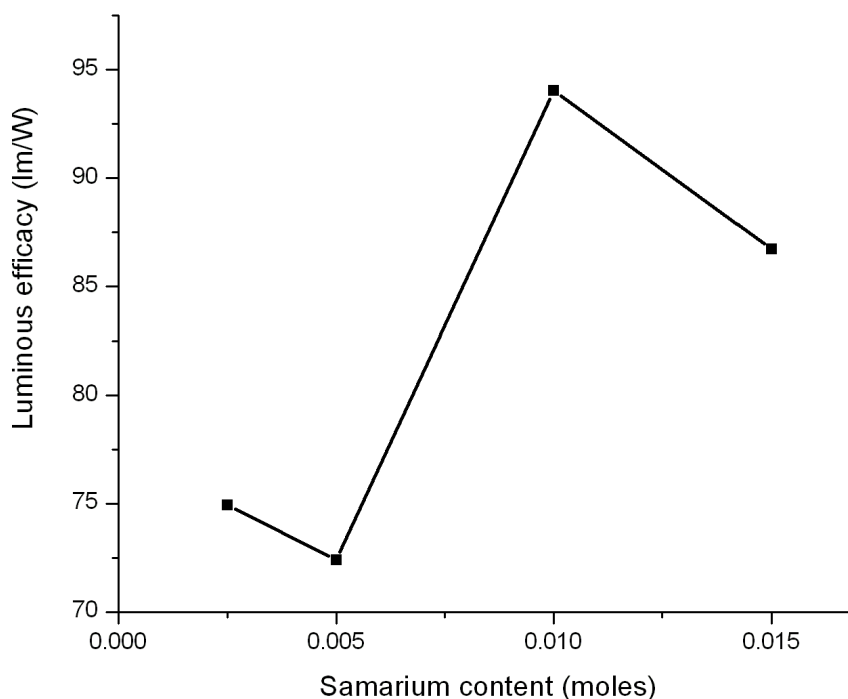
Figure 5.24: LE measurements of $LiEu_{0.2}Al_{0.67}(WO_4)_{0.5}(MoO_4)_{0.5}Sm_x$ as samarium concentration varied

5.6.4 Experimental Conditions

The firing time and temperatures in the synthesis of these materials were based on figures in the literature [1] [8] [9] for similar phosphors, which suggested a firing temperature between 600–900 °C for between 1–4 hours. In order to measure any effects the firing temperature led to in the phosphors, those made here were fired at temperatures between 800 °C and 1400 °C.

Firing Temperature

An aluminium phosphor containing tungsten and molybdenum of the formula $Li_{0.67}(WO_4)_{0.5}(MoO_4)_{0.5}Al_{0.33}Eu_{0.22}$ was fired at a range of temperatures for 3 hours and the efficacy results of the phosphors are shown in figure 5.25. These results shows that firing at 1200 °C was the most favourable temperature to attain the highest efficacy phosphor of this formula, when excited at 365nm. At 465nm excitation wavelengths, 800 °C and 1200 °C showed the greatest efficacy.

Firing temperatures are also dependent on the starting materials and changes to the host lattice will lead to an alternative optimum firing temperature. For example, after replacing the lithium with aluminium to give $(WO_4)_{0.5}(MoO_4)_{0.5}AlEu_{0.22}$ and firing at 1200 °C, this did not result in a phosphor powder as the reactants melted and became inseparable from the crucible.
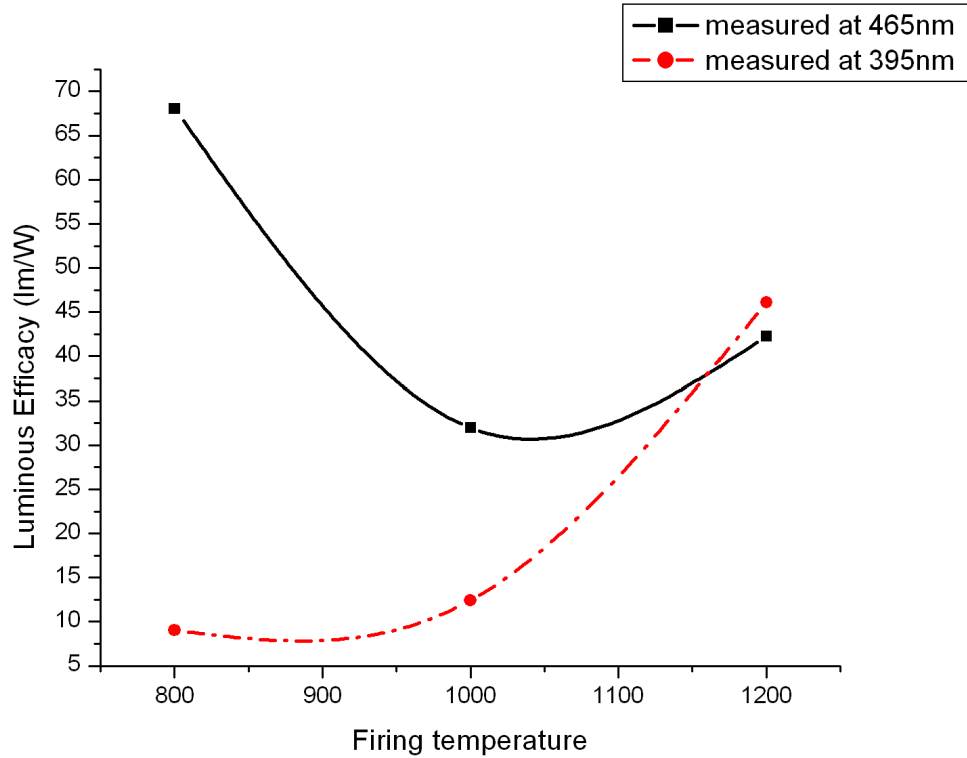
Figure 5.25: Luminous efficacies of the phosphor $\mathrm{Li}_{0.67}(\mathrm{WO}_4)_{0.5}(\mathrm{MoO}_4)_{0.5}\mathrm{Al}_{0.33}\mathrm{Eu}_{0.22}$ as the firing temperature was varied, measured over two excitation wavelengths

5.7 Double Tungstates/Molybdates

The double tungstates have been used more widely in phosphor research, including the replacement of tungsten with molybdenum [10] [11] and include alkali metals in the lattice structure. $\mathrm{LiEu}(\mathrm{WO}_4)_{2\text{-x}}(\mathrm{MoO}_4)_\mathrm{x}$ is one such example [1]. This was made here for $x = 1$ to give a phosphor of the form

$$\mathrm{LiEu}(\mathrm{WO}_4)(\mathrm{MoO}_4) \tag{5.3}$$

This was then compared with the novel phosphors reported earlier in this chapter. This phosphor, to be used as a benchmark, was measured with the Bentham Integrating Sphere to have a luminous efficacy of $158\,\mathrm{lm/W}$ and a quantum efficiency of 71%.

Samarium was added to this phosphor to see if the same line broadening effects occurred. As can be seen from figure 5.26, this did not have the same effects as previously and there was only a small effect at at three peaks of 363nm 368nm and 377nm wavelengths.

Some of the europium in these structures was replaced with aluminium and the efficacies of these phosphors were measured at 465nm excitation light. The stoichiometry and results are presented in table 5.6.

The introduction of aluminium into these phosphors significantly reduced the out-
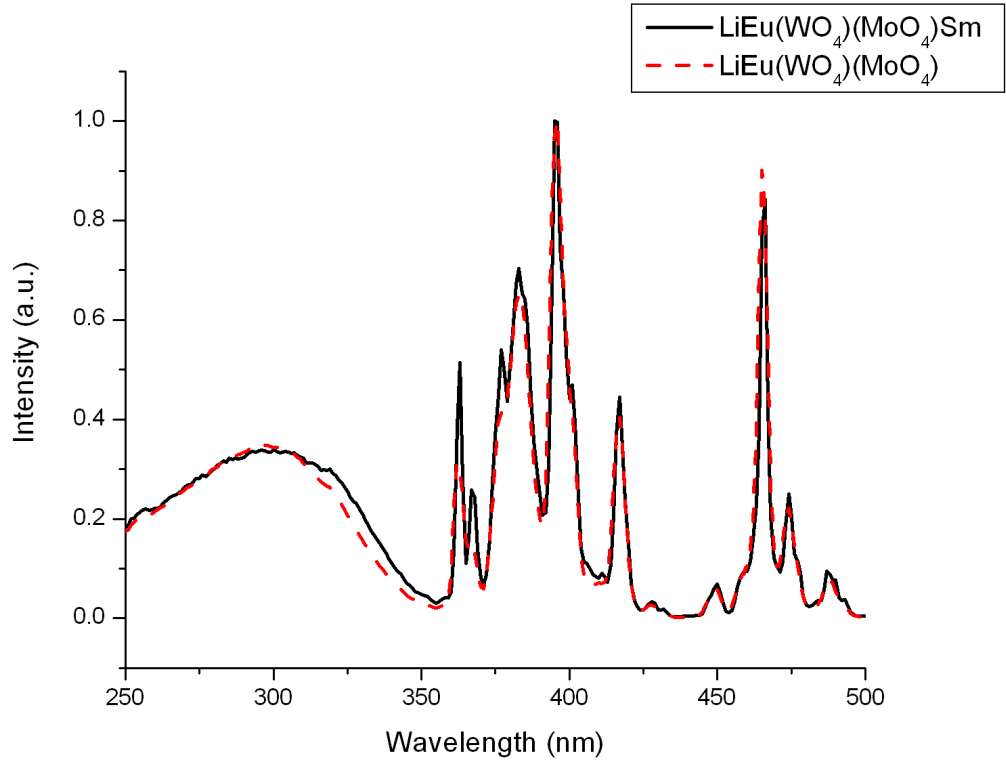
Figure 5.26: Excitation spectra comparing $EuLi(WO_4)(MoO_4)$ and $EuLi(WO_4)(MoO_4)Sm$

Table 5.6: Luminous efficacy measurements at 465nm excitation wavelength, with aluminium partially replacing europium

Phosphor	Efficacy (lm/W)
$LiEu_{0.44}(WO_4)(MoO_4)Al_{0.54}Sm_{0.02}$	54.3
$LiEu_{0.6}(WO_4)(MoO_4)Al_{0.38}Sm_{0.02}$	21.7
$LiEu_{0.8}(WO_4)(MoO_4)Al_{0.18}Sm_{0.02}$	65.5

put and was deemed an area not worth pursuing.

5.8 Alternative alkali metals

As with the single molybdates, the alkali metal used in the lattice can be varied. Table 5.7 shows these phosphors.

Table 5.7: Phosphor compositions of double tungsten molybdenum host lattices

Phosphor composition
$Ca_2WO_4MoO_4Eu_{0.22}$
$Na_2WO_4MoO_4Eu_{0.22}$
$LiWO_4MoO_4Eu_{0.25}Al_{0.5}Sm_{0.015}$
$Na_2WO_4MoO_4Eu_{0.44}Al_{1.34}Sm_{0.011}$
$K_2WO_4MoO_4Eu_{0.44}Al_{1.34}Sm_{0.011}$
$Ca_2WO_4MoO_4Eu_{0.44}Al_{1.34}Sm_{0.011}$

The excitation spectra for all three variations which include the Al^{3+} ions are shown in figure 5.27. Comparing the phosphors of the alkali metal cations, the main difference is that potassium showed wider excitation peaks for all wavelengths above 400nm. Ca^{2+} showed a relatively large charge-transfer band, with smaller excitation peaks at longer wavelengths.
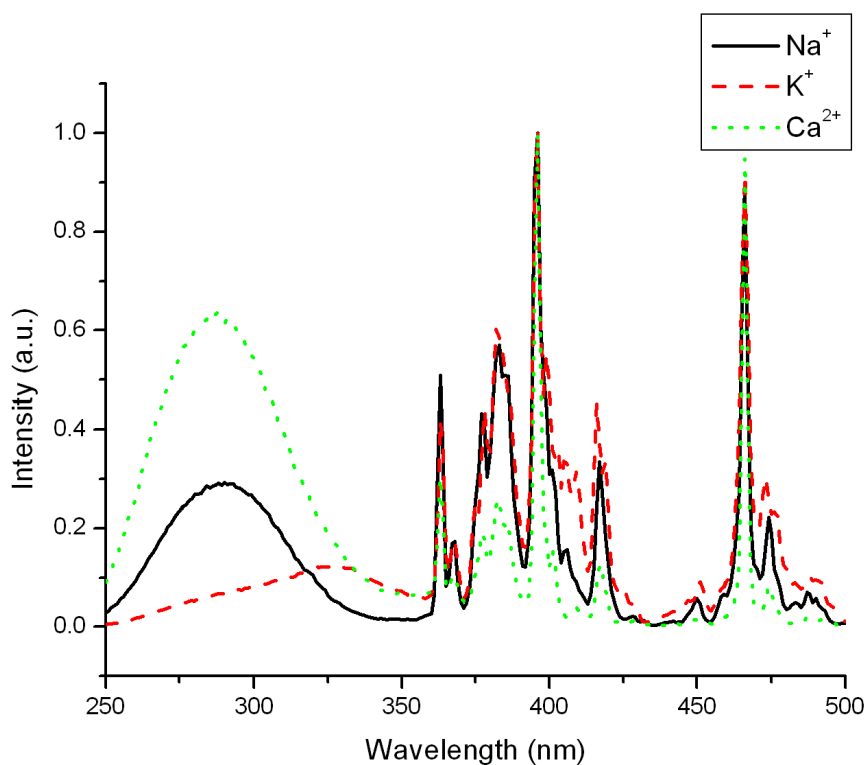
Figure 5.27: Excitation spectra comparison of $AWO_4MoO_4Eu_{0.44}Al_{1.34}Sm_{0.011}$ with (A = Na^+, K^+, Ca^{2+})

Perhaps resulting from these wider excitation bands, the phosphor that showed the highest efficacy was $Na_2WO_4MoO_4Eu_{0.44}Al_{1.34}Sm_{0.011}$, measured at $222.6\,lm/W$, greater than that of potassium ($151\,lm/W$) or calcium ($207\,lm/W$). The emission of this phosphor was measured over an increasing temperature range and the results for this are shown in figure 5.28. This showed a good temperature dependence and measured 79% of its room temperature efficacy at $175\,°C$.

The XRD for this phosphor was also analysed and the spectrum is shown in figure 5.29. This showed the phosphor, of the form, $LiEuAl(WO_4)(MoO_4)$ along with a very small excess of Al_2O_3 and MoO_4.

The fit here showed that the Eu^{3+} containing compounds should be $NaEu(MO_4)_2$ and $Na_5Eu(MO_4)_4$. While a phosphor of the form $NaEu(MO_4)_2$ was attempted earlier with less Eu^{3+}, without much success, an increase in the Eu^{3+} may result in a bright phosphor and is worth investigation.
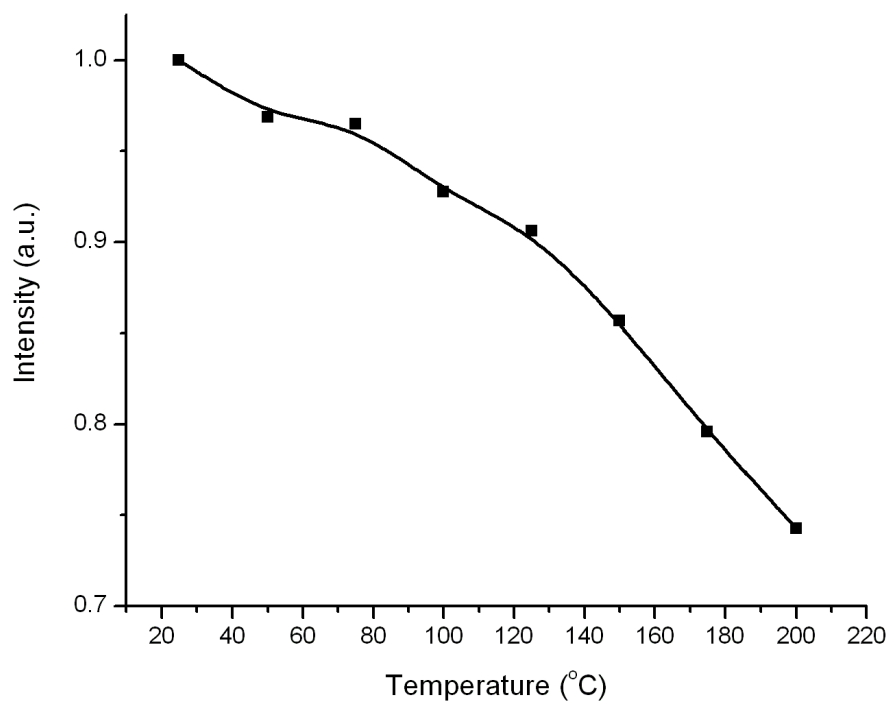
Figure 5.28: Temperature dependence of $Na_2WO_4MoO_4Eu_{0.44}Al_{1.34}Sm_{0.011}$
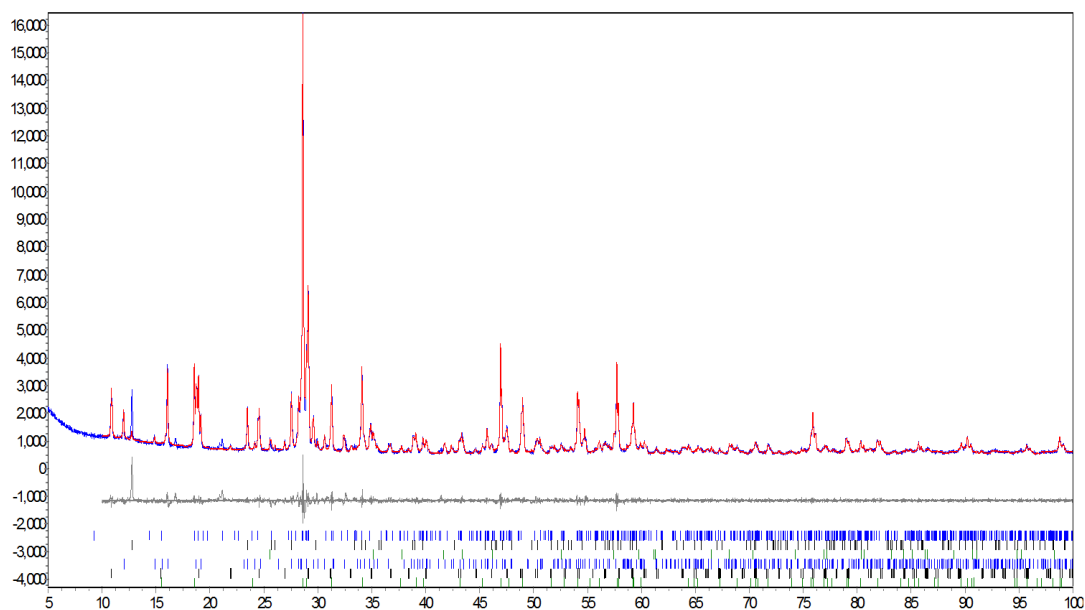
Figure 5.29: XRD analysis of $Na_2Eu_{0.22}Al(WO_4)_{0.5}(MoO_4)_{0.5}$

5.9   Yttrium Oxide

Returning to the phosphor $LiEu(WO_4)(MoO_4)$, an investigation of improved performance in this phosphor was attempted with the substitution of europium for yttrium. The efficacy measurements are shown in figure 5.30.
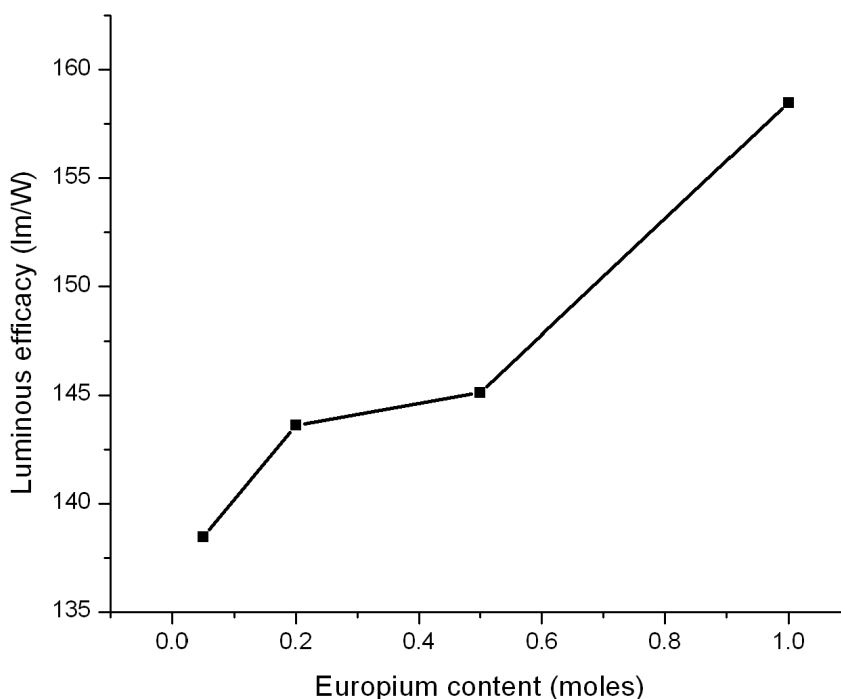
Figure 5.30: Luminous efficacy values for $LiY_xEu_y(WO_4)(MoO_4)$ excited at 465nm, with increasing yttrium content substituted in for europium

In one of these phosphors, the tungsten was completely replaced with molybdenum and gave the double molybdate $LiEu_{0.5}Y_{0.5}(MoO_4)_2$. Compared with the equivalent phosphor which included tungsten, the efficacy of this increased from $130\,\mathrm{lm/W}$ to $157\,\mathrm{lm/W}$.

5.9.1 Samarium Coactivator

Once again samarium was investigated as a possible coactivator for any increase in the efficacy of these phosphors. Two of the higher efficacy phosphors were remade with a small amount of samarium added to the reagents. The formula of the resulting phosphors were $LiEu_{0.5}Y_{0.5}(WO_4)_2Sm_{0.02}$ and $LiEu_{0.2}Y_{0.8}(WO_4)(MoO_4)Sm_{0.02}$. The efficacies of these phosphors and their counterparts without samarium, are shown in graph 5.31 and table 5.8. The table also shows some phosphors which have no tungsten component.

Samarium reduced the efficacies when yttrium replaced the europium and as the amount of yttrium increased, samarium had a greater reduction on the overall efficacy.

When the tungsten was completely replaced by molybdenum, there was a notable increase in the efficacy. Samarium also had the effect to increase the efficacy in these phosphors.

These novel phosphors were printed in an attempt to eventually compare their performance over LEDs and OLEDs. However, the size of the phosphor particles was
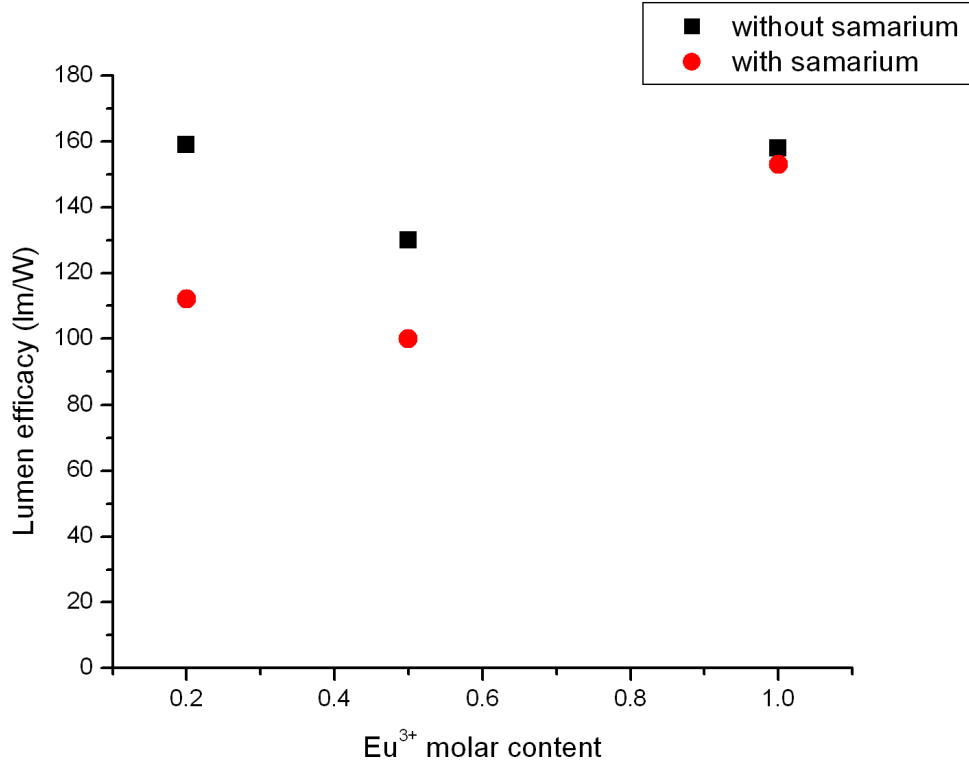
Figure 5.31: Efficacies for phosphors with and without Sm^{3+}

Table 5.8: Efficacies for phosphors with Y^{3+} partially substituted for Eu^{3+}

Phosphor	Efficacy (lm/W)
$LiEu(WO_4)(MoO_4)$	158
$LiEu(WO_4)(MoO_4)Sm_{0.02}$	153
$LiEu_{0.5}Y_{0.5}(WO_4)(MoO_4)$	130
$LiEu_{0.5}Y_{0.5}(WO_4)(MoO_4)Sm_{0.02}$	100
$LiEu_{0.2}Y_{0.8}(WO_4)(MoO_4)$	159
$LiEu_{0.2}Y_{0.8}(WO_4)(MoO_4)Sm_{0.02}$	112
$LiEu_{0.5}Y_{0.5}(MoO_4)_2$	157
$LiEu_{0.5}Y_{0.5}(MoO_4)_2Sm_{0.02}$	203

prohibitively large. Grinding the phosphors in a mortar and pestle reduced the size, however, this also reduced the efficacy. Dispersion in solution of the particles after firing was also attempted and lead to an even coating when printing. However, the smaller phosphor particles were those printed after dispersion. They were of very low efficacy and no calculable efficacy measurements were possible from the emission.

5.10   Conclusion

It was shown here that it was possible to substitute Y^{3+} for some Eu^{3+} in the lattice of $LiEu_xY_{1-x}(WO_4)(MoO_4)$ without losing any of the efficacy of the phosphor. This is an interesting and novel approach to reduce the cost of these narrow emitting red

phosphors.

However, it was the introduction of aluminium and replacement of the alkali metal lithium with sodium that saw the production of a novel high efficacy red emitting phosphor. $Na_2(WO_4)(MoO_4)Eu_{0.44}Al_{1.34}Sm_{0.011}$ was the phosphor which recorded the highest efficacy measurement at 227 lm/W. This also showed good temperature dependence as seen in figure 5.28, retaining 75% of its room temperature luminous efficacy at 200 °C. The synthesis method for these phosphors requires an improvement to produce small and uniform phosphor particles. Once this is achieved, they may be able to provide an alternative to existing commercial red emitting phosphors.

$NaEu(MoO_4)_2$ is also a potentially high efficacy red emitting phosphor based upon the structures seen in XRD analysis. This would require further experimentation of this compound to determine its luminous efficacy and properties.

Eu^{3+} narrow band emitters are currently in use for display lighting, or as a red component of white light where a CRI greater than 90 is not required. This has the potential to replace the existing phosphors, especially in lighting where good performance at high temperature is necessary, as in the case of LED lighting.

References

[1] Chuang-Hung Chiua, Ming-Fang Wang, Chi-Shen Leeb, and Teng-Ming Chen. Structural, spectroscopic and photoluminescence studies of LiEu(WO$_4$)$_{2-x}$(MoO$_4$)$_x$ as a near-UV convertible phosphor. *Journal of Solid State Chemistry*, 180:619 – 627, 2007.

[2] Wei Chen, Alan G. Joly, Collin M. Kowalchuk, Jan-Olle Malm, and Yining Huangand Jan-Olov Bovin. Structure, luminescence, and dynamics of Eu$_2$O$_3$ nanoparticles in mcm-41. *The Journal of Physical Chemistry B*, 106(28):7034–7041, 2002.

[3] Eun Young Lee, Mihail Nazarov, and Young Jin Kim. Red emission properties of (Y,M)NbO$_4$:Eu^{3+} (M: Al, Ga) phosphors under Near-UV excitation. *Journal of the Electrochemical Society*, 157(3):J102 – J105, 2010.

[4] Gwan-Hyoung Lee, Tae-Hyung Kim, Chulsoo Yoon, and Shinhoo Kang. Effect of local environment and Sm^{3+}-codoping on the luminescence properties in the Eu^{3+}-doped potassium tungstate phosphor for white LEDs. *Journal of Luminescence*, 128(12):1922 – 1926, 2008.

[5] Zhengliang Wang, Hongbin Liang, Menglian Gong, and Qiang Su. Novel red phosphor of Bi^{3+}, Sm^{3+} co-activated NaEu(MoO$_4$)$_2$. *Optical Materials*, 29(7):896 – 900, 2007.

[6] Xiao-xiao Wang, Yu-lun Xian, Gang Wang, Jian-xin Shi, Qiang Su, and Meng-lian Gong. Luminescence investigation of Eu^{3+}-Sm^{3+} co-doped Gd$_{2-x-y}$Eu$_x$Sm$_y$(MoO$_4$)$_3$ phosphors as red phosphors for UV InGaN-based light-emitting diode. *Optical Materials*, 30(4):521 – 526, 2007.

[7] Qiong Wei and Donghua Chen. Luminescence properties of Eu^{3+} and Sm^{3+} coactivated Gd(iii) tungstate phosphor for light-emitting diodes. *Optics & Laser Technology*, 41(6):783 – 787, 2009.

[8] Kyu-Seog Hwang, Young-Sun Jeon, Seung Hwangbo, and Jin-Tae Kim. Red-emitting LiEuW$_2$O$_8$ phosphor for white emitting diodes prepared by sol-gel process. *Optica Applicata*, 39(2):375 – 382, 2009.

[9] Yunsheng Hu, Weidong Zhuang, Hongqi Ye, Donghui Wang, Shusheng Zhang, and Xiaowei Huang. A novel red phosphor for white light emitting diodes. *Journal of Alloys and Compounds*, 390(1-2):226 – 229, 2005.

[10] Zhengliang Wang, Hongbin Liang, Menglian Gong, and Qiang Su. Luminescence investigation of Eu^{3+} activated double molybdates red phosphors with scheelite structure. *Journal of Alloys and Compounds*, 432:308 – 312, 2007.

[11] V. Sivakumar and U. V. Varadaraju. Intense red-emitting phosphors with white light emitting diodes. *Journal of the Electrochemical Society*, 152(10):H168 – H171, 2005.

Chapter 6

Screen Printing and ACEL Panels

The luminescent properties of phosphors command the applications for which the phosphor can be used; the properties of suitable phosphors are chosen based on the application. If the excitation light is of a blue wavelength, then the phosphor needs to have its excitation bands in this region. Furthermore, if there are multiple emissions from the device, or otherwise, then the phosphor must also not absorb light from any of these other wavelengths to avoid a reduction in efficacy and a change to the overall output spectrum that would be expected just viewing the emission spectra. Ideal utilisation of the phosphors can require some of their material properties to be improved upon in order that they function at maximum efficiency. This can include improvements in both their spectral properties and their material properties. As such, the synthesis and method for application of phosphors into the final light emitting package has to be considered. Changes in one area can lead to effects in another and in making these changes care has to be taken not to degrade or adversely alter the luminescent characteristics of the phosphor. Examples include shifting the emission bands in YAG:Ce^{3+} by introducing gadolinium to form a (Y,Gd)AG:Ce^{3+} phosphor, causing a reduction in the luminous efficacy as the gadolinium content is increased [1]. In addition, increasing particle size can also increase the luminous efficacy of the phosphor [2].

There are a large variety of applications where phosphors are used. These include television sets, Heads-Up Displays (HUDs), mobile phones as well as general and display lighting. The technologies that employ the use of phosphors have changed over time and new phosphors are often required, even within the same set of applications, as the technologies evolve. Televisions (TVs) are an example of this where new phosphors enabled the production of colour TV. Some of these phosphors contained cadmium and were later replaced as they posed environmental health risks [3].

To explore suitable phosphors, the methods of application to the products was studied; these include sputtering, spraying and screen printing. Screen printing and spraying techniques are discussed here and in the next chapter respectively, as the

most effective methods to apply the phosphors discussed in preceding chapters to end use applications.

6.1 Screen Printing

The screen printer was described in section 2.6 but the preferred phosphor properties are discussed here. Small, soft, homogeneous particles showed the best results for coverage and uniformity when printing and these were quantified experimentally and discussed later in this section. Grinding and sieving phosphors before printing was possible, though it is the larger phosphor particles removed in this process and these were usually the higher luminosity emitters present in a phosphor powder. This must be investigated in each case lest this process reduce the phosphor efficacy. The properties of the screens were not fixed in the sense that many were available which comprised a variety of specifications, including the number of threads and thread diameter. This affected the amount of phosphor that was deposited with each pass that the printer made over the substrate, as well as the largest particle size that could be used in the printing process.

The substrate that was used for printing depended on the properties required for the final application. Whilst glass is a common substrate for its excellent optical properties, plastics such as acetate were also used. The advantage of acetate was that it provided a cheap alternative to glass in printing the phosphors prepared for investigation in this chapter. When the optimal combination of phosphors was found they can then be printed onto glass if desired. The transmission spectra of these materials is shown in figure 6.1 for comparison. These both showed a high transmission over the entire range of the visible wavelengths. As expected, glass had a higher transmission at around 90% rather than 80% measured for acetate. This will lead to higher efficacy values when measured with glass as less light is absorbed or reflected. However, this may also lead to phosphor compositions being adjusted slightly to achieve specific colour requirements when using glass rather than acetate.

The screens described in the remainder of this chapter were created using an acetate substrate. A DuPont 7155 electroluminescent binder was mixed by hand with each phosphor in a 3:1 ratio by weight. This was printed onto the acetate sheet and dried in an oven at a temperature of $140\,^{\circ}\mathrm{C}$. To print a greater number of coats, each coat was allowed to dry before another was printed. A maximum of up to three coats were made using this method. The screen used for printing these phosphors had 48 threads per cm and a thread diameter of $80\mu\mathrm{m}$.

To increase the amount of phosphor deposited, either the ratio of phosphor to binder was increased, or the screen used in printing was changed to one with fewer threads per cm. An increase in phosphor deposition was preferred here as printing fewer runs will be cheaper and quicker. This was only viable up to a thickness where the printing quality, defined by the uniformity of the deposit, remained high. This is measured and described where appropriate for phosphor screens detailed in this and
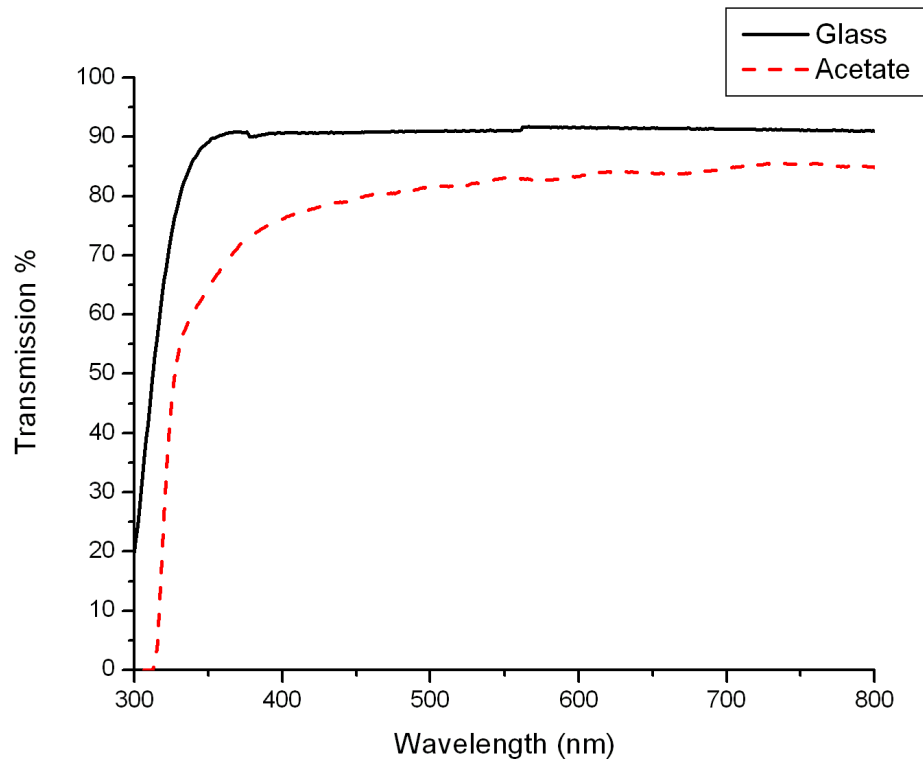
Figure 6.1: Transmission percentage for glass of 2mm thickness, over a wavelength range of 300nm to 800nm

the following chapters. This began to occur once the ratio dropped to less than 3:1. Using a higher ratio of binder resulted in a more even distribution of the phosphor although occasionally required printing a second layer. Printing a second layer can have an added advantage of a more even distribution of the phosphor relative to one thick layer. This was especially true for larger particles such as $SrS:Eu^{2+}$ and $CaS:Eu^{2+}$.

Measuring the weight of the deposited phosphor immediately after the screens were printed and after the screens had dried allowed the calculation of both phosphor deposited and thickness of the screens. For the $YAG:Ce^{3+}$ phosphor, 0.052g of phosphor was deposited in a layer which was measured visually using the SEM as approximately 35µm thick and is seen in figure 6.2.

The other phosphor screens were of comparable sizes with the $CaS:Eu^{2+}$ and $SrS:Eu^{2+}$ measured at a slightly smaller thickness of ~30µm due to less binder being used in their printing. This was to ensure a thicker layer of phosphor printed as these are less efficient than the others. The requisite amount would be deduced experimentally by interpolating the points on the CIE diagram between increasing amounts of phosphor and the excitation emission. The amount of coverage and the number of layers was adjusted for the requirements of the light output. This was discussed in more detail for LED emission in chapter 7 and PLED emission in chapter 8.
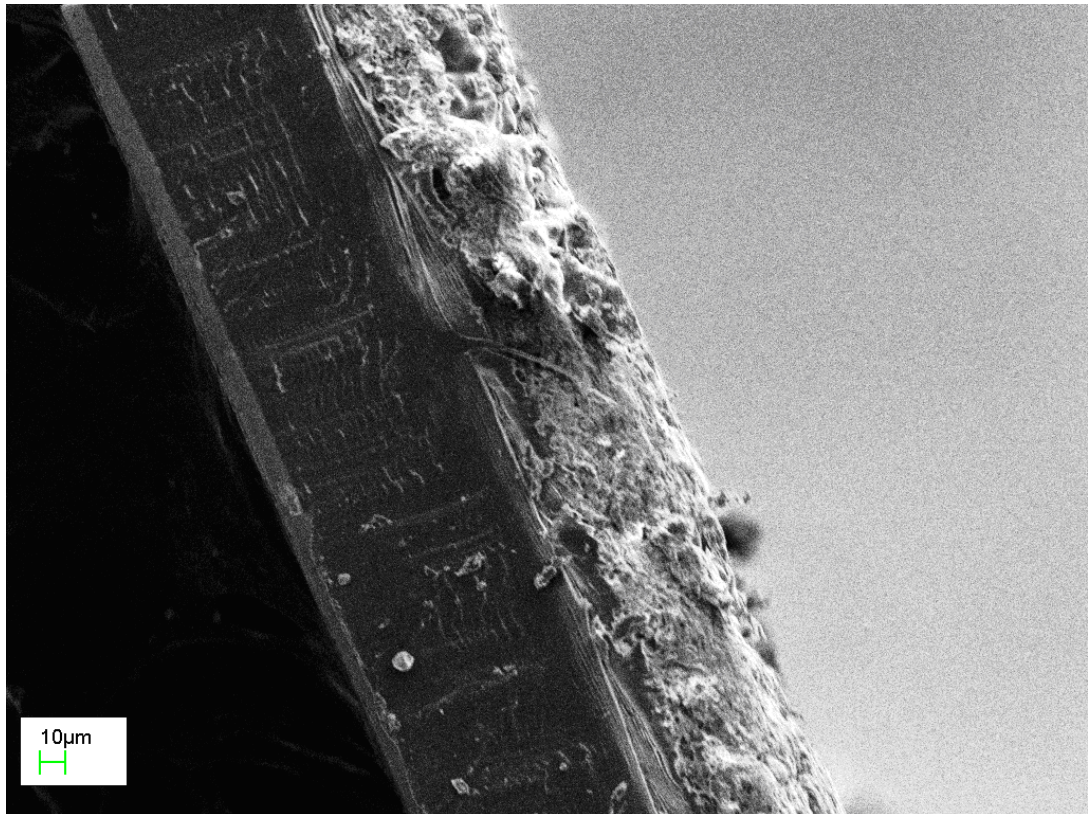
Figure 6.2: SEM image of acetate screen after printing with a binder and YAG:Ce^{3+} phosphor mixture.

6.2 ACEL Panels

One of the modern light emitting technologies is the alternating current electroluminescent panel (ACEL). A phosphor layer and a dielectric layer are printed in between two electrodes across which a voltage is applied. This potential difference provides the energy which excites electrons to the conduction band, leaving a hole behind. When these recombine a photon is emitted. The structure of these is such that they provide a surface emission across the entire panel. One of the electrodes is transparent whilst the other is reflective to maximise emitted light possible in one direction. A schematic is shown in figure 6.3 [4], depicting two possible architectures. 'Build Sequence Two' shows the reverse architecture where the substrate can be printed onto any solid surface, provided it is compatible with the inks.
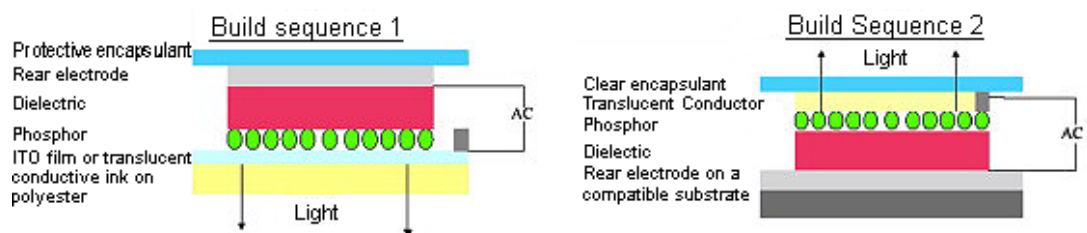
Figure 6.3: Diagram showing the typical structure of layers in an ACEL panel [4]

To find a phosphor that emits efficiently at the relatively low excitation energy

that is used in electroluminescent panels has not been easy as these are less common than when exciting at higher energies [5]. Zinc sulphide, doped with either manganese or copper are the only commercially available phosphors used in electroluminescent devices [6]. First discovered to have luminescent properties in the 19th century, it was initially used as a CRT phosphor and was able to function efficiently at relatively low voltages of 110V.

A copper activated zinc sulphide panel was made in-house. By increasing the frequency from 400Hz to 2000Hz the peak emission wavelength decreased from 500nm (green) to 455nm (blue), a well known effect [4]. These variations were measured using the JETI (see section 2.2 for equipment details) for the ZnS:Cu$^+$ ACEL panel and the resulting frequency against wavelength dependence is shown in figure 6.4. Increasing the frequency was controlled through increasing the voltage; the intensity is primarily determined by the voltage [7]. These ACELs were run by a sine wave AC power supply running at 110V.
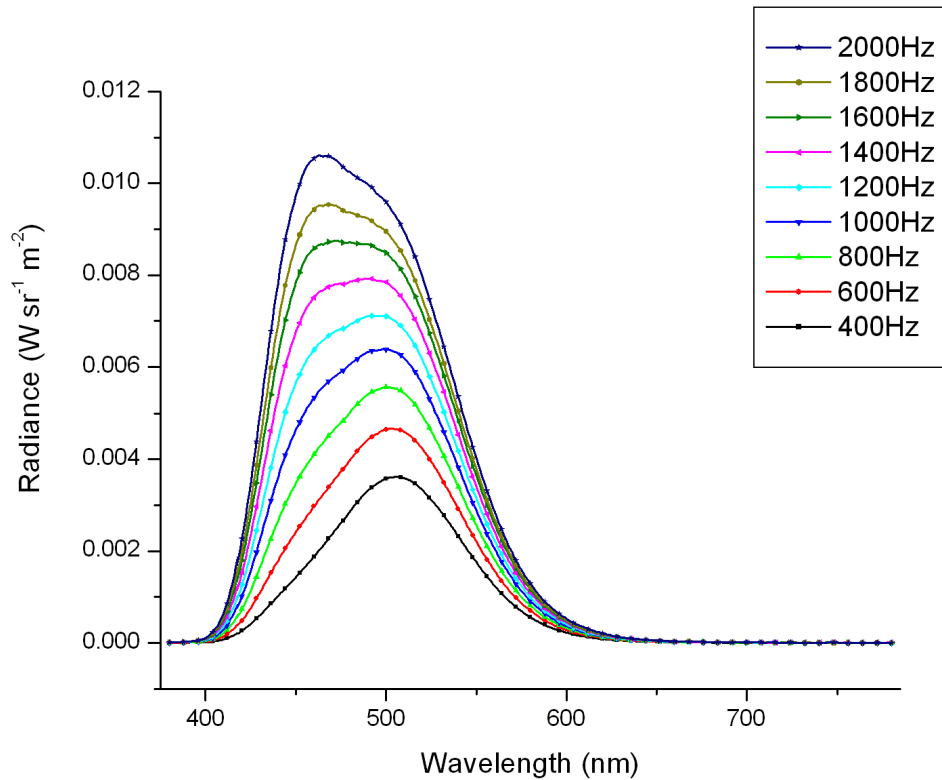
Figure 6.4: Spectrum of ACEL panel at fixed frequencies from 400Hz to 2000Hz

The changing emission was also recorded on the CIE spectrum and is shown in figure 6.5

The use of red emitting phosphors excited via this method have been largely overlooked in the literature and the most common method to produce a red light has been to make use of colour converting dyes, notably rhodamine. The fluorescence emission spectrum for rhodamine 6G is shown below in figure 6.6 [8], for 480nm excitation. A red emission from ACEL panels is required for use either as a component of white
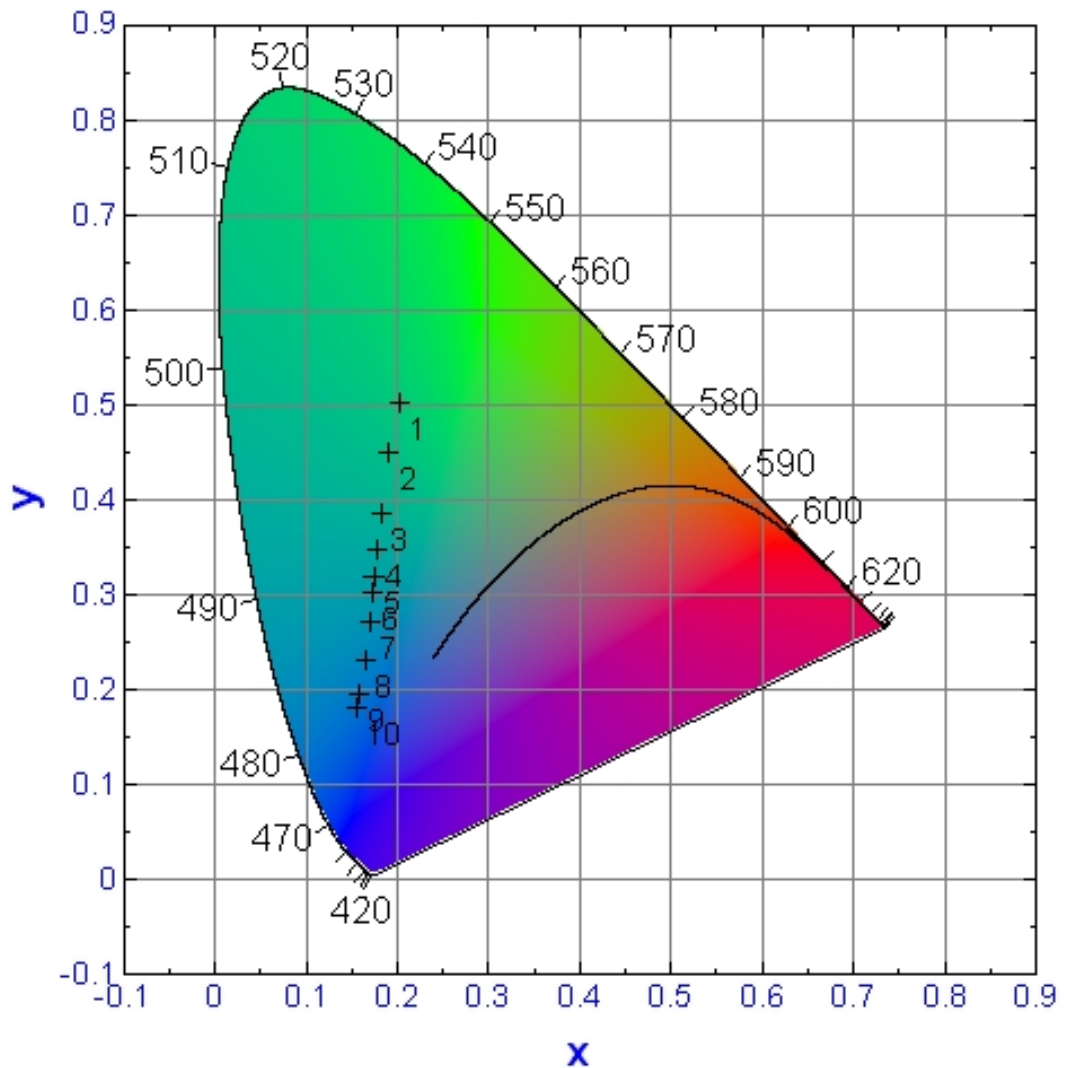
Figure 6.5: CIE colour points of ACEL panel as frequencies vary from 400Hz (1) to 2000Hz (10)

light or as a saturated red emission for display lighting. The main hurdle to overcome with dyes is their poor stability when exposed to sunlight. It is possible to protect them by dissolving them in resins, although care has to be taken to ensure that their properties are not hindered by making this change [9].

Applying phosphors to the ACEL panel instead of using dyes is an approach that was investigated and can be applied to situations where degradation of dyes is a problem. This was used to either convert all the emission or just to convert part of the blue/green and then combine this phosphor emission with the residual blue/green. Using a red phosphor this approach was taken and resulted in a high CRI white light emission.

6.2.1 Phosphors with ACEL panels

Once the phosphors were printed onto acetate sheets they were combined with the ACEL panels by fitting them on the top of the panel. A variety of phosphor coated
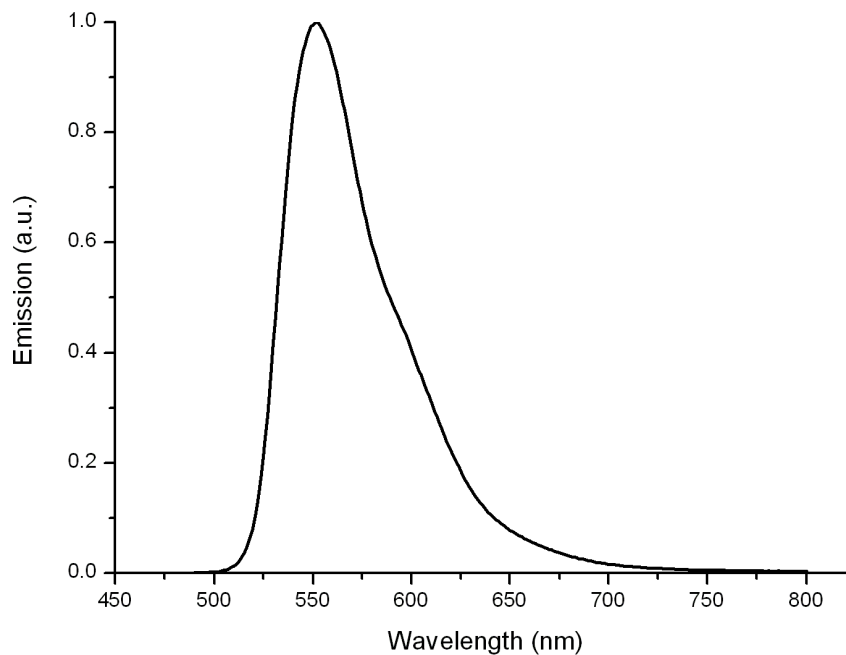
Figure 6.6: Fluorescence emission spectrum of rhodamine 6G, dissolved in ethanol

acetate sheets were used. The sheets were coated with various thickness by using one, two or three dry runs of the printer over the substrate. The phosphors used here were commercially produced phosphors, YAG:Ce^{3+}, SrS:Eu^{2+} and CaS:Eu^{2+}. The emission spectra of all three phosphors are shown in figures 6.7 6.8 and 6.9 respectively.

When applied to the ACEL panels, the frequency of the panel was important as this determined the emission wavelength of the panel and therefore the excitation efficiency of the phosphor. Another crucial factor in deciding the frequency of the ACEL panel emission is related to the desired output emission. This was based on the combination of the ACEL panel emission and that of the phosphor. When attempting to achieve a saturated light, tuning the ACEL panel to the peak excitation bands of the phosphor was necessary. This led to as much absorption of the light as possible by the phosphor and therefore the highest saturation level. However, to achieve a white light, saturation of the ACEL was not desired and a higher frequency was required. In this case, a frequency was used that provided enough blue light in the final emission and gave a greater coverage of the visible region of the electromagnetic spectrum and a higher CRI. There is one more factor, inherent in the panel characteristics, which cautioned against using too high a frequency. This is the reduction in the lifetime of the device as the frequency is increased. It is well known that the total number of cycles the phosphor experiences will determine its lifetime, as seen in figure 6.10 [10]. At 1500Hz a high CRI was attainable whilst keeping the lifetime of the device relatively high. These two factors need to be taken into account when choosing the desired operational frequency.
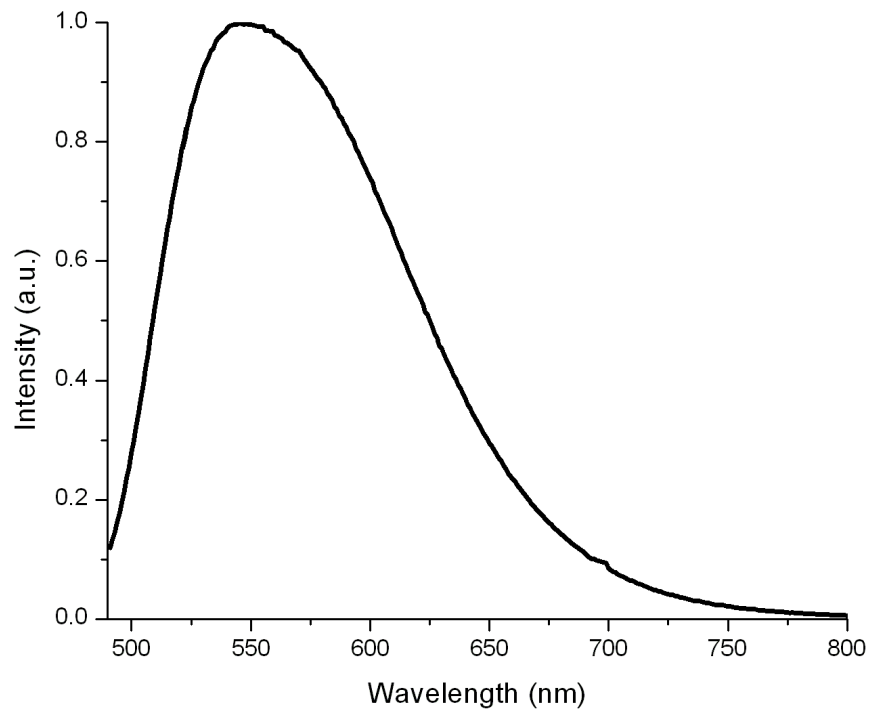
Figure 6.7: Emission spectrum of YAG:Ce^{3+} excited at 470nm
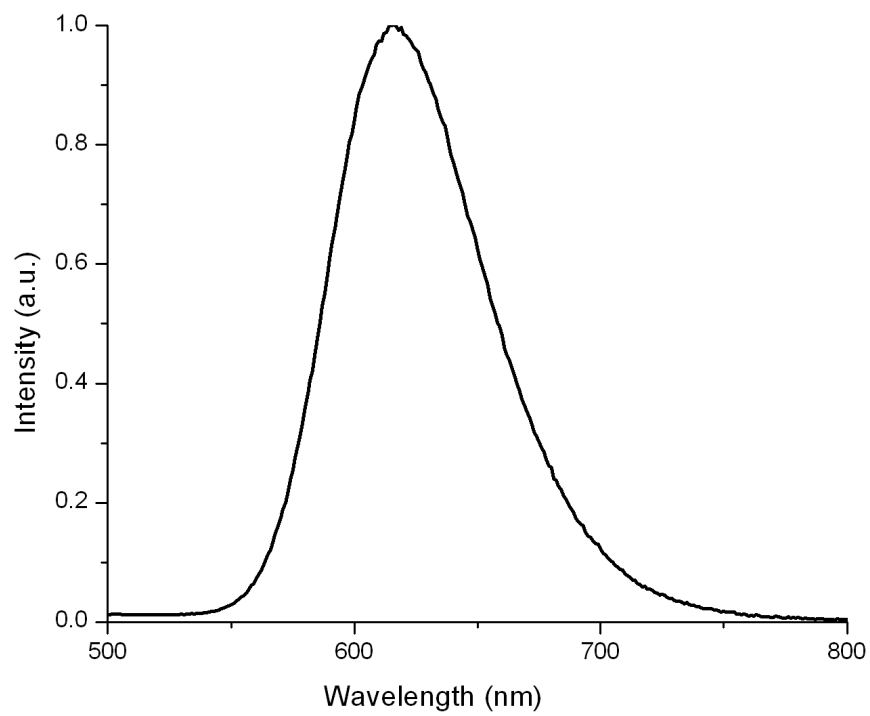
Figure 6.8: Emission spectrum of SrS:Eu^{2+} excited at 465nm
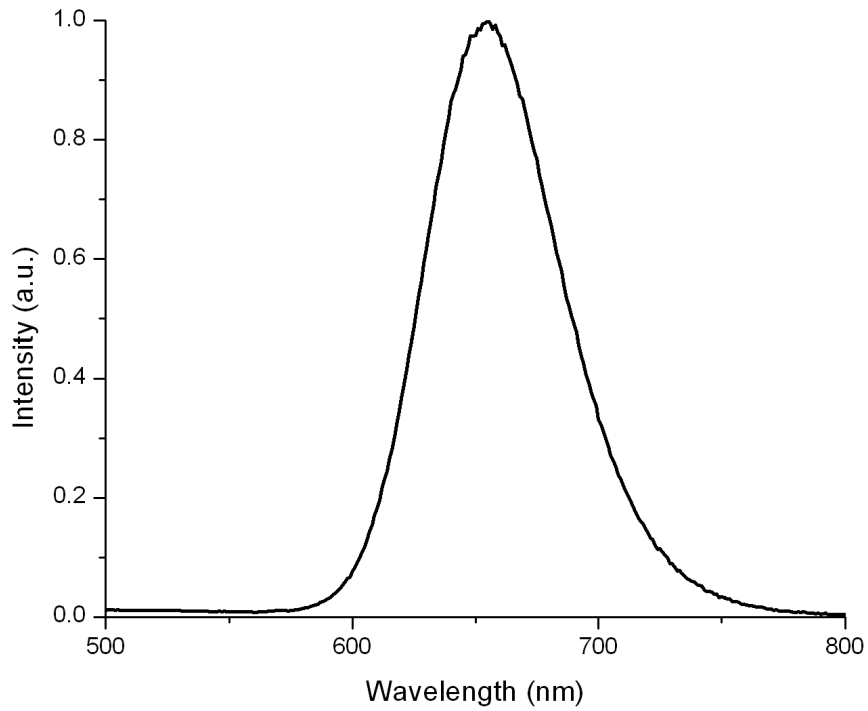
Figure 6.9: Emission spectrum of CaS:Eu^{2+} excited at 465nm
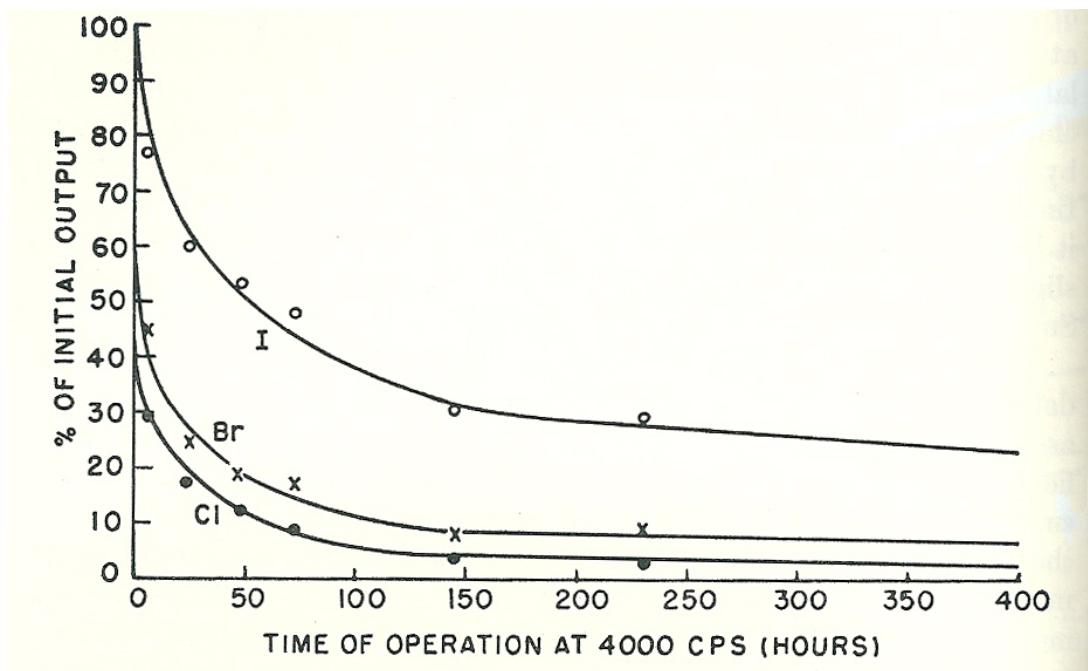
Figure 6.10: Reduction in efficacy of ZnS:Cu over lifetime, coactivated with different halides, 0.1% Cu and 0.3% halide added before firing [10]

In practice, a coating is applied to the phosphor to increase the lifetime of the phosphor. TiO$_2$ can be used as a coating for ZnS phosphors [11] to protect against moisture, as can aluminium oxide [12] and nitrides [13]. These increase the lifetime

such that commercial phosphors now have a half life in the thousands of hours when operated at 400-500Hz [14].

With the combination of the ACEL emission and the phosphor emission it was possible to produce a white light emission. YAG:Ce^{3+} showed the broadest emission spectrum, and has been used previously in combination with blue light to provide a white emission. The resulting spectrum shown in figure 6.11, presents the emission of the combination of the panel emission with the phosphor, using three YAG:Ce^{3+} screens of increasing thickness. At frequencies of 1500Hz the resulting luminance for each screen was measured at 221, 219 and 213 cdm^{-2} respectively.
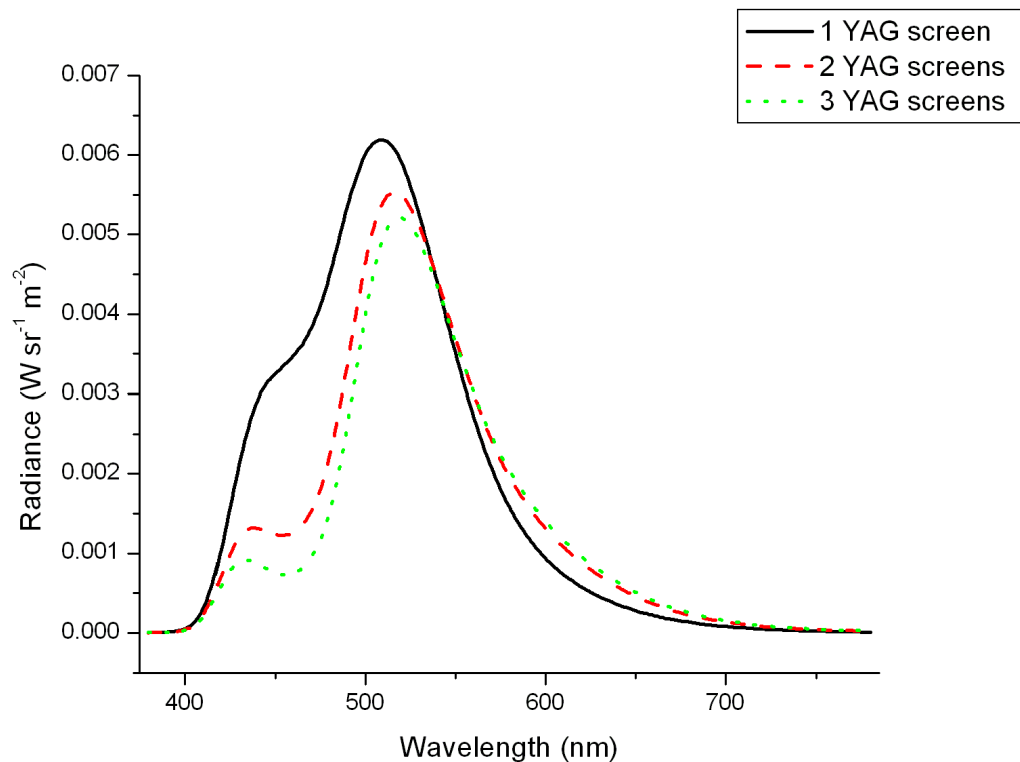
Figure 6.11: Spectrum of ACEL panel at 1500Hz, with acetate screens printed with YAG:Ce^{3+} phosphor of 1, 2 or 3 layers

However, none of the resulting emissions in these cases were close enough to the Planckian locus to provide a measure of CRI or CCT. The red emitting SrS:Eu^{2+} was then investigated alone with the ACEL panel and the emission of their combination is shown in figure 6.12. This was again an acetate screen with two printed layers of a commercially available SrS:Eu^{2+}, and run at 1500Hz. This emission covered a larger region of the spectrum and emitted close to the Planckian locus; the CRI was measured as 88.4 at a CCT of 5580K. The luminance of this screen was measured at 162 cdm^{-2}.

Changing the frequency of the ACEL panel will affect its emission when combined with the phosphors. This emission shift with increasing frequency was studied when used with SrS:Eu^{2+}. The frequency was varied from 1500Hz to 600Hz, and is plotted
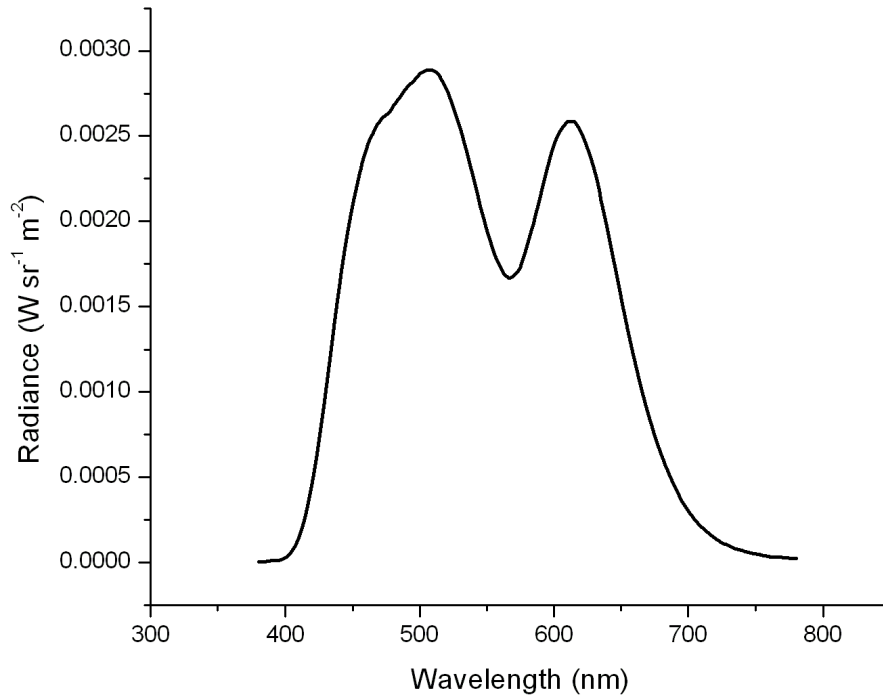
Figure 6.12: Spectrum of ACEL panel at 1500Hz with acetate screens printed with SrS:Eu^{2+} phosphor of 2 layers

in figure 6.13. The luminance, colour correlated temperature and CRI of these are laid out in table 6.1. The luminance increases with frequency as the ACEL panel output shifts to the shorter wavelength region of the spectrum. Both the CCT and CRI peak at 1200Hz.

Table 6.1: Luminance, colour correlated temperature of ACEL with SrS:Eu^{2+} phosphor panel

Freq. (Hz)	Luminance (cdm^{-2})	Efficacy (cdm^{-2}/W)	CCT (K)	CRI
1500	144	1.44	5494	88.37
1200	132	1.75	6067	90.02
1100	125	1.84	6020	90.00
1000	118	1.93	5970	89.54
900	109	1.99	5916	88.43
800	102	2.09	5869	87.31
700	93.1	2.12	5821	85.80
600	84.1	2.22	5770	84.06

This emission has a noticeable gap in the centre of the emission spectrum which had the potential to be filled by the addition of another phosphor. Attempts were made using a combination of one red phosphor, either CaS:Eu^{2+} or SrS:Eu^{2+}, with YAG:Ce^{3+}. As the order of phosphors may be important due to their efficiencies, the order in which they were applied was varied in each and every case to optimise the colour rendering. Finally, attempts were made using both red phosphors and the
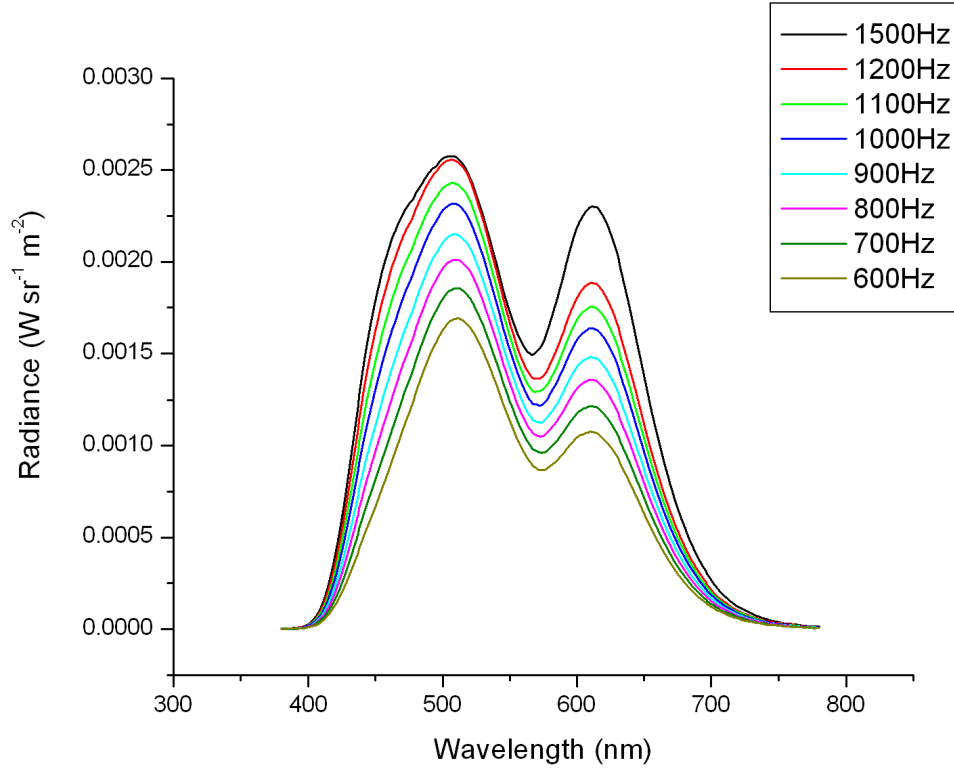
Figure 6.13: Spectrum of ACEL panel combined with $SrS:Eu^{2+}$ over frequency range of 1200Hz to 600Hz

yellow emitting $YAG:Ce^{3+}$. It was one of these combinations, with the red phosphor directly above the emitter, and the $YAG:Ce^{3+}$ above this, that gave the highest CRI of 90.6 at a temperature of 5660K, the spectrum of this combination is shown in figure 6.14. This has a luminance of $119\,cdm^{-2}$ and a CCT of $5658\,K$.

$YAG:Ce^{3+}$ was replaced with an alternative yellow/green phosphor, europium activated strontium thiogallate ($SrGa_2S_4:Eu^{2+}$). This gave a CRI measured as 92.9 at a very warm emission of 2570K. This combination gave a lower luminance relative to that of the $YAG:Ce^{3+}$ phosphor, of 73.9. These changes were due to the higher red content of $SrS:Eu^{2+}$ applied in order to achieve a white light emission and the narrow emission spectrum from the $SrGa_2S_4:Eu^{2+}$.

6.3 Conclusions

ACELs are a long standing low power light emitting technology that are efficient and have many niche uses, such as panels in the automotive industry. Using red emitting phosphors with the ACEL panels is promising and an avenue that can be researched further especially in cases where UV light can cause the breakdown of the dyes that are currently used [9]. To achieve this they will have to perform at least as well as the existing dyes that are currently used in commercial ventures. The performance of the dyes is strongly dependent on the production method and papers have reported
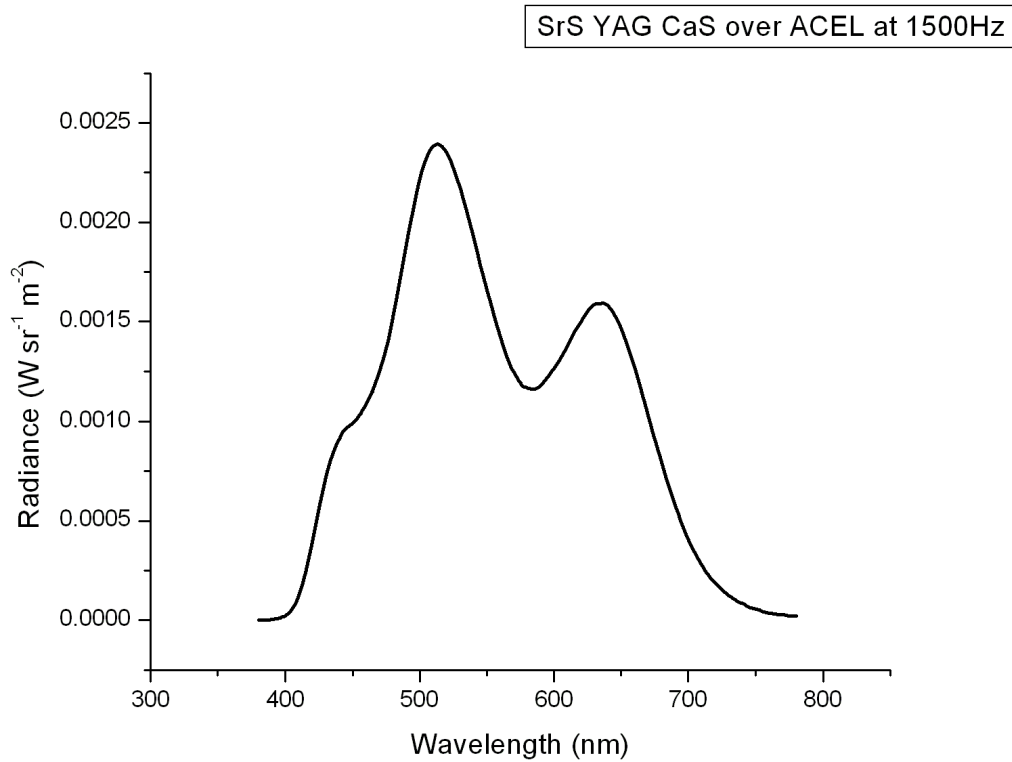
Figure 6.14: Spectrum of ACEL panel at 1500Hz with SrS:Eu^{2+}, YAG:Ce^{3+} and CaS:Eu^{2+} phosphors giving an emission with a CRI measured at >90

a luminance of up to $40 \, cdm^{-2}$ when run at $400 \, Hz$ from a source which has a green luminance of $46.8 \, cdm^{-2}$ and a blue-green of $34.1 \, cdm^{-2}$ [15]. Phosphors could replace dyes in situations where the dye will break down under UV light over a period of time, such as applications under sunlight. Should the efficiency, production methods or cost of phosphors be reduced then there is the potential for a greater scope in their usage within ACELs as well as an increase in use of ACELs in the lighting market.

Results here have shown that warm and cool white light of high CRI can be generated by ACEL panels with phosphors. At 600Hz the luminance was measured as 84 cdm^{-2} a CRI of 84 and a CCT of 5700K. It was also noted that the efficiency increases as the frequency decreases. As the emission is over a large angle, this represents an efficient output, comparable in lumens to those achieved by LED devices. While they are unlikely to compete directly against the narrow beam emitting LEDs, OLEDs (which are discussed in 8) are a more natural competitor for these devices.

References

[1] R. Withnall, J. Silver, G. Fern, T. Ireland, A. Lipman, and B. Patel. Experimental and theoretical luminous efficacies of phosphors used in combination with blue-emitting LEDs for lighting and backlighting. *Journal of the SID*, 16(2):359 – 366, 2008.

[2] Reilly Kenneth T. *Method for increasing the brightness and halflife of electroluminescent phosphors.* United States Patent 5110499, April 1991.

[3] Gordon C.C. Yang. Environmental threats of discarded picture tubes and printed circuit boards. *Journal of Hazardous Materials*, 34(2):235 – 243, 1993.

[4] J. Ibañez, E. Garcia, L. Gil, M. Mollar, and B. Mari. Frequency-dependent light emission and extinction of electroluminescent ZnS:Cu phosphor. *Displays*, 28(3):112 – 117, 2007.

[5] G Blasse and B.C. Grabmaier. *Luminescent Materials*, pages 11 – 32. Springer-Verlag, 1994.

[6] A. Vecht. D.C. Electroluminescence in zinc sulphide and related compounds. *Journal of Luminescence*, 7:213 – 227, 1973.

[7] Brigida Allieri, Stefano Peruzzi, Livio Antonini, Adolfo Speghini, Marco Bettinelli, Davide Consolini, Giordano Dotti, and Laura E. Depero. Spectroscopic characterisation of alternate current electroluminescent devices based on ZnS-Cu. *Journal of Alloys and Compounds*, 341(1-2):79 – 81, 2002.

[8] R. F. Kubin and A. N. Fletcher. Fluorescence quantum yields of some rhodamine dyes. *Journal of Luminescence*, 27(4):455 – 462, 1983.

[9] Shinkichi Tanimizu. *Phosphor Handbook*, page 770. Taylor & Francis Group, LLC, 2007.

[10] Henry Ivey. *Electroluminescence and related effects*, page 70. Academic Press, 1963.

[11] Sang-Do Han, Ishwar Singh, Devender Singh, You-He Lee, Gaytri Sharma, and Chi-Hwan Han. Crystal growth of electroluminescent ZnS:Cu,Cl phosphor and its TiO_2 coating by sol-gel method for thick-film EL device. *Journal of Luminescence*, 115(3-4):97 – 103, 2005.

[12] Kenton D Budd. *Electroluminescent phosphor particles encapsulated with an aluminium oxide based multiple oxide coating.* United States Patent 5958591, September 1999.

[13] Butchi Reddy Vaddi and Chen-Wen Fan. *Preparation of high-brightness, long life, moisture resistant electroluminescent phosphor .* United States Patent 9968156, May 2003.

[14] Jacob Stanley, Yu Jiang, Frank Bridges, Sue A Carter, and Laurel Ruhlen. Degradation and rejuvenation studies of AC electroluminescent ZnS:Cu,Cl phosphors. *J. Phys Condens. Matter*, 22:1 – 15, 2010.

[15] C. I. Zovko and T. C. Nerz. White polymer thick film electroluminescent lamps and their applications for backlighting liquid crystal displays in portable electronic devices. *Displays*, 20(3):155 – 159, 1999.

Chapter 7

Light Emitting Diodes

An introduction to light emitting diodes (LEDs) was provided in section 1.8. Application of phosphors to blue LEDs was one of the key ideas described at the outset of this research and is the focus of this chapter. The emission wavelengths that fall under the scope of blue LEDs lie from the high energy edge of the visible spectrum at 400nm to around 500nm. For general lighting a broad emitting blue is preferable as it will lead to a higher CRI, whereas for display lighting a short wavelength is desired in order to attain a higher range of the colour gamut.

The work here began with a look at general illumination; the LEDs used had an emission at a peak wavelength of 465nm. For white light illumination some of this blue light from the LED formed a component of the overall emission.

The detailed workings of an LED are not discussed here, but the extraction of light from the package is considered. The first step in the process of illumination studied here was how the phosphors were integrated into the device. Many methods were available, and they fell into two categories. Those where the phosphors were applied directly to the LED (usually in a silicone encapsulant) and those where they were applied remotely; each with its advantages and its disadvantages. The first application method explored is a variation of the former where phosphors were printed onto screens and applied directly to the LED. Printed in a similar method to those for the ACEL panels described in section 6.1, they provided a detailed analysis of the key elements of the phosphors in their application to the LEDs. The primary focus was the combination of light and the output characteristics. Following this, more detailed investigations were carried out to improve the output, in areas including efficacy, as best as possible.

Improvements in the efficiency of lighting are always sought after. For example, this can be done through an improvement in the design of the package to increase light extraction, or an increase in efficiency of the phosphor - by either improving the performance of existing ones, or through the use of alternative, and perhaps novel, phosphors.

7.1 LED characterisation

As seen in section 1.8, LED emission can not easily be tailored to desired requirements. The emission can be adjusted by altering the ratios of the semiconductors in the LED, though this often comes at the cost of efficiency as was seen in figure 3.2. There are many available semiconductor materials which generate an emission, each of their own specifications and so it was important to characterise exactly the LEDs that were used in this work. The stability of the LED over its lifetime, with LEDs ageing at different rates, is an issue that can affect the consistency of the output as the device ages [1] [2]. The operating temperature can also affect the emission from the blue LED and may lead to an increase in CCT as the temperature rises. Differences can occur even for LEDs of the same material. While this problem lay beyond the scope of the research, it is a known problem and as mentioned in Chapter 3, there are measures in place to correct for ageing effects when using a variety of sources by using a feedback loop to retain the desired output [3]. Characterisation of the LED allowed for the appropriate phosphors to be chosen based on the combination of emission of the LED and the excitation wavelengths of the phosphor. The LED array used with the phosphor screens was a 6x6 array and was run from 22.5V up to 26V in 0.5V increments whilst the current increased from 3mA to 127mA over this range. The range of input powers were therefore from 0.0675W to 3.3W. The LED had a peak wavelength of 465nm at lower voltages which decreased to 463nm as the power increased, and full width half maximum of 18nm $\pm$1nm. This emission spectrum with increasing power is shown in figure 7.1 and the shift in peak wavelength was focussed on in figure 7.2. These high brightness LEDs had a lumen output of 33.2 lm at 127mA with an efficacy of 10.0 lm/W at this power.

7.2 Phosphor screens

Phosphor screens were initially printed for four commercially available phosphors, $YAG:Ce^{3+}$, $SrG_2S_4:Eu^{2+}$, $CaS:Eu^{2+}$ and $SrS:Eu^{2+}$ all purchased from Phosphor Technology. The $YAG:Ce^{3+}$ was expected to combine with the blue LED source to create a white light emission, based on ideas described in section 3.1.1. This was therefore an ideal starting point to test this concept and to compare it to other white light emission technologies. Once again, the use of screens was primarily a cheap and quick method for testing the phosphors in a setting where the measured output approximates closely to the environment in which it will be used. Once a picture of the interactions has been built up the optimal method to introduce them based on the package conditions (e.g. the substrate) is a small, but crucial step. This is to print the phosphors on the desired substrate and make adjustments to the thickness of the phosphor layer based on the output if necessary.

A variety of screens were made of increasing $YAG:Ce^{3+}$ thickness by dry printing successive layers. The weight of phosphor deposited by this method was calculated and was the same as those described in section 6.1.
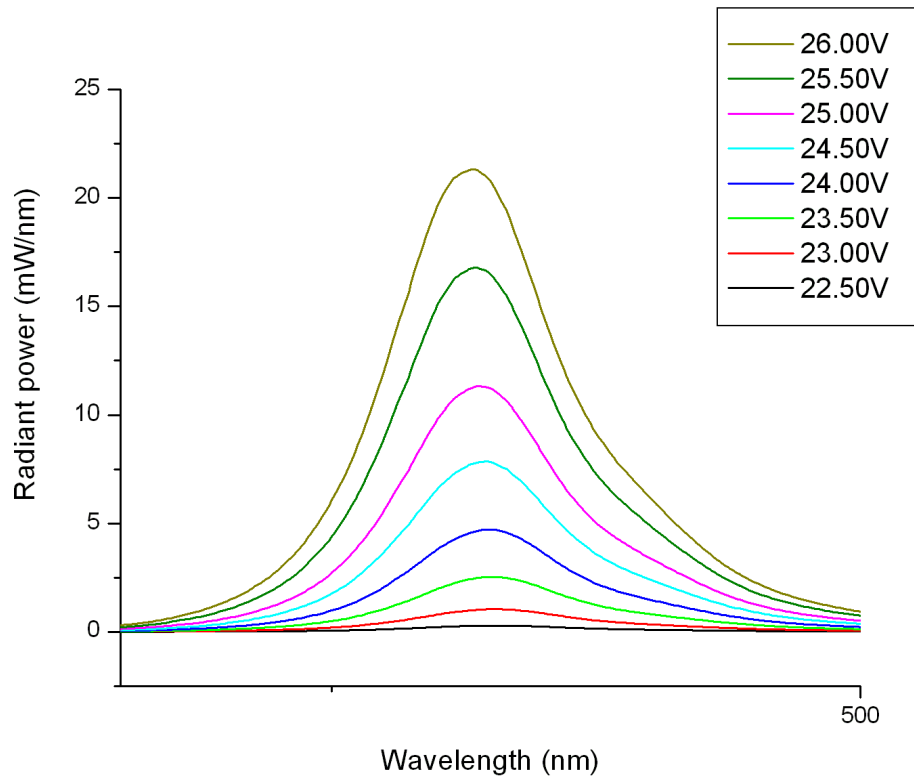
Figure 7.1: Emission spectrum of LED array as voltage increases incrementally from 22.50V to 26.00V

These screens were placed directly above the blue LED whose emission is depicted in figure 7.1. The LED was run for each screen at a range of voltages from 23.0V to 26.0V, and the resulting spectra are shown in figure 7.3 for the measurement taken at 26.0V over an increasing thickness in phosphor deposited.

$SrG_2S_4:Eu^{2+}$ is also a phosphor which emits in the central region of the visible spectrum and was investigated for its potential application to the LEDs. This was in place of a $YAG:Ce^{3+}$ as a component for a one or two phosphor system to create white light. Once again, the LED was run at voltages from 23V to 26.0V and the resulting spectra are shown in figure 7.4 for the measurement taken at 26.0V over an increasing thickness in phosphor deposited.

For completeness, and to see how the red phosphors responds to the LED, $CaS:Eu^{2+}$ and $SrS:Eu^{2+}$ were also measured over the LED running in the same conditions. One or both of these phosphors were to be used as the red constituent of any potential white light emission. A red component to the white light was something seen to be lacking in the emission spectra in figures 7.3 and 7.4 when the blue LED was combined with either a $YAG:Ce^{3+}$ or $SrGa_2S_4:Eu^{2+}$.

These spectra for europium activated calcium sulphide and europium activated strontium sulphide europium are shown in figures 7.5 and 7.6 respectively.

When comparing the two it was clear that the $YAG:Ce^{3+}$ phosphor emission was much broader than that of $SrGa_2S_4:Eu^{2+}$. They both emitted from 500nm, and
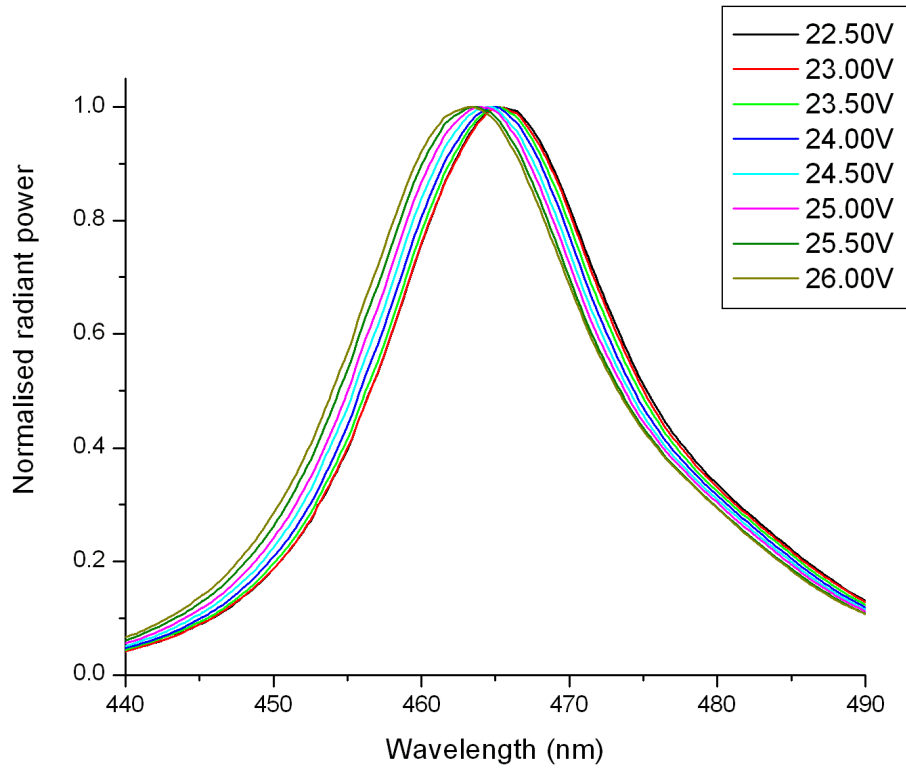
Figure 7.2: Peak shift in normalised emission spectrum of LED array as voltage increases incrementally from 22.50V to 26.00V
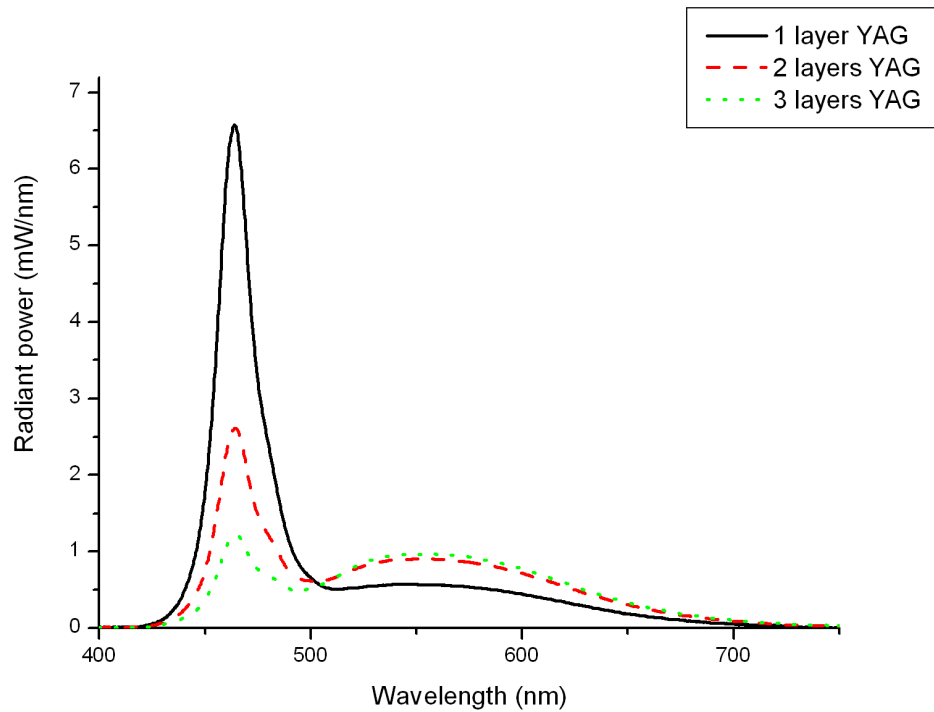
Figure 7.3: Emission from YAG:Ce^{3+} screens over blue LED
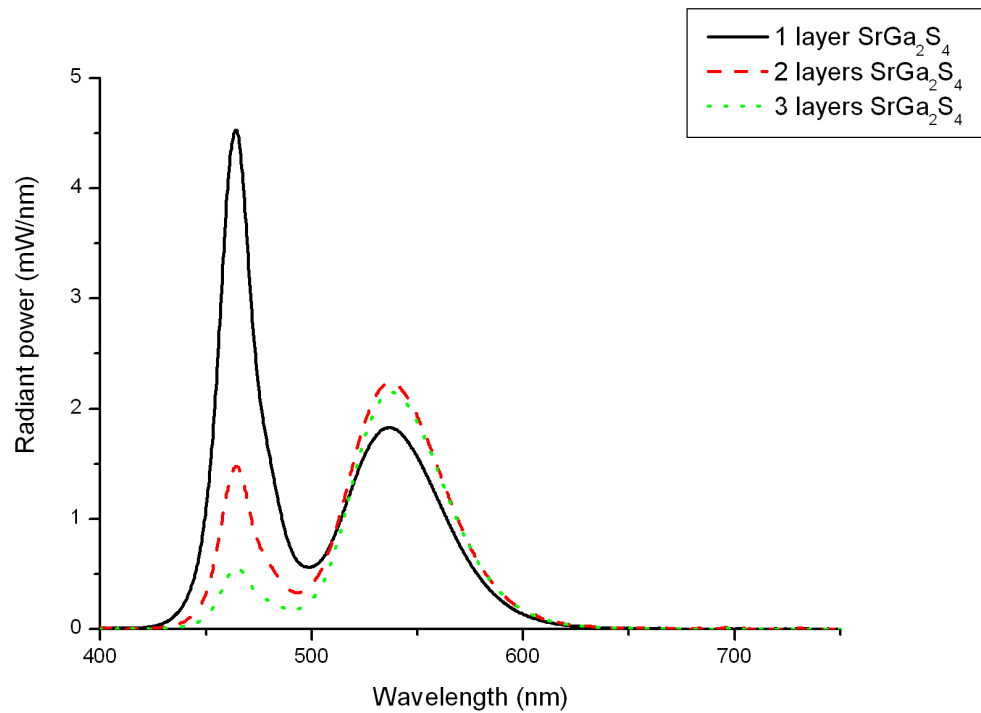
Figure 7.4: Emission from $SrGa_2S_4$:Eu^{2+} screens over blue LED
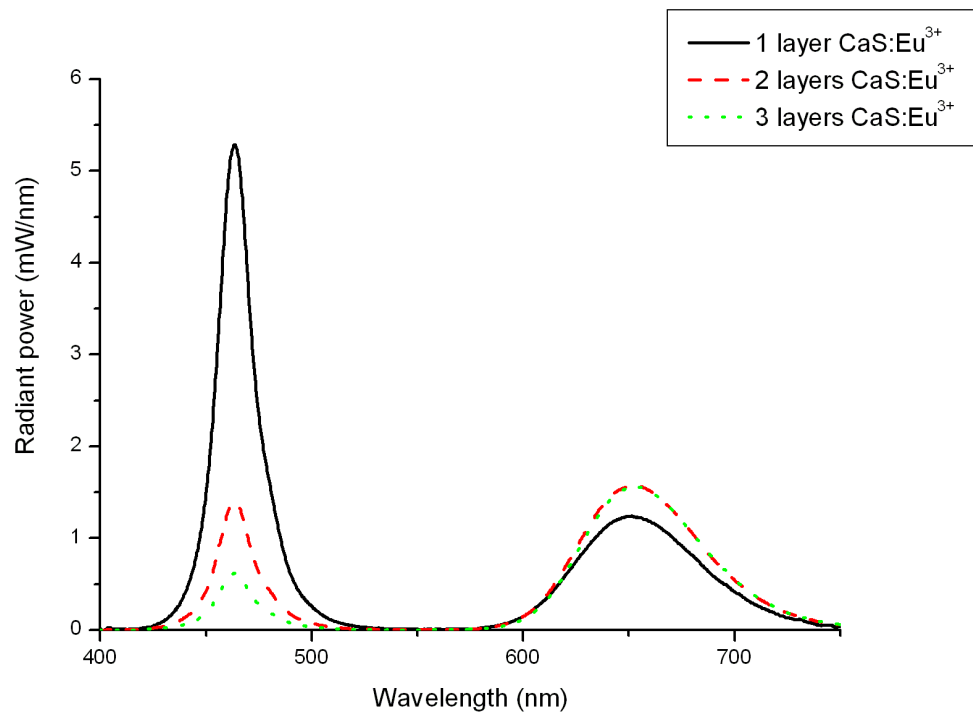
Figure 7.5: Emission from CaS:Eu^{2+} screens over blue LED

covered the central, high lumen output region, of the visible region, however, the YAG:Ce^{3+} extended into the red region of the spectrum. This explained why the YAG:Ce^{3+} is a very good phosphor for white light generation from a one phosphor
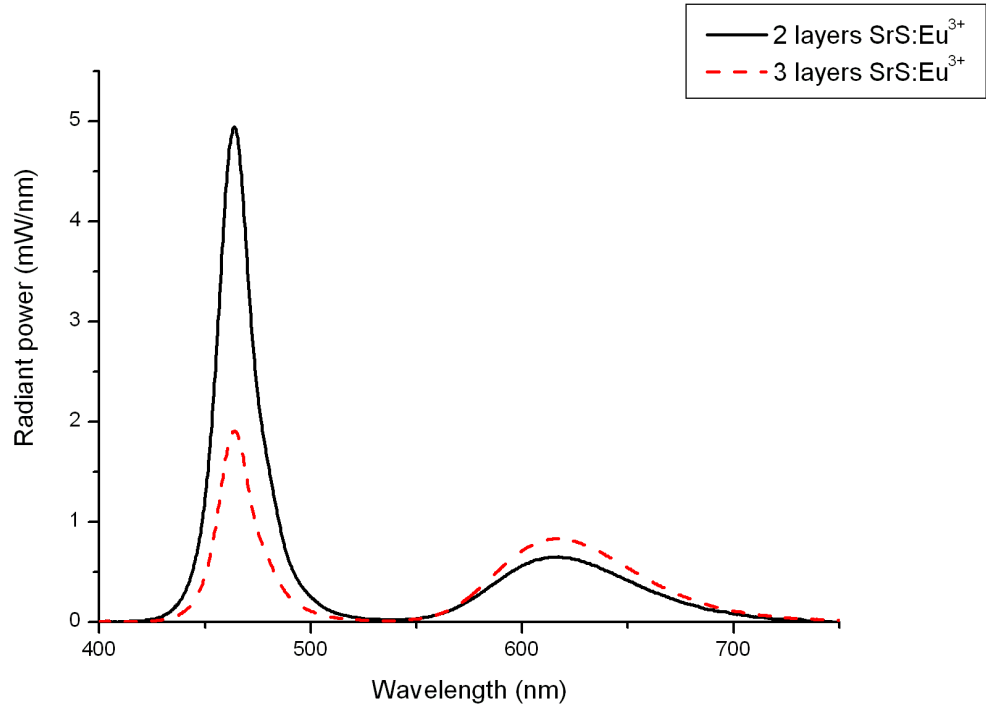
Figure 7.6: Emission from SrS:Eu^{2+} screens over blue LED

system. It was also observed that in both cases, there appeared to be an indication that the efficiency of the phosphor decreased as more was added. However, further addition of phosphor will still absorb the emission from the LED.

Before looking at improving the white light emission, there were further phosphors with the potential to be used in these cases.

7.3   Novel Phosphors

Further screens were printed using phosphors described in chapter 5, as well as another phosphor that was made at Brunel, Li$_2$SrSiO$_4$:Eu^{2+}. This is a broad band green emitting phosphor which can also be doped with Ce^{3+} and has been studied recently [4] [5].

7.3.1   Experimental Method Li$_2$SrSiO$_4$:Eu^{2+}

Li$_2$SrSiO$_4$:Eu^{2+} phosphor powder was synthesised by solid state reaction [6] of the starting materials, Li$_2$CO$_3$, SrCO$_3$, SiO$_2$ and Eu$_2$O$_3$. Stoichiometric amounts were ball milled in IPA for 2 hours and after drying, the powder was preheated in air at 600 °C for 12 hours. The powder was then placed in a alumina boat and fired at 800 °C for 12 hours under a reducing atmosphere of 5%H$_2$ 95%N$_2$. The rate of heating and cooling was controlled at 5 °C per minute. After firing, the powder was ground using a mortar and pestle.

7.3.2 Properties of Li$_2$SrSiO$_4$:Eu^{2+}

The phosphor particles were investigated under SEM and were seen to be quite large in size at 100μm and greater, images of which are shown in figure 7.7. A barium chloride flux was introduced in an effort to reduce the particle size. This phosphor was then remade as described in the previous section (7.3.1), with the inclusion of BaCl$_2$. This was added solely in order to control the particle size of the phosphors after the firing. This was assessed for a range of fluxes, from 1% to 3% by weight, and the resulting phosphors were analysed under SEM. These images are shown in figures 7.8, 7.9 and 7.10.
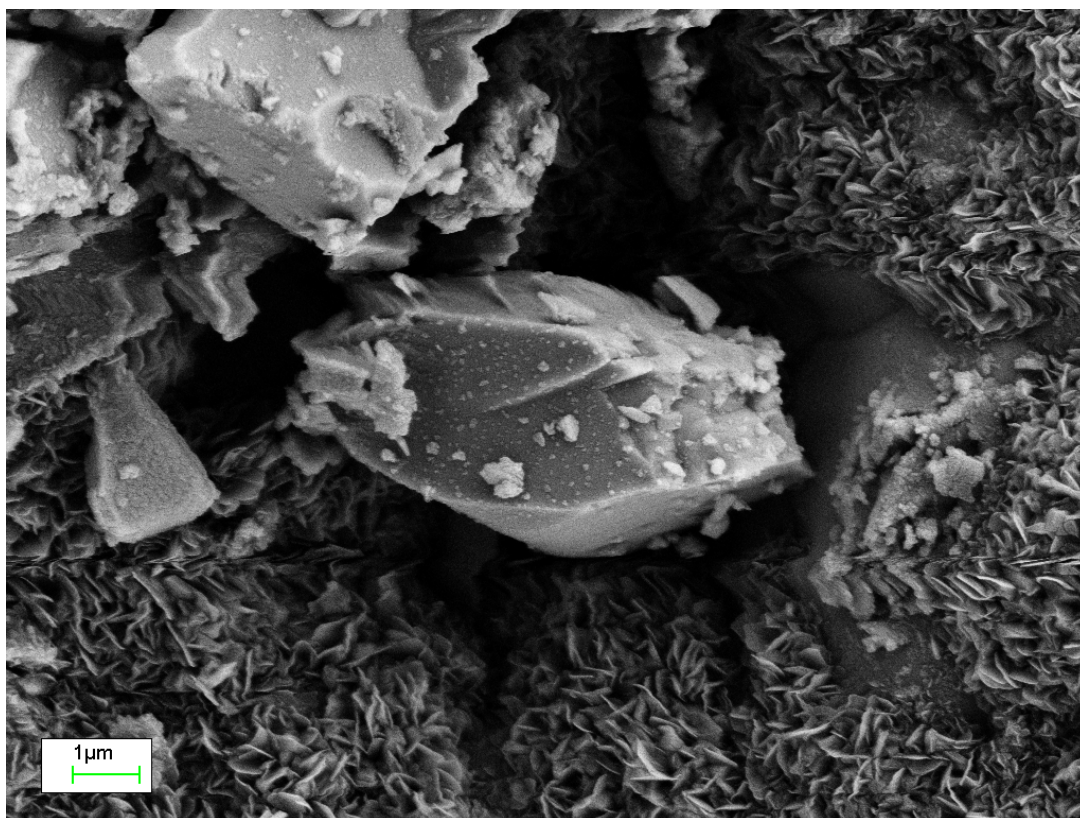
Figure 7.7: SEM of particles of Li$_2$SrSiO$_4$:Eu^{2+} showing small particles, 5μm in size, at 23K magnification

These images showed that not until a 3% flux was introduced was there a noticable reduction in the particle size. However, whilst there were many particles now of the order of 10μm in size, which were relatively large when sub micron particles are often a requirement, in addition there were a large number of particles of greater sizes. The effect of the flux on the excitation and emission spectra was also investigated. The normalised overlay of these spectra are presented in figures 7.11 and 7.12. The excitation spectrum was not altered significantly with the addition of a flux, although there was a noticable trend in the emission spectra to a slight narrowing of the emission bands, especially below the peak wavelength.

This phosphor was screen printed, after firing with a 3% flux and was found to have very poor properties for printing dues to the size of the particles. This led to
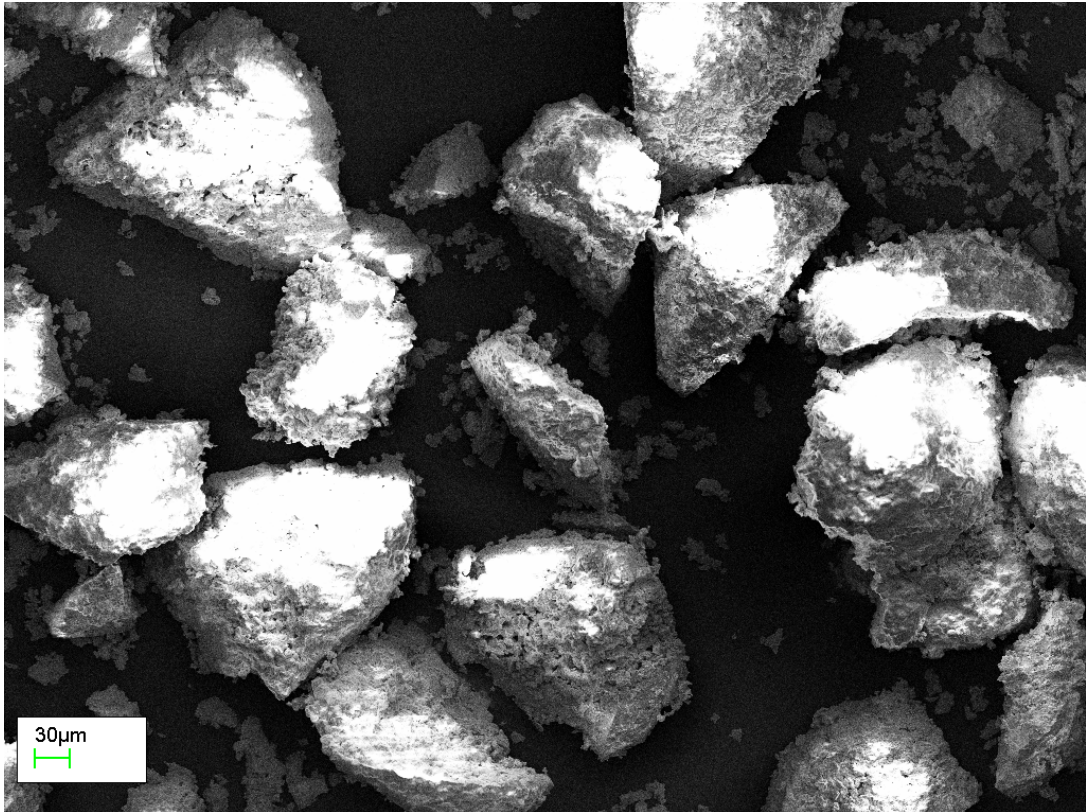
Figure 7.8: SEM of particles of Li_2SrSiO_4:Eu^{2+} with 1% $BaCl_2$ flux, at 400X magnification
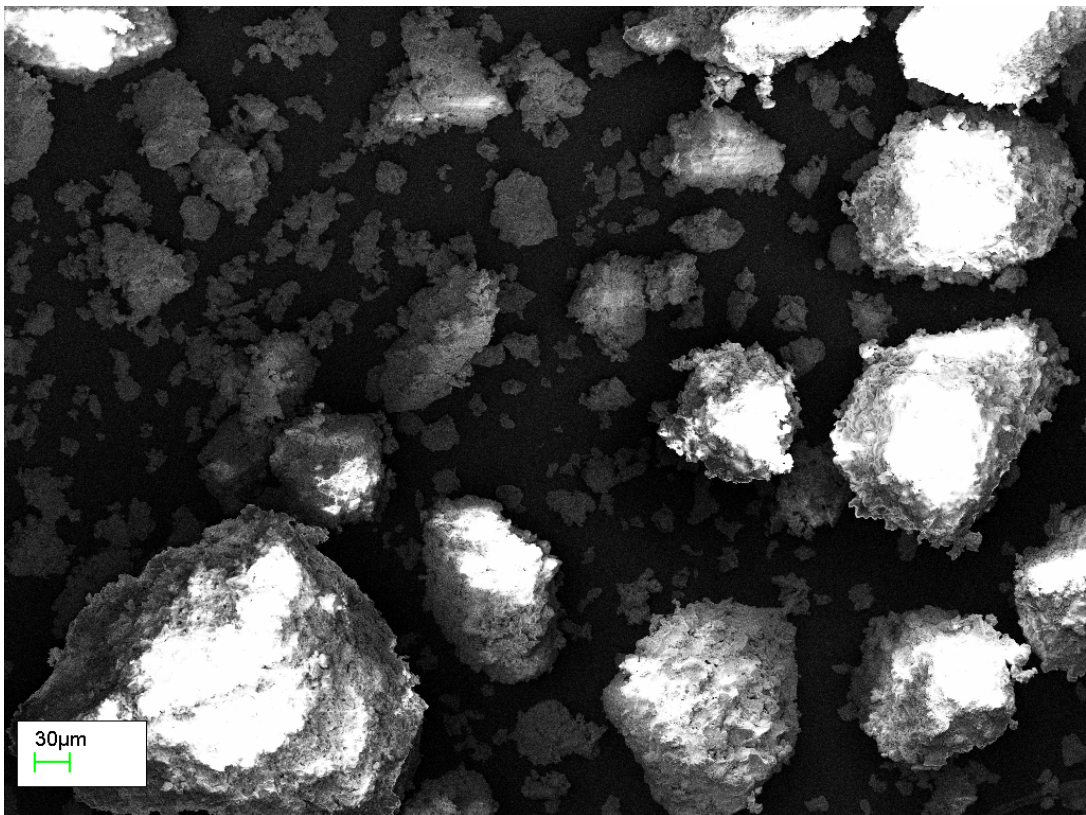
Figure 7.9: SEM of particles of Li_2SrSiO_4:Eu^{2+} with 2% $BaCl_2$ flux, at 400X magnification
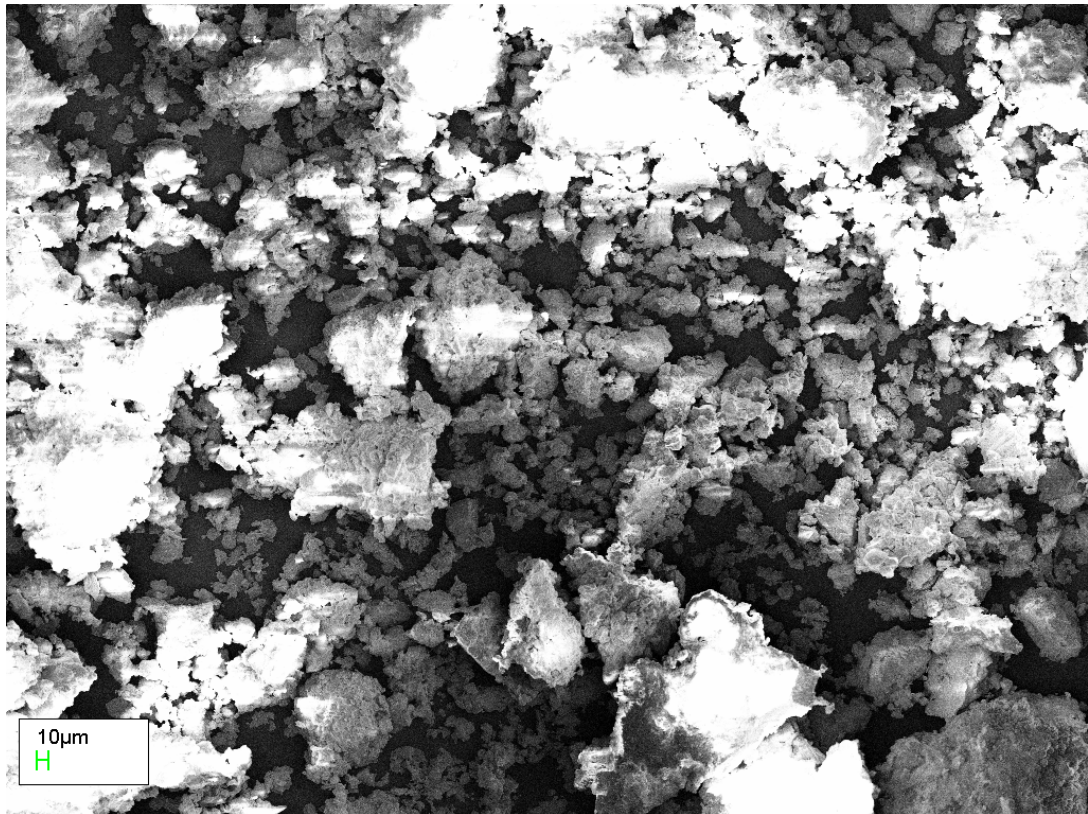
Figure 7.10: SEM of particles of $Li_2SrSiO_4:Eu^{2+}$ with 3% $BaCl_2$ flux, at 400X magnification

a very grainy finish to the screens even after printing a few dry runs and therefore further evaluation of this phosphor was discontinued. However, its emission was a very broad band covering deeper into the red than the $YAG:Ce^{3+}$ and if an alternative deposition method, or method to decrease the size of the particles while retaining the luminance is discovered, this phosphor would show great potential for use in a myriad of applications.
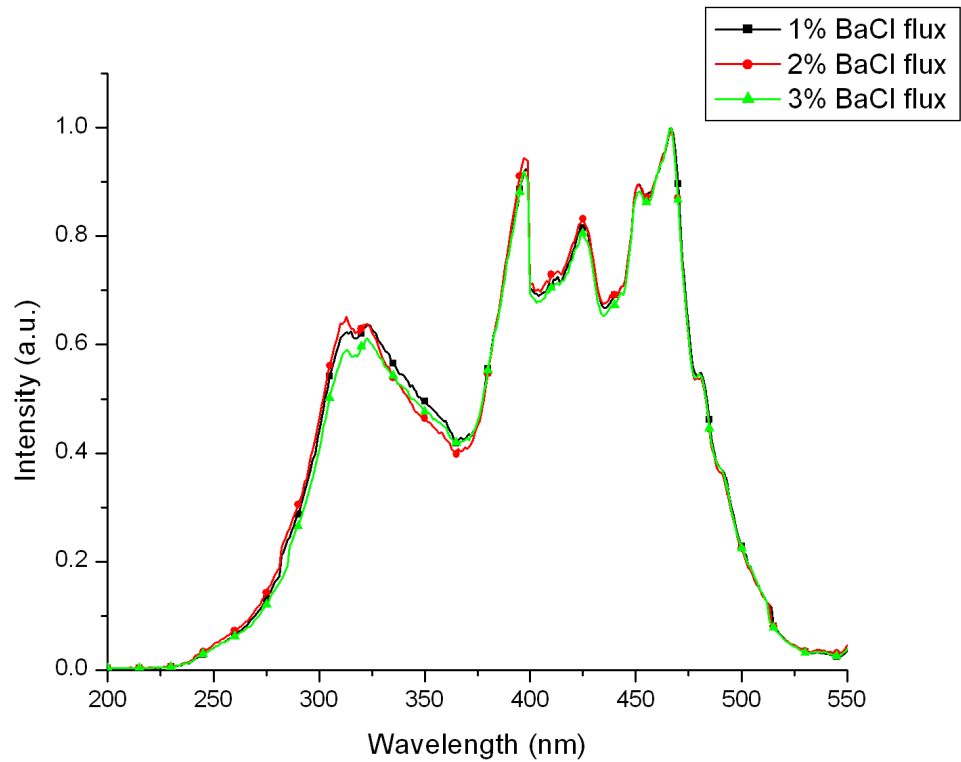
Figure 7.11: Excitation spectra of Li_2SrSiO_4:Eu^{2}+ for increasing $BaCl_2$ flux content, monitored at 580nm
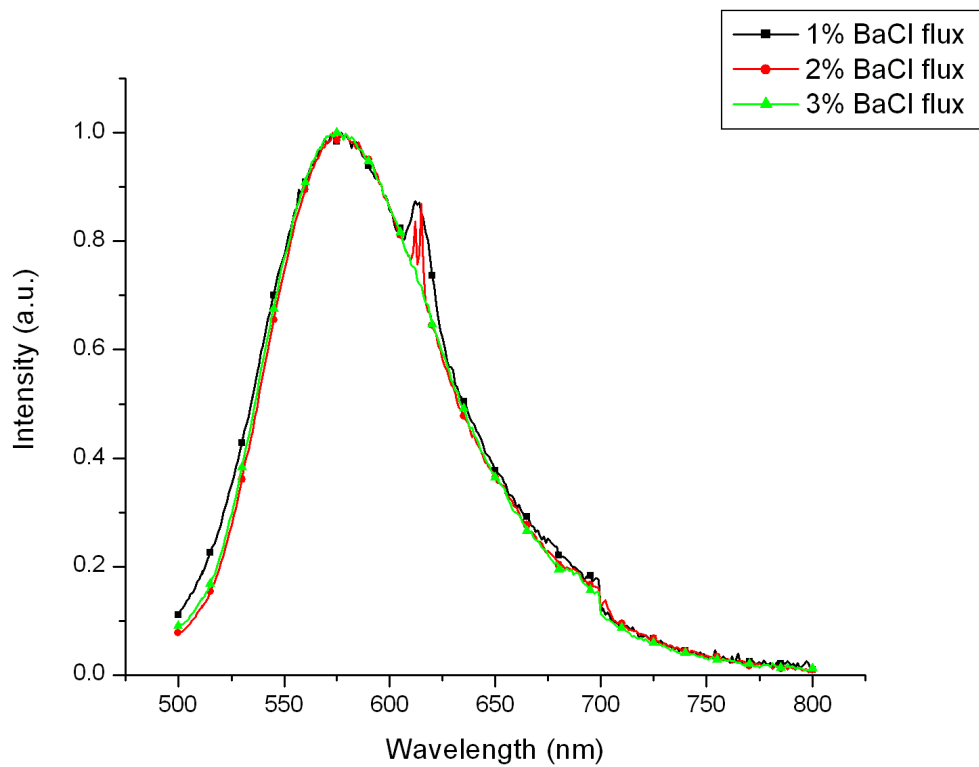
Figure 7.12: Emission spectra of Li_2SrSiO_4:Eu^{2}+ for increasing $BaCl_2$ flux content, excited at 465nm. The shoulder at 620nm was an artefact of the excitation lamp

7.4 White light emission

All the commercial phosphors were compared in their individual performance over the LED array. Their efficacies and efficiencies combined with the blue LED are shown in table 7.1. The $SrGa_2S_4$:Eu^{2+} was the superior phosphor in terms of its luminous efficacy, because its emission lay in the centre of the photopic response curve and was therefore measured at a very high luminosity. The red emitting phosphors were at much lower efficacies than even the LED and this was due to the distance from the centre of the photopic curve that the emissions lie. CaS:Eu^{2+} emitted deeper in the red than the SrS:Eu^{2+} explaining its lower value.

Table 7.1: Efficacies and efficiencies from varying thickness screens over blue emitting LED running at 25.00V

Emitter	No. of layers	Output (lm)	Efficacy (lm/W)
Array	-	17.9	9.9
YAG:Ce^{3+}	1	25.2	16.1
	2	32.3	20.7
	3	30.9	21.2
$SrGa_2S_4$:Eu^{2+}	1	37.9	24.1
	2	42.4	26.0
	3	39.6	24.5
CaS:Eu^{2+}	1	9.4	5.8
	2	6.8	4.1
	3	5.8	3.5
SrS:Eu^{2+}	2	13.7	8.3
	3	13.9	7.9

With the LED and individual phosphors categorised it was possible to study their combinations in order to achieve a high CRI white light output. The excitation spectra of each of the phosphors, and the emission profile of the LEDs (over varied power applied) was measured and these overlaying spectra were normalised and are shown in figure 7.13. The peaks of the excitation of the phosphors matched well with the LED confirming their suitability. However, it must be noted that as the power of the LED increases, and the peak shifts to lower wavelengths, slightly more of the blue light would be expected to penetrate beyond the phosphor. This was seen in all the emissions of the phosphors listed above with slight shifts in the CIE_x and CIE_y coordinates, and corresponding shifts in the CCT.

The YAG:Ce^{3+} and $SrGa_2S_4$:Eu^{2+} were then compared for their white light emission properties over the blue LED. CCT and CRI were additional measurements taken. Colour points were important in this case, and the closest achievable for each of these screens was the use of 2 layers of YAG:Ce^{3+} measured at (CIE_x, CIE_y) of (0.29, 0.33) and 1 layer of $SrGa_2S_4$:Eu^{2+} measured at (CIE_x, CIE_y) of (0.20, 0.31). Nevertheless, all the measured values are shown in table 7.2.

The most beneficial comparison of a white light emission was between the phosphor screens closest to a white point. With the $SrGa_2S_4$:Eu^{2+} situated to the left edge of
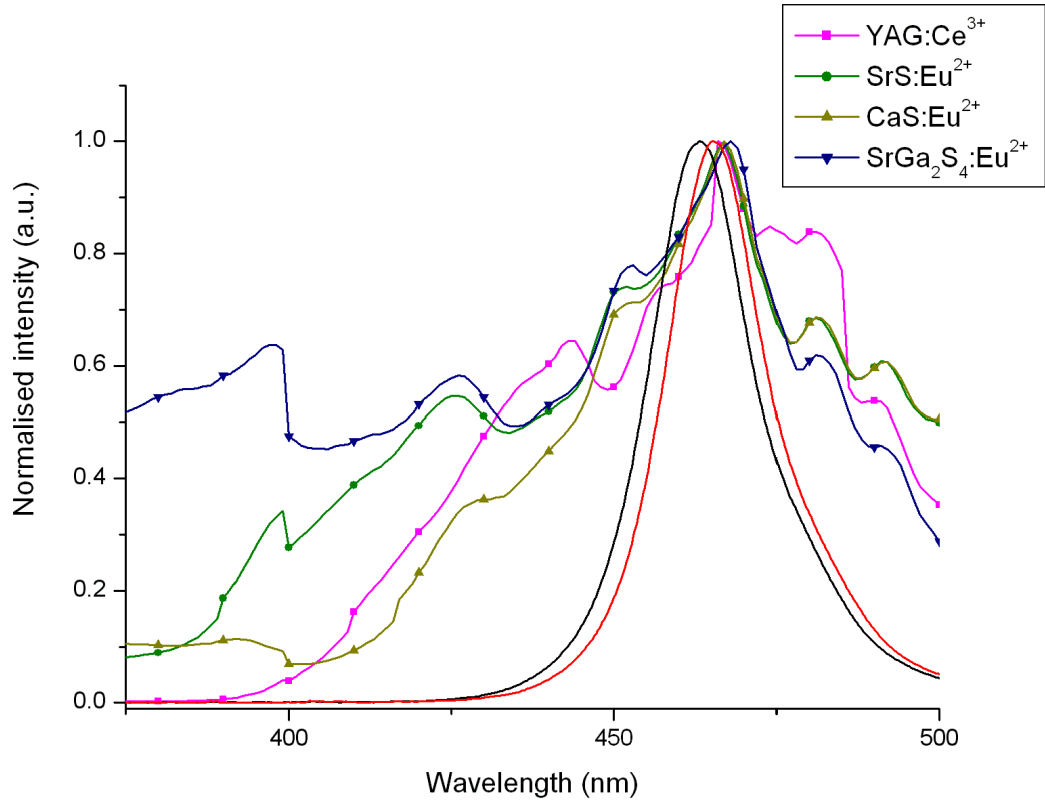
Figure 7.13: An overlay of the emission spectrum of the LED array, at the extremities of its peaks, and the excitation spectra of the phosphors described in this section

Table 7.2: Colour correlated temperature (K) and CRI for yellow/green phosphors of varying thickness screens over blue emitting LED running at 25.00V

Emitter	No. of screens	CCT(K)	CRI
YAG:Ce^{3+}	1	n/a	n/a
	2	7678	78
	3	5080	71.4
SrGa$_2$S$_4$:Eu^{2+}	1	20863	37.2
	2	74.82	25.6
	3	64.74	20.7

the Planckian locus, it was no surprise that the colour temperature was at such a high figure. However, the CRI was very low at just 37.2. As expected from the emission spectrum, this result showed that the peak was not broad enough to allow use of just this phosphor. The YAG:Ce^{3+} was much closer to the Planckian and has a reasonably high CRI of 78. R4 and R8 (defined in section 1.2.3) were the two lowest numbers in the colour rendering index (from R1 to R8), and although R9 was lower than these, it is not used for the overall CRI calculation. (R9 is a measure of a deeper red wavelength than any of those used in calculating R1 - R8.)

7.4.1 Problems with screens

The problems with screens were due to directly applying phosphors to the LEDs and the temperature increase they will experience. Even though there was a heat sink and fan when running the LED, heat was generated within the package and this adversely affects the performance of the phosphor. The operating temperature of LEDs can reach over $150\,^{\circ}$C, and the phosphors' performance at these temperatures was measured. As seen in figure 7.14 the luminous efficacy of these phosphors drops significantly with increasing temperature, except for the YAG:Ce^{3+} which retains its efficacy to 89% of its room temperature value at $150\,^{\circ}$C. For $SrGa_2S_4$:Eu^{2+}, the phosphor would not heat beyond temperatures greater than $160\,^{\circ}$C when the heat transfer to it was equalled by the losses suffered by the phosphor powder.

It was well known that the sulphides have poor thermal quenching; however, the measurements on $SrGa_2S_4$:Eu^{2+} show that it lost its efficacy almost entirely at a relatively low temperature. This was unexpected, as other sulphides such as CaS:Eu^{2+} and SrS:Eu^{2+} do not suffer this fate until reaching greater temperatures. It was posited that this effect was due to the high thermal conductivity of the phosphor. If high thermal conductivity describes the case with which electrons may be excited to the conduction band where they are lost non-radiatively, then thermal conductivity, which is a function of the lattice, may be proportional to temperature quenching.
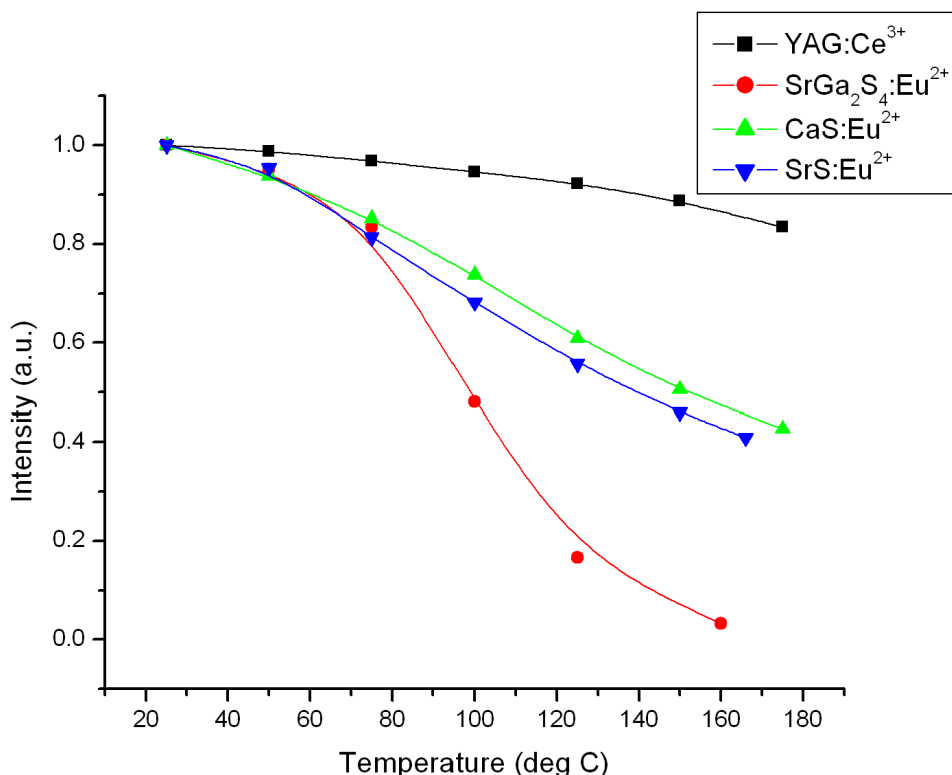
Figure 7.14: Normalised spectra showing decrease in efficacy of phosphors with increasing temperature

This thermal quenching, especially in the cases of sulphide phosphors, led to a new

approach when attempts were made to achieve high efficacy LED based emission. The aforementioned alternative technique for applying phosphors, namely using a remote method (screens or domes), were investigated for these same phosphors.

7.5 Remote Phosphors

Overcoming a reduction in performance at high temperature was the major advantage in the application of the phosphor on remote screens or on other remote supports. Light extraction also required study, including the effect this had on backscattered light and diffusion of light. As the phosphor emits isotropically, not all the emission was in the desired direction, and a portion of this was absorbed by the chip. Extraction of these photons has been seen to lead to an increase of up to 60% in lumen output [7]. There are a plethora of methods for the extraction of these photons, many of which have been registered in patents [8] [9]. Commonly, these will include the use of a reflector as well as a short wave filter in some region between the phosphor and the LED, again to increase the emission. One of the early registered patents, held by Philips, shows the use of reflectors and filters (although in this case does not involve remote phosphors) and is reproduced in figure 7.15 [8].
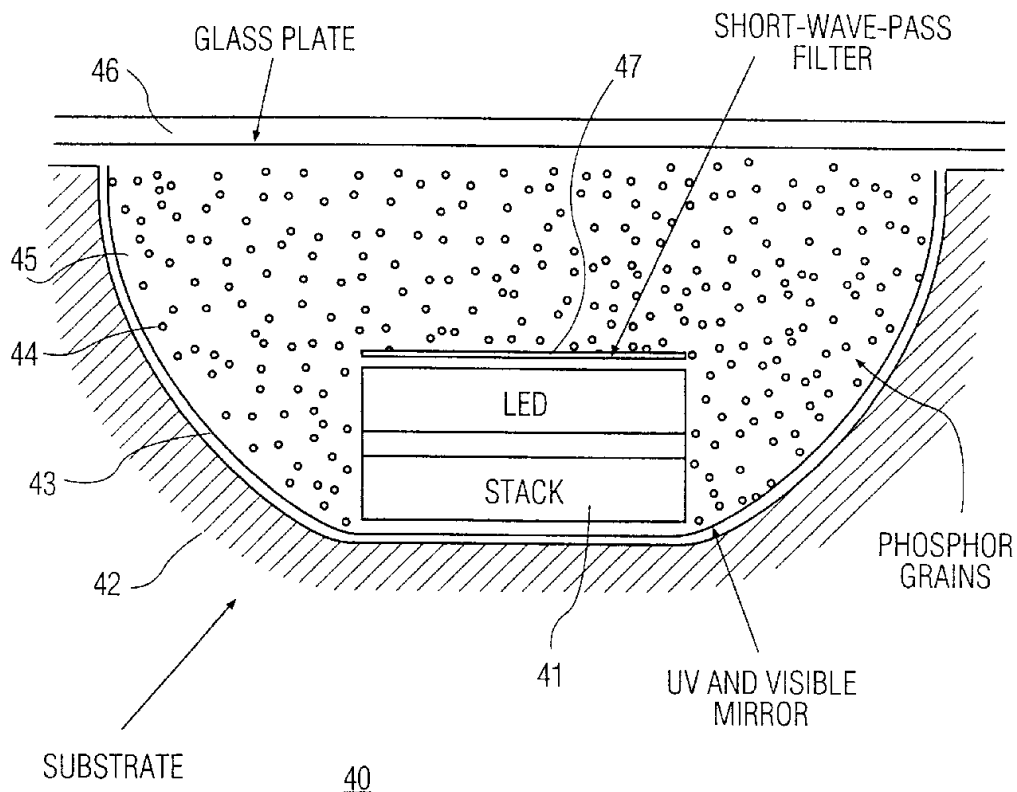
Figure 7.15: Early patent describing application of short wave pass filters and mirrors

These relatively early patents applied the phosphors directly, as seen, and this arrangement has drawbacks. The most noticeable is a 'halo effect', due to the varied

thickness in the phosphor layer that the light passes through. This was corrected in later patents by the use of a uniform, and usually thinner, layer of phosphor for which the light will pass through [10]. Ensuring that this layer was produced at constant thickness is one of the technical aspects of current LED arrays. This uniform emission needs to take into account the fact that the LED is directional and the light is emitted in a narrow manner, unlike that which is emitted from the phosphors.

One of the advantages of applying the phosphors remotely is that they act as a diffuser for the exciting light and a brief investigation into diffusion of LED chips was conducted.

7.5.1 Light Diffusion from Phosphors

Achieving isotropic emission from light sources was not solely confined to the application of phosphors. Prior to application of phosphors, other methods were available and investigated to achieve a diffuse emission from an LED. Should any diffusion problems arise following application of phosphors these may prove useful.

Those that were attempted here included a diffusion film, the introduction of a random surface diffusion and particle suspension diffusion.

Diffusion Film

A diffusion film was added on top of the surface of the device. This was a thin diffuser and was moulded to allow it to fix to the device. However, this was not suitable for integration into the device as it melted when trying to mould to the shape of the LED. To attach remotely required more work to ascertain the best optical arrangement for the diffuser including a method of support, which was deemed beyond the scope of the research.

Random Surface Diffusion

The idea here was to introduce a rough surface for the encapsulate of the device. Following the introduction of domes to the surface (described in the following section) the domes were subjected to the sandblaster to introduce a randomness to the surface. This led to a very even distribution of the emission and halos which were present prior to this process, were no longer apparent. This method was also successful for a multicoloured array of LED chips within a device.

Particle Suspension Diffusion

A final alternative which was investigated was the addition of reflective particles suspended within solid domes. Whilst this is not a remote application, it merited investigation as a method to diffuse the emission and prevent a halo effect seen previously, without altering the device in any other way. This was achieved using titanium dioxide, a material which is close to 100% reflective in the visible light region. It has a refractive index of 2.6 – 2.9 and as this increases the overall refractive index of the

silicone surrounding the chip, it has a positive effect on light extraction [11]. Using just 0.5% by weight relative to the total weight of the silicone gel in producing the dome led to a very cloudy dome. The lumen output in this case dropped to 29% of the output of the LED. At 0.1%, the lumen output was at 64% and at 0.05% the output was at 83% of the array's output. Whilst this does achieve the necessary diffusion, too much of the light was deemed to be lost in backscattering and absoprtion to continue with this approach.

Phosphors produced the same effect as these diffusion layers, and their use suspended remotely at a distance in a thin layer was investigated. This was carried out using solid hemispherical domes, to which a layer of phosphor was applied. Hemispherical shells have already been used to apply phosphors remotely and improve the light extraction [9].

7.6   Domes

A method for applying phosphors remotely is to use a spherical apparatus around the LED. This has properties conducive to the increase in extraction of light from the LED by reducing the amount of light reflected back to the array from any interface. A change in refractive index from one surface to another leads to some reflection and a larger refractive index leads to a greater reflection. The LED chips used were encapsulated by silicone which formed a flat surface. The domes reduced this reflection by reducing the amount of large angles that are met by the isotropically emitted light of the phosphor.

7.6.1   Making the domes

Domes were made using a GE Toshiba silicone gel, IVS4632. This was a two component gel which required equal mixing of each part of the A and B components. This was experimentally achieved using a speedmixer run at 1500-2000 rpm. Using a speedmixer was preferable to other methods, such as mixing by hand, as it was highly efficient in removing any bubbles. Without using the speedmixer degassing would be required to prevent bubbles expanding as the gel cured. Once mixed, to prevent introducing bubbles to the mixture, either the gel was extracted using a syringe or poured directly into a specially crafted aluminium mould. This mould was designed to allow an LED array to be affixed such that the gel would cure into a dome shape and be attached to the array located directly and centrally above the LED chips. The gel was cured in an oven at 80 °C for 2 hours to complete the process.

Spraying the domes

The materials used in order to coat the domes with the phosphors included a GE Toshiba silicone gel IVS4632, the desired phosphors and acetone which was added to thin the mixture to allow for smooth spraying. The same silicones that were used to create the domes was used here to limit change in refractive index at the interface.

The phosphors had a refractive index at ~2.1 for the sulphides and ~1.83 for the YAG:Ce^{3+}, with the silicone gel having a refractive index of 1.40. The LED wafers have a refractive index of ~2.4 and this combination led to better light extraction for sulphides. Furthermore, the sulphides having similar indices allowed their mixing without causing an increase in light scattering [12].

A basic airbrush was used as the equipment to spray the domes. The ratio of silicone to phosphors was around 3:1 although decreased to 4:1 if less phosphor was required as was the case in some situations for the red phosphors. The amount of acetone used also varied depending on the phosphor used, with the sulphide red phosphors requiring more acetone for uniform spraying, possibly due to the larger particle size. The exact ratios used also depended on the properties required from the light source, and those for white light emission were discussed in section 7.6.2.

After spraying the domes, they were placed in an oven at 80 °C for 10–30 minutes to evaporate the acetone and cure the silicone within which the phosphor was now contained. Sulphide based phosphors curing time were greater than those for other phosphors such as YAG:Ce^{3+}. The amounts of phosphors that should be deposited to generate a white light were calculated experimentally. The method for spraying these was adjusted to balance optimisation of the quality and ease in spraying with amounts required to generate the desired output.

7.6.2 White light emission from domes

Simply incorporating the domes onto the array increases the efficacy of the light output. At 30W, the arrays would emit at approximately 5.5 lm/W, and this increased to 10.4 lm/W with a dome built onto the array.

Using the commercial phosphors listed in the preceding sections it was possible to create a white light emission from a blue LED source. The amount of each phosphor necessary and the order that they were deposited on the dome were important in creating such emissions in a repeatable process. The process began with the phosphor, silicone and acetone ratios being derived experimentally to form a mixture that was a suitable viscosity for spraying.

The amount of silicone used to YAG:Ce^{3+} was in a ratio of 3g YAG:Ce^{3+} for each 10g of silicone, and added to this was 2g of acetone. Both the CaS:Eu^{2+} and SrS:Eu^{2+} required 18g of silicone for 3g of phosphor. To attain the highest CRI an even weighting of each of these two phosphors was used. 6g of acetone was used to thin this mixture for spraying.

Initially, each of the phosphors was applied separately, beginning with CaS:Eu^{3+} and SrS:Eu^{3+}. The spectra are shown in figures 7.16 and 7.18. The associated colour points are shown in figures 7.17 and 7.19 respectively. (Points A-E on this spectrum are reference points to standard white light sources).
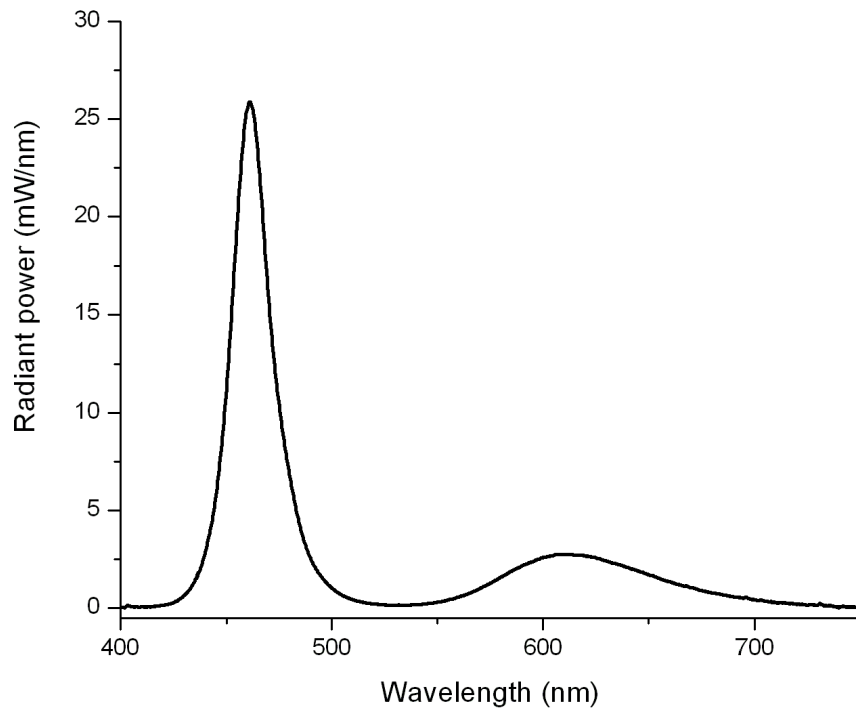
Figure 7.16: Blue LED emission with a SrS:Eu^{2+} coated dome
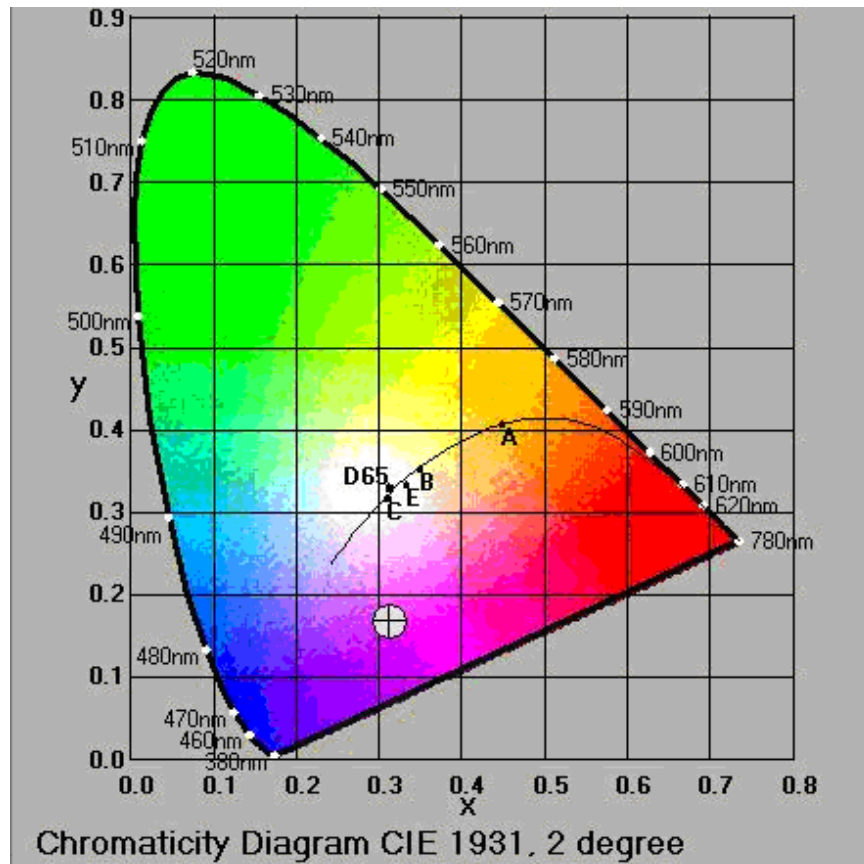

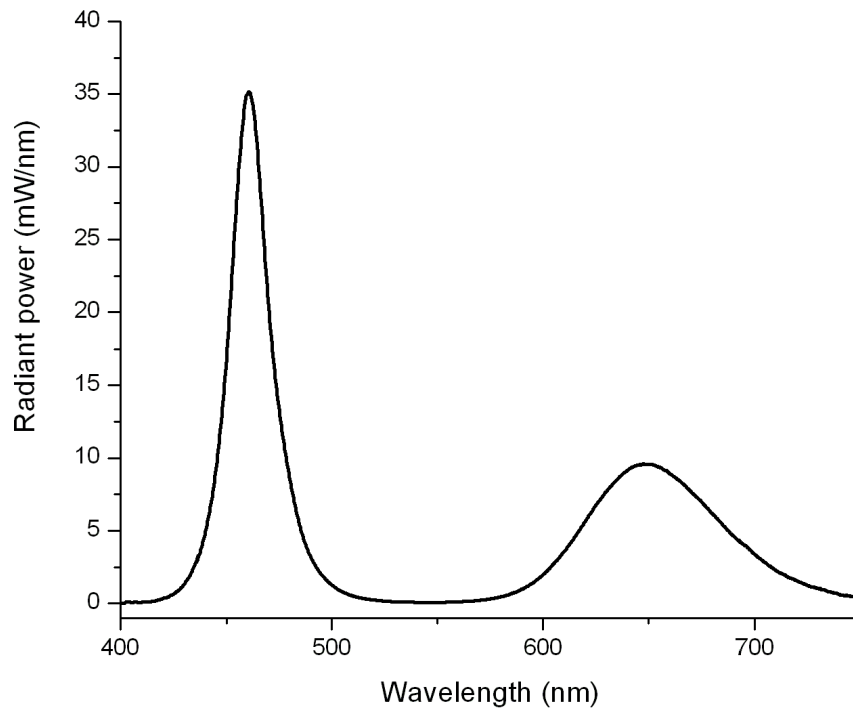Figure 7.17: CIE coordinates of blue LED emission with a SrS:Eu^{2+} coated dome

Figure 7.18: Blue LED emission with a CaS:Eu^{2+} coated dome
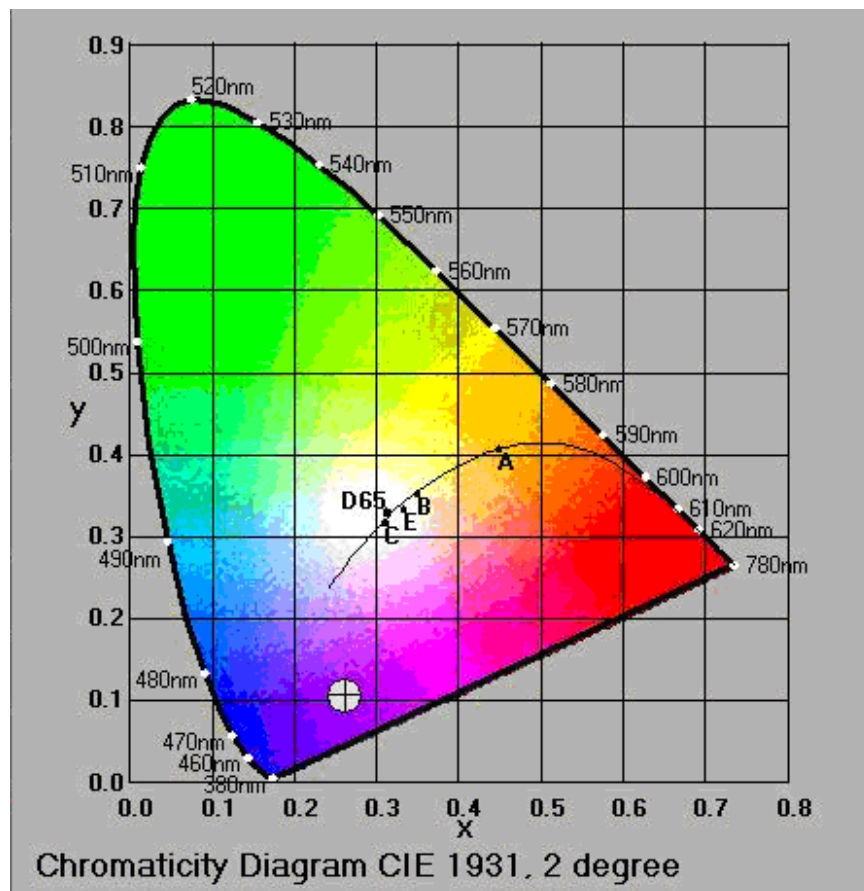
Figure 7.19: CIE coordinates of blue LED emission with a CaS:Eu^{2+} coated dome

An even mix, by weight, of $CaS:Eu^{3+}$ and $SrS:Eu^{3+}$ was used to broaden the emission spectrum compared with each individually and is seen in figure 7.20. This broader emission spectrum increased the CRI for white light emission. As the amount of phosphor was increased, the CIE coordinates seen in figure 7.21, also shifted further towards the red than with those shown earlier. As expected this shift with increasing phosphor remains on a straight line from the colour point of the LED.
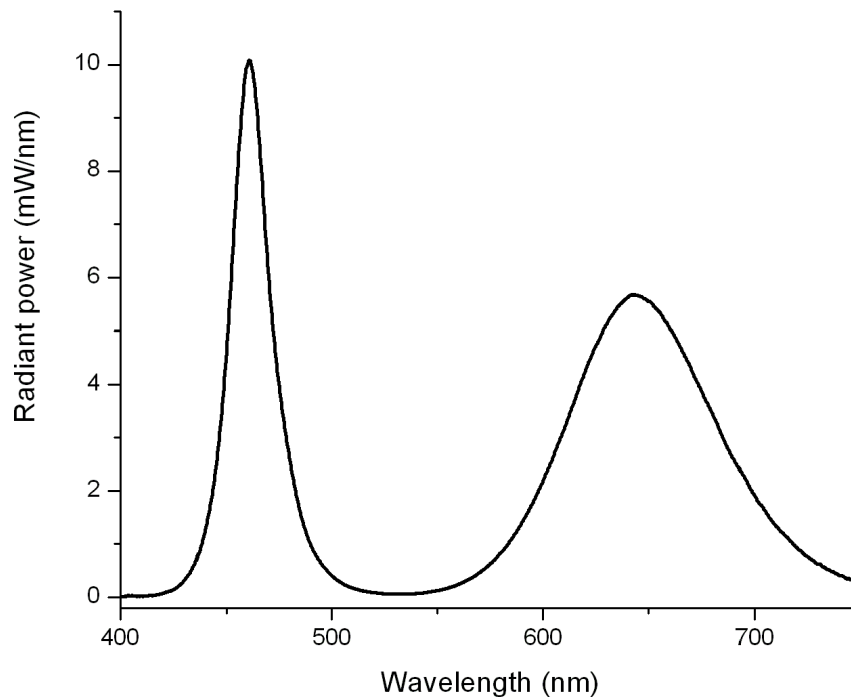
Figure 7.20: Blue LED emission and dome coated with an even mix of $CaS:Eu^{2+}$ and $SrS:Eu^{2+}$

$SrGa_2S_4:Eu^{2+}$ was added to the red emitting combination of phosphors. The emission is shown in figure 7.22. As was clear from the image, there were large gaps in the emission spectrum between the emission from the LED blue, the green and the red phosphors. This led to a low CRI of between 72 and 80 depending on the power to the blue LED. In this case, as the power increased, the CRI increased although the CCT increased from around 15000 to as high as 45600 when at a CRI of 80, with colour points of (0.27, 0.25). Whilst it would be possible to add more of each of the phosphors and keep the emission at the Planckian, the CRI would be unlikely to increase much beyond this figure recorded.

Further to this, $SrGa_2S_4:Eu^{2+}$ was seen to emit efficiently only over a narrow temperature range, and became inefficient as the temperature increased, especially when compared to $YAG:Ce^{3+}$, it was no longer used with the LED arrays. Therefore, $YAG:Ce^{3+}$ was the phosphor that provided the yellow emission with $CaS:Eu^{2+}$ and/or $SrS:Eu^{2+}$ were used for the red emission.
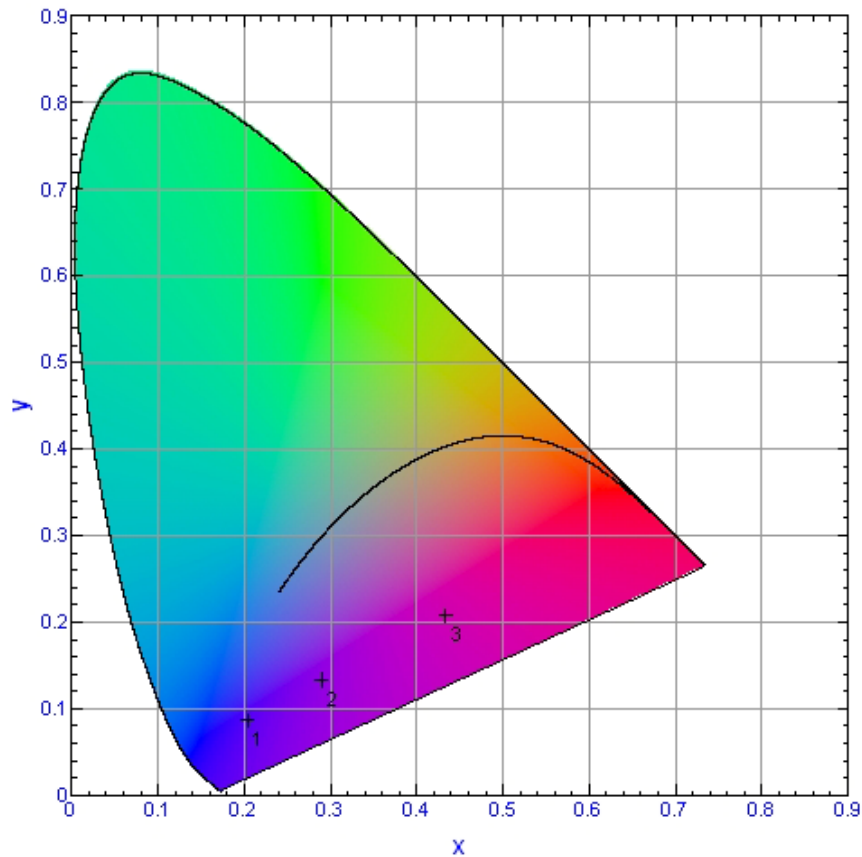
Figure 7.21: CIE coordinates of blue LED emission and dome coated with an even mix of
CaS:Eu^{2+} and SrS:Eu^{2+}

The red phosphor was applied first for two reasons. As was the case with screens
tested over ACEL panels in the previous chapter, the red phosphor was less efficient
and more is required to achieve the same final output if it comprises the top layer.
Secondly, in this method the YAG:Ce^{3+} phosphor mixed with silicone dried more
rapidly and had a smoother appearance, which was more aesthetically pleasing and
provided a more durable outer layer.

This combination of phosphors led to the spectra in figure 7.23. This showed
the emission spectrum when the amount of YAG:Ce^{3+} used combined with the red
phosphor and the remaining blue light to give an overall white emission. Changing
the thickness of each layer led to many different colour points, including some on the
Planckian locus. The CIE diagram for each of the four spectra of figure 7.23 is shown
in figure 7.24 and labelled in respect of the legend in the former.

This white light emission (labelled (2) in figure 7.23) followed the Planckian as the
power was increased in the blue LED and the CCT increases from 3466 to 4032 as the
power to the LED increases. The measured CRI, as the power increased, decreased
from 92.20 to 90.6.
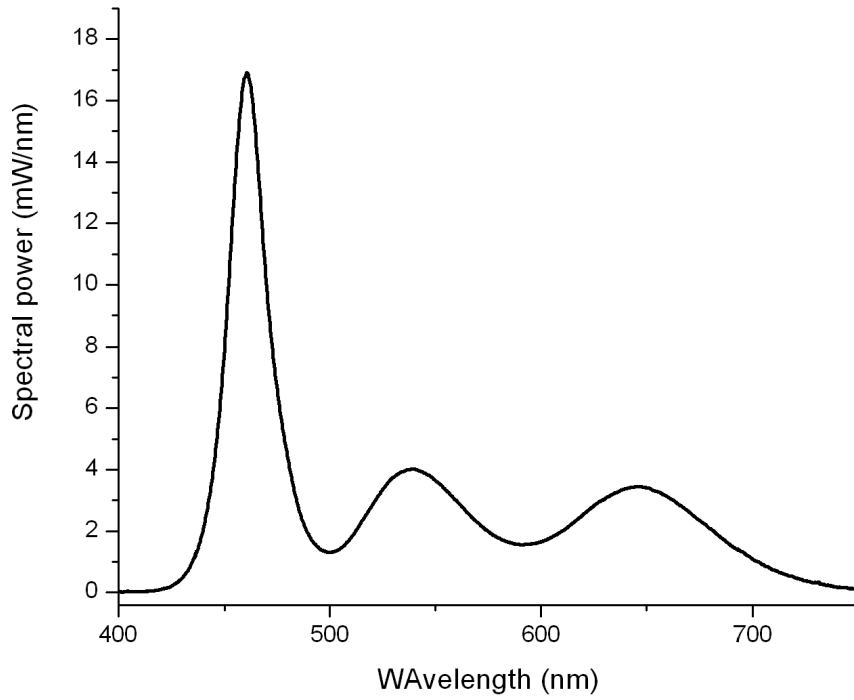
Figure 7.22: Blue LED emission and dome coated with a mix of CaS:Eu^{2+}, SrS:Eu^{2+} and SrGa$_2$S$_4$:Eu^{2+}
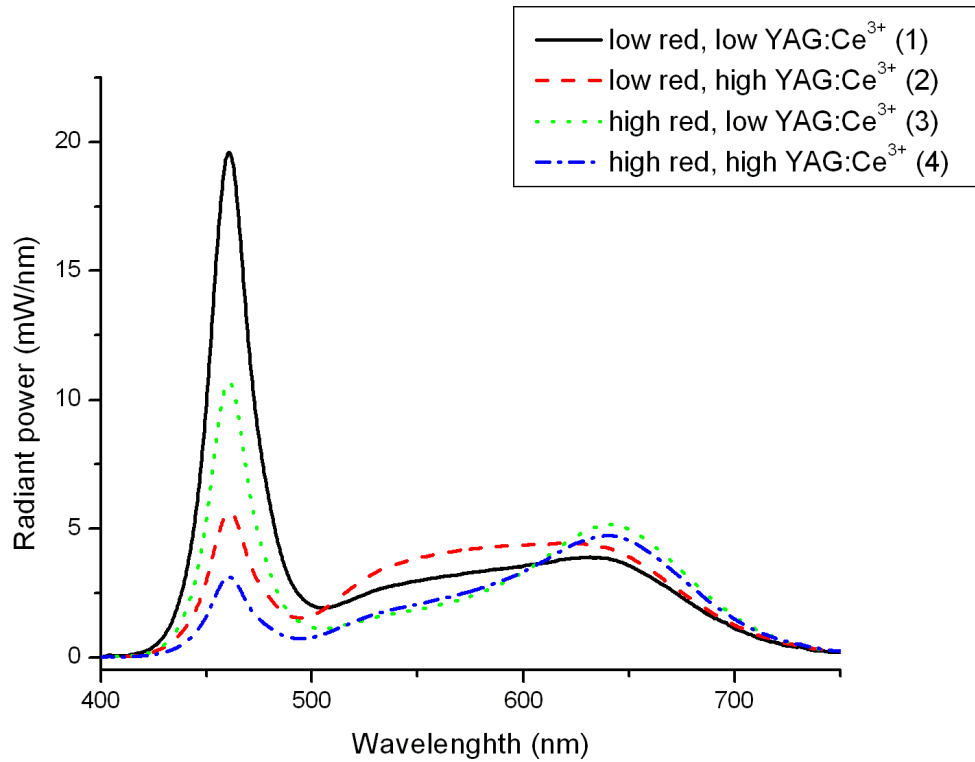
Figure 7.23: Blue LED emission and dome coated with a mix of YAG:Ce^{3+}, CaS:Eu^{2+} and SrS:Eu^{2+}
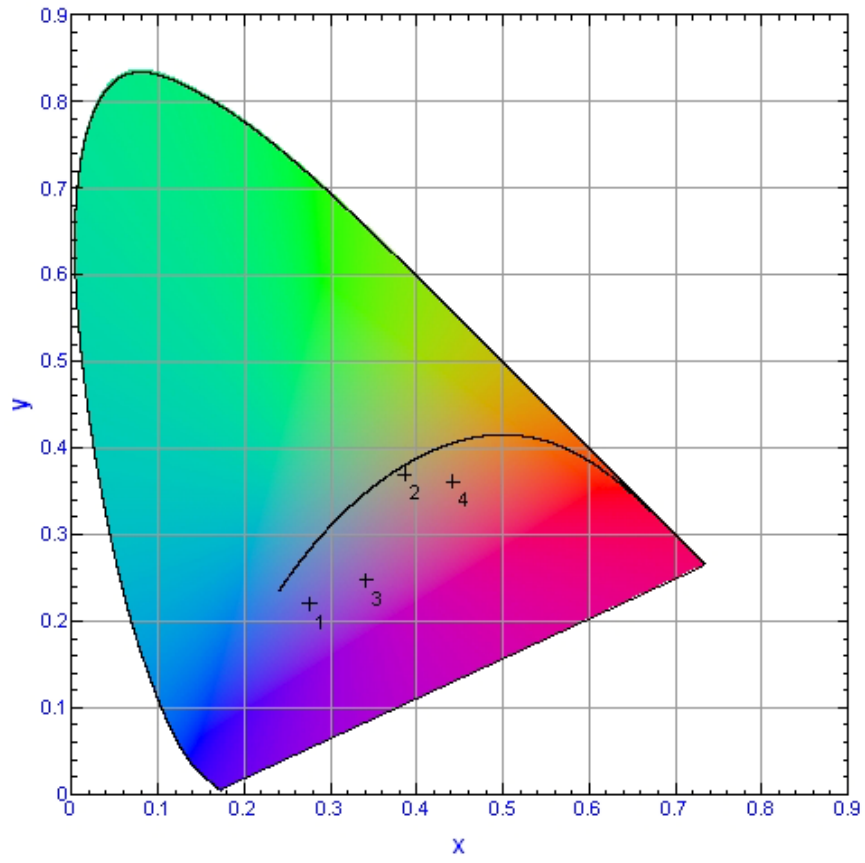
Figure 7.24: CIE coordinates of blue LED emission and dome coated with a mix of YAG:Ce^{3+}, CaS:Eu^{2+} and SrS:Eu^{2+}

With a greater amount of red phosphor and YAG:Ce^{3+} deposited, the emission appears as labelled (4) on the spectra in figure 7.23. This had CIE (x, y) coordinates of ~(0.45, 0.36) depending on the input power. This is just below the Planckian locus, and with a CCT of ~2400K is a warm red emission. The CRI is also high at > 90.

For a dome of 18mm radius, by varying the deposited amount of red phosphor, from 0.043g to 0.006g, a CCT from 2600 to 7300 can be achieved. The CRI peaked at 93.7 for that with greatest red content, and for the highest CCT was measured at 87.0 which is high enough for almost all applications.

The relationship between CRI and amount of red phosphor deposited is shown in figure 7.25. The corresponding amount of YAG:$^{3+}$ phosphor required to achieve very close to a white light emission, based on the weight of the red phosphor deposited, is shown in figure 7.26. These results can be converted to a thickness if the measurements of the domes are precisely taken. The error in the measurements of domes here proved too great to calculate the thickness accurately.
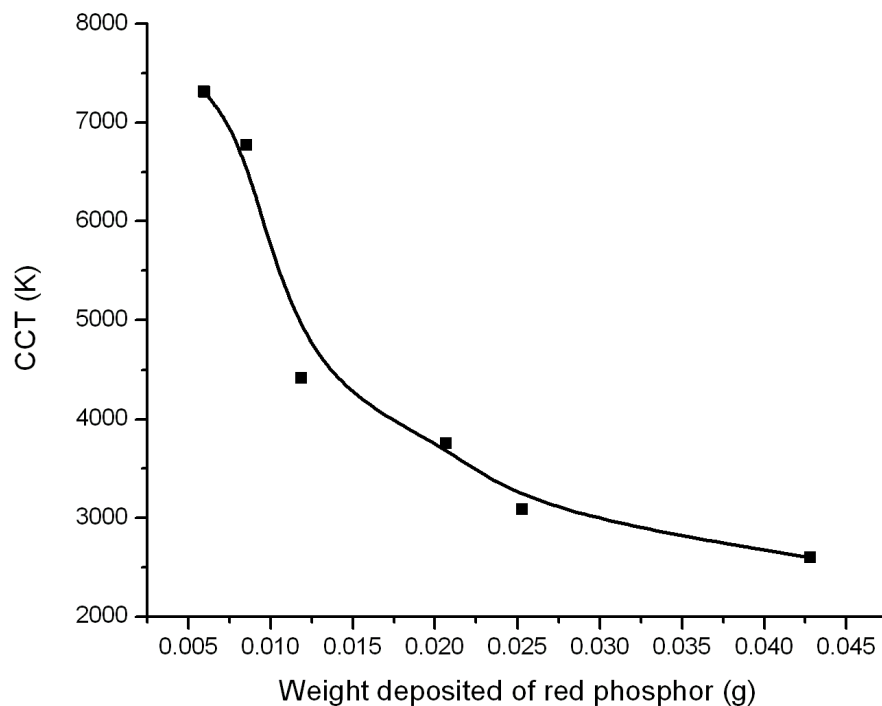
Figure 7.25: Relationship between weight of red phosphor (combined SrS:Eu^{2+} and CaS:Eu^{2+}) deposited and CCT of final product after YAG:Ce^{3+} was added

For a white light emission, the weight after drying the red phosphor combination for 30 mins (the acetone will have evaporated after a few mins) should be around 0.050g for low CCT requirements. At 25W this gives a CCT of 3280K. This much red phosphor requires 0.166g of YAG:Ce^{3+} deposited to give a white light emission. With 0.040g of red phosphor, 0.091g of YAG:Ce^{3+} was required to give a white light of 4000K at 25W.
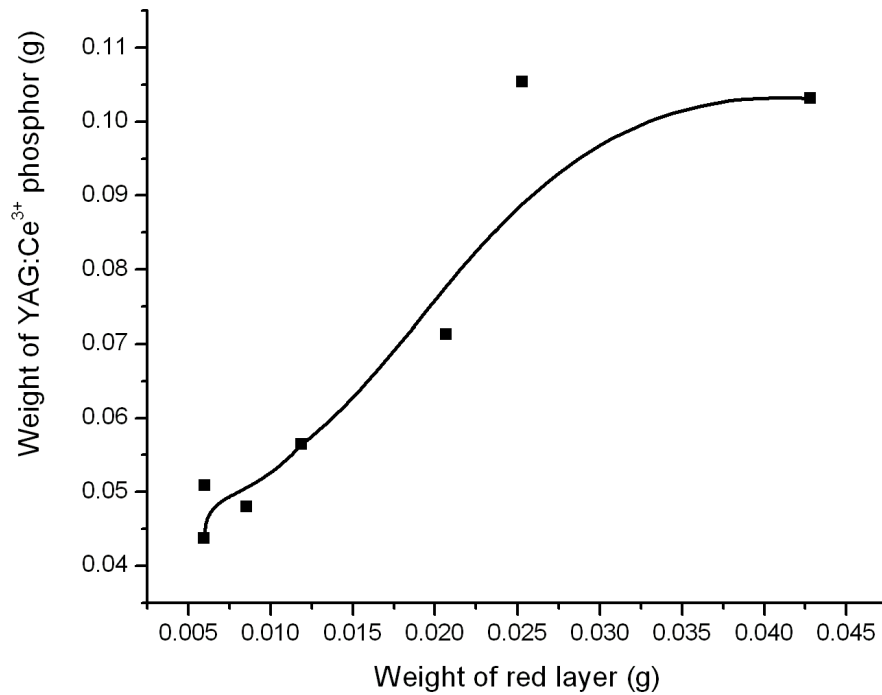
Figure 7.26: Relationship between weight of YAG:Ce^{3+} and red phosphor (combined SrS:Eu^{2+} and CaS:Eu^{2+}) to achieve a white light emission when excited with a blue LED

In every situation after weighing the deposited amounts of red phosphor of this mixture, it was possible to calculate the amounts of YAG:Ce^{3+} phosphor necessary to be added that result in a white light emission. Based on these results, it was then possible to control the initial amount of red phosphor deposited, in order to define the desired final CCT that would be achieved once the YAG:Ce^{3+} was added.

7.6.3 Refractive Index and scattering considerations

The scattering effects that occur in these designs warrants mention. The factors under consideration were wavelength of excitation light, particle size, and refractive index of the particles and the silicone. Mie scattering is applicable here due to the size of the particles. When the particles were encapsulated, a greater difference in the refractive index between the phosphors, which as inorganic materials are usually in the range of 1.75 – 2.25, and the silicone gel at 1.40, leads to a greater scattering effect. This is exacerbated at lower wavelengths, and the values for scattering against refractive index were calculated and are shown in figure 7.27 [13].
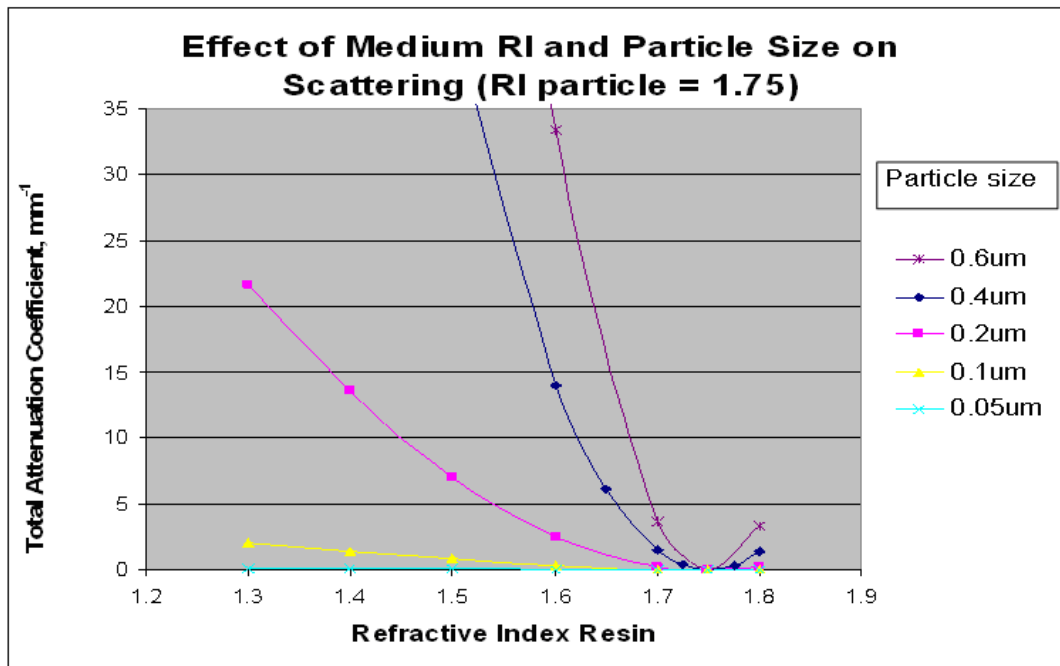
Figure 7.27: Mie scattering calculation, at 600nm

As is seen, as particles size is reduced the scattering is reduced, and the other major effect is the dispersion as the concentration of particles per cubic micron is proportional to the total attenuation coefficient. For white light emission, less dense packing is necessary to allow some blue emission to pass although, if attempting to saturate the emission a densely packed layer would suffer from this effect.

7.6.4 Improving the efficacy of emission from dome

There were two avenues pursued to increase the efficacy from the domes that were created thus far in this chapter. They were the inclusion of a short wave filter, and the addition of some silicone gel to remove the air gap that lay between the dome and the surface of the encapsulation of the LED. The latter was needed as production of the LED package would allow for the dome to be built directly onto the LED. The increase in efficacy was measured for domes that had the air gap eliminated by the direct placement of the dome onto the array.

This efficacy increase would be expected to be seen over all the results reported earlier in this chapter.

Short Wave Filters

Two short wave filters were purchased from Edmund Optics and used by positioning them between the LED array and the dome. This was to reflect any of the phosphor emission which was not in the forward/desired direction. The short wave pass filters had their cut-offs listed at 500nm and 550nm. The transmission spectrum of these filters are shown in figures 7.28 and 7.29 and also shows the positions of the LED emission and phosphor emission. The 500nm pass filter has a cut-off that appeared to be in a more suitable location based on the emission spectrum of the LED although the filter's reflection at higher wavelength was a concern. Furthermore, a reduction due to absorption or reflection of the blue light needed to be compensated for by the increase in reflected light.
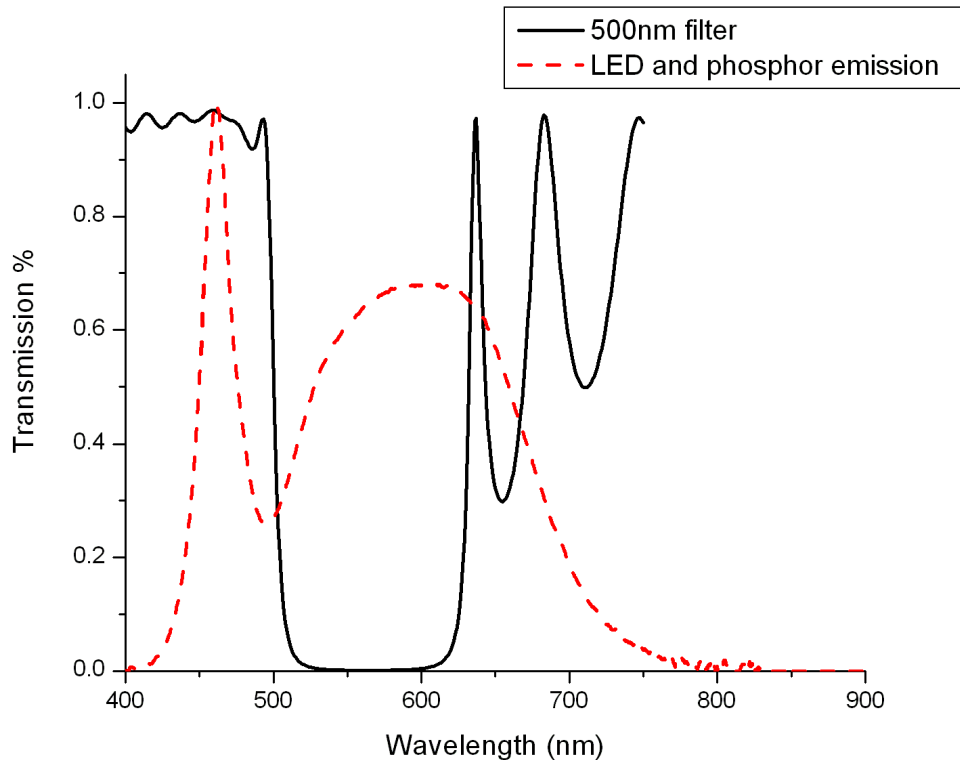
Figure 7.28: Transmission of the 500nm filter, the normalised LED and phosphor emission is shown for comparison

The filter is made on a substrate, which in this case was glass. As the glass is thicker than the filter layer, there was a noticeable difference in the application of the filter depending on which way round it was positioned. The first method was to have the filter above the LED, with the substrate above the filter. When reversed, the filter was above the substrate, further from the emission of the LED. The arrangement of layers is shown in figure 7.30.
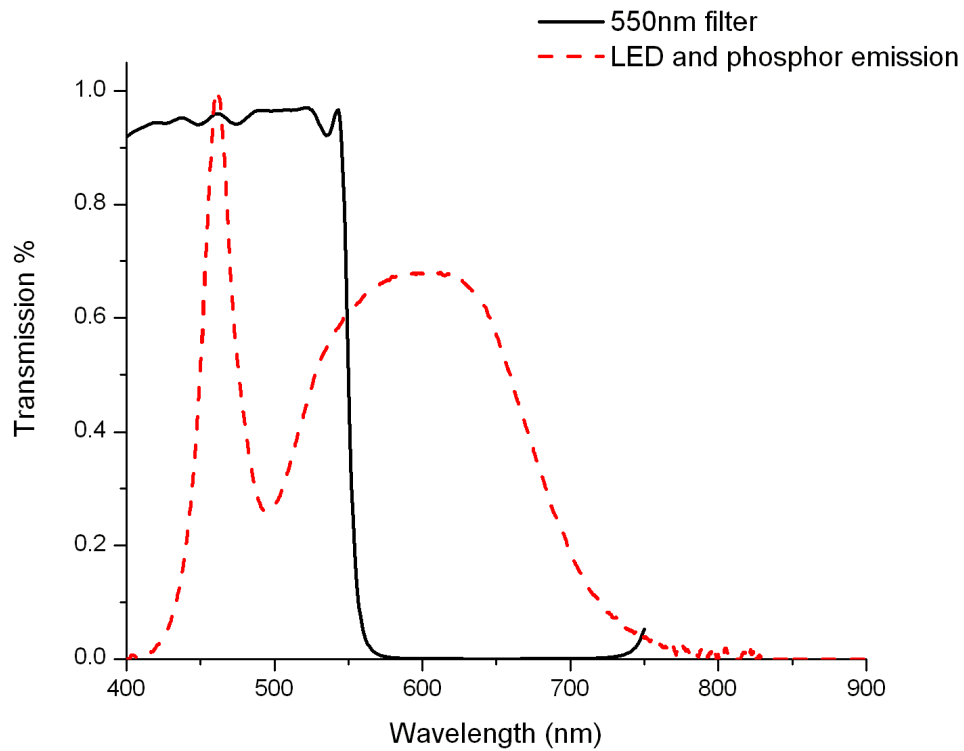
Figure 7.29: Transmission of the 550nm filter, the normalised LED and phosphor emission is shown for comparison

Figure 7.30: Schematic showing the order of the filter and architecture as described in the text

This difference is apparent in the emission spectra and is shown in figures 7.31 and 7.32. The results from this attempt to increase the emission is shown in table 7.3.

It was seen that when using the 500nm filter with the phosphors there was a decrease in efficacy, with the filter appearing to reduce the edge of the LED emission. However, the 550nm filter increased the efficacy by 15%. This was not at the expense of CRI and the colour correlated temperature was only slightly affected by this change. While the addition of a filter does have clear benefits the addition of filters into commercial products will be based on whether or not they are cost effective.
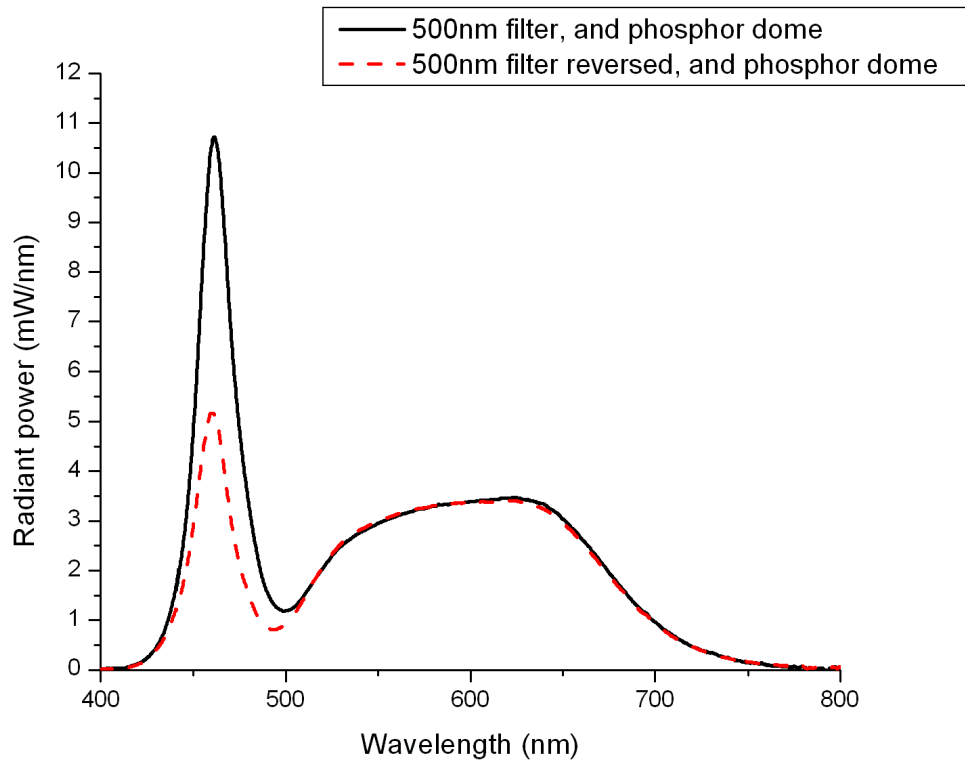
Figure 7.31: Comparison of the emission using phosphor domes and 500nm filter when the position of the filter on substrate was reversed

Table 7.3: Efficacy measurements from the inclusion of a filter between the LED and the phosphors.

Setup	Output (lm)	Efficacy (lm/W)	CRI	CCT(K)
Array	138.3	5.3	n/a	n/a
Phosphor dome	265.3	10.2	90.6	3770
500nm filter	88.69	3.4	n/a	n/a
500nm filter, dome	214.5	8.3	83.3	6040
500nm filter reversed, dome	206.6	8.0	90.1	3880
550nm filter	124.1	4.8	n/a	n/a
550nm filter, dome	291.9	11.1	90.1	3690
500nm filter reversed, dome	304.2	11.6	90.1	3540

Figure 7.32: Comparison of the emission using phosphor domes and 550nm filter when the position of the filter on substrate was reversed

Temperature dependence of phosphors

When the domes were produced on a large scale for testing, they were not built directly on the array each time, but produced unattached to allow easy testing of measurements. To compare these domes to those built directly on the arrays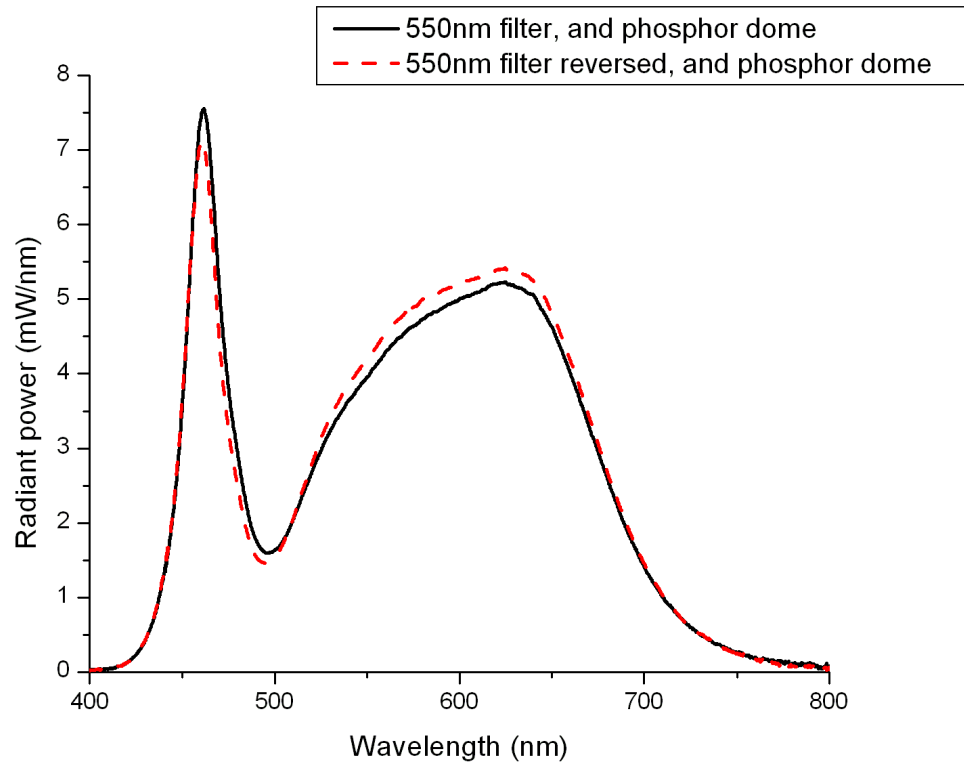, the small air gap was removed by application of uncured silicone gel. The air gap between the dome has the effect creating an interface which reduced the light extraction, and at the same time insulating the dome somewhat from the heat transfer from the LED. How they affected the output over an increased temperature was investigated. The results were measured with and without an air gap to compare the LED and phosphor performance. The results for this are shown in table 7.4.

Table 7.4: Efficacy measurements comparing the efficacies when including an air gap between the domes and the LED array

Setup	time delay	Efficacy (lm/W)	CRI	CCT(K)
Array	initial	5.10	n/a	n/a
	1 minute	4.90	n/a	n/a
	5 minutes	4.95	n/a	n/a
Dome with air gap	initial	11.2	88.3	4530
	1 minute	10.8	88.2	4820
	5 minutes	10.6	88.5	5040
Dome without air gap	initial	18.2	89.4	5750
	1 minute	17.3	89.1	6230
	5 minutes	16.7	88.7	6540

From these results, it is clear that whilst an air gap can help insulate the phosphors by having a small reduction in the efficacy decrease as the LED heats up, the overall efficacy is reduced. The effect is so dramatic that it is preferable to run this arrangement with no air gap, building the dome directly onto the LED. The change in CCT is noticeable as the LED heats up although within ten minutes this was stabilised once the temperature of the phosphor had stabilised.

7.7 Conclusion

The experimental data in this chapter accurately portrays much of the discussion in section 1.4.1 regarding broad band emitters and their use in applications. The broad band emitters, especially in the red region of the spectrum, will tend to lead to low lumen output where a narrow emitter, such as the Eu^{3+} emitters seen in chapter 5, can lead to a higher luminous efficacy. However, to achieve good colour rendering a broad emitter is necessary.

The novel phosphors reported earlier in this work were tested in conjunction with blue emitting LEDs (of peak wavelength 465nm) and compared to existing commercial phosphors. These existing phosphors showed superior luminous efficacies at least in part due to the physical attributes of the phosphor powder notably homogeneous small particle size, a key attribute for printing process. This importance of applica-

tion of the phosphors to the screens was clear, even between commercially available phosphors where YAG:Ce^{3+} showed greatest light output. Further research into the manufacturing methods of the novel phosphors reported should improve the printing properties of these red emitting phosphors and lead to an increase in the efficacy of white light based on blue light emitting diodes.

However, applying these existing phosphors to the LED had problems especially at high temperature. A novel manufacturing method for the domes to increase light extraction, and application of phosphors was described here. The advantages in light extraction and temperature performance are clear as the total output achievable for a white light at high power (~30W) was in excess of 11 lm/W with a CRI of 90 at a CCT of 3600K.

References

[1] A. Uddin, A.C. Wei, and T.G. Andersson. Study of degradation mechanism of blue light emitting diodes. *Thin Solid Films*, 483(1-2):378 – 381, 2005.

[2] Matteo Meneghini, Lorenzo Trevisanello, Gaudenzio Meneghesso, Enrico Zanoni, Francesca Rossi, Maura Pavesi, Ulrich Zehnder, and Uwe Strauss. High-temperature failure of GaN LEDs related with passivation. *Superlattices and Microstructures*, 40(4-6):405 – 411, 2006. E-MRS 2006 Symposium S: Material Science and Technology of Wide Bandgap Semiconductors, 2006 Spring Meeting of the European Materials Research Society.

[3] Subramanian Muthu, Frank J. P. Schuurmans, and Michael. D. Pashley. Red, green, and blue LEDs for white light illumination. *IEEE journal on selected topics in quantum electronics*, 8(2):333 – 338, 2002.

[4] Hong He, Renli Fu, Yongge Cao, Xiufeng Song, Zhengwei Pan, Xinran Zhao, Qingbo Xiao, and Ran Li. $Ce^{3+} \rightarrow Eu^{2+}$ energy transfer mechanism in the Li_2SrSiO_4:Eu^{2+}, Ce^{3+} phosphor. *Optical Materials*, 32(5):632 – 636, 2010.

[5] V.P. Dotsenko, S.M. Levshov, I.V. Berezovskaya, G.B. Stryganyuk, A.S. Voloshinovskii, and N.P. Efryushina. Luminescent properties of Eu^{2+} and Ce^{3+} ions in strontium litho-silicate Li_2SrSiO_4. *Journal of Luminescence*, 131(2):310 – 315, 2011.

[6] Terry Ireland. *conversation with R Stone*, April 2008.

[7] N. Narendran, Y. Gu, J. P. Freyssinier-Nova, and Y. Zhu. Extracting phosphor-scattered photons to improve white LED efficiency. *Physica status solidi (a)*, 202:R60 – R62, 2005.

[8] Leendert Vriens, Gerard Acket, and Cornelius Ronda. *UV/blue LED-phosphor device with efficient conversion of UV/blues light to visible light*. United States Patent 5813753, September 1998.

[9] Thonas F. Soules, Stanton Weaver Jr., Chen-Lun Hsing Chen, Mathew Sommers, Boris Kolodin, Anan Achyut Setlur, and Thoman Elliot Stecher. *Coated LED with improved efficiency*. United States Patent 7479662, January 2009.

[10] Christopher Haydn Lowery. *Multiple encapsulation of phosphor-LED devices*. United States Patent 5959316, September 1999.

[11] Frank W. Mont, Jong Kyu Kim, Martin F. Schubert, E. Fred Schubert, and Richard W. Siegel. High-refractive-index TiO_2-nanoparticle-loaded encapsulants for light-emitting diodes. *Journal of Applied Physics*, 103(8):083120–1 – 083120– 6, 2008.

[12] Dongdong Jia and Xiao jun Wang. Alkali earth sulfide phosphors doped with Eu^{3+}/Eu^{2+} and Ce^{3+} for LEDs. *Optical Materials*, 30(3):375 – 379, 2007.

[13] Paul Harris. *E-mail to R Stone*, July 2011.

Chapter 8

Organic Light Emitting Diodes

An introduction to organic light emitting diodes (OLEDs) was described in section 1.9. OLEDs are still advancing rapidly in both their efficacy and their emission [1]. They already have advantages over other light emitting devices including a high contrast ratio, thin film and wide viewing angle [2]. PLEDs are the basis for light generation discussed in this chapter and the substrate for these was glass. Initially supplied with a peak wavelength of 466nm, this was followed by PLEDs emitting at shorter peak wavelengths. This was first followed by one with a peak wavelength of 463nm, and was later surpassed by one having a peak wavelength located at 456nm. The associated shift in CIE coordinates (x, y) was from (0.150, 0.210) to (0.145, 0.180) and later (0.147, 0.156). These spectra are shown in figure 8.1. As is seen in the spectra, the change in peak wavelength from these devices was quite a significant shift, and in the latest device supplied, rather than having a shoulder, a separate second peak emerges. This affects the full width half maximum (FWHM) which was measured as 47.5nm for the initial PLED and 23.9nm for that of the lower wavelength. However, this improvement was relatively recent and as such much of the work utilised is based on the PLED emitting at 463nm.

As with LEDs, generating white light using a single light emitter has advantages over the use of three emitters in a red, green and blue (RGB) system [3]. A single emitter offers better colour stability with ageing as it is determined by just one emitter, and the electronic and physical architecture are simpler. In this case, down conversion phosphors were utilised for both general lighting and display lighting, although each would have the choice of phosphors guided by the requirements of the emission. In the case of display lighting, a saturated light with the emission coordinates tailored to create as wide a colour gamut as possible is desired. For use with general lighting, a broad band emitter is key to achieving a high CRI emission [4]. Both of these cases are studied for the PLEDs in this chapter.

8.1 Phosphor Screens

The interaction between the PLEDs and the phosphors were studied using acetate screens to build up a picture of their interactions.
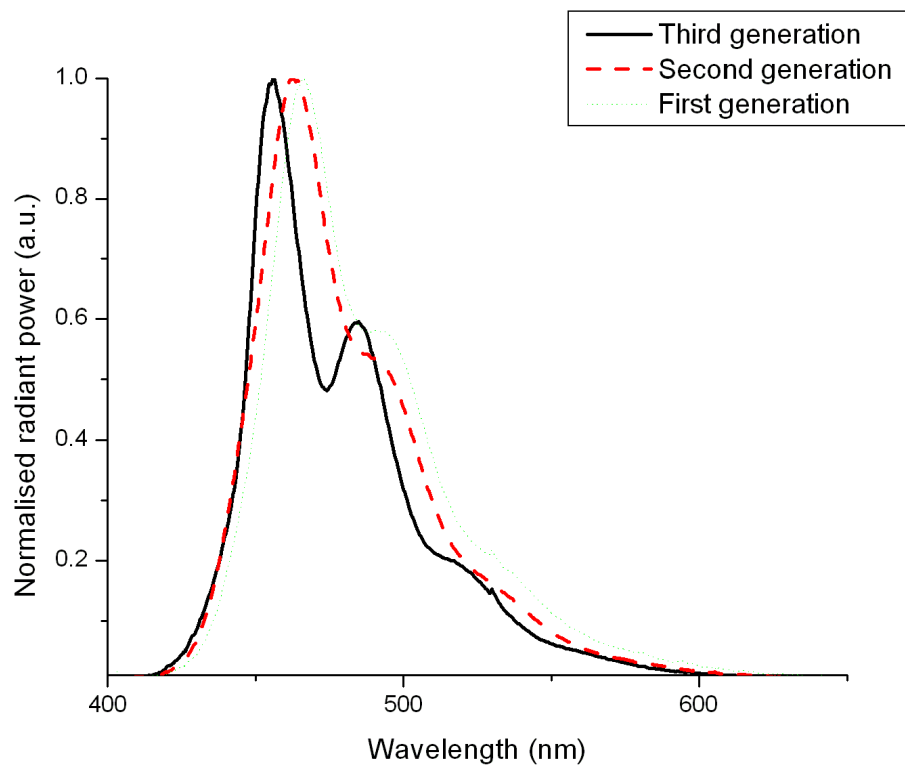
Figure 8.1: Emission spectra of first generation, second generation and third generation PLEDs showing decreasing peak emission wavelength

The YAG:Ce^{3+} phosphor screen was the first that was tested with the PLEDs. What was clear from this emission, seen in figure 8.2, was that the higher wavelength edge of the PLED emission was less readily absorbed than the peak emission wavelength. This was not the case for the other phosphors. $SrGa_2S_4$:Eu^{2+} was also a broad band green emitter although its emission did not extend into the red, and the combined emission with the PLED is presented in figure 8.3.

The excitation from the red emitting phosphors, CaS:Eu^{2+} and SrS:Eu^{2+}, combined with the blue PLED emission, is shown in figures 8.4 and 8.5 respectively.

The efficacies of the PLEDs along with the performance when the phosphors were included are presented in table 8.1.
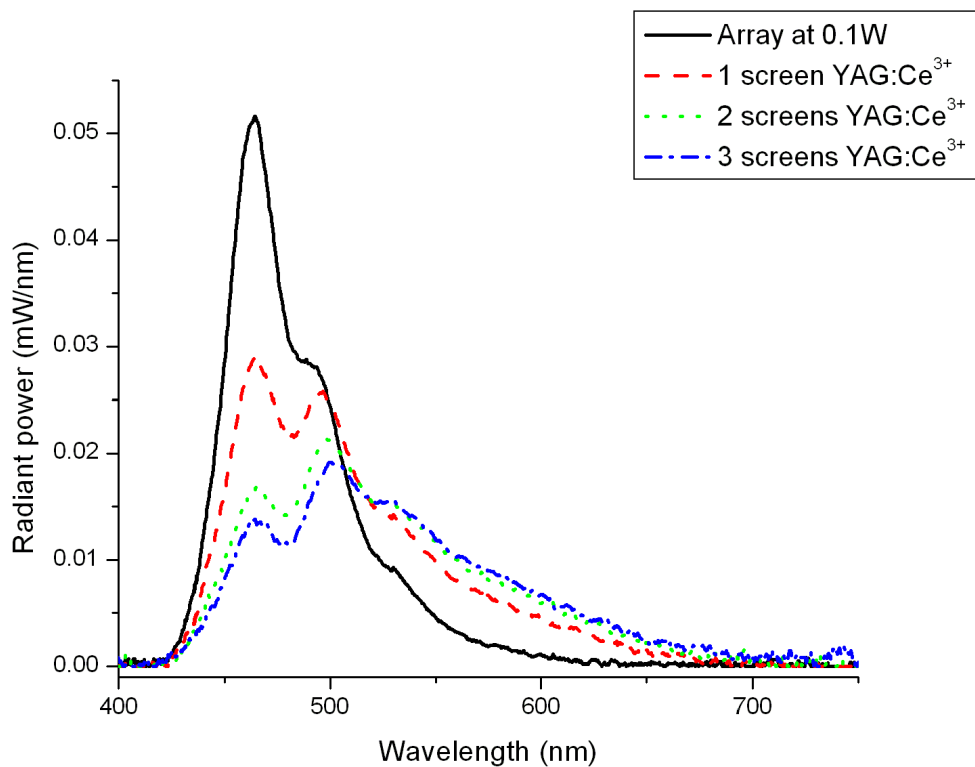
Figure 8.2: YAG:Ce^{3+} screens over blue PLED
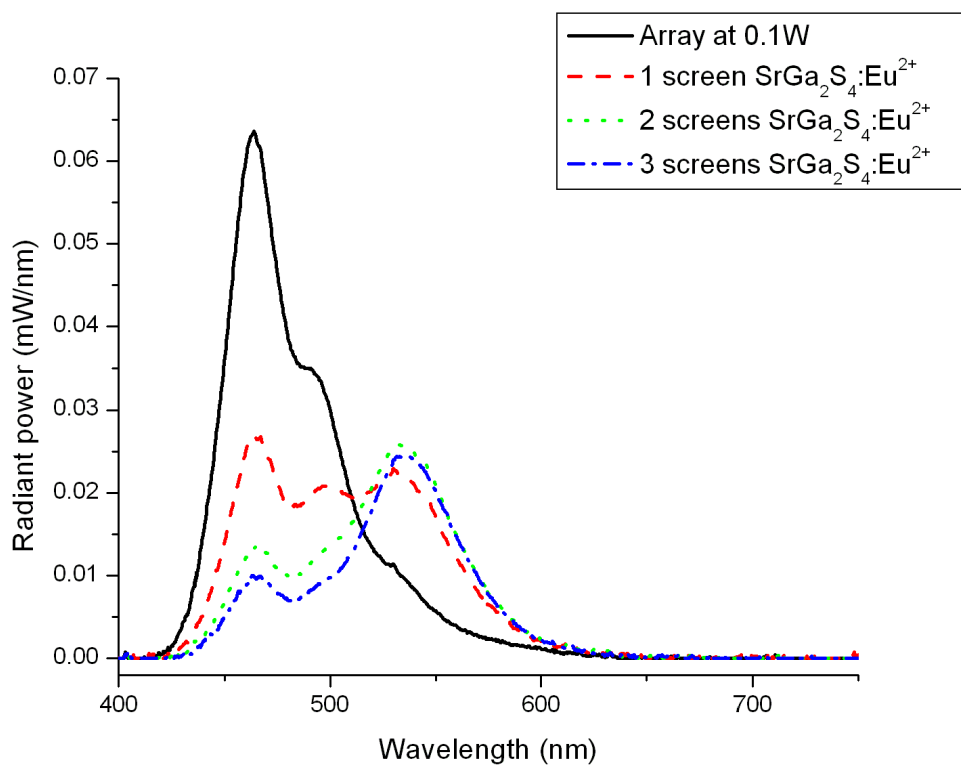
Figure 8.3: SrG$_2$S$_4$:Eu^{2+} screens over blue PLED
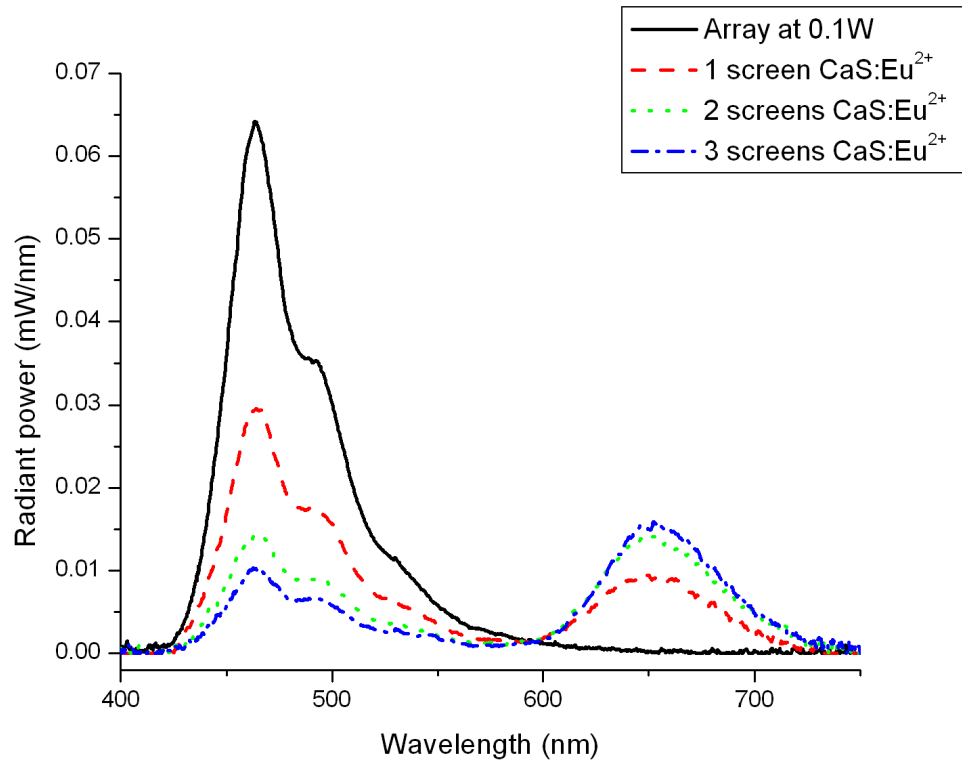
Figure 8.4: CaS:Eu^{2+} screens over blue PLED
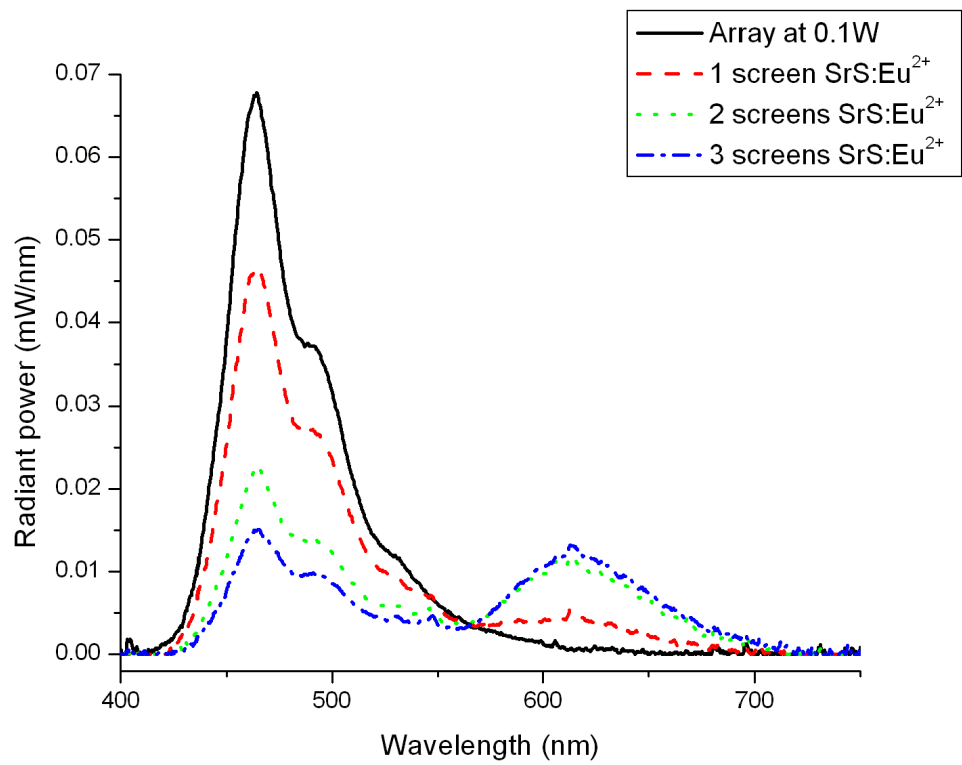
Figure 8.5: SrS:Eu^{2+} screens over blue PLED

Table 8.1: Emissions from varying thickness screens over blue emitting PLED, run at 5V and 20mA

Emission	Number of layers	Lumen output (lm)	Efficacy (lm/W)
Array	-	0.60	6.01
YAG:Ce^{3+}	1	0.72	7.2
	2	0.77	7.7
	3	0.79	7.9
SrGa$_2$S$_4$:Eu^{2+}	1	0.87	8.74
	2	0.93	9.25
	3	0.85	8.52
CaS:Eu^{2+}	1	0.38	3.84
	2	0.27	2.74
	3	0.23	2.29
SrS:Eu^{2+}	1	0.57	5.71
	2	0.52	5.16
	3	0.47	4.68

The excitation spectra of the phosphors were then measured and this is shown with an overlay of the PLED emission, for both the $CIE_y = 0.21$ and $CIE_y = 0.18$ PLED devices. This appears in figure 8.6.

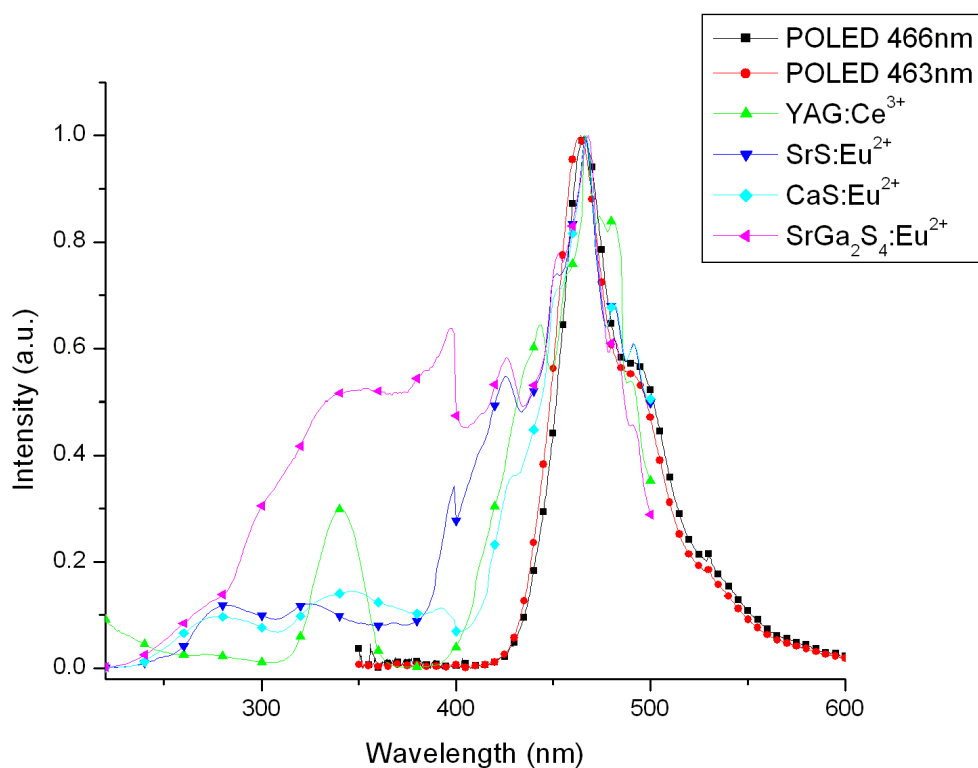Figure 8.6: Overlay of excitation wavelength of phosphors and emission spectra of PLEDs

8.2   Saturation of PLED emission

In the case of display lighting, each RGB component is required at colour points as far to the extremes of the CIE diagram as possible to generate the greatest colour gamut and therefore the largest number of colours available for display. The best position for the green, to allow the full range of white colour points within the colour gamut, was towards the right of the CIE colour space. The most important aspects of the emission is to reach as close to the edge of the Planckian locus as possible. When measuring the phosphors alone, the registered emission showed their true colour points. However, to achieve this in practice was not as easy. All the blue excitation light needed to be absorbed else it was seen in the output. However, addition of excess phosphor reduced the efficacy of the overall light through energy losses in scattering and absorption.

Table 8.2 shows the performance of the phosphors as measured directly in the Bentham Integrating Sphere.

Due to the structure of the device, not all the emission was directed in the forward direction, and some scatters and emits from the sides of the device. It appeared in all the emissions in figures 8.2 to 8.5 that the phosphor was becoming saturated with

some blue emission still exiting the device and this was due to the structure of the device and blue light 'leaking' from the sides of the PLED. Corrections for this were therefore addressed in section 8.2.1.

It was possible to analyse the phosphor on the PLED device by using a ProMetric imaging colorimeter which took images and measured the emission from directly above the emitter in high resolution. This was able to analyse CIE coordinates over many points, with each point registered on a 1931 CIE chromaticity diagram. Results are shown for the greater thickness screens of $SrGa_2S_4:Eu^{2+}$ (figures 8.7 and 8.8) and $CaS:Eu^{2+}$ (figures 8.9 and 8.10) [5].

These showed the accuracy and precision needed in the phosphor layer that is applied to the surface of the light emitting region to obtain a consistent emission from the combination of the two. These results indicated a more uniform deposition method was required for phosphor particles of this size. While the $SrGa_2S_4:Eu^{2+}$ showed uniform a emission, especially notable in the high resolution image, $CaS:Eu^{2+}$ showed poor uniformity. This is due to the printing quality which is a function of the particle size. Based on the scattering from $YAG:Ce^{3+}$ particles and emission spectra from other phosphors, this did show that in principle, if particle size can be controlled, this would provide a suitable method for generation of light for displays.

Table 8.2: Direct measurements of phosphor powder

Phosphor	Luminous efficacy (lm/W)	Quantum efficiency (%)	Max. Theoretical Efficacy (lm/W)	(CIE_x, CIE_y)
$YAG:Ce^{3+}$	320.7	78.0	380.7	(0.43, 0.55)
$SrGa_2S_4:Eu^{2+}$	339.0	65.5	487.9	(0.29, 0.68)
$CaS:Eu^{2+}$	43.1	61.6	77.2	(0.70, 0.30)
$SrS:Eu^{2+}$	119.4	59.2	212.7	(0.64, 0.36)

Figure 8.7: High resolution image of $SrGa_2S_4$:Eu^{2+} screen, the black bar represents one mm

Figure 8.8: CIE diagram over high resolution for individual points on $SrGa_2S_4$:Eu^{2+} screen
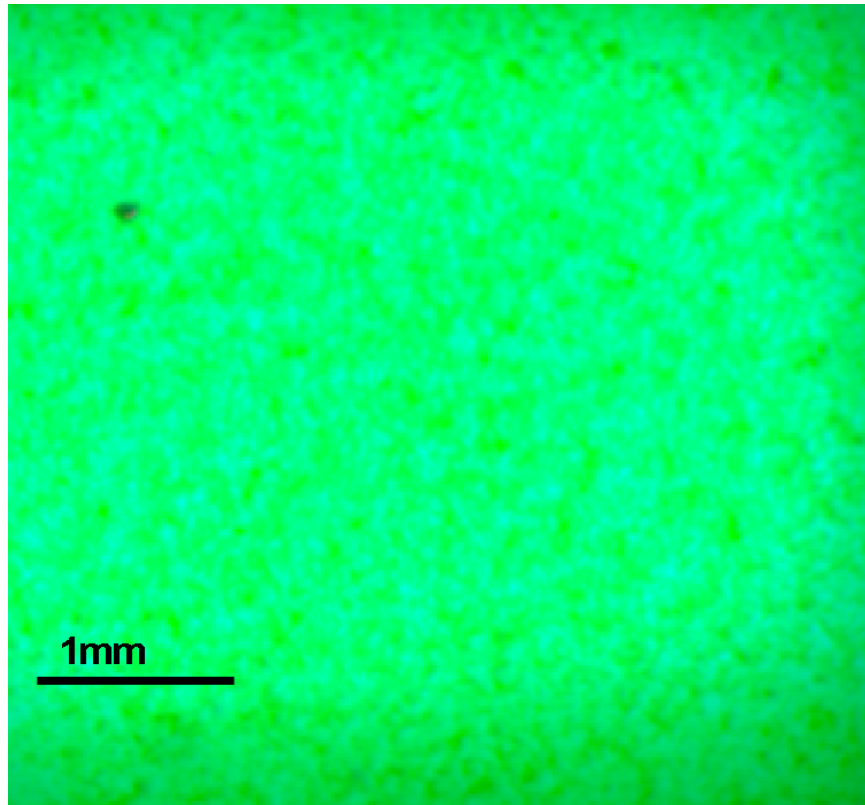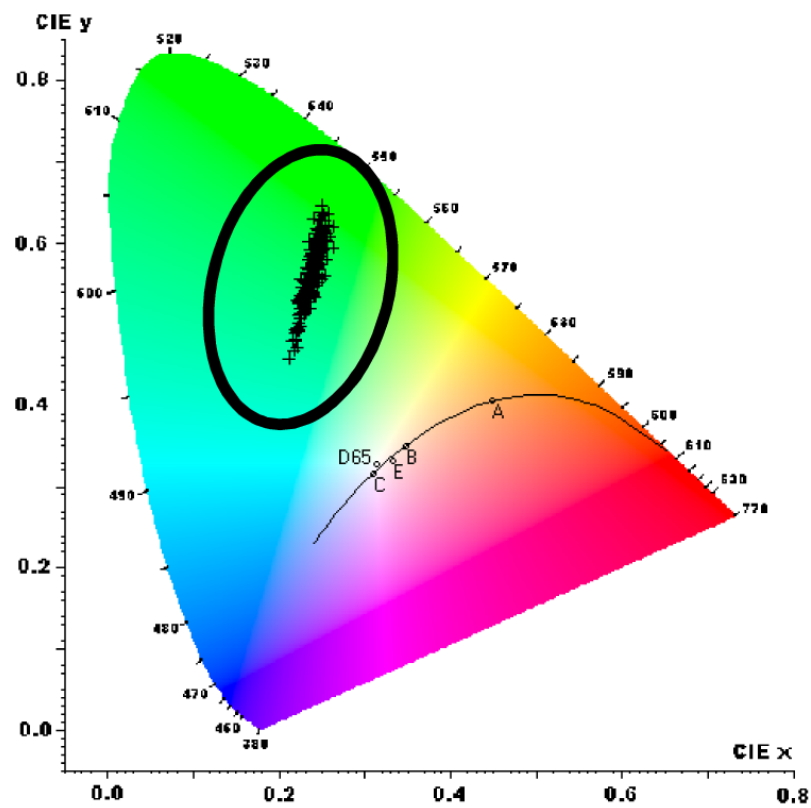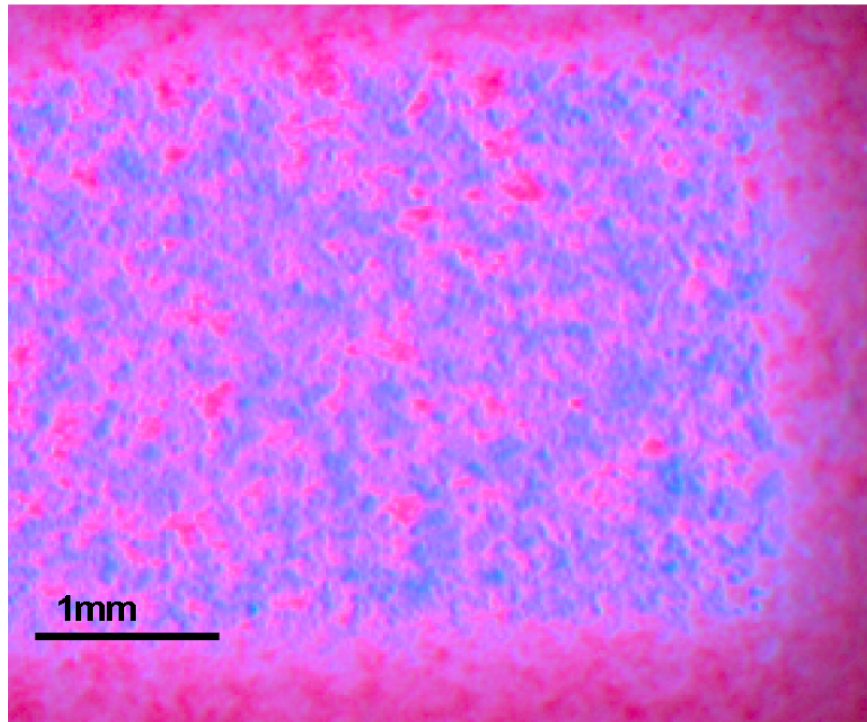
Figure 8.9: High resolution image of CaS:Eu^{2+} screens, the black bar represents one mm
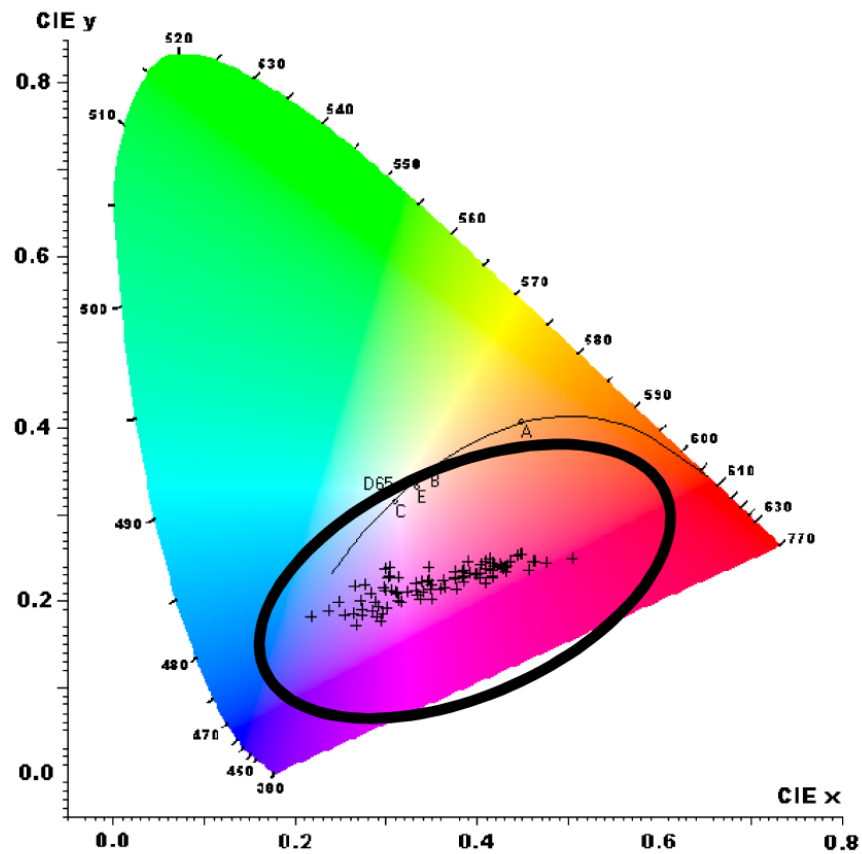

Figure 8.10: CIE diagram over high resolution for individual points on CaS:Eu^{2+} screen

8.2.1 Removing light leaking from the PLED

For saturated devices, the aim was to extend the colour gamut to as large an area as possible. In order to test these devices and the power they can achieve, all the blue emitting light needed to be converted by the phosphors. However, as mentioned earlier, some of the blue light was leaking from the side of the device and this prevented accurate measurements for colour points achievable when using the Pro-Lite Integrating Sphere. In order to correct for this, the device was blackened around the edges from where the light was leaking. This covered a small area and so did not adversely affect the overall results as absorption by this material should be low relative to the total area. Using this arrangement, the phosphor screens were again tested, with $SrGa_2S_4$:Eu^{2+} and CaS:Eu^{2+} as these showed the deepest red and green emissions. These spectra are shown in figures 8.11 and 8.12 with (x, y) CIE coordinates of (0.30, 0.63) for $SrGa_2S_4$:Eu^{2+} and (0.59, 0.29) for CaS:Eu^{2+}. These results show, by comparing to the phosphor emission in table 8.2, the $SrGa_2S_4$:Eu^{2+} saturated the emission although the CaS:Eu^{2+} did not completely saturate the blue emission. In both cases, however, a lot of phosphor was used to achieve the saturation in these measurements and this strongly reduced the efficacies resulting in values of $3.6\,lm/W$ for $SrGa_2S_4$:Eu^{2+} and just $0.44\,lm/W$ for CaS:Eu^{2+}.
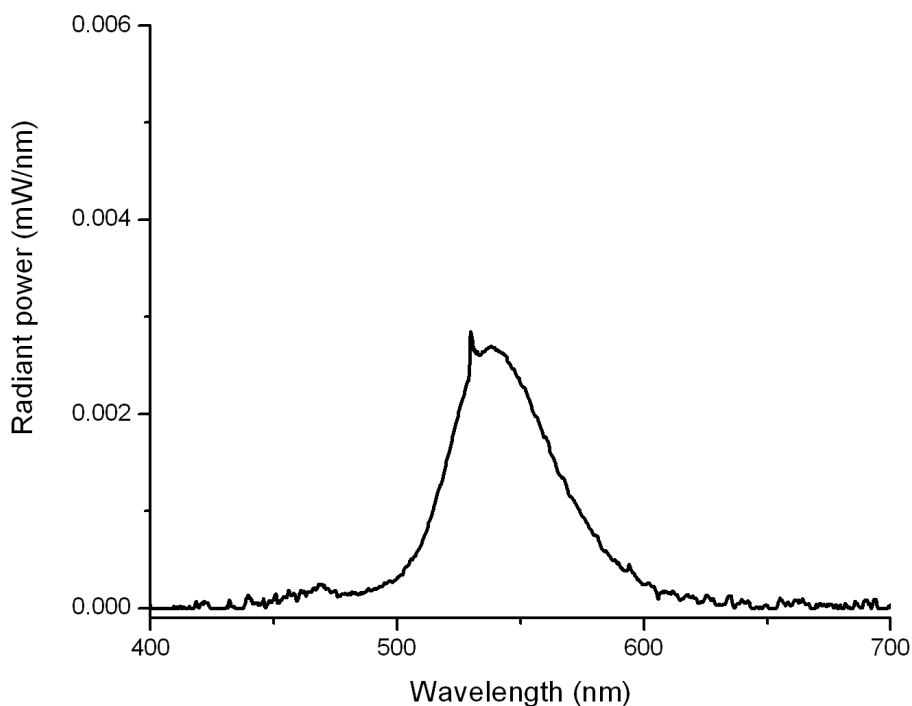

Figure 8.11: Complete colour conversion of PLED emission by $SrGa_2S_4$:Eu^{2+}

These CIE_x and CIE_y coordinates were compared with the results in table 8.2 and showed a high level of saturation of the emission.
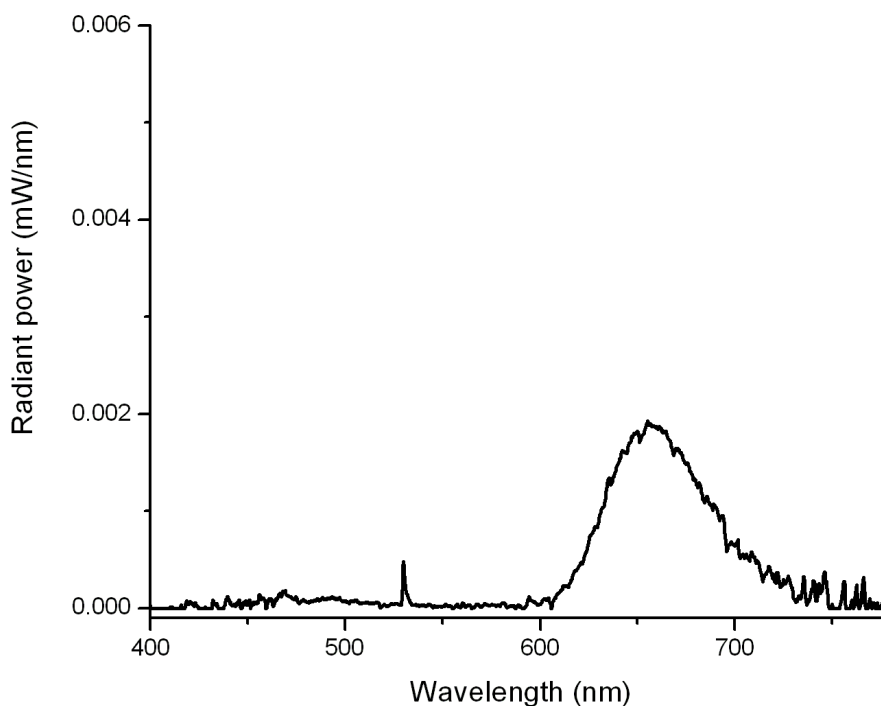
Figure 8.12: Complete colour conversion of PLED emission by $CaS:Eu^{2+}$

8.3 White light emission

One aim of using these phosphors with the blue light was to create a white light emission using the blue PLED. In this case, with certain phosphor concentrations a measurable white light was recorded. With the $YAG:Ce^{3+}$ screen, CIE coordinates (0.29, 0.33) were achieved with a CCT of 7611 K, and its position in the CIE diagram is shown in figure 8.13, marked with a 2. Point 1 shows the PLED with less $YAG:Ce^{3+}$, and point 3 shows $YAG:Ce^{3+}$ screen of greater thickness.

$SrGa_2S_4:Eu^{2+}$ alone can not get as near the Planckian locus as $YAG:Ce^{3+}$ and its CIE colour coordinates are (0.20, 0.32). The $YAG:Ce^{3+}$ phosphor has a CRI measured at 76 which is the minimum required for general lighting. To increase the CRI, the individual breakdown of R numbers was measured and, as expected, R8 was poor measured at 58 (as with CRI, this is measured out of 100); R9, not used in CRI calculations but a measure of deeper red, was even lower and measured at 0. These are related to the deep red measurements and thus the addition of a red phosphor to this was the next step to achieve a high CRI white light.

8.3.1 Two Phosphor Mix with Blue PLED

A white light emission was created by adding a red emitting phosphor to the blue PLED and yellow phosphor. Both the $CaS:Eu^{2+}$ and $SrS:Eu^{2+}$ were included to widen the deep red emission as much as possible. The order that the phosphors were
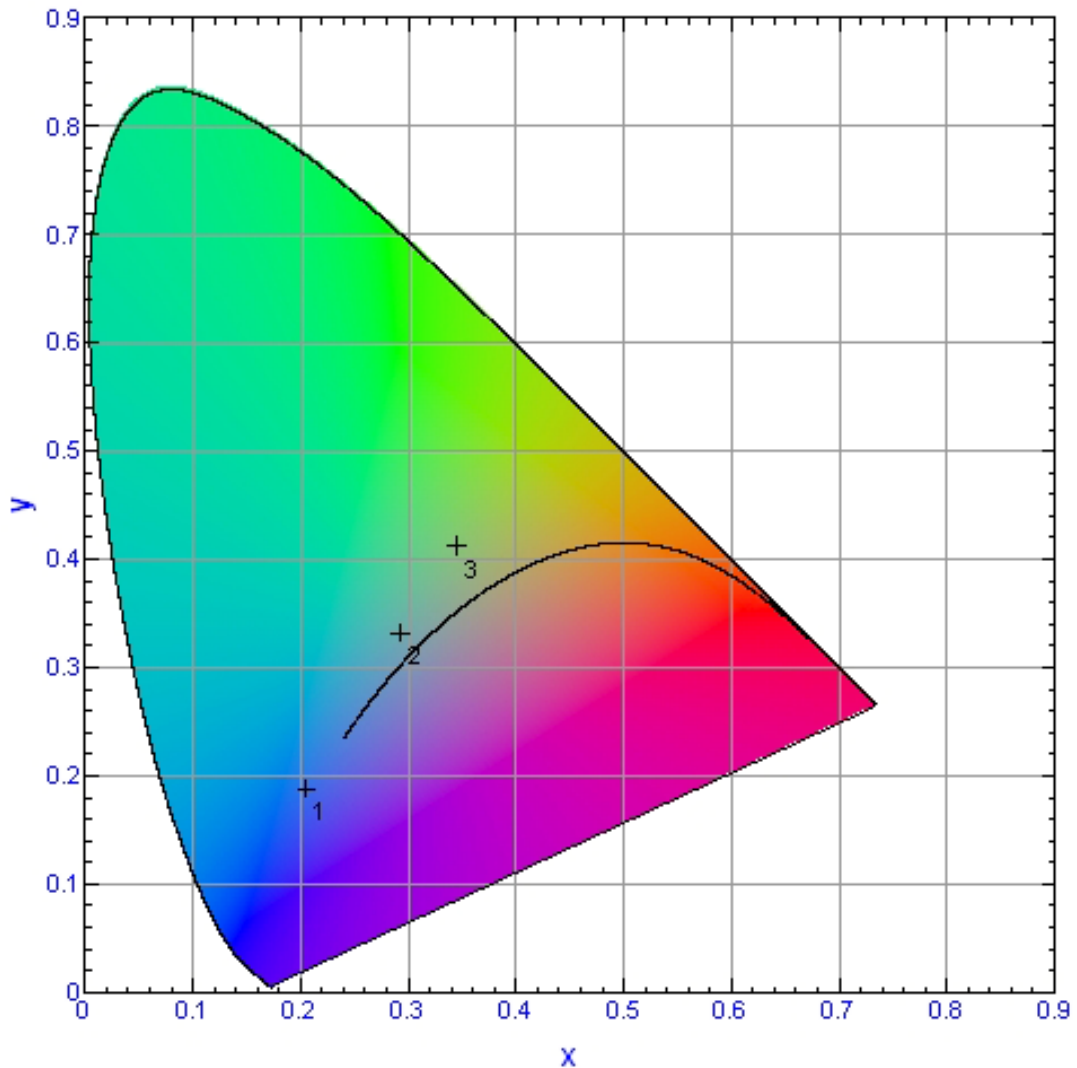
Figure 8.13: Colour point for blue PLED alone and in combination with increasing thickness YAG:$^{3+}$ phosphor screens

combined was important and the CRI can vary greatly based on the arrangement, with value measured anywhere between 70 and 90. The use of too much red phosphor led to the lower measurement of this value, although it provided an emission closer to the Planckian locus. These differences were seen most clearly by comparing an arrangement where SrS:Eu^{2+} was directly above the PLED, followed by YAG:Ce^{3+} and then CaS:Eu^{2+}. An increased thickness of the YAG:Ce^{3+} layer led to a lower CRI reducing to 79 from its peak at 90, while the CIE coordinates shifted from (0.32, 0.38) to (0.34, 0.35). These are shown in figure 8.14, the thicker layer is point 1. The efficacies of these measurements were similar at 4.5 lm/W to 4.3 lm/W as the thickness of the YAG:Ce^{3+} increased. Adjusting the phosphor content increased or decreased the colour temperature, although this led to a reduction in the CRI, from this peak value.
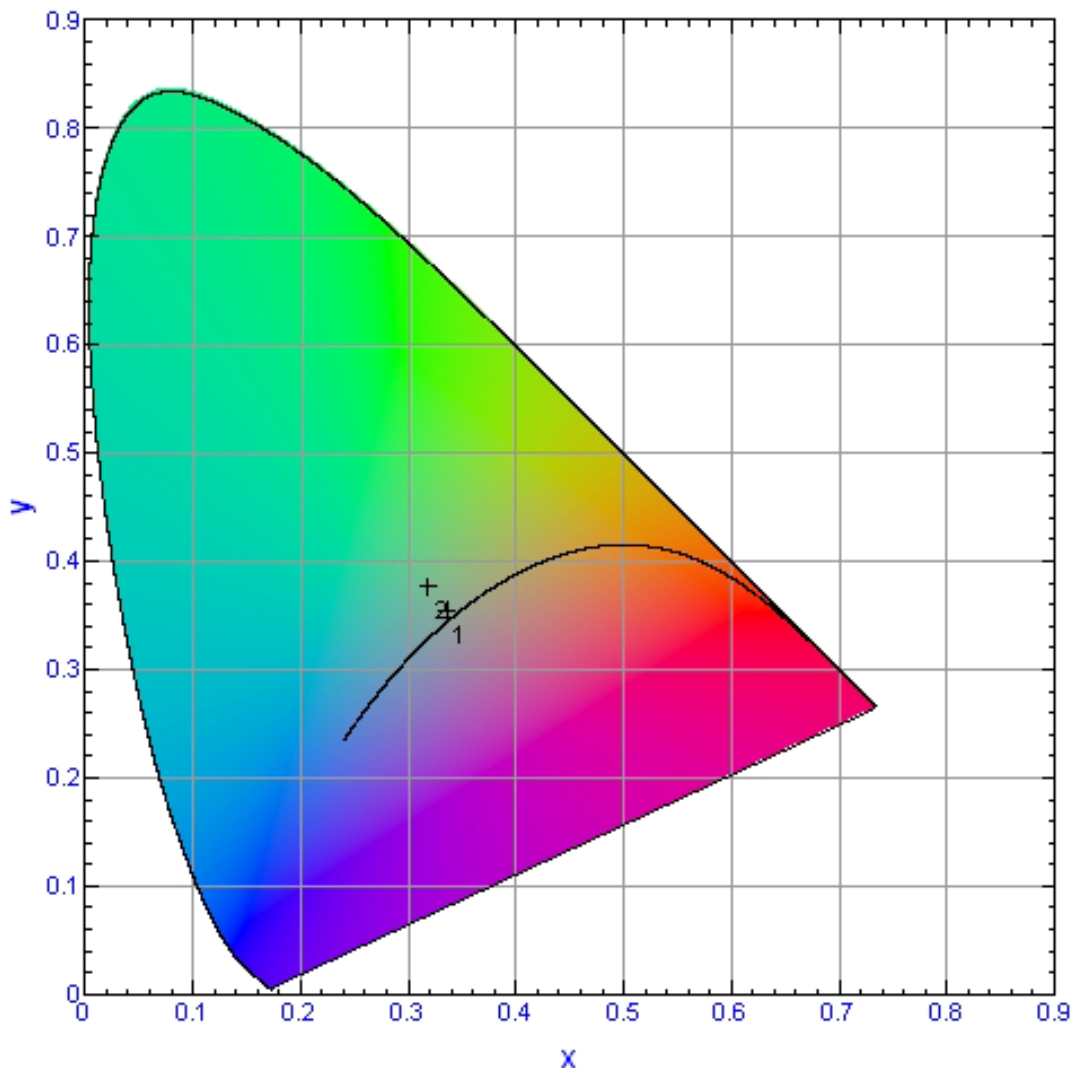
Figure 8.14: Emission on the Planckian locus has a reduced CRI (79 to 90) and decreased CCT of 5367K to 6014K

8.3.2   Combining Red And Blue PLEDS

An alternative arrangement to generate a white light is to combine a blue and a red PLED device [6]. This may also require a a green emitting phosphor. The YAG:Ce^{3+} and SrG_2S_4:Eu^{2+} were investigated in this arrangement, and the combination of the emission spectra are shown in figure 8.15.

A decrease in red emission is seen when YAG:Ce^{3+} and $SrGa_2S_4$:Eu^{2+} were compared; this was attributed to greater scattering of the emission by the $SrGa_2S_4$:Eu^{2+}. A thicker screen showed a greater decrease.

The CIE coordinates for each phosphor combined with both PLEDs, are shown in figure 8.16. Extrapolating the line for YAG:Ce^{3+} showed that after the thickness is increased to the Planckian, the emission will measure a low temperature of ~ 2000K. However, the location of the $SrGa_2S_4$:Eu^{2+} emission was on the Planckian locus at 2700K and CIE coordinates of (0.47, 0.43). It was clear that the long tail of the YAG:Ce^{3+} had very little advantage when a red PLED supplements the blue PLED.
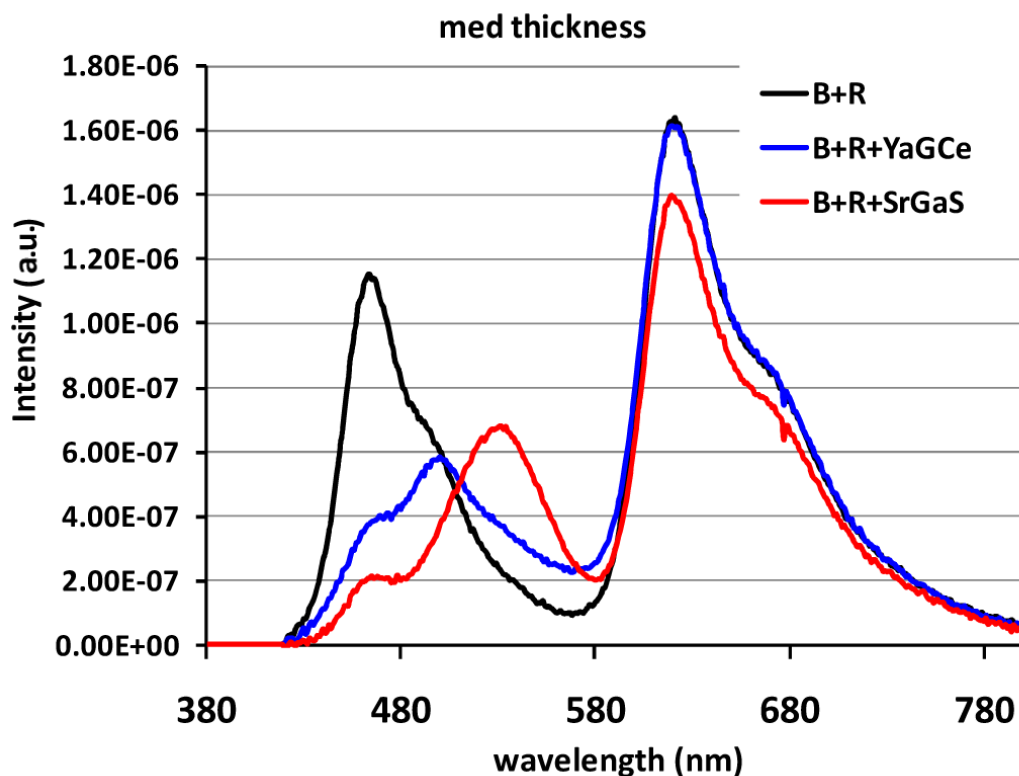
Figure 8.15: Emission spectra of combination of blue PLED (B), red PLED (R), and either YAG:Ce^{3+} or SrGa$_2$S$_4$:Eu^{2+} phosphor

Furthermore, the SrGa$_2$S$_4$:Eu^{2+} showed superior performance as its peak emission was at a higher wavelength. These results indicated using this method for generation of white light, SrGa$_2$S$_4$:Eu^{2+} would be the phosphor of choice.

To investigate this arrangement in greater detail, screens of varying thickness were compared. These were measured using a power supply run at 9mA (which led to a higher luminous efficacy than measured earlier when run at 20mA). The results are seen in figure 8.17 and the thickness of the layers increase from left to right on the x axis. CRI, external quantum efficiency (EQE) and luminous efficacy (in lm/W) are shown.

These results showed where the thickness of the screen would need to lie and can be calculated based on chosen emission characteristics. These results also showed the trade off between increasing CRI at a cost of a decreasing efficacy.

8.4 Silicone gel

When using the screens, the air gap between these and the device was expected to lead to a reduction in efficacy [7]. This interface caused a change in refractive index and therefore can lead to losses between the emission of the PLED and excitation of the phosphor. To counteract this effect, the air gap was removed using a silicone gel between the PLED and phosphor screen. The transmission of this gel was measured
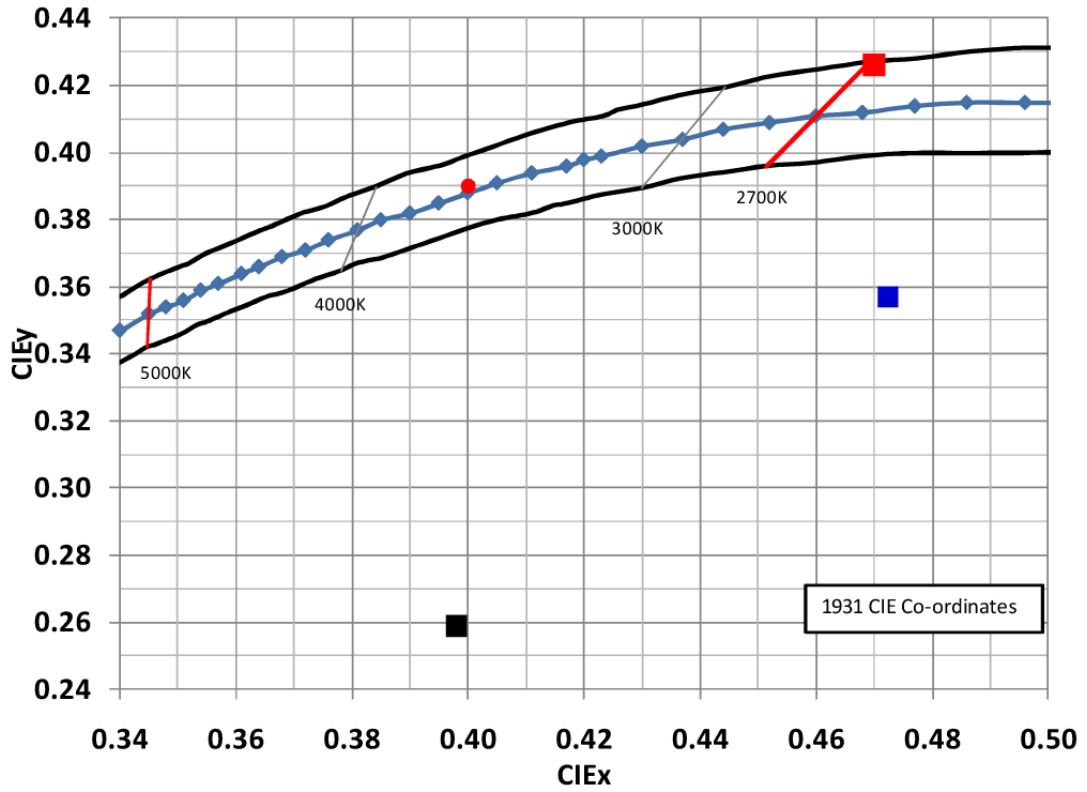
Figure 8.16: CIE coordinates of PLED combination (black), with addition of YAG:Ce^{3+} (blue) or addition of SrGa$_2$S$_4$:Eu^{2+} (red)
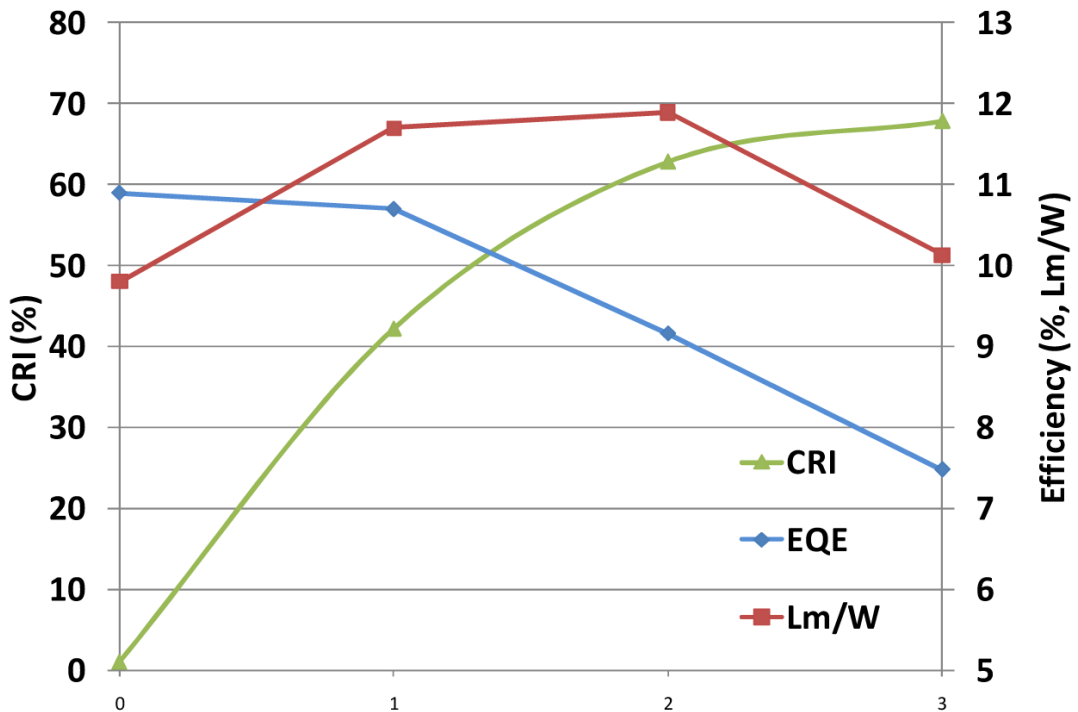
Figure 8.17: Efficiency and CRI measurements with increasing layers of SrGa$_2$S$_4$:Eu^{2+} screens
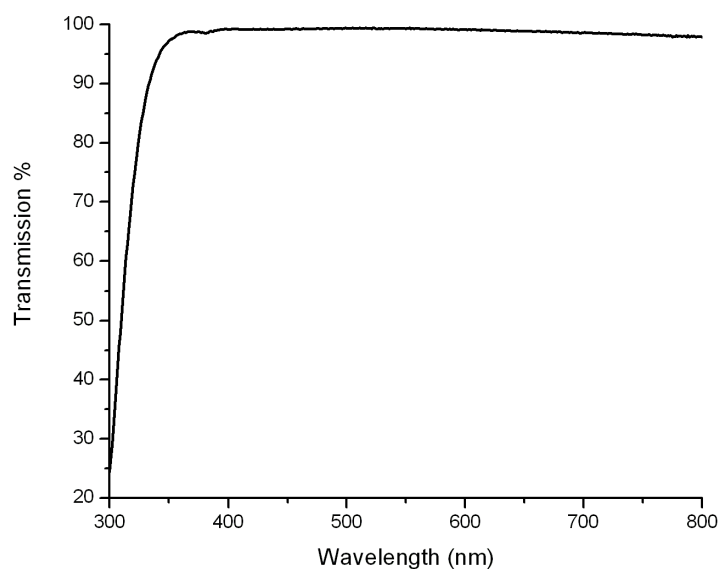
Figure 8.18: Transmittance efficiency of uncured silicone used, of 1mm thickness

and is close to 100% over the visible wavelengths and this spectrum is shown in figure 8.18.

This was used here to measure the effect that this air gap had on the measured efficacy, something that would not be present in a final product where the phosphor would be either a part of the substrate or directly applied to the substrate. The results are shown in figure 8.19. The increase in luminous efficacy can be up to 40% greater than without using the gel and shows that it will be necessary to directly apply the phosphors to the device.

Figure 8.19: Emission spectra depicting difference with and without silicone gel between screens and PLED device

8.5 Conclusions

As with LEDs, colour converting phosphors show promise for general and display lighting utilising PLEDs as the light source and have similar advantages. The application of the phosphor to the device will comprise unique challenges which must be overcome to provide efficient packages for these devices. The difference in lighting and displays is once again clear 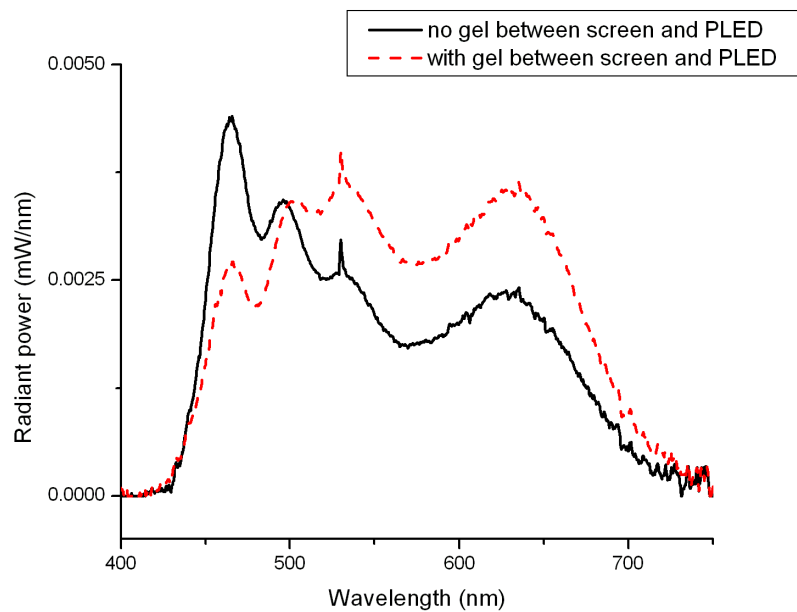in the choice of phosphors for the application. For display lighting the focus needs to shift to the manufacture and deposition of the phosphors to produce small particles uniformly arranged to achieve a high efficacy saturated emission. The effects of scattering in this case is clearly crucial and improvements in extraction of light will greatly increase the efficacy of these devices. While YAG:Ce^{3+} has shown good properties for light extraction it is the other phosphors which may play a greater role in display lighting. Further work is required which looks set to have a large and immediate impact on the growing market of PLED devices for displays.

In general lighting, even though a blue emission 'through' the phosphor is required and phosphors are already well suited to the application, it is again the extraction of light for maximum efficiency is where the next improvements will arise. Due to the availability of high efficacy red PLED emitters, it may be that only one phosphor is required to generate an efficient high quality white light emitter. As the blue emitting devices are made at lower wavelengths, more phosphor can be applied such that the emission will remain close to the Planckian locus with the possibility of an increased CRI.

The nature of the emission from these devices, as well as their architecture could lead to them replacing ACEL panels in many of their applications as the efficiency of these devices is superior and energy efficiency concerns begin to dictate lighting requirements.

References

[1] P. Coppo. *SPR Photochemistry*, volume 37, pages 393 – 406. A. Albini ed., 2009.

[2] Bernard Geffroy, Philippe le Roy, and Christophe Prat. Organic light-emitting diode (OLED) technology: materials, devices and display technologies. *Polymer Internationl*, 55(6):572–582, 2006.

[3] Benjamin Krummacher, Markus Klein, Norwin von Malm, and Albrecht Winnacker. Optical analysis of down-conversion OLEDs. *Proc. SPIE*, 6910(1):691007, 2008.

[4] Cees R. Ronda. *Emission and excitation mechanisms of phosphors*, pages 1 – 20. Weinheim: Wiley-VCH, 2008.

[5] Martial Berry. *E-mail to R Stone*, May 2010.

[6] M. Suzuki, T. Hatakeyama, S. Tokito, and F. Sato. High-efficiency white phosphorescent polymer light-emitting devices. *Selected Topics in Quantum Electronics, IEEE Journal of*, 10(1):115–120, 2004.

[7] Siddha Pimputkar, James S. Speck, Steven P. DenBaars, and Shuji Nakamura. Prospects for LED lighting. *Nature Photonics*, 3:180–182, 2009.

Chapter 9

Conclusions

Questions addressed at the outset of the work were based upon an investigation into an attempted increase in efficiency of existing lighting technology. The two approaches taken herein were in improving the performance of phosphors and improving the efficacy of existing lighting packages. The former included the potential for both amending existing phosphors and creation of novel phosphors.

In improving the phosphor performance the double tungstate/molybdate phosphors were investigated and a novel red phosphor was synthesised and shown to have high efficacy. $Na_2WO_4MoO_4Eu_{0.44}Al_{1.34}Sm_{0.011}$ was the best of these in terms of luminous efficacy and was measured at 140% of previously reported Eu^{3+} phosphors [1] at $227\,lm/W$. This also has a lower europium content than many other Eu^{3+} phosphors and this will lead to the benefit of a reduced cost of the phosphor. These phosphors reported herein also showed other positive attributes including the position of the excitation bands to match the emission of blue LEDs and position of emission bands for use in display and general lighting as with other Eu^{3+} phosphors. Furthermore, they also showed a good temperature dependence of close to 90% at $175\,°C$. However, the luminous efficacy of the phosphor did not match that of current commercial phosphors when tested in applications and this was due to the poor printing onto a substrate. This appeared to be a problem due to a large particle size which lead to the poor print quality. It is hoped that with further improvements to the synthesis method that small homogenous particles for this phosphor may be made which would lead to its widespread use in many applications.

With respect to the amendment of existing phosphors, yttrium was used to replace europium in the lattice. Whilst this did not prove fruitful for current commercial phosphors, for the double tungstate/molybdate phosphors which are currently a topic of research, it was shown that this could lead to an improvement in the luminous efficacy without a compromise to any of the other properties that were investigated. $LiEu_{0.5}Y_{0.5}(MoO_4)_2Sm_{0.02}$ showed a 28% increase in luminous efficacy and was the best of those reported in this work. Again, as well as the increase in luminous efficacy, a great benefit is the reduction in cost of production of the phosphor due to the lowered europium content.

There was also a improvement made in extracting light from LED packages based

upon a novel method of manufacture of a solid dome encapsulant for the LED array. This also included the application of the phosphor powder to the dome. This manufacture method was put to use in commercial applications as there was a measured increase in efficacy using these which doubled the light output from the LED array.

Following this success with this application to LEDs, phosphors were also applied to ACEL and PLED panels in order to ascertain whether an increase in efficacy of the package would result. Phosphors were seen to work well with both technologies and whether they will see widespread use depends on the cost offset against the properties required. Red emitting phosphors will be competing against red dyes (notably rhodamine 6G) and in outdoor applications can find an advantage as they do not break down over time under UV light [2].

For PLEDs to compete with ACELs the cost will be a crucial factor; once they are of comparable luminous efficacy, PLEDs will need to match the price to be able to compete effectively in all low cost applications.

A further finding reported herein was that there may be a potential relation between thermal quenching and the host lattice. Insulators suffered from thermal quenching at low temperatures, while conductors retained their luminous efficacy at high temperatures. The mechanism for quenching has been studied and many proposals have been put forward. A literature study has indicated that thermal excitation to a conduction-band-like state [3] is the means by which quenching occurs. The result found herein should be studied further in mind of these reported results to see if they point the way for successful new phosphor design based on the thermal properties of lattices.

References

[1] Chuang-Hung Chiua, Ming-Fang Wang, Chi-Shen Leeb, and Teng-Ming Chen. Structural, spectroscopic and photoluminescence studies of LiEu(WO$_4$)$_{2-x}$(MoO$_4$)$_x$ as a near-UV convertible phosphor. *Journal of Solid State Chemistry*, 180:619 – 627, 2007.

[2] Shinkichi Tanimizu. *Phosphor Handbook*, page 770. Taylor & Francis Group, LLC, 2007.

[3] P Dorenbos. Thermal quenching of Eu^{2+} 5d-4f luminescence in inorganic compounds. *Journal of Physics: Condensed Matter*, 17(50):8103, 2005.